Exploring stem cell dynamics, clonal expansion and pseudopolyps in inflammatory bowel disease

Noor Jawad

PhD thesis

Supervisors: Professor Sir Nick Wright, Professor of Histopathology

Professor Andrew Silver, Professor of Cancer Genetics

Professor Ian Sanderson. Professor of Paediatric Gastroenterology

ABSTRACT

Inflammatory bowel disease (IBD) confers a high risk of development of colitis-associated colorectal cancer in patients with extensive colitis. Crypt fission is a mechanism of clonal expansion in the intestinal epithelium. Although fission is rare in the normal colon, many crypts in IBD patients are in the process of fission. Protumourigenic mutations can spread through the entire inflamed colon relatively quickly indicating that stem cell dynamics are altered in IBD. Some patients with IBD develop pseudopolyps as a result of mucosal ulceration and epithelial regeneration. The aim of this PhD was to investigate the effect of inflammation on niche succession, the crypt cycle and the expansion of clones in the IBD intestine. Pseudopolyps were examined as potential sites for clonal expansion by determining the frequency of mutated pseudopolyps and proliferative potential, and examining their microRNA (miRNA) profile relative to inactive, active and dysplastic mucosa, and adenoma and cancerous tissue. This thesis will show that crypt fission cycles in inflammatory bowel diseased colon are protracted and that each stage of crypt fission appears to be slow. Overall, clonally related adjacent IBD crypts seem to share a more recent common ancestor than non-related IBD crypts, supporting increased crypt fission rates in IBD. The proliferative drive induced by continuous inflammation and mucosal repair in ulcerative colitis (UC) appears to promote the expansion of CCO-deficient patches. Furthermore, niche succession appears to be faster in active IBD. Pseudopolyps are a source of regeneration within the epithelium and, as shown here, have a faster proliferative drive than background mucosa in IBD patients. Pseudopolyps are not genetically inert and are a potential source of protumourigenic mutations in UC. Hence, pseudopolyps are a potential reservoir within the inflamed epithelium where mutations are harboured and where there is no competition from neighbouring

epithelium, as it has been denuded following previous inflammation. MiRNA expression in pseudopolyps differs from that of UC-dysplasia and mucosa. In particular, the MiR-29 family was downregulated in pseudopolyps, a miRNA family that has been implicated in intestinal fibrosis formation in stricturing Crohn's disease.

Pseudopolyps have been traditionally thought of as benign, genetically inert and incidental findings characteristic of chronic inflammation. My research runs counter to this view indicating an exciting paradigm shift in the way we consider pseudopolyps, which may eventually alter the endoscopic management of these lesions in the future.

ACKNOWLEDGEMENTS

First and foremost my thanks go to Professor Sir Nick Wright who has supported me throughout this incredible journey into the world of science. You have been a source of great inspiration to me and I am so grateful and privileged to have been part of your phenomenal work.

Words cannot express my sincerest gratitude towards Professor Andy Silver, who has been exceptionally supportive, kind and encouraging throughout my studentship. I would not be here without your unremitting support and wisdom.

I would also like to thank Professor Ian Sanderson for his ongoing support and guidance.

I must next thank Dr Manuel Rodriguez-Justo, Professor Roger Feakins and Dr Ibtisam Saeed for all their time and pathology expertise. I would also like to thank Vitor for all his tuition on the LCM technique and Chung-Yin Lee for his incredible knowledge and skill.

My thanks also go to the outstanding medical students, Charlotte, Jonathan and Erin for all their enthusiasm and excellent work with data collection, to Rosemary and Richard for help with *in situ* hybridisation, to Anna for her kind help with tissue collection, and to Amy and Cecilia for their help on the miRNA study.

My brilliant colleagues, Annie, you are my guardian angel, and to the fabulous crew, Bianca, Danielle, Laura, Shahab, Arielle, Anna and Seb I will miss your wonderful conversation and friendship.

To the wonderful Simon, you are a genius, thank you for your guidance. To dear Trevor and Stuart thank you both so much for all your advice, intellectual support and ideas throughout my PhD.

This has been an incredible challenge, but the one I am most proud of in my life to date; and I dedicate this thesis, to my beloved children, Niall and Tamara, my PhD babies, to my fantastic and loving parents and sister Farrah for all their kindness, support and encouragement they have given me, and to the love of my life, my husband Jamie, who has been my rock throughout. What an incredible 4 years.

I acknowledge support from the Bart's and The London Charity and the Medical Research Council for funding my work.

Declaration: I, Noor Jawad confirm that the work presented in my thesis is my own. Where information has been derived from other sources, I confirm that this has been indicated in the thesis.

PUBLICATIONS ARISING FROM THIS THESIS

- **Oral Prize Presentation**

British Society of Gastroenterology-Regional Meeting - Oral Prize Presentation

Pseudopolyps can be linked spatially and temporally with pre-malignancy and colorectal cancer in some cases of inflammatory bowel disease.

Noor Jawad, Charlotte Johnson, Erin Butterworth, Roger Feakins, Ibtisam Saeed, Manuel Rodriguez-Justo, Stuart McDonald, Trevor Graham, Andrew Silver, Nicholas Wright.

Royal College of Physicians, February 2015.

PRIZES

British Society of Gastroenterology's Prize for Best Poster in Category Inflammatory Bowel Disease

Methylation signatures of non-expressed genes reveal insights into the effects of inflammation on stem cell dynamics and crypt fission in inflammatory bowel disease.

N Jawad, T Graham, M Novelli, M Rodriguez-Justo, N Wright, S McDonald

British Society of Gastroenterology 27th June 2013, Glasgow

British Society of Gastroenterology - Regional Meeting - Best Oral Abstract Presentation Prize

Are Pseudopolyps the Source of Tumorigenic Mutations in Ulcerative Colitis?

N Jawad, T Graham, M Novelli, M Rodriguez-Justo, R Feakins, A Silver, N Wright, S McDonald.

Royal College of Physicians, March 2013.

British Society of Gastroenterology Poster Of Distinction

Are Pseudopolyps the Source of Tumorigenic Mutations in Ulcerative Colitis?

N Jawad, T Graham, M Novelli, M Rodriguez-Justo, R Feakins, A Silver, N Wright, S McDonald

Digestive Diseases Federation Liverpool, UK, **19th June 2012**

PROJECTS AND PUBLICATIONS

N Jawad, TA Graham, SAC McDonald, NA Wright.
Clonal Expansion May Explain patterns of Cytochrome c Oxidase Deficiency in Ulcerative Colitis. ***Journal of the National Cancer Institute***, 2014 Feb;106(2).

N Jawad and NA Wright
Stem Cells: A Potential Target in Colorectal Cancer?
Colorectal Cancer. February 2012. Volume1, No 1, Pages 7-9.

Jawad N, Direkze N, Leedham SJ
Inflammatory Bowel Disease and Colon Cancer
Recent Results Cancer Res. 2011; 185-99-115. Review.

Graham TA, **Jawad N**, Wright NA.
Spindles losing their bearings: does disruption of orientation in stem cells predict the onset of cancer?
BioEssays vol **32**, Issue 6, June 2010.

BOOK CHAPTERS

Humphries A, **Jawad N**, Ignjatovic A, East J, Leedham S. Carcinogenesis in Ulcerative Colitis, Ulcerative Colitis from Genetics to Complications, Mustafa M. Shennak (Ed.), ISBN: 978-953-307-853-3, InTech Publishing 2012.

Jawad N, Direkze N, Leedham S 'Inflammatory bowel disease and colon cancer', in '"Inflammation and Cancer: concepts, consequences and clinical management", 2011, Springer publishing. Editor Janusz Jankowski.

ABSTRACTS

N Jawad, J Crook, A-M Baker, B Cereser, M Rodriguez-Justo, T Graham, N Wright, S McDonald.
Determining stem cell and crypt dynamics in inflammatory bowel disease. ***Gut***, June 2014, Vol 63, (Suppl 1): A161-A162.

N Jawad, T Graham, M Novelli, M Rodriguez-Justo, N Wright, S McDonald
Methylation signatures of non-expressed genes reveal insights into the effects of inflammation on stem cell dynamics and crypt fission in inflammatory bowel disease. ***Gut***, June 2013 Vol 62 (Suppl 1):A245.

N Jawad, T Graham, M Novelli, M Rodriguez-Justo, R Feakins, A Silver, N Wright, S McDonald Are Pseudopolyps the Source of Tumorigenic Mutations in Ulcerative Colitis? ***Gut***, June 2012, Vol 61, A236-A236.

List of Figures

List of Tables

CHAPTER 1 GENERAL INTRODUCTION

1.1 Inflammatory bowel disease

Ulcerative colitis (UC) was first described in the medical literature in 1859 (Wilks 1859) and Crohn's disease (CD) first became known as a medical entity following an article published in 1932 by Crohn, Ginsberg and Oppenheimer, and was described as "regional ileitis" (Crohn et al. 1932).

UC and CD, collectively known as inflammatory bowel disease (IBD), are disorders of modern society, and their incidence in developed countries has been rising since the mid-20th century. Currently, UC and CD both have a prevalence of two per 1,000 people in northern Europe, with an incidence of 10 and 6 per 100,000 people per year, respectively, in Western countries (Shivananda et al. 1996). UC is the most common form of IBD worldwide (Danese and Fiocchi 2011).

IBD is thought to be a consequence of incongruous and ongoing activation of the mucosal immune system driven by the presence of normal luminal flora. This process might be assisted by defective barrier function of the intestinal epithelium and the mucosal immune system.

IBD usually presents between the ages of 15 to 30 years of age (Loftus and Sandborn 2002). It is common for UC and CD to be grouped together and diagnosed as IBD, as both conditions can involve the colon and share clinical symptoms and signs. They are characterized by chronic, relapsing and remitting inflammation, affecting the colon in UC or any portion of the gut in CD. However, UC and CD are evidently discrete

pathophysiological entities. UC is a disease of the mucosal lining of the large bowel that involves the rectum (proctitis) and may affect part of the colon, or the entire colon (pancolitis); the inflammation is continuous. UC is less prone to complications, and in some patients, its clinical course is mild. In contrast to CD, UC can be cured by colectomy (Solberg et al. 2009). CD most commonly affects the ileum and colon, yet it can involve any region of the gastro-intestinal tract, from the oral cavity to the anus. In CD the inflammation is frequently transmural, and interrupted. The disease often features intestinal granulomas, which are atypical in UC. CD is often complicated by structuring and fistula formation, which are not seen in UC.

In 1925 the first documented case of a colitis-associated cancer was described by Crohn and Rosenberg (Greenstein 2000). It is now recognized that IBD confers a high risk of development of a number of malignancies especially colorectal cancer (CRC), with a standardised incidence ratio of 2.4 (95% CI 0.6–6.0) in patients with extensive or pan UC. This risk is associated with longer disease duration, an earlier age of onset (Ekbom et al. 1990), the degree of severity of inflammation (Rutter et al. 2004a), and the presence of concomitant inflammatory conditions such as primary sclerosing cholangitis (PSC). This suggests that the acquired cancer risk is a consequence of the inflammatory process, which results in cycles of recurrent ulceration and tissue restitution. It is now accepted that the cancer risk in both CD and UC is approximately the same if similar disease patterns are compared (Gillen et al. 1994), and this is further evidence for inflammation-associated tumorigenesis. Furthermore, the molecular pathways and histopathology of colitis–associated CRC (CACRC) is distinct from that of sporadic CRC (SCRC). This needs careful consideration in order to advance and perfect screening programmes for patients with longstanding IBD.

This chapter will now discuss the intestinal stem cell, the stem cell niche, and how a mutation within a stem cell comes to dominance and fixation, and leads to clonal expansion within the gut potentially forming a dysplastic lesion.

1.2 Carcinogenesis in inflammatory bowel disease: an introduction to stem cells

Cancer is thought to arise from a mutation in a single stem cell. Stem cells possess a unique property of longevity that permits the potential acquisition of multiple tumorigenic mutations, a prerequisite of carcinogenesis.

It is clear that intestinal epithelium is a highly susceptible cancer site, facilitated by the fact that the intestinal epithelium is a rapidly proliferating and perpetually differentiating epithelium. The large number of cell divisions, in order to maintain gut homeostasis, increases the likelihood of accruing genetic mutations by chance. In addition, the gut is exposed constantly to a harsh milieu from potential toxins and carcinogens within digested food, which has particular relevance because of the recent trend towards the consumption of processed foods (Loh et al. 2011).

The intestinal epithelium has a highly organised architecture in the form of crypts, which are dynamic structures with the intestinal stem cells residing in the niche at the base of each crypt (Wright 2000). These stem cells are defined by their ability to self-renew and their potential for multi-lineage differentiation. First coined by Cheng and Leblond, the Unitarian theory (1974) was used to describe the notion (Cheng and Leblond 1974) that all cell types are derived from a single multipotential stem cell through a number of committed progenitors. Stem cells divide and move slowly up from the base of the crypt to become the transit-amplifying cells. As these cells ascend

the crypt to the lumen, the cell divisions rapidly increase in order to produce the committed progenitor cells, which in turn become one of the four characteristic mature intestinal cell types, or terminally differentiated cells that are shed into the lumen within 5- 7 days (Leedham and Wright 2008) (Figure 1.1). These are known as the columnar absorptive cells or enterocytes, the mucus-secreting goblet cells or the endocrine cells (neuroendocrine or enteroendocrine cells), which secrete a variety of peptide hormones in an endocrine or paracrine fashion, and the Paneth cells (Figure 1.2). The latter cell types are predominantly located at the base of the small intestinal crypt. Occasionally, in normal individuals, Paneth cells can also be seen in the ascending colon. The Paneth cells function remains elusive, although they are thought to produce defensins and anti-microbial peptides that, in turn, play an integral part in innate immunity (Salzman et al. 2007). More recently Sato and colleagues demonstrated that Paneth cells are long-lived and, indeed, critical in the maintenance of stem cells within the niche in the small intestine (Sato et al. 2011).

The specialized microenvironment which houses the putative stem cells, the so-called 'niche', is formed by a group of epithelial and mesenchymal cells and extracellular substrates, providing the optimal setting for stem cells to differentiate (Leedham and Wright 2008). A fenestrated sheath of mesenchymal cells or pericryptal fibroblasts regulate stem cell proliferation through paracrine secretion of various signalling factors (Powell et al. 1999). The Wnt-β-catenin pathway is one of these signalling pathways and is paramount in controlling stem cell behaviour. This pathway will be discussed further in sections 1.11 and 1.12.

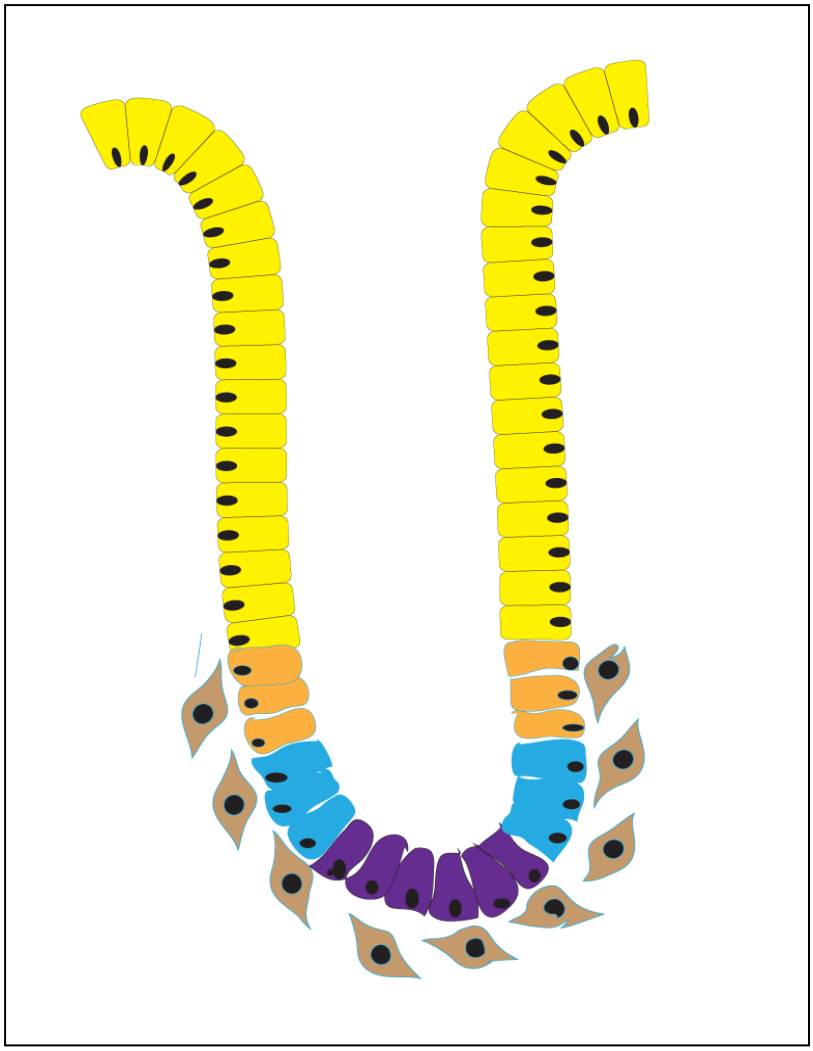

Figure 1.1 The intestinal crypt and stem cell niche. Stem cells reside at the base of the crypt (purple) and are surrounded by myofibroblasts (brown) and, together, comprise the 'niche'. Stem cell divisions produce the transit amplifying cells (blue), which proliferate rapidly. As cells migrate up the crypt they become committed to a lineage, so-called committed progenitor cells (orange) and are terminally differentiated once they reach the top (yellow).

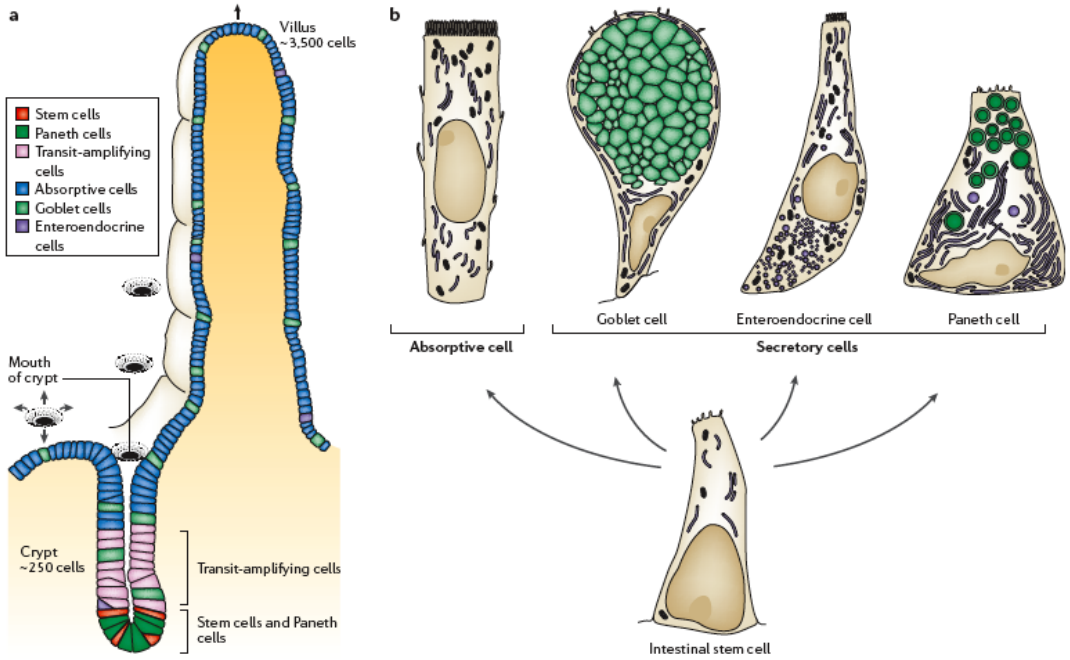

Figure 1.2 Characteristic mature cell types of the intestine. Absorptive cell: enterocytes, simple columnar epithelial cells involved in nutrient and water absorption; glycocalyx surface coat contains digestive enzymes plus secretion of immunoglobulins. Goblet cell: glandular simple columnar epithelial cell; secretion of gel forming mucins, the major component of mucus. Enteroendocrine cell: specialized endocrine cells produce hormones or peptides that act as chemoreceptors, initiating digestion and detecting harmful substances and initiating protective actions. Paneth cell: sense bacteria via MyD88-dependent toll-like receptor activation triggering secretion of antimicrobials: defensins, lysozymes; protects stem cells.

1.2.1 Cancer stem cells

Over 30 years ago the concept of the cancer stem cell (CSC) was first proposed. Only 1 in 1000 to 1 in 5000 of human myeloma tumour cells could form colonies when cultured *in vitro*. The implication was that not all cancer cells boast replicative competence (see Figure 1.3) (Hamburger and Salmon 1977). More recent studies have provided further verification for the existence of CSC. Bonnet and colleagues demonstrated, using a human tumour cell xenotransplantation model, that in immunosuppressed mice (non-obese diabetic/severe-combined immunodeficient mice (NOD/SCID) mice), a subset of leukaemic cells $CD34^{++}/CD38^{-}$ could instigate leukaemic cell growth (Bonnet et al. 1997). Subsequent studies using the same human tumour cell xenotransplantation model have provided further corroborative evidence for the existence of a CSC population. This population has also been demonstrated using primary CRCs, breast, brain, pancreas and prostate cancers (Al-Hajj et al. 2003; Singh et al. 2003; Dalerba et al. 2007; Li et al. 2007; O'Brien et al. 2007; Ricci-Vitiani et al. 2007; Cocciadiferro et al. 2009).

CSCs are proposed to be a population of stem cells within tumours that are capable of propagating the tumour (Wicha et al. 2006). These stem cells act in a similar way to normal organ specific stem cells that maintain homeostasis, yet these cells cause tumour expansion. CSCs are also similar to stem cells in their use of the signaling pathways that are required for persistence (Reya et al. 2001). CSC may be derived from normal stem cells, but with aberrations to the regulatory processes controlling normal stem cell function that allows for consequent cancer formation (Vermeulen et al. 2008). However, this has by no means been proved.

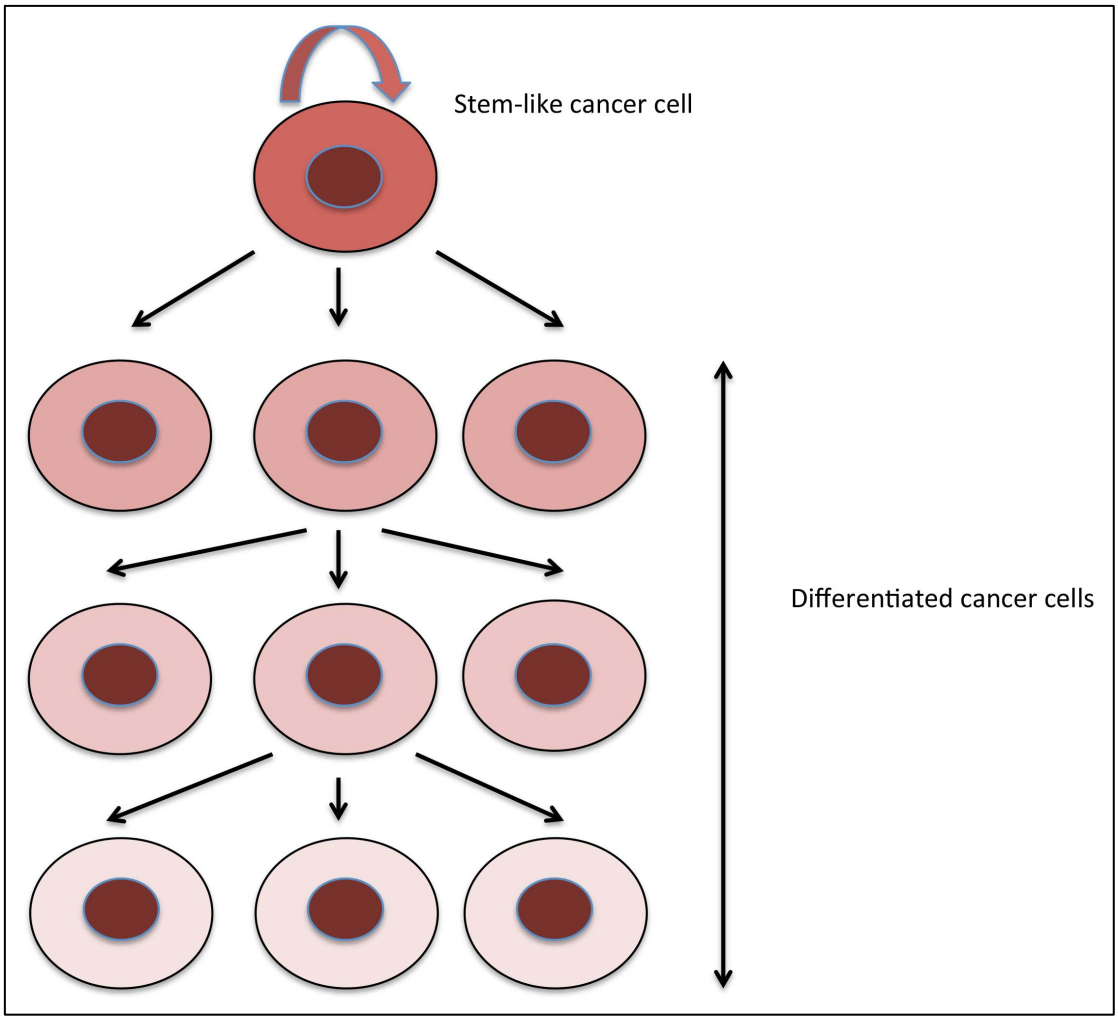

Figure 1.3 Cancer stem cell hypothesis. Only the Cancer Stem Cells (CSC) can accrue the necessary genetic changes to progress to a tumour. The progeny of the CSC are differentiated and are unable to self-renew.

The question why tumour bulk reduction with certain chemotherapeutic agents does not always equate to increased patient survival may be due to the differential survival of this CSC population (Visvader and Lindeman 2012). Unsuccessful eradication of such a potent cell population will consequently lead to cancer recurrence.

1.2.2 The identification of cancer stem cells

Using flow cytometric analysis demonstrated that the putative CRC initiating cells expressed the surface molecule CD133(O'Brien et al. 2007; Ricci-Vitiani et al. 2007). Further supportive evidence came from single-cell cloning studies, which showed that 1 in 16 $CD133^{+}$ cells were able to produce tumour spheroids (Vermeulen et al. 2008). Furthermore, a single cell could initiate tumour formation *in vivo*. However, CD133 may not be relevant to all tumours, as it appears to be tumour specific. In addition, CD133 has been challenged as a marker in gastrointestinal cancers. Shmelkov and colleagues demonstrated that CD133 expression was not exclusively present on intestinal stem or cancer-initiating cells. Furthermore, in metastases, $CD133^{+}$ tumour cells could give rise to the more aggressive sub-population, which are $CD133^{-}$. The $CD133^{-}$ population were also competent tumour-initiators in NOD/SCID mice (Shmelkov et al. 2008).

Alternative colon CSC markers have been proposed. Dalerba and colleagues identified the epithelial cell adhesion molecule (EpCAM) and the expression of antigen, $CD44^{+}$ and CD166 ($EpCAM^{high}$,/$CD44^{+}$/$CD166^{+}$) as surface markers of cancer-initiating cells, as exemplified by their tumourigenic potential in transplantation experiments (Dalerba et al. 2007). CD166 is associated with a poor clinical outcome in colon cancer, but how robust these molecules are as individual

markers of CSCs is debatable. However, this combination of markers appears more impressive, as $CD44^+$ cells can be seen in $CD133^-$ cancer cell populations (Dalerba et al. 2007). CSCs are thought to be rare, but recent work by Quintana and colleagues indicate that in malignant melanoma they may be numerous (Quintana et al. 2008). However, this result may be because they used a more immunologically deprived mouse, which highlights a potential fault line in the CSC hypothesis: so-called CSCs are those cells which can survive in the harsh immunological milieu of the mouse, even in those animals engineered with a compromised immune system.

Novel research data has emerged in support of the controversial proposal that solid tumours are not accumulations of equivalent cells, but alternatively contain cancer stem cells that sustain tumour preservation. Three independent studies of murine models of brain, skin and intestinal tumours deliver primary evidence that CSCs do exist and arise *de novo* during neoplastic development in intact organs (Chen et al., 2012; Driessens et al. 2012; Schepers et al. 2012). Using permanent *in vivo* fluorescent labeling of stem cells and their progeny, so-called lineage tracing, intestinal stem cells that give rise to various cell types that make up intestinal epithelial tissue in mice has been demonstrated (Barker et al. 2009). The same group showed that deletion of the *APC* gene led to the formation of intestinal adenomas.

Schepers and co-workers utilized lineage-tracing to verify whether the murine intestinal tumours were sustained by CSCs (Schepers et al. 2012). This study involved knocking out *Apc* in murine intestinal stem cells using the multicolour Cre-reporter R26R-Confetti mouse model. Here, the cells stochastically assumed one of four fluorescent tagging colours when the mice were administered a low dose of tamoxifen

to conditionally knock-out (KO) *Apc* in the gut. The first dose frequently led to 'clonal' adenomas, which were single-colour, signifying that they originated from single intestinal stem cells. Curiously, a further tamoxifen dose converted the colour of individual cells in the adenomas and the progeny of these newly coloured cells populated the tumour. These included differentiated tumour cells. This identified the parent cells as CSCs (Schepers et al. 2012) (Figure 1.4).

Further corroborative evidence for CSCs comes from a murine model of a benign skin tumour, a papilloma (Driessens et al. 2012). Lineage tracing of individual papilloma cells revealed that only 20% of cells are able to divide into daughter cells that populated large areas of the tumour. These studies gave sophisticated evidence of stem-cell activity in intact benign tumours. Driessens et al then went on to examine cell hierarchies maintained by CSCs in invasive malignant tumours using a mouse model of squamous cell skin cancer (Driessens et al. 2012). The malignant tumours comprised much larger numbers of long term replicating cancer cells that demonstrated only modest evidence of cell differentiation. This raises the question as to whether cancers deviate as they progress from being benign to malignant from a hierarchical organization into relative chaos (Figure 1.4).

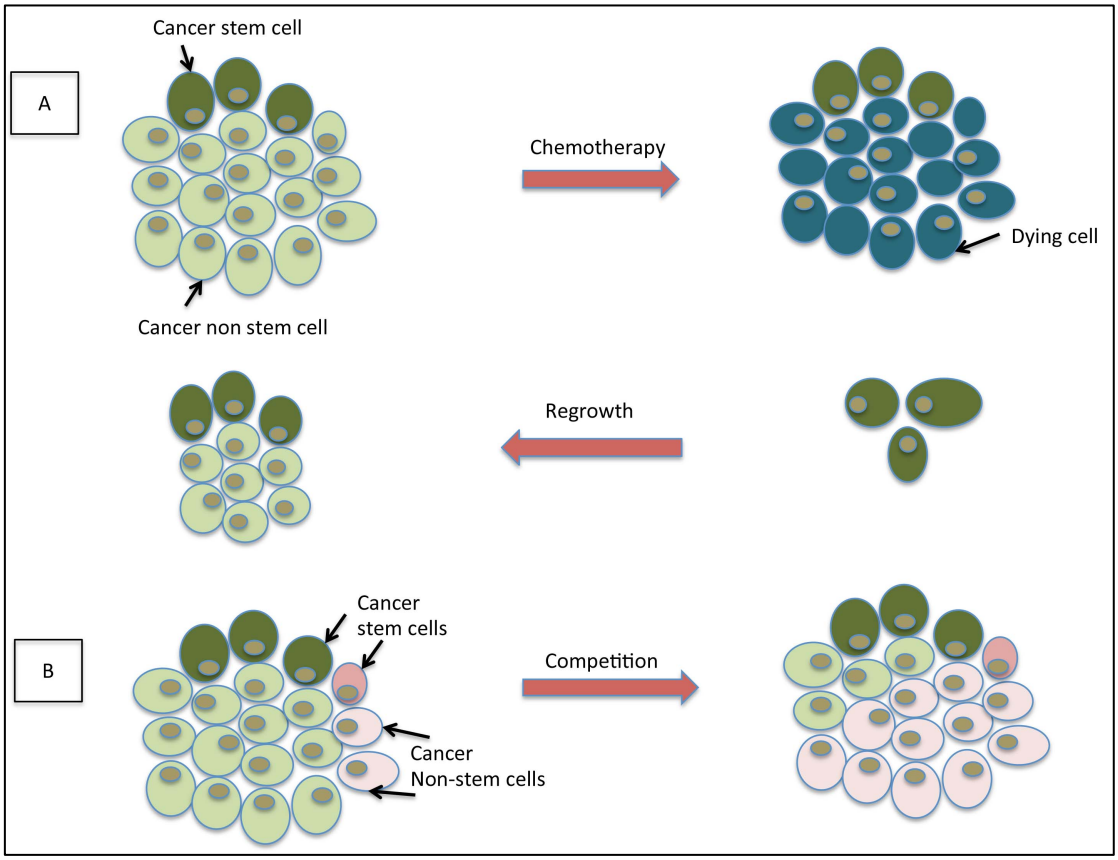

Figure 1.4 Not all tumour cells are equal. Brain, skin and intestinal tumours include CSCs that are capable of self-renewal and give rise to other, more-differentiated (non-stem) cells that comprise the majority of the tumour-cell population, as demonstrated by (Chen et al. 2012; Driessens et al. 2012; Schepers et al. 2012). **A.** Chemotherapeutic agents can destroy the bulk of the dividing non-stem cells, yet the surviving CSCs can repopulate the tumour. Thus, by focussing therapy on both CSCs and the diving cells, this would permit entire tumour eradication. **B.** Pink and green cells indicate different clonal populations, each one primarily derived from an individual CSC. CSCs constantly compete with each other for a position in the tumour to ensure their daughter cells prevail (Driessens et al. 2012).

Chen and colleagues produced further convincing data that malignant tumours comprise CSCs (Chen et al. 2012). Using a model of murine brain tumours (glioblastomas), they demonstrated elegantly that CSCs repopulated the cancer after chemotherapeutic agents removed the bulk of the tumour. By targeting both the CSCs and their daughter cells with an amalgamation of 'suicide-gene' technology that selectively kill glioblastoma CSCs and chemotherapeutic agents that eliminate the bulk of the dividing cancer cells, the study showed the inhibition of glioblastoma growth *in vivo* (Figure 1.4) (Chen et al. 2012). Whilst the work reported using mouse models epitomises a significant new era in the CSC debate, future work will need to include studies on how well mouse CSCs reiterate their human equivalents, and whether model systems can be used to evaluate future treatments prior to use in humans.

1.2.3 Cancer stem cells as a useful therapeutic target

The prospect of selectively targeting the CSC population is extremely attractive. Many chemotherapeutic agents successfully debulk tumours, but ultimately this can result in tumour recurrence since these therapies fail to target the CSC population. To selectively target the maintenance pathways and the microenvironment that drive and support these CSCs would be a potential therapeutic approach. One example of a key maintenance pathway is the Notch/Delta signalling pathway, which is crucial in the maintenance of stem cell homeostasis (Bigas and Espinosa, 2012). This pathway is considered vital for maintenance of the stem cell and for retaining the stem cells in their undifferentiated state. *In vivo* experiments within the mouse intestine have shown that conditional ablation of the Notch pathway results in the entire loss of the proliferative zone, with transit amplifying cells rapidly differentiating (Bigas and

Espinosa 2012). This was also seen in cells within murine adenomas (van Es 2005). Conversely, when Fre and colleagues conducted *in vivo* experiments to strongly activate Notch signalling, the proliferative zone grew and there were very few cells that had differentiated phenotypes (Fre et al. 2005). Promising data from *in vivo* experiments in colon cancer have shown that γ-secretase inhibitors can inhibit activated Notch signalling. Van Es and colleagues used the $Apc^{min/+}$ mouse model to show that with γ-secretase inhibitor administration there was a marked differentiation of immature proliferative adenomatous cells into terminally differentiated goblet cells (van Es 2005).

Other experiments have offered exciting therapeutic potential. For example, Todaro and co-workers observed that a subgroup of $CD133^{+}$ colon CSCs were safeguarded from apoptotic events stimulated by chemotherapy agents by producing IL-4 (Todaro et al. 2007). Thus, the use of IL-4 inhibitors as a treatment for colon cancer is promising.

1.2.4 Cancer stem cells: conclusions

The CSC hypothesis remains surrounded by many controversies. There is considerable evidence for their existence, across a range of tumour types, yet a major stumbling block has been the ongoing challenge of achieving successful isolation of the putative stem cell sub-population from their natural milieu. This is a necessary first step before we gain the ability to control their behaviour. However, there has been impressive progress in our quest to identify and characterise the intestinal stem cell, so perhaps the search to accurately define the CSC sub-population is not too far in the future.

The CSC theory, if correct, has significant clinical and therapeutic implications. The use of chemotherapy may well be streamlined in the future by sub-typing tumours to identify the putative stem cell population driving tumour expansion. In the meantime, we need to move away from methods that employ *in vitro* and xenotransplantation methods for studying CSC behaviour to those that allow the monitoring of their expansion and growth in primary tumours.

Inherent to the CSC hypothesis is that after malignant transformation a larger fraction of stem cell divisions will be for self-renewal, which in turn promotes adenoma growth. Winton's lab in 2013 demonstrated that this process was wholly ineffective (Kozar et al. 2013). The bulk of self-renewing divisions serve to replace stem cells lost from the adenoma either due to commitment or cell death. This results in clones populating intratumoural zones maintained by a common stem cell pool (Kozar et al. 2013). This would support the notion that the majority of tumour stem cells are primed for displacement and ultimate extinction and that medical therapies enhancing this predilection could shape the foundations for novel drug therapies.

1.3 Inflammation and the stem cell niche

The effect of inflammation on the mammalian intestinal niche is an area of great interest. There is no hard evidence for a direct effect of inflammation on the stem cell niche. However, from a histopathological perspective, IBD has a characteristic microscopic finding of an inflammatory mucosal infiltrate, from which activated mesenchymal myofibroblasts and infiltrating leucocytes secrete various morphogens, pro-inflammatory cytokines and growth factors, which can influence the surrounding stem cell niche (Powell et al. 1999).

In the context of IBD, one potential mechanism by which inflammation may drive tumorigenesis is through an affect on the surrounding stem cell niche. Corroborative evidence for this comes from a study, which demonstrated in the Drosophila intestine that mucosal inflammation increased stem cell proliferation via dysregulation of the evolutionary conserved Hippo (Hpo) signaling pathway (Ren et al. 2010). Further substantive evidence comes from the fact that numerous human cancers have disruption of the Hpo pathway (Harvey et al. 2013). Importantly, disruption of the Hpo pathway suggests one possible mechanism whereby inflammation may be driving tumourigenesis in IBD through a direct effect on the stem cell niche.

The next section will explore the transition of a single stem cell to an autonomous mutated clone.

1.4 Crypt fission and clonal expansion

How does a single mutation within a stem cell cause cellular expansion to form a tumour? How a cancer can arise from one mutation in a stem cell can be explained by examining stem cell dynamics within the normal colonic crypt unit. The niche located at the crypt base is thought to house a few clonally related stem cells, a number that is closely regulated (Williams et al. 1992; Campbell et al. 1996; Yatabe et al. 2001; Barker et al. 2007). A single stem cell and its progeny can stochastically expand via a process termed niche succession (Figure 1.5). Subsequently, all the progeny of that stem cell lineage take over the crypt, and this is known as monoclonal conversion (Yatabe et al. 2001). This progression is believed to be gradual; the estimated

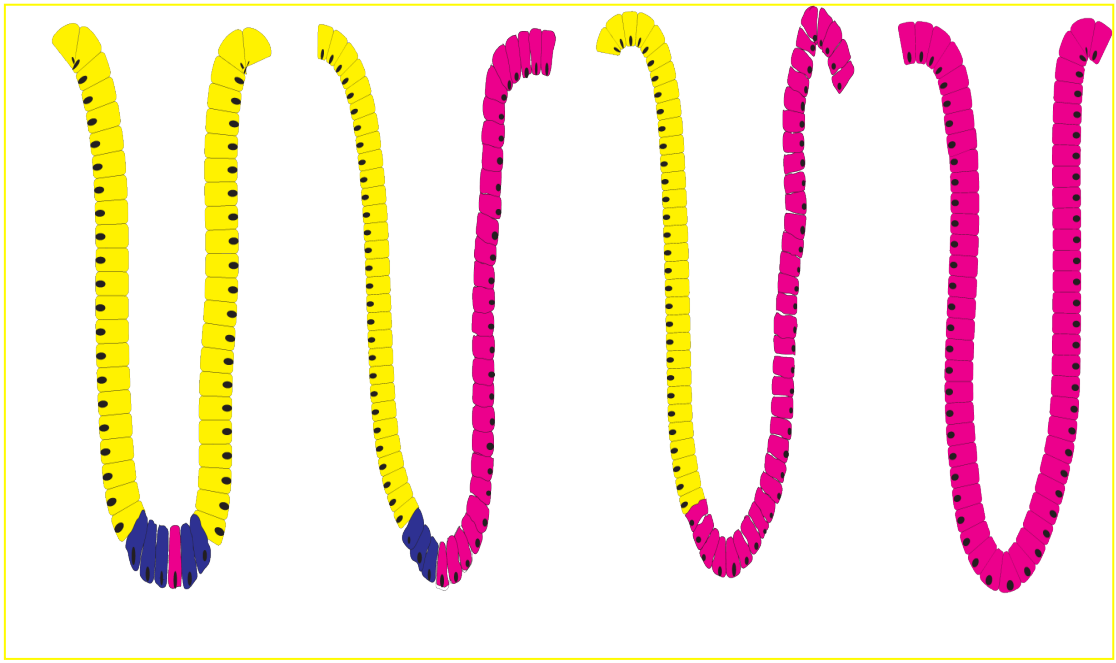

Figure 1.5 Niche succession and monoclonal conversion. Stem cells reside at the base of the crypt (blue cells); a mutated stem cell (highlighted in pink) within the niche is able to expand via niche succession. Subsequently, all the progeny of that stem cell lineage take over the crypt – monoclonal conversion.

incidence of sequential niche succession phases in the normal human colon being every 8-9 years (Graham et al. 2011). During infancy and childhood and, indeed, following inflammatory insults to the intestinal epithelium, the normal intestine needs a system to allow growth and restoration of intestinal crypts. Crypt fission is a process by which a single parent crypt bifurcates into two daughter crypts, permitting epithelial regeneration. In the healthy colon this is believed to be a slow process, although in the diseased bowel this expansion has the potential to be accelerated. Inflammation, or indeed, an oncogenic mutation in a stem cell which possesses a selective advantage, could represent prospective up-regulation of the regeneration process. It is by this process of crypt fission that a dysplastic lesion is said to occur (Park et al. 1995; Wong et al. 2002; Greaves et al. 2006).

It has been well documented that crypt fission is the mechanism behind the expansion and spread of individual crypts, not only in the colon (Greaves et al. 2006), but throughout the entire gastrointestinal tract, the small intestine (Gutierrez-Gonzalez and Wright 2008) and the stomach (McDonald et al. 2008). It is probable that this is the method governing clonal expansion in CACRC. In the context of IBD and a chronic inflammatory milieu, a flaw in the normal inhibitory pathways regulating stem cell proliferation could lead to a potentially oncogenic mutation acquiring a selective advantage. This mutant clone could accrue further deleterious mutations as it rapidly expands via niche succession and crypt fission. Crypt fission is a well-documented histological trait in colitis and dysplasia (Park et al. 1995; Wong et al. 2002). One study of a UC patient used fluorescent *in-situ* hybridization to exhibit the spread of *TP53* mutations in the daughter crypts of a crypt in the process of fission in UC (Chen et al. 2005).

1.4.1 Paradigms of tumorigenesis in the intestinal epithelium.

There are two schools of thought regarding the development of spontaneous adenomatous lesions and both share the notion that a founder mutation within a stem cell in the colonic crypt expands. However there are distinct differences in the two models (Figure 1.6).

In the 'bottom up' hypothesis expansion of a mutated stem cell at the crypt base, whether it is a stochastic mutation or one that possesses a selective advantage, results in the formation of an adenomatous clone (Figure 1.6). Consequently, the dysplastic cells come to occupy the whole crypt leading to a clonal monocryptal adenoma (Novelli et al. 1996). Wong et al. (2002) showed that in the histogenesis of colorectal adenomas, hyperplastic colonic polyps and IBD the percentage of crypts in fission, the so-called, 'crypt fission index', was up-regulated (Wong et al. 2002).

The contrasting models centre on the theory that the mutated stem cells are distributed in-between crypt orifices, the intracryptal zone. The dysplastic tissue is thought to expand laterally and downwards into the adjacent crypts; the so-called 'top down' hypothesis (Figure 1.6). It has been postulated that once the stem cells have been mutated, they then migrate to the intracryptal zone, and then undergo adenomatous spread (Wright 2000). Certainly this has been observed in large adenomas. Indeed, it may be that a combination of the two models occurs, with the bottom up mechanism forming a monocryptal adenoma and the top down model permitting the formation of larger adenomas via lateral spread into adjacent crypts (Brittan and Wright 2004; Giannakis et al. 2006).

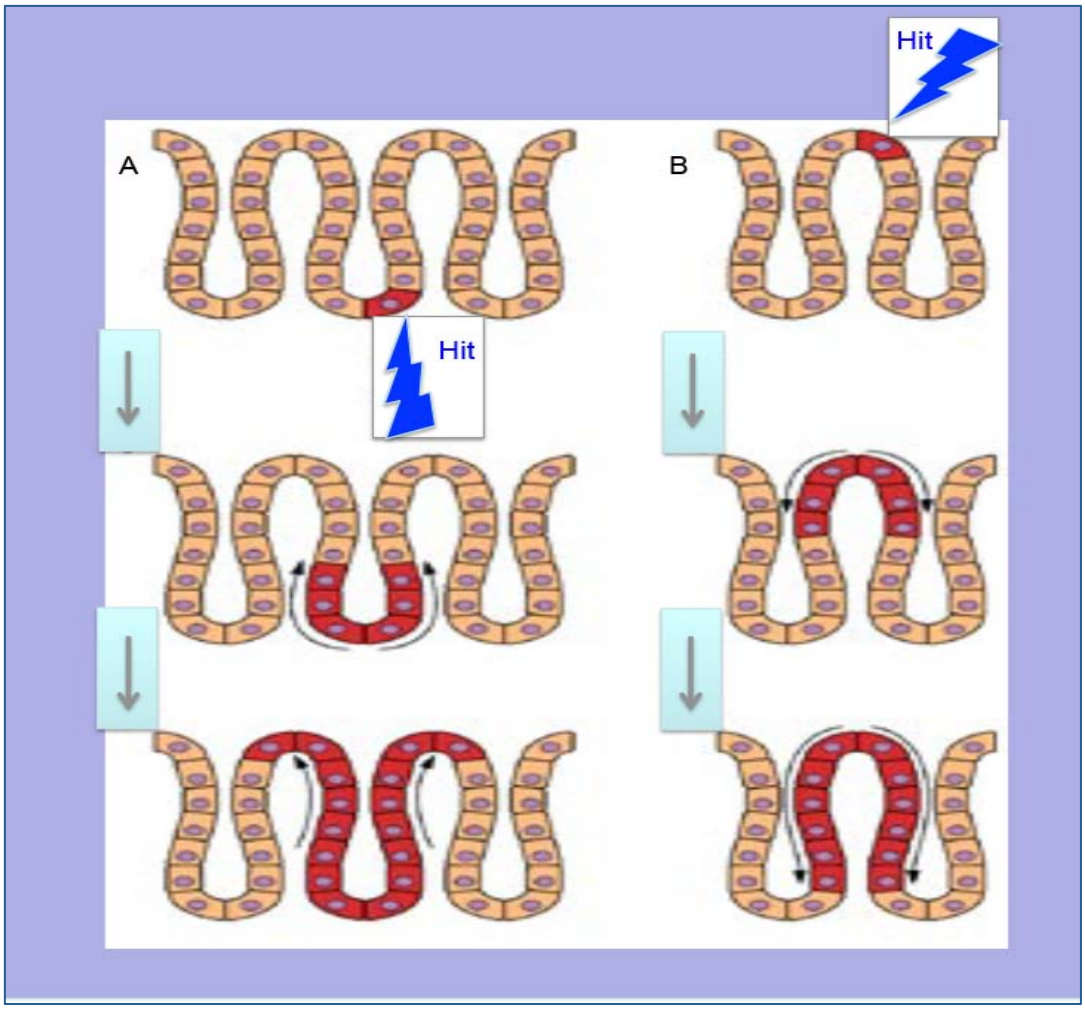

Figure 1.6 Schematic of the 'top-down' and 'bottom-up' models of adenoma histogenesis in the colonic crypt. Red cells denoted those carrying mutation(s). Arrows indicate direction of spread.

1.5 Comparison of carcinogenesis pathways in sporadic and colitis-associated colorectal cancer

SCRC and CACRC are thought to be distinct disease entities. This comes from genetic, histopathological, and functional evidence. There are several distinguishing clinical features apparent when comparing CACRC to SCRC. Firstly, CACRC arises in a younger patient population, often from flat, not polyploid, dysplasia and has a more proximal distribution. Furthermore, there is a greater frequency of mucinous or signet cell histology and a higher incidence of multiple synchronous lesions (Itzkowitz and Yio 2004). From a histological perspective, sporadic tumours tend to follow the adenoma-carcinoma sequence (Vogelstein et al. 1988), whereas CACRC progresses from no dysplasia to indefinite dysplasia, usually through low (LGD) and high-grade dysplasia (HGD) to carcinoma. The stepwise accumulation of genetic mutations in onco- and tumour suppressor genes that underpins the SCRC carcinogenesis pathway is well established (Vogelstein et al. 1988) and has significantly altered worldwide clinical practice. For example, mutations in *KRAS* appear to have importance as predictive factors for lack of response to certain oncological therapies. Activating *KRAS* mutations, which are identified in approximately 40 to 45% of CRCs, are associated with resistance to treatments that target the epidermal growth factor receptor (EGFR), such as cetuximab and panitumumab (Allegra et al. 2009). The CACRC carcinogenesis pathway is less explored and significantly differs in the requirement and timing of genetic and epigenetic alterations.

1.6 Control of cell proliferation in the intestinal crypt: canonical Wnt signalling in sporadic and colitis-associated colorectal cancer

Cell proliferation in the intestinal crypt is under the control of a large family of secreted glycoproteins known as Wnts. They are expressed in numerous species from *Drosphila* to man, and comprise a minimum of 19 known members in humans (Anastas and Moon 2013). Wnt signalling is an essential regulator of homeostasis in the intestinal epithelium with many functions including regulating epithelial cell proliferation and confinement, secretory lineage expansion, conservation of the stem cell phenotype and Paneth cell maturation (Scoville et al. 2008; Anastas and Moon, 2013). One fundamental function of Wnt signalling is to serve as the principal proliferative driver in the injured epithelium permitting intestinal epithelial restitution.

A significant element of the canonical Wnt pathway is a protein termed Adenomatous Polyposis Coli *(*APC*)*, which is responsible for the control of the transcription factor β-catenin (CTNNB1). In normal growth (absence of Wnt signalling) intracellular β-catenin undergoes serial serine phosphorylation by an APC destruction complex and degradation via the ubiquitin-proteasome pathway. This results in low levels of cytosolic β-catenin. Hence, truncation or deficit of APC disturbs the β-catenin degradation complex. This leads subsequently to stabilised β-catenin translocating into the nucleus leading to upregulation of Wnt target gene expression, a process responsible for cellular proliferation (Bienz and Clevers 2000; Sieber et al. 2000).

In CACRC *APC* mutations are found relatively infrequently, approximately 3-6% of cases (Tarmin et al. 1995; Aust et al. 2002). In contrast, somatic *APC* mutations are the initiating gate-keeping mutations in SCRC (Kinzler and Vogelstein 1996), which

are observed in over half of sporadic adenomas (Powell et al. 1992) and 80% of carcinomas (Miyoshi et al. 1992). In 2003 Preston and colleagues corroborated this fact by observing that many adenomas exhibited abnormal nuclear β-catenin expression when examined by immunohistochemical staining (Preston et al. 2003). β-catenin is mutated in sporadic CRC but much less frequently than *APC*.

1.7 Alternative activation of the Wnt pathway in mucosal healing

It has been suggested that an alternative, inflammation-induced mechanism of β-catenin stabilisation is responsible for Wnt activation in colitis (Boland et al. 2005). Wnt is upregulated in epithelial regeneration with upregulated expression of ligands and CMYC and other Wnt target genes (You et al. 2008). Paradoxically activation of Wnt by *APC* or β-catenin mutation is seen infrequently in CACRC. In dextran sulfate sodium (DSS) induced mouse models of colitis knock-out of *DKK-1*, a Wnt antagonist, precludes the initiation of colitis and advances epithelial restoration; activation of Wnt via R-spondin also deters the initiation of DSS induced colitis and enhances recovery (Zhao et al. 2007).

Lee and colleagues showed that phosphorylation of β-catenin at moiety serine 552 occurs with the *PI3* kinase/Akt pathways (Lee et al. 2010). *PI3K* phosphorylation leads to nuclear translocation and target gene activation. This mechanism effectively bypasses the destruction complex and explains why *APC* mutation is rarely selected for in CACRC.

In an acute inflammatory setting, Wnt signalling is paramount in tissue healing, however chronic inflammation causing Wnt activation can be tumourigenic (Ashton et

al. 2006). The pathways for inflammation and tumorigenesis can coincide. Possible tumorigeneic drivers in chronic intestinal inflammation are the potential feedback loops between Wnt target genes and *PI3K*-mediated Wnt activation. This was demonstrated in a mouse model by conditionally deleting focal adhesion kinase *(FAK)*, a downstream c-Myc target (Ashton et al. 2006). Following insult, the murine intestine could not be restored, yet on *FAK* obliteration, induced tumorigenesis following loss of *APC* was abolished. This was via downregulation of phosoph-Akt levels, which indicated that *FAK* is a downstream target of Wnt signalling and upstream of *P13K/Akt/mTor* activation. Following *APC* loss, *FAK* facilitates not only intestinal regeneration, but also tumour transformation.

The next section will micro-dissect the adenoma-carcinoma sequence in sporadic colon cancer and contrast to the colitis-associated colorectal cancer pathway.

1.8 Genetic instability

1.8.1 Chromosomal instability

In sporadic cancer carcinogenesis, chromosomal instability (CIN) leading to aneuploidy, detectable by both image and flow cytometry, is rare in established precursor lesions before the development of high-grade dysplasia or cancer (Sieber et al. 2000). Yet, in UC, CIN can be detected in histologically non-dysplastic tissue from high-risk patients (extensive inflammatory disease distribution and long duration of disease), by comparative genomic hybridization (Willenbucher et al. 1997), image (Keller et al. 2001) or flow cytometry; CIN is thought to precede the development of dysplasia in these patients (Rubin et al. 1992; Befrits et al. 1994). It has been

suggested that CIN occurs as a consequence of the effect of inflammation and reactive oxygen species encouraging telomere shortening thereby permitting chromosomal end fusion. This shortening results in cycles of chromatin bridge breakage and fusion, promoting the accumulation of chromosomal aberrations (O'Sullivan et al. 2002). Indeed, it has been demonstrated that premature telomere length shortening and increased DNA damage occurs as a consequence of chronic inflammation in UC patients compared to age-matched normal control individuals (Risques et al. 2008). A mutator phenotype ensues as a result of this damage propagating mutations (Loeb and Loeb, 1999) and eventually causing a 'field' defect, whereby localized regions within the colon have accrued the same mutation(s) or other genomic alterations (Salk et al. 2009).

A recent study by Lai et al. 2012 used bacterial artificial chromosome arrays to examine genomic instability along the length of the UC colon (Lai et al. 2012). The authors demonstrated that genomic instability increased with disease progression and biopsies more proximal to dysplastic areas had increased instability. Smaller changes (<1Mb) in field copy number (gain or loss) were especially seen in UC 'progressor' patients who had dysplasia or cancer. Larger gains or losses in chromosomal copy numbers were largely restricted to dysplastic biopsies (Lai et al. 2012). This data supports the study by Greaves and colleagues in which the mean patch size of CCO deficient crypts increased with age (Greaves et al. 2006). Thus, not only does chronic inflammation and mutator phenotype contribute to the large field defects, but perhaps also due to premature aging of the UC colon, in which a 30 year old UC patient's colon is more analogous to the colon of a 60 to 70 year old without UC.

1.8.2 Initiating genetic mutations

In SCRC, mutations in *APC* are found in about 60% of sporadic adenomas and 80% of carcinomas (Powell et al. 1992) and are gate-keeping, initiating mutations (Kinzler and Vogelstein 1996). It is clear that the inflammation and restitution processes that underly IBD select for alternative initiating genetic mutations in CACRC (Figure 1.7). A recent clonal ordering study determining the spatial distribution of shared mutations in UC-associated neoplasia allowed insight into the timing of genetic mutations (Leedham et al. 2009). *TP53* was the most common single founding mutation with *KRAS* mutations as the only other detected unique gate-keeping mutation (Figure 1.7). *APC* mutations were uncommon suggesting that *APC* is unlikely to have a gatekeeper function in colitis-induced neoplasia. This is consistent with other work. Point mutations in the *TP53* gene can be detected in non-dysplastic tissue from patients with UC preceding the development of aneuploidy and loss of heterozygosity (LOH), and appear to be linked to the presence of inflammation (Brentnall et al. 1994; Hussain et al. 2000). Additionally, LOH for *TP53* correlates with malignant progression, occurring in 6% of non-dysplastic biopsies, 33% of LGD, 63% of HGD and 85% of cancers (Burmer et al. 1992). The mutation spectrum in *TP53* is dominated by transition mutations (Yin et al. 1993; Hussain et al. 2000; Yoshida et al. 2003), and this is likely to reflect the effect of the inflammatory process causing oxidative DNA damage and deamination of 5-methylcytosine, promoting G:C to A:T transitions (Hussain et al. 2000; Seril et al. 2003). It is simple to comprehend why *TP53* may act as an initiating mutation in colitis. If underlying chromosomal instability throughout the colon were the main tumourigenic driving force in colitis (Chen et al. 2005), early *TP53* would be selected for on the basis that disruption of a mitotic checkpoint would permit the survival and selection of clones with gross chromosomal changes.

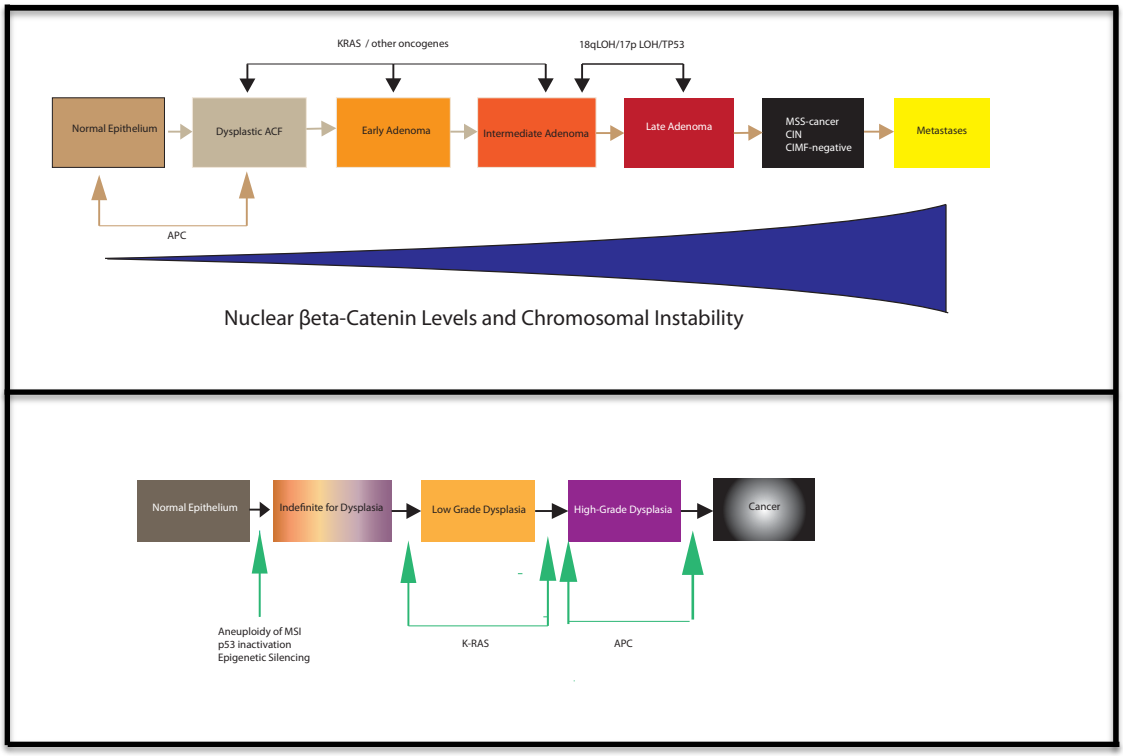

Figure 1.7 Comparison of colitis associated and sporadic colorectal cancer pathways. Upper panel, sporadic colorectal cancer pathway; bottom panel, colitis associated colorectal cancer pathway. Both types of cancer show multistep development with sequential mutation in tumour suppressor and oncogenes. The main differences between the pathways are in the timing of these mutations. Abbreviations: *APC*, Adenomatous Polyposis Coli; DCC, Deleted in Colon Cancer; LOH, loss of heterozygosity; MSI, Microsatellite instability.

There is further compelling evidence to show that *p53* mutant clones have an increased prospect of becoming fixated in an inflamed gut (Vermeulen et al. 2013). This is likely due to the advantageous power of *p53*-mutated cells in handling colitis-associated reactive oxygen species production. This was demonstrated in a mouse model of chronic colitis using DSS, given a week prior to clone induction, and sustained until examination of clone size distributions. Colitis triggers an alteration in stem cell dynamics in the colon, predominantly through lowering the replacement rate. The particular mutation that was used was the dominant-negative hotspot mutation $P53^{R172H}$, and whilst it bestowed no advantage to colon stem cells under normal conditions, in the colitic gut it considerably improved cell fitness. Broadly speaking, this demonstrates that the competitive advantage of mutations arising during the formation of cancer alters depending on the milieu in which they occur.

It is well established that cancer arises in cells accumulating genetic abnormalities, which bestow a benefit on a clone of cells over surrounding cells. Vermeulen and colleagues recently investigated using models of intestinal tumour initiation how oncogenic mutations can confer an advantage on a clone harbouring such mutations by their action on stem cell dynamics (Vermeulen et al. 2013). Murine studies have shown that cancer occurs following an initial transformation event occurring principally, but not solely in the stem cell compartment (Barker et al. 2009; Schwitalla et al. 2013). It is known that normal intestinal crypt homeostasis is typified by competition between equipotent stem cells that constantly replace each other stochastically (Snippert et al. 2010; Lopez-Garcia et al. 2010). To enable lineage tracing of WT and mutated cell lineages low-level intestinal recombination, either

specifically in the crypt base using *Lgr5*-EGFP-Cre^{ER} mice or more commonly *Ah*Cre^{ER} mice (both crossed to R26-Lox-STOP-Lox-*tdTomato* (tdTom$^{fl/fl}$) reporter strain) was used (Snippert et al. 2010; Lopez-Garcia et al. 2010). Clones were observed and quantified at the crypt base permitting robust clone size quantification around the circumference of the crypt. Their findings corroborated other previous studies showing that constant rudimentary neutral replacements dominated intestinal stem dynamics in murine small and large intestine (Lopez-Garcia et al. 2010; Snippert et al. 2010). A previous notion that a large proportion of *Lgr5*$^{+}$ cells are in fact more committed progenitor cells and do not function as stem cells in homeostasis was confirmed (Buczacki et al. 2013). Their findings also indicate that mutations such as *Apc* loss and *Kras* activation do not govern the outcome, and many mutated stem cells are replaced by wild type stem cells following biased but still random events.

1.9 Alternative and Serrated pathways

There has been considerable research into genetic pathways to CRC since Vogelstein's original proposal and the discovery of the alternative and serrated pathways. *KRAS* or *BRAF* oncogenic mutations, activation of the mitogen activated protein kinase pathways, in conjunction with acquired MSI and methylation of promoter CpG sites in multiple genes (CpG island methylator phenotype – CIMP), have been found to be pivotal pathways in the evolution of colorectal cancer. They are independent of *APC* mutation (Jass 2002; Leggett and Whitehall 2010) (Figure 1.8). Within the promoter regions of a gene panel associated with carcinogenesis *(p16*, *MLH1*, *MINT1*, *MINT2*, *MINT31*, *RUNX3, CACNA1G, IGF2, NEUROG1, SOCS1*), CIMP denotes specific, age independent methylation of a number of CpG islands (Samowitz et al. 2005; Weisenberger et al. 2006).

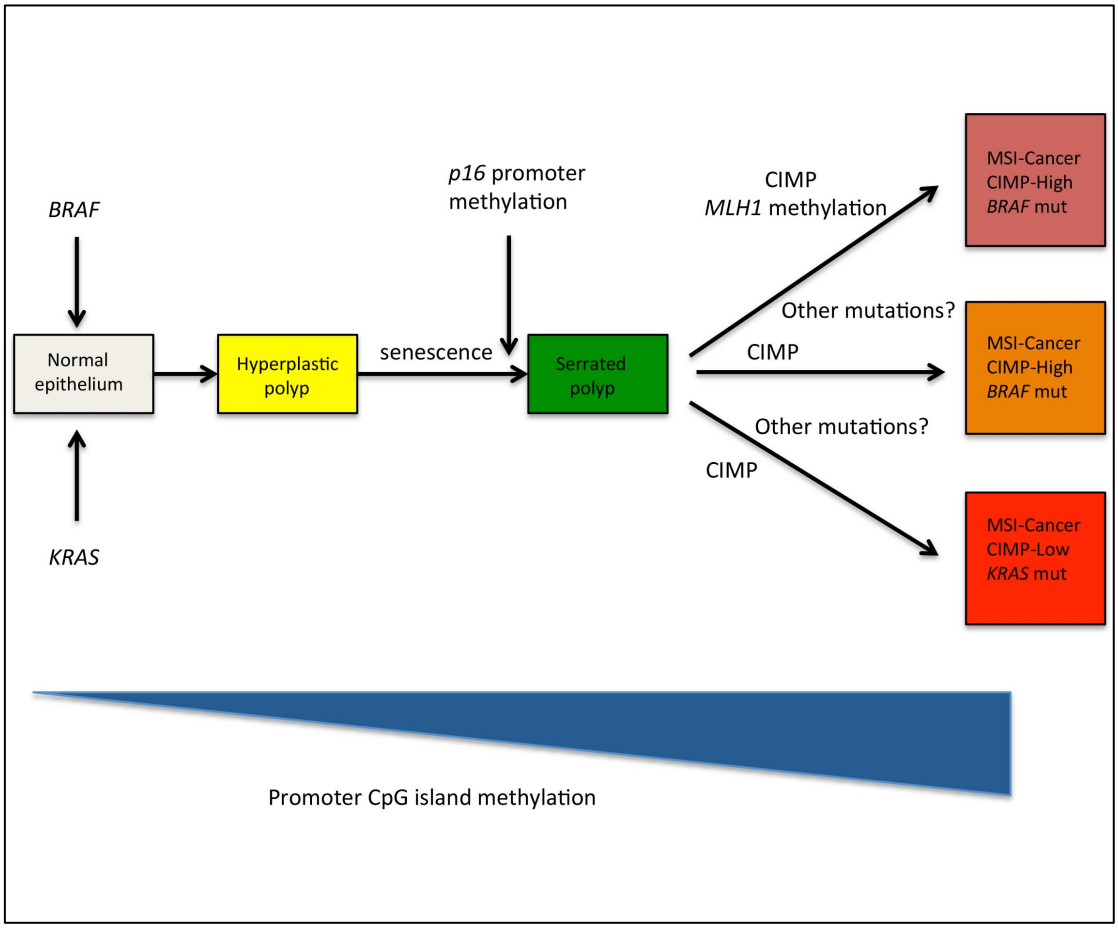

Figure 1.8 Alternative and serrated pathways to colorectal cancer: *BRAF* or *KRAS* mutations lead to a proliferative drive that is followed by *p16*-induced senescence. The increase in CIMP permits escape and advancement to serrated polyps. *BRAF* mutations are associated with a high level of CIMP and MSI cancers, whereas *KRAS* mutant lesions tend to be CIMP-low and MSS. This is a simplification of the main pathways, and there is overlap between the two, with many other oncogenes and tumour suppressor genes likely involved that remain to be completely clarified. Abbreviations: MSS microsatellite stable; MSI microsatellite instability; CIN chromosomal instability; CIMP CpG island methylator phenotype.

Thus commonly, lesions are categorised as CIMP-negative, CIMP-low (one or two CpG islands are methylated), or CIMP-high (3 or more of the gene panel are methylated). Indeed, a discrete subgroup of CRCs has been identified which are CIMP-high. They are usually located in the proximal colon, are poorly differentiated, *TP53* wild-type and are highly associated with *BRAF* mutations and MSI (Curtin et al. 2011; Weisenberger et al. 2006; Ang 2010).

A universal characteristic of serrated polyps is a *saw-toothed* infolding of the epithelium. In the past, these lesions were categorised into another subgroup along with hyperplastic polyps and, importantly, believed to carry no malignant potential. Yet, it is now well recognised that a strong association exists between serrated polyps, in particular, sessile serrated adenomas, and sporadic MSI colorectal cancer. Indeed it has been demonstrated that cancers can specifically arise from adjacent serrated polyps with a transition zone of dysplasia (Snover 2005). Most commonly *BRAF* mutations are believed to be the initiating events in the *serrated pathway*, although *KRAS* mutations can also initiate this pathway, although they are mutually exclusive (O'Brien 2006). The second event is *p16* induced senescence, and methylation with the early development of CIMP. Later progression of the lesions is associated with MSI (O'Brien 2006; Leggett 2010) (Figure 1.8).

Almost all *BRAF* mutations are a result of a single point mutation (V600E). This leads to constitutive activation of the MAPK pathway downstream of *KRAS.* Despite *BRAF* mutations being extremely common in serrated polyps, they are seldom seen in conventional adenomas (Kambara 2004). Conversely there is a distinct link between

the development of CIMP and MSI in colorectal cancers (Kambara 2004; Wiesenberger 2006).

In conclusion, there are numerous genetic pathways implicated in colorectal carcinogenesis. In early adenomas the initiating genetic events still remain as *APC* and *KRAS* mutations, yet alternative pathways have been identified, pertaining to the histology and location of the colonic lesion. Indeed, Fearon and Vogelstein deduced that '*it is the accumulation of events, rather than their order of occurrence with respect to one another, that is likely to be most important in colorectal tumor progression'* (Fearon and Vogelstein 1990). It is currently believed that the critical factor in determining whether a lesion will progress to cancer is the actual timing of genetic events (Fodde et al. 2001; Leggett et al. 2010).

1.10 Mutator phenotype versus clonal expansion

Multiple aneuploidy detection techniques have shown that gross chromosomal changes occur in non-dysplastic tissue in UC. Chen and colleagues used arbitrarily-primed (AP)-PCR and inter-simple-sequence repeat (ISSR)-PCR genetic fingerprinting techniques to further analyse genomic instability in colitis (Chen et al. 2005). The identification of DNA fingerprint abnormalities throughout normal and dysplastic areas of the colon allowed the subdivision of patients with IBD into UC progressors: patients with identifiable genomic instability who are likely to progress to dysplasia or cancer, and UC non-progressors, patients with normal DNA fingerprints who do not (Chen et al. 2003). The authors proposed that this colon-wide genomic instability in UC progressors provides a field from which dysplasia develops, and is evidence of a mutator phenotype where mutations in genes maintaining genetic

stability result in an increased mutation rate driving colitis-associated tumourigenesis (Loeb and Loeb 1999; Chen et al. 2003; Chen et al. 2005). This is a controversial subject and proponents of an evolutionary theory of carcinogenesis argue that the mutator phenotype theory underestimates the power of natural selection (Bodmer 1999; Tomlinson and Bodmer 1999). The recent identification of colitis-associated neoplasia clonality with *TP53* as the commonest initiating mutation (Leedham et al. 2009) lends weight to a Darwinian model where natural selection and clonal expansion are the dominant forces driving CACRC evolution - the somatic mutation theory of carcinogenesis. Thus, CACRC appears to follow the somatic mutation theory of carcinogenesis, where initial mutations in key target genes introduce a selective growth advantage to a cell and then the forces of natural selection and evolution act to expand this clone — a so called *selective sweep* (Maley et al. 2004). When a mutation has spread through an entire population it is said to have gone to fixation, as there are no longer any competing alleles. Further mutations within this clone can then cause expansion producing regional selective sweeps and clonal diversity.

Clonal ordering studies utilise the spatial distribution of shared mutations within various areas of dysplasia and cancer to make inferences about the timing of mutations and selective sweeps. A recent clonal ordering study of colitis-associated lesions identified *TP53* as the most common single founding mutation, with *KRAS* mutations the only other detected unique gate-keeping mutation (Leedham et al. 2009). Not only is mutated *TP53* frequently observed in colitis-associated lesions, but also the frequency of both point mutations and 17qLOH correlates with malignant progression (Burmer et al. 1992; Brentnall et al. 1994; Hussain et al. 2000). It is relatively

straightforward to comprehend the high frequency of initiating *TP53* mutations in colitis, certainly from an evolutionary standpoint. There would be a strong selective pressure for *TP53* mutation in predysplastic lesions surrounded by chronic inflammation, with chromosomal instability a consequence of inactivation of this protein through disruption of mitotic checkpoints. The survival of stem cells with gross chromosomal changes would then be permitted.

The close association between the cell cycle and DNA repair suggests that a number of genes involved in the cellular response to DNA damage, such as *TP53,* may have a two-fold responsibility in controlling DNA repair and growth. Consequently, mutations in these genes may provide both a selective growth advantage and an increased mutation rate driving selection and the mutator phenotype simultaneously. However, evolutionary geneticists argue that the mutator phenotype component is a coincidental by-product of direct selection of mutation of these genes for their anti-apoptotic effects (Bodmer et al. 2008). The debate continues.

Recently, it has become evident that the stroma may play a pivotal role in tumourigenesis (Alspach et al. 2014). There is a symbiotic relationship between stromal and epithelial cancer cells (Mueller and Fusenig 2004). Stromal cells produce growth and angiogenic factors to support the tumour cells. Indeed, Karnoub and co-workers showed that mesenchymal stem cells within tumour stroma promote breast cancer metastasis (Karnoub et al. 2007).

1.11 Field cancerisation and the importance of clonality and passenger mutations in early cancer

It is well recognised that cancer occurs as a result of a natural selection phenomenon in cells carrying somatic mutations that confer a proliferative benefit. Only a minority of the thousands of mutations within a tumour will actually serve to promote tumour growth. Most of the mutations are simple passengers with insignificant importance. However, any mutation can be used as a surrogate label to mark a cell's clonal progenies. With this technique, it is possible to detect the aberrant proliferative signature of pre-malignant tissue and discern the development of clonal cancers. Clearly the possibility of early cancer diagnostics in the future with the ability to detect anomalous cells as a prelude to macro- and microscopic dysplasia has significant potential.

The prospect of detecting aberrant genetic changes before cancer growth begins is an extremely attractive one and very attainable. There is an overwhelming and ever-increasing amount of data to suggest that areas of tissue or 'fields' of tissue can display pro-tumourigenic mutations, which are, in themselves, of minimal biological influence, morphologically speaking, but possess certain characteristics which confer a predilection for subsequent neoplastic growth. This was coined 'field cancerisation', after it was proposed by Slaughter et al. back in 1953 to explain the presence of multifocal head and neck cancers developing out of a field of precancerous change that had developed following carcinogen exposure (Slaughter et al. 1953). Coinciding with the arrival of high end molecular techniques came an expansion of this theory. Braakhuis and colleagues (Braakhuis et al. 2003) proposed that the field was actually a clonally expanded area of mutated cells, and, by definition, pre-neoplastic.

Microscopically, the tissue may be normal, hyperplastic or indeed dysplastic.

There is ever increasing evidence to support field cancerisation in IBD and indeed in IBD associated cancers. For example, metachronous tumours are seen in almost a third of all Crohn's patients (Gyde et al. 1980; Connell et al. 1994). The continual cycle of mucosal damage and repair characteristic of IBD presents a palpable stimulus for crypt growth. UC tumours have been shown to arise in fields of cells with short telomeres (O'Sullivan et al. 2002). Furthermore, Garrity-Park and colleagues presented data recently to show that IBD-associated tumours often display identical anomalous methylated loci as neighbouring and disparate non-cancerous mucosa (Garrity-Park et al. 2010).

Clonally expanded mutated patches have been documented previously in dysplastic and phenotypically normal mucosa of colitis patients (Lyda et al. 1998; Lyda et al. 2000). Leedham and associates identified field cancerisation in one patient when they demonstrated that three left-sided tumours and some of the intervening chronically inflamed but phenotypically non-dysplastic mucosa shared the same founder mutation (Leedham et al. 2009). This suggested widespread clonal expansion of a progenitor clone from which the three spatially independent tumours arose. Niche succession and crypt fission are likely to be the mechanisms behind clonal expansion in CACRC. Symmetrical division of individual crypt stem cells results in the extinction or amplification of one cell lineage (Kim and Shibata 2002). This process will occur faster if the mutation provides a growth advantage. Crypt fission is responsible for the spread of individual clones into daughter crypts in the colon (Greaves et al. 2006) and this process is a histological feature of colitis and dysplasia (Park et al. 1995). Chen

and colleagues used a fluorescent *in-situ* hybridisation technique to demonstrate the spread of *TP53* mutations into the daughter crypts of a crypt in the process of fission in UC (Chen et al. 2005). Furthermore, in UC, diverse *TP53* mutations have been identified in disparate areas of the bowel. Single *TP53* mutated clones were seen in cancer (Yoshida et al. 2003). Furthermore, several groups reported that in UC patients, examination of non-cancerous tissue revealed that cells was commonly aneuploid or chromosomally unstable (CIN). This was extrapolative to cancer risk (Melville et al. 1989; Levine et al. 1991; Burmer et al. 1992; Chen et al. 2003).

Further corroborative evidence for field cancerisation in IBD comes from a recent study from Galandiuk and co-workers (Galandiuk et al. 2012). This work demonstrated elegantly that extensive field cancerisation occurs in the chronically inflamed large bowel of some patients with CD (Galandiuk et al. 2012). In seven of 10 patients, mutations found in the tumour mucosa could also be detected in non-tumour mucosa, suggesting a clonal relationship between these tissues. Examination of the longitudinal samples revealed evidence of extensive growth of pre-tumour clones in non-dysplastic epithelium several years prior to the development of neoplasia; in one case mutations in the *TP53*, *p16* and *KRAS* genes were present in the same non-dysplastic crypts. In a second patient, a *p53* mutant clone was focally detected in the sigmoid colon, and then 4 years later was detected throughout the entire length of the patient's colon. This mass expansion of a mutant clone over a considerable distance over a very short period of time was quite remarkable, perhaps drawing attention to potential need for close follow up of pre-tumour clones. A possible mechanism to explain this overwhelming clonal migration could be through elevated crypt fission rates which have been noted in inflamed tissue (Cheng et al.

1986).

So can mutational burden in IBD crypts act as predictive factors of future development of carcinoma? In the same study by Galandiuk, a 65 year old male with pancolonic CD and perianal fistulation since the age of 37 developed a well-differentiated mucinous adenocarcinoma in a perineal proctectomy scar that was resected. The tumour contained an exon 7 *TP53* mutation at c.733G>A, a *KRAS* mutation at c.37G>A and a *p16* mutation at c.238C>T, and the nearby non-dysplastic crypts in the inflamed resection margin contained the same mutations. This would indicate field cancerization. Remarkably, the same three mutations were also detected in a proctectomy specimen collected 4 years earlier. Analysis of a nearby perianal fistula tract in the earlier proctectomy specimen detected the identical *KRAS* c.37G>A mutation, although there was a different *TP53* mutation present and no *p16* mutation was found (Galandiuk et al. 2012). This is compelling evidence indicating that *KRAS* c.37G>A was the initial pretumour mutation in this patient. The second *TP53* mutation could not be identified in subsequent samples suggesting that the clone had perhaps become extinct. In addition, this patient had a further *KRAS* mutation in an early small bowel biopsy; yet it had disappeared 2 years later implying that clonal extinction had occurred. Thus, the colonic crypts bear a considerable mutational burden, in this case mutations in two tumour suppressor genes and an oncogene. This illustrates the complex correlation between key clonal mutations and the dysplastic phenotype, and that it is not possible to delineate the genotype that is associated specifically with dysplasia. In early FAP adenomas, for example, single mutations can induce dysplastic changes (Lamlum et al. 2000). However, in the case examined by Galandiuk and colleagues the mutational burden is considerable and associated

with a non-dysplastic phenotype. Mutations in tumour suppressor genes such as *TP53* have been noted in non-dysplastic mucosa before (Brentnall et al. 1994), although not in association with other mutations. This explains the extensive dispersion of pre-tumourigenic clones in non-cancerous tissue. Non-dysplastic crypts concealing tumourigenic clones highlights the controversial fact that dysplastic tissue could be a capricious cancer risk indicator.

Clonal expansion is a potential tool to predict cancer risk in UC patients. Alterations in the number of base-pair repeats at mutable polyguanine tracts can act as a surrogate clonal marker (Salk et al. 2009). Salk and associates demonstrated that UC patients with cancer had evidence of clonal expansion across non-neoplastic mucosa whilst UC patients without cancer did not have evidence of clonal expansion. This supports the notion that in IBD pre-tumour clones can prognosticate tumour occurrence.

The evidence for field cancerisation in IBD has a number of clinical implications, raising questions about the use of molecular genetic analysis of non-dysplastic tissue in high-risk cancer patients to detect fields from which future tumours may arise. On the other hand, an important concern is that despite endoscopic resection of visible dysplastic lesions preventing tumour progression in that lesion, fields of clonally expanded genetically mutant, but non-dysplastic, crypts, may well be left behind.

1.12 DNA methylation

CpG island hypermethylation often starts in normal mucosa as a function of age and is markedly increased in cancer (Issa et al. 2001) (Figure 1.9). Such silencing is clonal

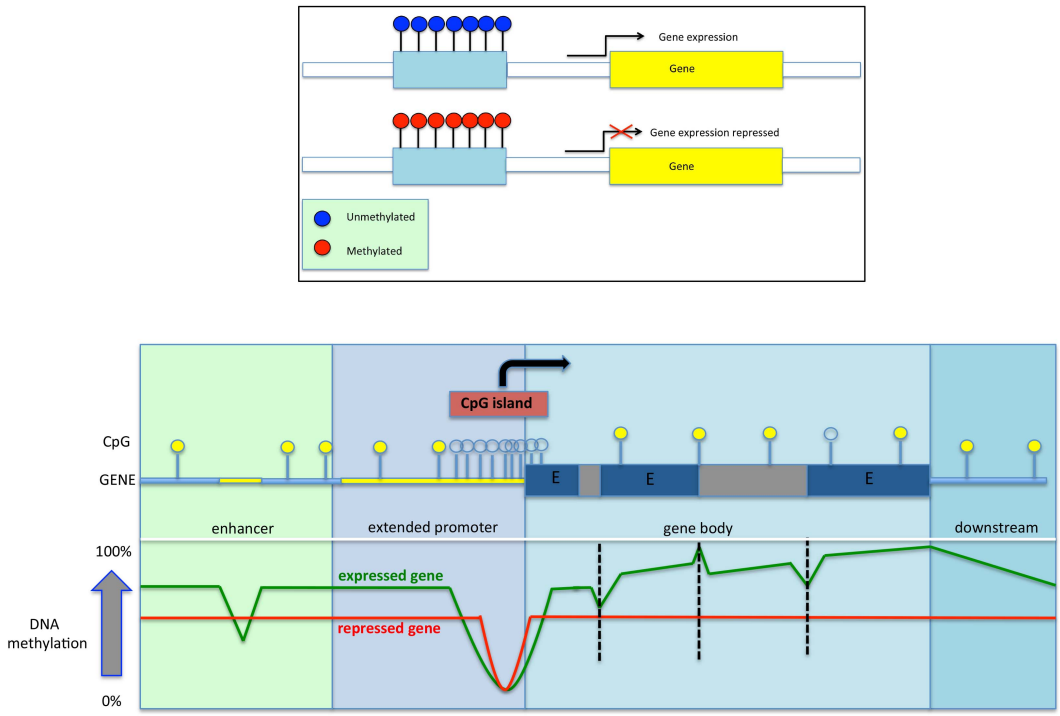

Figure 1.9 Mechanism of methylation. Methylation causes suppression of gene expression. Blue circles represent unmethylated regions of DNA, Red circles represent methylated regions of DNA.

and thought to be physiologically irreversible in somatic cells. Neoplastic cells often display aberrant promoter region methylation with epigenetic silencing of multiple genes including genes that regulate critical processes such as cell cycle control, DNA repair, and angiogenesis (Kulis and Esteller 2010). In the colon, CpG islands methylated in cancer have been divided into two groups: those that display cancer restricted methylation (type C), and those that are methylated initially in aging normal epithelial cells (type A) (Issa et al. 2001). It has been proposed that age-related methylation contributes to an acquired predisposition to colorectal neoplasia because methylation alters the physiology of aging cells and tissues (Issa et al. 2001; Kulis and Esteller 2010). This hypothesis predicts that higher levels of age related methylation are associated with a heightened susceptibility to developing CRC, and it may be present in conditions of rapid cell turnover that mimic premature aging such as IBD.

1.13 Stem cells – longevity and multipotency

There is much deliberation on the exact location of the stem cell niche, and the number of stem cells located within that niche, and indeed over the stem cell dynamics within the niche. Most of the existing evidence comes from small intestinal murine labelling experiments using somatic mutagens or chimeric mice, in which one strain carries a recognizable marker. This is due to the technical limitations of using human tissue.

It was a study by Williams and associates in 1992 (Williams et al. 1992) that supported the notion that multiple stem cells are housed within a niche rather than a single stem cell as first assumed (Winton et al. 1990). Using a mutagen-induced loss of the X-linked enzyme glucose-6-phosphate dehydrogenase (G6PD) in crypt cells,

they were able to mark cells. They compared the time-course of mutated phenotypes in both the small and large intestine of mice. A large number of partially mutated crypts were seen, quickly following administration of the mutagen. With time there was a rapid growth of wholly mutated crypts that plateaued at the same time that partially mutated crypts became extinct. The time taken for the appearance of wholly mutated crypts in the large intestine was approximately 4 weeks, but 21 weeks in the small intestine. Williams and colleagues deduced that these findings corroborated the idea that a number of stem cells reside in the niche, and that this number varies depending on the small or large intestine (Williams et al. 1992). More stem cells might be housed in the small intestinal crypt niche to account for the contrast in time differences. The hypothesis that the intestinal crypt is maintained by a stem cell niche, housing multiple related stem cells, has since been supported by further studies in both the mouse and human (Bjerknes and Cheng 1999; Yatabe et al. 2001; Barker et al. 2007; Sangiorgi and Capecchi 2008).

To clearly identify stem cells morphologically versus other cells within the crypt is unachievable. Early attempts were based on the assumption that stem cells were essentially quiescent, and could be recognised by long-term retention of DNA labels (Potten 1978; Potten et al. 2002). However, this may not be the case (Potten et al. 1992). Researchers then pursued markers positioned in the crypt base, including Musashi 1, an RNA-binding protein believed to be involved in asymmetrical cell divisions during Drosophila neural development, and *DCK1*, a calmodulin dependent protein kinase (Nishimura et al. 2003; Potten et al. 2003; Dekaney et al. 2005). The limited evidence for these as stem cell markers was based on the detection of a small number of cells in the reputed stem cell position at the crypt base labelled with such

markers. Lineage labeling has not yet been demonstrated with these markers (Nishimura et al. 2003; Potten et al. 2003; Dekaney et al. 2005).

Clevers then went on to describe, in a seminal paper, leucine-rich-repeat-containing G-protein-coupled receptor 5 (*Gpr49* or *Lgr5*) an intestinal Wnt target gene, found to be solely expressed in the crypt base (Barker et al. 2007). Barker and colleagues demonstrated that within the small intestinal crypt, amidst the basal Paneth cells, *Lgr5* expression was restricted to 6-8 columnar based cells (CBCs), and several CBCs at the crypt base. This finding was in concordance with Leblond and colleagues so called "stem cell zone" model proposed back in 1974 (Cheng and Leblond 1974). This was in contrast to the "+4 position model" previously described by Potten in 1974 and in 1997, in which they had identified, using DNA-label retention studies, the stem cell niche in the small intestine as being above the basal Paneth cells, around cell position +4 (Potten et al. 1974; Potten and Booth 1997).

A very crucial experiment then followed: the use of a mouse model with an inducible *Lgr5-Cre* knock in allele and an inducible Rosa26-lacZ reporter demonstrated that *Lgr5* positive columnar cells at the crypt base demonstrated multipotency over a 60-day period. Namely, all epithelial lineages could be created, and all exhibited lineage labelling (Sato et al. 2009). Sato and colleagues (Sato 2009) demonstrated that they could develop unequal, self-propagating, crypt-villus like constructs containing stem and Paneth cells within the base of the crypt. This was achieved by simply using a laminin matrigel, several growth signals, and murine small intestinal stem cells. The same group more recently demonstrated, via murine studies, the potential role of the Paneth cell in stem cell maintenance within the niche microenvironment (Sato et al.

2011). They demonstrated that small intestinal Paneth cells and basal Paneth-like cells in the mouse colon produced Wnt and other niche signals crucial for the maintenance of intestinal stem cells within their niche, hence probing the role of the peri-cryptal myofibroblast in stem cell maintenance. This raises the question to what degree does the niche milieu control stem cell maintenance. Indeed, it may well be predetermined genetically by the stem cells themselves via their respective differential responses to peripheral signalling pathways, such as Wnt.

A further study used polycomb ring finger oncogene (*BMI1*) as a lineage marker. *BMI1* encodes a chromatin remodeling protein of the polycomb group and was initially described as the protein product of an oncogene implicated in the induction of leukaemias. *BMI1* main role is involvement in the self-renewal of hematopoietic and neural stem cells (Baylin et al. 1998; Bea et al. 2001; Kim and Morshead 2003). *BMI1* appears to reliably mark long-lived cell clones (>12 months) populated by all intestinal lineages and serves as a specific marker of a cell population located at the +4 position of the crypt. This was demonstrated using an inducible Cre recombinant mouse, under the control of the *Bmi1* locus, and crossing with a mouse strain with the inducible Rosa26-LacZ reporter. Twenty hours after tamoxifen injection, *BMI-1*$^{+}$ cells appeared four cells up from the crypt base in some of the proximal small intestinal crypts of the mice progeny (Sangiorgi and Capecchi 2008). What is more, ablation of *BMI-1*$^{+}$ cells by targeted expression of the diphtheria toxin resulted in crypt loss (van der Flier et al. 2009). However, *BMI-1* is not expressed in the colon and is only seen in 10% of small gastrointestinal crypts in mouse models (van der Flier et al. 2009). Thus the integrity of *BMI-1* as a *bone fide* stem cell candidate marker is questionable.

Montgomery and colleagues have identified a subpopulation of slowly cycling intestinal stem cells marked by mouse telomerase reverse transcriptase (*mTert*) expression that could contribute to all differentiated intestinal cell types as well as the *Lgr5*$^{+}$ cell population (Montgomery et al. 2011). *mTert*-expressing cells were found to distribute in a pattern along the crypt–villus axis analogous to long-term label-retaining cells (LRCs) and were impervious to tissue injury following irradiation (Montgomery et al. 2011). Lineage-tracing studies demonstrated that *mTert*$^{+}$ cells not only could give rise to all differentiated intestinal cell types, but they persisted long term, and could contribute to the regenerative response following injury. Consistent with other highly regenerative tissues, their results further demonstrated that a slowly cycling stem cell population exists within the intestine (Montgomery et al. 2011).

There have been various debates regarding the exact identity of the stem cells that maintain the intestinal epithelium: is it the *Lgr5*$^{+}$ intercalated cells at the crypt base or the supra-Paneth cells that express markers such as *Hopx*? Both Itzkovitz et al. (2012) and Munoz et al. (2012) have homed in on the overlap in expression between the two populations, implying that *Lgr5* expression defines all putative stem cell populations and cell locations. Confirming that only 30-50% of the lower crypt population serve as the genuine stem cells may indicate that such cells necessitate the expression of other factors in addition to *Lgr5*, or that division within the population may suggest that only a fraction truly achieve stem cell status.

Potten and colleagues in 1997 and 1998 carried out an array of experiments to exploit the sensitivity of stem cells to radiation to alter crypt stem cell population numbers to varying degrees (Cai et al. 1997; Potten and Booth 1997; Potten and Grant 1998).

Potten and colleagues calculated the number of apoptotic cells and the number of crypts actively being renewed, to allow an approximation of the quantity and position of the clonogenic cells within the crypt (Cai et al. 1997; Potten and Booth 1997; Potten and Grant 1998). Their estimations led to the assumption that within each murine small intestinal crypt, there were approximately 300-450 cells with 4-6 ultimate-lineage ancestor stem cells in the +4 position, above the Paneth cells. A tiered crypt stem cell structure was suggested. Namely, that there were two levels of transit-amplifying cells situated above the antecedent stem cell, which maintained clonogenic stem cell properties and were capable of self-renewal, in addition to having the ability to repopulate the crypt epithelium and regenerate the lower tier stem cells if the lower cells are damaged. In the large intestine the results were generally similar but a differing regional distribution of the putative stem cell niche was observed (Cai, 1997; Potten 1997; Potten 1998). It was estimated that between 5-36 clonogenic cells existed within the colon and this estimate was dependent on the irradiation dosage administered. The greatest numbers of apoptotic cells were identified at the crypt base, within the transverse colon and rectum in 10 strains of mice (Cai 1997; Potten 1997; Potten 1998). The caecum was comparable to the small intestine. Hence, there seems to be considerable variance in apoptotic cell numbers between the small intestine and the proximal and distal colon. The groups of Barker in 2007, and Sangiorgi in 2008, identified in the mouse small intestine contradictory stem cell sites and, indeed, stem cell activity (Barker et al. 2007; Sangiorgi and Capecchi 2008). This could be explained by overlapping sub-populations of stem cells distinguished by the particular stem cell markers utilised.

These papers resulted in a paradigm shift in our understanding of the intestinal stem cell: that they are *actively* cycling and have a doubling time of approximately once every 24 hours. This contradicted the theory that stem cells were necessarily slow cycling and that this helped to protect them from replicative DNA errors. Hence, the study of the monoclonal conversion process allowed for the identification of stem cells, their niches, and for the study of lineage tracing in the gut.

1.14 Stem cell dynamics

There is an entrenched dogma that intestinal crypt stem cells divide asymmetrically, where each division results in the production of one stem cell and one daughter cell. The daughter cells would become a transit amplifying (TA) cell and eventually become terminally differentiated (Yamashita and Fuller 2005). This was logical as it supported the immortal strand hypothesis put forward by John Cairns in 1975 that stated that stem cells retained a template DNA strand and always passed on the copy strand to the daughter cell therefore protecting the genome of the stem cell (Cairns 1975). More recently, evidence from the mouse points to stem cell homeostasis within the intestinal niche exhibiting what is termed *population asymmetry* (Lopez-Garcia et al. 2010; Snippert et al. 2010; Simons and Clevers 2011), whereby stem cells are either lost or gained via symmetrical divisions on an equal basis in order to maintain homoestasis and a constant stem cell population. However, Snippert and colleagues carried out fate mapping of individual stem cells by generating a multicolour Cre-reporter mouse model. Short- and long-term clonal tracing data of individual *Lgr5*^{hi} cells were collected (Snippert et al. 2010). These disclosed that most *Lgr5*^{hi} cell divisions occur symmetrically. In addition, a further study demonstrated that due to niche constraints on space and number there was neutral competition between stem

cells resulting in clones expanding and diminishing arbitrarily, pending one lineage coming to dominance within the niche (Lopez-Garcia et al. 2010). Furthermore, the rate of stem cell replacement was equivalent to the cell division rate, implying that neutral drift and symmetrical cell divisions are crucial to stem cell homeostasis. Thus, the regulation of stem cells is extremely adaptable to the dynamic environment, allowing any stem cell to be in prime position to differentiate into a number of cell types and replace neighbouring stem cells as necessary (Lopez-Garcia et al. 2010).

1.15 Intestinal crypts are clonal populations

The theory that adult crypts are monoclonal and contain cell populations ultimately derived from a single multipotential stem cell is well documented. We have discussed how *niche succession* with subsequent *monoclonal conversion* is inherent to the dynamics of a stem cell niche. We will now consider the Unitarian hypothesis (Cheng and Leblond, 1974), that all cells are derived from a single multipotential stem cell through a number of committed progenitors. This hypothesis has been examined, most frequently, by the use of chimeric mice, in which one strain has a demonstrable marker. This technique is known as lineage labelling and has shown that all cell types within intestinal crypts are clonal populations. However, studying the dynamics of human colonic stem cells using invasive labelling studies is unfeasible. However, naturally occurring mutations have provided an alternative. The first human study involved a mutation in the gene coding for the enzyme O-acetyl transferase (OAT), which is accountable for the O-acetylation of sialic acid in goblet cell mucus. It is thought that only 9% of the human population is homozygous ($OAT^{-/-}$) - such that only mutated goblet cells stain positively with mild periodic acid-Schiff reagent (mPAS). Heterozygoytes ($OAT^{+/-}$) make up 42%, and will only stain positive if the

remaining allele receives a 'hit'. Once the second hit occurs, the crypt undergoes monoclonal conversion; hence, initially there is only partial crypt staining which then becomes homogeneous (Fuller et al. 1990). Irradiation results in an increase in the percentage of fully stained crypts; this number also increases with age. The 'clonal stabilisation time' – the time taken for an entire crypt to become clonal, is thought to be one year in humans (Campbell et al. 1996).

The rare autosomal dominant condition familial adenomatous polyposis (FAP) provides further evidence for clonality. Patients with FAP develop colorectal adenomas at an early age, and have an accelerated progression to cancer. The mutation that causes FAP occurs within the *APC* gene, which encodes a component of the Wnt pathway. The discovery of a rare patient with FAP and XO/XY mosaicism who had undergone a prophylactic colectomy allowed analysis of their tissue, using *in situ* hybridisation of the Y chromosome. This revealed that each colonic crypt was either XO or XY and there were no mixed crypts indicating each crypt had a clonal origin (Novelli et al. 1996).

A subsequent study by the same research group looked at a cohort of mediterranean female patients heterozygous for Glucose 6-phosphate dehydrogenase; (G6PD deficiency is X-linked and the most common enzymatic disorder of red blood cells in humans. The clinical expression of G6PD deficiency variants encompasses a spectrum of haemolytic syndromes - from being asymptomatic to episodic anaemia, to chronic haemolysis. Examination of the tissue of these patients' revealed large fields of monoclonal crypts containing only the defective gene product and polyclonality was

not identified. This was further endorsement for clonality in human colonic crypts (Novelli et al. 2003).

More recently researchers have used mitochondrial DNA (mtDNA) mutations, which are associated with a loss of cytochrome c oxidase (CCO), as a clonal marker to study stem cell dynamics in humans (Taylor et al. 2003). The mitochondrial genome is a 16.5 kb circular loop of DNA. It is replicated autonomously of the cell cycle by organelle-specific machinery. Each cell contains multiple mitochondria. In turn, each mitochondrion can comprise up to ten genomes and, therefore, certain tissues contain hundreds of mtDNA genomes (Wallace 2005). Mitochondria are deficient in protective histones and have defective DNA repair machinery, and are continually exposed to reactive oxygen intermediates from the electron transport chain. This results in a higher mtDNA mutation rate than genomic DNA (Taylor et al. 2003). During mitosis, mtDNA mutations are passed on to daughter cells, hence functioning as a marker of cell ancestry. MtDNA mutations occur stochastically, increase with age, and can affect a percentage of the copies (heteroplasmy) or all copies (homeoplasmy) of the mitochondrial genome. In order for a mutation to lead to a mutated cellular phenotype, heteroplasmy needs to be extensive or homoplasmy is required (Sciacco et al. 1994). MtDNA encodes for CCO, which is one of the components of complex IV of the respiratory chain. Two colour-immunohistochemistry for nuclear-DNA-encoded succinate dehydrogenase can be used to identify CCO activity: CCO-negative cells stain blue and wild type cells stain brown. Using PCR it can be shown that CCO negative crypts share the same mutation and are therefore clonal in origin (Taylor et al., 2003).

Greaves et al. (2006) who pioneered this technique utilised it to distinguish the stem cell compartment at the base of the colonic crypts and showed that patches of genetically related crypts form and increase in size with age. The same group have gone on to demonstrate the putative stem cell compartment for regenerative units in the stomach (McDonald et al. 2008), small intestine (Gutierrez-Gonzalez and Wright 2008), skin and pancreas (Fellous et al. 2009b), and liver (Fellous et al. 2009a). In addition, this group have depicted the clonality of cirrhotic liver nodules (Lin et al. 2010).

Stem cell dynamics in human epithelial tissues, such as the colonic crypt, remain uncertain due to the inherent limitations of using human tissue. The next section will explore a serendipitous means to study dynamics and infer rates of clonal expansion in human tissues.

1.16 Understanding stem cell dynamics with the use of methylation patterns

Through the process of niche succession, a particular stem cell lineage can come to dominate a niche, either by neutral drift or by a selective advantage offered by a mutant clone. Following this process, a particular stem cell lineage can come to occupy the whole crypt, so-called monoclonal conversion (Figure 1.5).

CpG islands found within non-expressed genes are CpG dense regions, which demonstrate age-related methylation (Chu et al. 2007). Methylation at these loci is somatically inherited: in the zygote, CpG islands are unmethylated initially and during mitosis these islands attain stochastic methylation *de novo*. This can be exploited to study the clonal origin of cells. Thus, by using the disparity between any two cells'

methylation signatures, their clonal origin may be inferred. If two cells share similar methylation patterns, they are likely to share a recent common ancestor. Conversely, it is less probable that unrelated cells have comparable methylation signatures. This allows the inference of the ancestry of cells within the human body without the need for invasive labelling techniques.

It is possible to manipulate this stylish technique to compose a phylogenetic tree to examine cell population dynamics. Epigenetic signatures represent a molecular clock, as the rate of change of methylation status (methylation or de-methylation) at CpG sites is low, estimated at approximately $2x10^{-5}$ per CpG site per division (Yatabe et al. 2001; Kim and Shibata 2002). Methylation occurs at mitosis and, therefore, more mitotically active tissues have more methylated sites within a CpG island. This is termed the percent methylation, which increases with the mitotic age of the tissue (Chu et al. 2007). In a pivotal study by Yatabe and colleagues, these workers exploited this technique to permit the examination of stem cell population dynamics in the crypt (Yatabe et al. 2001). Proof that the crypt housed multiple long-lived stem cells came from the observation that individual crypts have a limited number of distinctive methylation signatures. In addition, the diversity between methylation signatures within a crypt was symptomatic of the fact that the stem cells were challenging each other to remain within the niche (Yatabe et al. 2001; Nicolas et al. 2007). This has been demonstrated within the small intestine (Kim et al. 2005) and also outside of the gastrointestinal tract, in endometrial glands (Kim et al. 2005; Kim et al. 2006) and hair follicles (Kim et al. 2006). The data demonstrated that niche succession cycles is an innate consequence of the actuality of symmetric stem cell divisions and neutral drift within the niche in human colonic crypts (Simons and

Clevers 2011). Within the human colon all stem cell lineages within a niche, bar one, are destroyed every 8.2 years approximately equating to 9 to 10 periods of complete renewal in a lifecycle (Kim and Shibata 2002). Thus, an integral characteristic of a niche is clonal succession. It is paramount to comprehend, however, that this process can occur without a mutation. Mutations essential for carcinogenesis may not necessarily confer any survival advantage, but may come to govern the niche through 'hitchhiking' these niche succession cycles (Maley et al. 2004).

The Winton lab recently used a functional approach independent of stem-cell specific markers to characterise stem cell populations and quantify the dynamics of clonogenic stem cell replacement. They used a method in which genetic labelling in the intestinal epithelium is acquired as a mutation-induced clonal mark during DNA replication (Kozar et al., 2013). The technique exploits the relative instability of dinucleotide repeat tracts during DNA replication by placing a $[CA]_{30}$ tract within a reporter gene. The reporter gene is only expressed if there is a frameshift mutation. Analysing the *in vivo* mutation rate and combining this data with the known neutral drift dynamics that describe intestinal stem cell replacement could quantify functional stem cells in crypts and adenomas. Conflictingly, this approach identified significantly fewer numbers of 'working' stem cells than were considered to be present in the intestinal epithelium (5-7 per crypt) and in adenomas (9 per gland). Furthermore, stem cell replacement was occurring at a markedly lower rate. These observations would imply that the majority of tumour stem cell divisions act merely to replace stem cell loss, with only a limited number of clonal stem cells successfully driving gland repopulation and tumour progression.

1.16.1 Clonal expansion in tumour evolution

The model of clonal evolution preceding the formation of a malignant tumour remains unknown. It is well established that human adenomas have relatively low malignant potential. Indeed some longitudinal analyses have demonstrated fewer than 1 in 10 adenomas undergo malignant transformation within 10 years of initial identification (Stryker et al. 1987). Longitudinal and barium observational studies suggest that adenomas stay stagnant in size for many years, with some lesions even degenerating over time (Welin et al. 1963; Hofstad et al. 1996; Tada et al. 1984). Jones and colleagues modelled the relative mutation burden of CRCs versus adenomas and proposed that it takes 17 years for a large adenoma to become malignant (Jones et al. 2008). Our laboratory performed lineage tracing in human adenomas using both nuclear and mitochondrial DNA lesions and epigenetic markers (Humphries et al. 2013). The data identified a stem cell population within adenomas and suggested that new growth of intratumour clones arises intermittently, and not in a continual course as expected. This feature was demonstrated in six colonic adenomas. They were microdissected and characterised for genetic lesions and clones deficient in CCO^- as detected by histochemistry were then analysed using mtDNA sequencing. Methylation patterns of adenomatous crypts were determined by clonal bisulphite sequencing. Adenomas were epigenetically diverse. Compared to the tumour as a whole, intratumour clones demonstrated less diverse methylation patterns (Humphries et al. 2013). In summary, adenomas appeared to be relatively mitotically old populations, containing sporadic recently formed subclones that had developed following recent rapid clonal expansion.

1.17 Pseudopolyps

Inflammatory pseudopolyps are a consequence of mucosal ulceration and epithelial regeneration, a classic feature of IBD. They appear as irregularly shaped islands of residual intact colonic mucosa. Polyps are multiple, frequently filiform and distributed throughout the colitic region of the colon. In regions of more active recent inflammation they can be more isolated and semipedunculated, with mucus discharge on their apices (Figure 1.10). Clustered pseudopolyps may be associated with surrounding dysplasia, and meticulous biopsying of this area is paramount. Surveillance colonoscopy can be more problematic when these lesions are present, as inflamed polyps can be vascular. These characteristic lesions are best left *in situ*.

Pseudopolyps are often seen in UC occurring in approximately 20% of all cases, although they are not specific to the condition. Their size varies from a few millimetres in diameter to a centimetre or more, and pseudopolyps are often taller than wide. They may mimic neoplastic lesions, but biopsy is confirmatory (Waye et al. 1977). Pseudopolyps are associated with increased severity and more extensive involvement in UC (Rutter et al. 2004b; Velayos et al. 2006; Rubin et al. 2013).

1.17.1 Pseudopolyps as a predictor of cancer risk

Two important studies published in the last decade examined predictive factors associated with CRC in UC. The first study examined cancer surveillance in longstanding UC, specifically looking at endoscopic appearances to help predict cancer risk (Rutter et al. 2004b). This study from St Mark's Hospital reported an association between postinflammatory pseudopolyps and CRC. A 2.3-fold increase in odds of CRC for pseudopolyps was based on results from extensive surveillance colonoscopy (Rutter et al. 2004b). Pseudopolyps were indeed common:

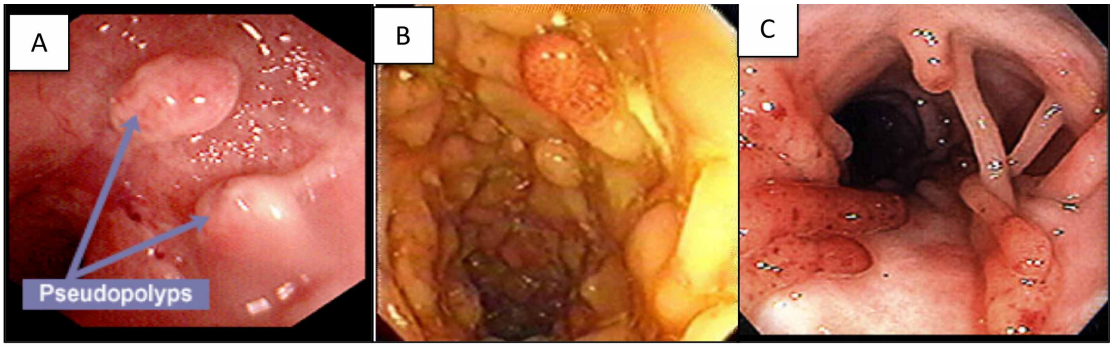

Figure 1.10 Endoscopic views of pseudopolyps. A, several pseudopolyps at endoscopy; B, a 'carpet' of pseudopolyps at endoscopy; C, large filiform pseudopolyps at endoscopy. Taken from www.uptodate.com

in the study by Rutter and colleagues a total of 62% of cases and 39% of controls were found to have them (Rutter et al. 2014b). These findings were further corroborated by a study by Velayos and colleagues in 2006 in which they found a 2.5-fold increase in odds of CRC for pseudopolyps. Pseudopolyps were also common in this study, present in 56% of cases and 42% of controls (Velayos et al. 2006).

Pseudopolyps are not considered to be intrinsically premalignant (Kelly and Gabos 1987). Any association between pseudopolyps and CRC is representative of pseudopolyps being a visible surrogate marker of significant inflammation predisposing to cancer; or is there an alternative explanation? Studies conducted to date on pseudopolyps add additional complexities to endoscopic surveillance in patients with multiple post-inflammatory polyps (Rutter et al. 2004b; Velayos et al. 2006; Rubin et al. 2013). They have demonstrated that UC patients are at increased risk of CRC, yet detecting dysplasia or neoplasia is challenging in a colon populated by pseudopolyps. Such cases may influence the patient and clinician towards a prophylactic colectomy even though the malignant potential of individual pseudopolyps remains uncertain. Certainly, further investigation is very necessary and a successful determination of the role of pseudopoyps in cancer development would warrant an exciting paradigm shift in the management of UC patients. The questions are: how do we establish what role pseudopolyps have in tumour formation? And, can we identify biomarkers that can inform our management of patients with pseudopolyps? MicroRNAs may help in providing answers to both questions.

1.18 MicroRNAs

MicroRNAs (miRNAs) were discovered nearly 20 years ago as a class of non coding

RNAs consisting of 18-24 nucleotides (Bartel 2009). They are post-transcriptional regulators of both gene expression and protein function and are part of a group of other small RNAs (small interfering RNAs (siRNA) and piwi-interacting RNAs (piRNAs) (Bartel 2009). MicroRNAs bind to the 3' untranslated region of messenger RNA (mRNA) and cause either translational inhibition or cleavage of the mRNA complex (Bartel 2009). More than 60% of mRNAs have complementary binding sites for miRNA (Friedman et al. 2009). Each miRNA can target several hundred mRNAs, within a specific cell type.

1.18.1 Synthesis

MiRNAs are transcribed in the nucleus by RNA polymerase II and assembled into a hairpin loop arrangement. This is known as primary miRNA (pri-miRNA). Drosha, an RNase-III enzyme severs this complex into precursor miRNA (pre-miRNAs). Pre-miRNAs are then transported into the cytoplasm where they are spliced further by an RNAse-III enzyme termed Dicer into short miRNAs. MiRNAs can alter protein expression once they have been integrated into an RNA-induced silencing complex (RISC) that permits mi-RNA binding to a complementary mRNA. The disintegration of the mRNA complex or indeed the translational inhibition controls post-transcriptional gene expression (Figure 1.11) (He and Hannon 2004; Jeffrey 2008).

The same targets that miRNAs police frequently control synthesis of miRNAs. Hence, a target protein can moderate miRNA expression, which if expressed would simulate functional deficit of the target protein in a double-negative feedback loop (He and Hannon 2004; Jeffrey 2008).

1.18.2 Function and prediction of targets

The function of miRNAs is to control gene expression. This is achieved by miRNAs binding to mRNA resulting in heightened mRNA breakdown, site-specific splicing or translational inhibition (Chekulaeva and Filipowicz 2009). The latter is the most common method (Figure 1.11).

The prediction of miRNA and their targets has been an ongoing challenge as not all the 23 nucleotides of miRNA have a complementary mRNA. However, one of the many scientific breakthroughs during this search was the detection that miRNA pairing to mRNA targets was concentrated on the so-called 'seed', nucleotides 2-7 of the 5' end of the miRNA (Bartel 2009). This was augmented by the computational power to explore the ribosomal post-initiation sites (3' UTR) of mRNA to find the conserved 6-8 nucleotide matches (Bartel 2009). MiRNAs with identical nucleotide sequence from positions 2-8 share all the same targets, and are classified into families based on this. Approximately 300 targets per miRNA family were predicted (Bartel 2009).

The effectiveness of the seed match of miRNAs to mRNA is reliant on numerous variables: the seed match site on the mRNA; the type and number of bound nucleotides; and the spacing and number (Bartel 2009). The traditional canonical miRNA binding is a seed match (nt 2-7) plus further matches at positions 1, 8 or both. An alternative, less efficient type of binding occurs with only a seed match or a counterbalance seed match (nt 3-8). Less commonly seen is the most efficient binding type, consisting of either an additional 6-7 nucleotide seed match or an offset binding for an incongruity within the seed (Bartel 2009).

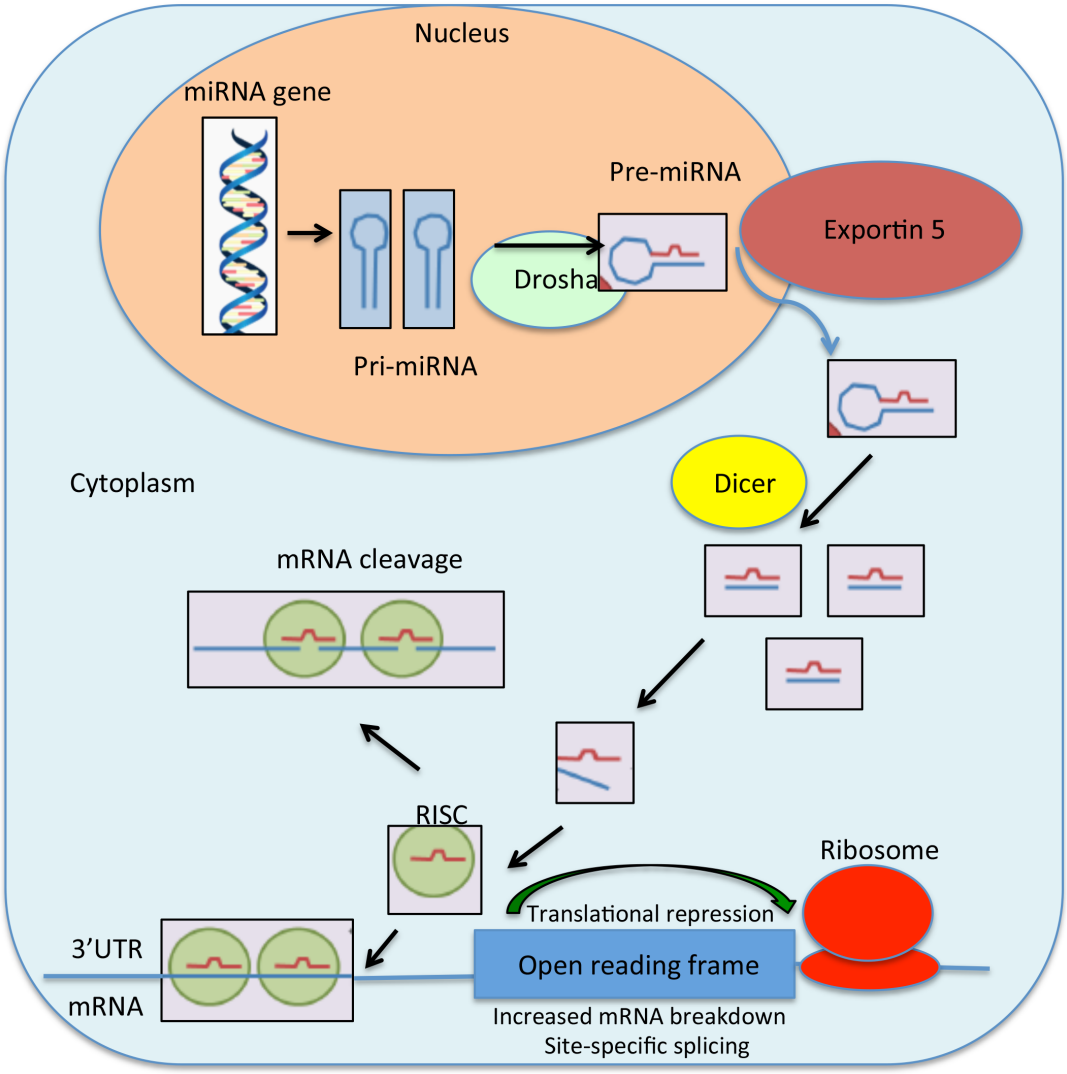

Figure 1.11 The synthesis and effects of microRNA in a cell. Pri-miRNA is transcribed from a gene in the nucleus, modified into pre-miRNA, which is exported into the cytoplasm. Dicer processes the pre-miRNA into short fragments and subsequently into mature miRNA. MiRNA within RISC binds to mRNA to either suppress translation or to cleave the mRNA.

1.18.3 MicroRNAs and cancer

It has been well documented that miRNA controls protein expression and abnormal miRNA expression is observed in many cancers. MiRNAs have a pivotal role in signal transduction, cell differentiation, proliferation and apoptosis (Liu et al. 2011). Hence, it is unsurprising that miRNAs play a key role in normal stem cell proliferation and epithelial cell differentiation. Also, miRNAs play a crucial part in tumourigenesis via modification of tumour expansion, differentiation, adhesion, invasion, apoptosis and indeed metastasis (Liu et al. 2011). In oncogenesis, miRNA can become dysregulated, and can act as oncogenes or tumour suppressors (Ambros 2004).

1.18.4 Tissue and serum microRNAs and inflammatory bowel disease

It is well recognized that IBD is a consequence of interactions between host genetic susceptibility, environmental factors, and immune dysregulation. Gene expression profiles can differentiate CD from UC and also help stratify patients according to probable therapeutic response rates (Arijs et al. 2009; Rybaczyk et al. 2009).

Characteristic miRNA expression profiles have been found in active UC, Crohn's ileitis and Crohn's colitis, at the tissue level. Furthermore, serum miRNAs expression profiles in UC and CD patients have been shown to be quite distinct. These changes follow the stepwise progression from a histological perspective, from normal, non inflamed tissue through to dysplastic tissue.

It was back in 2008 when Wu et al. (2008) first identified miRNA expression in colonic mucosa samples from IBD patients. 11 miRNAs were differentially expressed in active UC compared to controls. They also showed an inverse relationship between

macrophage inflammatory peptide-2α (implicated in IBD previously) and MiR-192. A more recent study by Olaru et al. identified 30 miRs that were differentially expressed between chronically inflamed mucosae and IBD cancers. MiR-224 levels increased sequentially at each stage of IBD progression and correctly distinguished cancers from normal or chronically inflamed IBD tissues. Using mRNA arrays with bioinformatic analyses it was proposed that miR-224 plays a role in cell cycle regulation. Cell cycle experiments indicated that miR-224 regulates the G1-S checkpoint. *In silico* prediction analyses, corroborated by Western blotting and luciferase assays, demonstrated p21 as a specific direct mRNA target of miR-224, establishing the role of miR-224 in IBD carcinogenesis (Olaru et al. 2013).

No characterization has been performed on pseudopolyp tissue to date. Pseudopolyps are thought to be benign lesions occurring as a result of inflammation. Further work is needed to fully comprehend the role of miRNAs in IBD and may also help us to better define disease activity mechanisms, potentially offering better diagnostic and therapeutic agents.

1.18.5 MiRNAs as Biomarkers

MiRNAs could be exploited as biomarkers of disease processes given their presence and stability in peripheral blood. For example, a recent study by Nijhuis et al. (2014) compared sera levels of miR-29a, miR-29b and miR-29c between patients with stricturing CD to patients with inflammatory CD and healthy controls. Relative to healthy controls, miR-29a, miR-29b and miR-29c were elevated in the circulation of inflammatory CD patients, demonstrating that disease affects the levels of miR-29 family. This observation was consistent with Iborra and colleagues who demonstrated

an increase in miR-29a in UC patients (Iborra et al. 2013). In CD patients, the mean levels of miR-29a were significantly lower in both the sera and intestinal mucosa of stricturing CD patients. These observations in CD patients are consistent with those of Roderburg and colleagues who described reduced levels of miR-29a in the sera of patients with liver cirrhosis (Roderburg et al. 2011). Furthermore, reduced levels of miR-29a and miR-29c in urine exosomes is also related to renal fibrosis in chronic kidney disease patients (Lv et al. 2013). Yet, the significant overlap in expression of miR-29a between stricturing and inflammatory CD patients suggests that, alone, miR-29a has limited potential as a serological biomarker of intestinal fibrosis. Further investigations are warranted to determine the true predictive value of circulating miRNAs.

1.18 Hypotheses and aims

1.18.1 Hypotheses

Chronic inflammation in patients with UC results in crypt hyperplasia. However, it is unknown if crypt stem cell dynamics are affected. Combining mtDNA mutations with additional markers of clonal expansion that change over a relatively quick time period, such as methylation patterns of non-expressed genes, reveals stem cell dynamics. I will use these two methods to investigate if a) the stem cell compartment is expanded and b) the rate at which a stem cell takes over the entire stem cell zone, (so-called *niche succession*) is increased. Furthermore, analysis of the stem cell marker *LGR5* by *in situ* hybridisation will assist in determining any increase of stem cell number in UC crypts. It has been shown that in normal colonic mucosa, patch size increases with age

due to multiple crypt fission events. ***I hypothesise that fission, and therefore patch size would be greater in patients with UC than in aged-matched normal controls.***

Crypt fission is the mechanism behind the spread of mitochondrial DNA mutations in the normal gut and ***I hypothesise that the increase in the crypt fission rate in colitis may be responsible for widespread clonal expansion of mutated cells in this condition.***

Pseudopolyps may be the areas where mutations are harboured, acting as a 'nursery' for the genesis of repopulating cells that carry mutations. ***A secondary hypothesis is that pseudopolyps are clonal expansions of crypts that have acquired a protumourigenic survival advantage over surrounding normal epithelium that frequently perishes in the inflammatory milieu.*** Here, the aim is to test the hypothesis *in vivo*, to determine the genetic status of pseudopolyps and frequency of mutated pseudopolyps**,**

The other hypothesis is that the inflammation-associated changes to the intestinal mucosa that drive progression to dysplasia and CACRC result in dysregulated expression of miRNAs and that pseudopolyps have profiles more akin to dysplasia than IBD intestinal mucosa. A further hypothesis is that there would be more proliferation in the form of $Ki67^+$ cells in pseudopolyps compared with control crypts because of a stronger survival advantage and reduced apoptosis, and the number of $LGR5^+$ cells would be increased as a consequence of expansion of the stem cell compartment.

1.18.2 Aims

1. Use mitochondrial DNA mutations, in conjunction with methylation patterns of non-expressed genes to analyse stem cell dynamics in the context of IBD.
2. To analyse mtDNA patch size to model the rate of crypt fission in UC and compare this with established normal mucosa data.
3. To determine the genetic status of pseudopolyps and frequency of mutated pseudopolyps.
4. Assess the differential expression of miRNAs in pseudopolyps, active IBD, inactive IBD and dysplasia.
5. Assess Ki67 proliferation index in pseudopolyps versus control IBD tissue.
6. Identify *LGR5*-positive cells in pseudopolyp crypts using *in situ* hybridisation as a measure of stem cell number.

CHAPTER 2 MATERIALS and METHODS

The general methods used are detailed here. The section numbers from this chapter indicate specific methods relevant to each of the results chapters. Any variations from the techniques given below are discussed in the appropriate results chapter.

2.1 Tissue collection and sectioning

2.1.1 Fresh frozen tissue

UC tissue samples were obtained from patients undergoing surgery at University College Hospital, and The Royal London Hospital. Ethical approval and informed consent was obtained in accordance with the United Kingdom Human Tissue Act (2006), REC reference numbers 07/Q1604/17 and 11/LO/1613. Fresh tissue was immediately frozen in liquid nitrogen using isopentane as a cryoprotectant, and then stored at minus 80°C until further use. Isopentane is not a cryoprotectant in the usual sense, although it does speed up freezing to minimize damage caused by ice crystal growth.

Serial sections of tissue were then cut either 'on-edge' or '*en-face*' depending on the requirements of the project at thicknesses ranging from 8 μM to 20 μM. For laser-capture micro-dissection (LCMD), sections were mounted onto P.A.L.M. laser capture slides (P.A.L.M. Microlaser, Technologies, Germany) that had been pre-exposed to 254nm UV light to improve section adhesion. For tissue designated for immuno-histochemistry (IHC) then sections were cut at 4-8 μm and mounted onto charged glass slides (Thermo Scientific, Germany).

2.1.2 Formalin-fixed paraffin embedded tissue

Archived normal human colon blocks were obtained from University College Hospital London and The Royal London Hospital in accordance with the requirements of the United Kingdom Human Tissue Act (2006), REC reference numbers 07/Q1604/17 and 11/LO/1613. Serial sections were cut at 6 μM onto charged glass slides (Thermo-Scientific, Germany).

2.2 DNA extraction

Proteinase K digestion buffer (Arcturus Bioscience, USA) was used for all DNA extractions. All equipment, gloves and reagents, excluding proteinase K enzyme, were sterilised by 45 minutes of 254nm UV light treatment (UV hood, ASTEC Microflow, UK). Prepared proteinase K digestion buffer was kept on ice to prevent autodegradation.

2.2.1 Tissue macro-dissection

To allow somatic mutation screening of genes commonly mutated in CACRC, 3-5 serial sections from each section were needle macro-dissected into a 1.5 μl micro-centrifuge tube containing 150 μl of Proteinase K digestion buffer. Tubes were incubated for a minimum of 16 hours at 65°C, briefly centrifuged and then incubated for 10 minutes at 95°C to deactivate proteinase K. The clear lysate was removed via a pipette into a clean 1.5 μl micro-centrifuge tube, in order to remove residual protein. DNA concentration was then measured using a NanoDrop® analyser, and lysate diluted to a DNA concentration of 100-200ng per μl, which is the optimum concentration for stock solutions to be used for setting up PCR analysis. DNA lysate was then stored at -20°C until further use.

2.2.2 Laser capture micro-dissection

LCMD of single crypts or single cells from UC and CD tissue was performed using the P.A.L.M. Laser Micro-dissection system (P.A.L.M., Zeiss, Germany). Crypts or single cells were micro-dissected and then catapulted into the adhesive caps of the P.A.L.M. LCMD tubes (P.A.L.M., Zeiss, Germany). An appropriate volume of freshly prepared Proteinase K buffer was then added and the tubes incubated at 65°C for a minimum of 3 hours for frozen tissue and 16 hours for paraffin tissue. Tubes were then centrifuged at 3000 rpm for 1 minute before heating at 95°C for 10 minutes to deactivate Proteinase K. Following further centrifugation at 3000 rpm for 1 minute, DNA lysate was stored at -20°C until further use.

2.3 DNA amplification and sequencing techniques

2.3.1 Polymerase chain reaction

The PCR reaction was used extensively in this study for DNA amplification. Typically a 25 µl PCR reaction contains 30-50ng of template DNA, 0.4 pmols of each primer, 2.5 µl Mg^{2+} -free PCR buffer (Promega, Madison, WI), 1-2 mM MgCl2 (Promega, USA), 0.2 mM of each dNTP (Amersham), a variable amount of Q solution (Qiagen, Crawley, UK) and 1 unit of Taq polymerase (Qiagen). PCR reactions were performed in 96 well plates (ABgene, Epsom, UK). DNA samples were aliquoted into the plate and the PCR master mix added after vortexing. The plate was sealed with Thermowell sealers (Corning, UK) and immediately run on a Tetrad 2 PCR machine (Bio-Rad, UK), or on a G-Storm PCR machine (Labtech, UK). Typical reaction conditions are given in Table 2.1.

Table 2.1. PCR reaction conditions.

Number of cycles	Step	Temperature (^{O}C)	Time (mins)
1	Initial denaturing	95	4
35	Denaturing	94	1
	Primer annealing	55, 58 or 60	1
1	Final extension	72	10

2.3.2 Primer design

Formalin fixation of tissue causes cross-linkage and breakage of DNA, thus DNA extracted with this technique is usually fragmented and of relatively poor quality. In view of this, when utilising this DNA for PCR, primers should be designed to amplify small amplicons of approximately one to two hundred base pairs. However this approach does permit the analysis of historical samples, which may be up to 40+ years old. Individual experiments used different PCR based methodological techniques and necessitated specific oligonucleotide primers, which were individually designed using the Primer3 programme designed by the Whitehead Institute of Biomedical Research (http://www-genome.wi.mit.edu/cgi-bin/primer/primer3_www.cgi). Custom oligonucleotides were obtained from Sigma Genosys (Sigma, UK). All primers underwent optimisation for magnesium content and annealing temperature prior to experimental use and these conditions are listed in addition to the primers in Tables 2.2 to 2.4.

Table 2.2 *p53* 1st and 2nd round primers

Primer name	Sequence (5' to 3')	25mM $MgCl_2$ (μl)	Q (μl)	Annealing Temp (^oC)
p53 5F p53 5R	CACTTGTGCCCTGACTTTCA GAGCAATCAGTGAGGAATCAGA	1	5	55
p53 6F p53 6R	AGAGACGACAGGGCTGGTT TGGAGGGCCACTGACAAC	2	5	60
p53 7F p53 7R	TGCTTGCCACAGGTCTCC GGTCAGAGGCAAGCAGAGG	1	5	60
p53 8F p53 8R	TTTTTAAATGGGACAGGTAGGA CACCCTTGGTCTCCTCCAC	2	5	60
p53 5 2ndF p53 5 2ndR	TCTGTCTCCTTCCTCTTCCTACA AACCAGCCCTGTCGTCTCT	1	5	60
p53 6 2ndF p53 6 2ndR	CAGGCCTCTGATTCCTCACT CTTAACCCTCCTCCCAGAG	1		60
p53 7 2ndF p53 7 2ndR	CTTGGGCCTGTGTTATCTCC GTGTGCAGGGTGGCAAGT	1	5	60
p53 8 2ndF p53 8 2ndR	GCCTCTGCTTCTCTTTTCC GCTTCTTGTCCTGCTTGCTT	2		60

Table 2.3 CDKN2A *(p16)* 1st and 2nd round primers

Primer name	Sequence (5' to 3')	25mM $MgCl_2$ (μl)	Q (μl)	Annealing Temp (^oC)
1st round				
p16 2A F p16 2A R	GTGAGGGGGCTCTACACAAG CAGGTACCGTGCGACATC	2	5	60
p16 2B F p16 2B R	CTGTTCTCTCTGGCAGGTCA TGTGCTGGAAAATGAATGCT	2	5	60
2nd round				
p16 2A 2ndF p16 2A 2ndR	CCTGGCTCTGACCATTCTGT CAGCTCCTCAGCCAGGTC	2	5	60
p16 2B 2ndF p16 2B 2ndR	CTTCCTGGACACGCTGGT TGGAAGCTCTCAGGGTACAAA	2	5	60

Table 2.4 *KRAS* 1st and 2nd round primers

Primer name	Sequence (5' to 3')	25mM $MgCl_2$ (μl)	Q (μl)	Annealing Temp (^oC)
1st round				
KRAS 1st F *KRAS* 1st R	GAGTTTGTATTAAAAGGTACTGGTGGA ATCAAAGAATGGTCCTGCAC	2	5	60
2nd round				
KRAS 2nd F *KRAS* 2nd R	TTTGATAGTGTATTAACCTTAT TATTAAAACAAGATTTACCTC	2	5	55

2.3.3 Agarose gel electrophoresis

Following PCR, 5 µl of product was mixed with 1 µl of loading dye (0.25% w/v bromophenol blue, 0.25% w/v xylene cyanol, 30% v/v glycerol). This was loaded onto a 1-2% (w/v) agarose gel containing gel red (1 in 20,000 dilution) and electrophoresed at 55V for 1 hour in TBE buffer (National Diagnostics, Atlanta, USA). 1kb DNA ladders (Promega, USA) were inserted into a separate well. After electrophoresis, PCR products were visualised using a UV light box, and were diluted with nanopure water according to the strength of the observed product.

2.3.4 Nested PCR

Nested PCR techniques were utilised to amplify the small amounts of DNA obtained from individual crypt lysis to permit mutation analysis of p53, p16, and K-RAS genes. UV-light stable reagents and PCR equipment (plates, pipettes, PCR plate films, eppendorfs and gloves) were exposed to 254nm wavelength UV light for 30 minutes prior to use, and all PCR preparation stages were carried out in an Omni PCR UV hood (Biaquell, UK) to minimise contamination.

2.3.5 First round PCR reaction

First round oligonucleotide primer pairs were specially constructed to amplify a DNA region that included the amplicon covered by the primers utilised in the second PCR round. The first round PCR product was then used as DNA template for the second round reaction. Primers and conditions are listed in Tables 4.1- 4.3. Typical PCR reaction contents and conditions are detailed in section 2.3.

2.3.6 Second round PCR reaction

Every second round primer pair was designed to be within the region of the gene amplified as the corresponding first round PCR product. Primers and conditions are listed in Tables 2.2-2.4. Typical PCR reaction contents and conditions are outlined in section 2.3. The second round product underwent agarose gel electrophoresis as detailed in section 2.3.4. Crypt lysate product was purified and sequenced only if the control blank cap was negative. Every product with a visualised control band on electrophoresis was excluded at this stage.

2.3.7 DNA purification and sequencing

PCR products were purified using the ExoSap-IT® (GE healthcare, UK) clean-up kit for enzymatic removal of unused primers and nucleotides; ExoSAP-IT® contains exonuclease I which removes unincorporated primers, and shrimp alkaline phosphatase which removes leftover dNTPs. 2 µl of ExoSap-IT® was added to 5 µl of each PCR product and then run on a thermal cycler using the protocol detailed in Chapter 9 Appendix.

All sequencing was performed using the BigDye Terminator cycle sequencing method on an ABI Prism Genetic Analyzer: automated sequencing that uses four terminator nucleotides labelled with distinguishable fluorophores. ExoSAP-IT products were diluted with 10-20 µl of distilled H_20, depending on the strength of the PCR product bands on the agarose gel. The sequencing reaction was prepared according to the reagent protocol detailed in Chapter 9 Appendix using the ABI Biosystems BigDye Terminator (Applied Biosystems, USA). For sequencing thermal cycler protocols see Chapter 9 Appendix. Purified sequencing products were vacuum dried using a

Eppendorf 5301 Concentrator (Eppendorf, UK) for 30 minutes at 45°C. Re-suspended residues were transferred to a 48 capillary ABI 3730 DNA Analyser (Applied Biosystems, USA) for sequencing and sequence data analysed with the 4Peaks software (Mekentosj, Netherlands).

2.4 Crypt isolation technique

Fresh IBD tissue biopsies were sampled immediately after endoscopic removal. The biopsy tissue was incubated at 37°C for 10 minutes in calcium- and magnesium-free Dulbecco's modified eagle medium (DMEM) containing 30 mmol/L ethylene – diaminetetraacetic acid (EDTA). Following this, the tissue was shaken in DMEM containing calcium and magnesium, and the crypts were separated from the lamina propria mucosa or fibrous stroma in 30 seconds. The mixture of isolated crypts and lamina propria mucosa or fibrous stroma was then sedimented by gentle centrifugation at 300 g.

Crypts were observed and collected under a dissecting microscope (model SZ60; Olympus, Tokyo) and digested in 14 µl of proteinase K for 16 hours. The samples were then denatured at 95°C for 10 minutes at 95°C and then stored at minus 20°C.

2.5 Mitochondrial DNA mutation detection

2.5.1 Enzyme histochemistry

Two-colour enzyme histochemistry was used to simultaneously detect the mtDNAencoded enzyme CCO and nuclear DNA-encoded succinate dehydrogenase (SDH) (Taylor et al. 2003), a component of complex II of the respiratory chain.

Mutated cells lacking in CCO activity appear blue; non-mutated cells appear brown. Frozen sections air-dried for 45 minutes and first incubated in cytochrome c oxidase medium (100 mmol/L cytochrome c, 20 μg/mL catalase and 4 mmol/L diaminobenzidine (DAB) tetrahydrochloride in 0.2 mol/L phosphate buffer, pH 7.0, all sourced from Sigma-Aldrich, Poole, UK) for a maximum of 45 minutes at 37°C. Crypts or cell populations within crypts with normal activity of CCO subsequently appear brown. In order to counter-stain CCO-deficient cells, sections then underwent three 5-minute washes in phosphate-buffered saline (PBS), pH 7.4, before being incubated in SDH medium (130 mmol/L sodium succinate, 200 mmol/L phenazine methosulfate, 1 mmol/L sodium azide, and 1.5 mmol/L nitroblue tetrazolium in 0.2 mol/L phosphate buffer, pH 7.0; all sourced from Sigma-Aldrich, Poole, UK) for a maximum of 45 minutes at 37°C, or until a strong blue stain had developed in the unstained crypt cell populations. Sections again were washed in PBS for 3x 5 minutes and dehydrated in a graded ethanol series (70%, 90%, 100%, 100%). If tissue was for LCMD, slides were air-dried for 1 hour before being stored at -80°C; sections that were on normal glass slides were cleared in Histoclear (Lamb Laboratory Supplies, UK) and mounted with Permount® (Fisher Scientific, USA).

2.5.2 Laser-capture micro-dissection of intestinal crypts stained for cytochrome *c* oxidase activity

After enzyme staining for CCO activity, three different types of intestinal crypts are observed: (i) wild-type brown crypts, (ii) wholly-mutated blue crypts and (iii) crypts containing populations of both brown and blue cells (mixed or partially mutated crypts). LCMD was then performed on both wholly mutated and partially mutated blue crypts, and adjacent brown wild-type crypts, in order to sequence the

mitochondrial DNA and confirm the presence of clonal point mutations in the blue cells. Laser-capture slides were allowed to thaw at room temperature for 1 hour before micro-dissection. Single cells from CCO-deficient crypts and adjacent wild-type crypts were individually micro-dissected. If required for genomic and/or methylation analysis, the remaining regions of the whole crypt were then dissected from serial sections. 14 μl of Proteinase K digestion buffer was added to each tube for a minimum of 3 hours digestion. A negative control tube containing only digestion buffer and no laser-capture material was also included. In partially CCO-deficient crypts, CCO-deficient cells were micro-dissected separately from CCO-proficient cells, and then the remaining blue and brown cell populations from the whole crypt micro-dissected into two tubes for methylation analysis. After digestion, tubes were briefly centrifuged and proteinase K deactivated by heating to 95°C for 10 minutes. DNA lysate was stored at - 20°C until further use.

2.5.3 MtDNA sequencing

LCMD followed by PCR together with mtDNA sequencing validates the presence of clonal mitochondrial mutations in wholly or partially CCO-deficient crypts, and this has been demonstrated to be a consistent indicator for detecting the clonal expansion of mutated stem cells (McDonald et al. 2006). Extracted DNA lysate was used to sequence the entire mitochondrial genome from micro-dissected areas. This was followed by a two-round amplification step. The first round consisted of amplifying 9 fragments spanning the entire mitochondrial genome. These initial large PCR products of approximately 2 kb decrease the risk of amplifying pseudo-genes when using DNA extracted from small quantities. The second round consisted of 36 M13-tailed primer pairs to amplify overlapping segments of the first-round products, resulting in

amplicons of 500-700 bp that span the entire mitochondrial genome (see Chapter 9 Appendix for primer sequences and detailed PCR protocols). PCR product from the second round reaction was run on a 2% agarose gel, and only those reactions where the negative controls were blank on the agarose gel were taken forward for sequencing. DNA purification and sequencing was performed as previously described (see Methods 1.3.2) and then compared to the revised Cambridge reference sequence (http://www.mitomap.org/MITOMAP) using sequence alignment software of the European Bioinformatics Institute (http://www.ebi.ac.uk). Once a potential mutation was identified, the PCR was repeated using the original DNA lysate and multiple samples from the mutated blue cells and adjacent wild-type, brown cells in order to confirm its validity.

2.6 Immunohistochemistry

All FFPE sections were de-waxed to water, with an additional hydrogen peroxide blocking step for endogenous peroxidases if required, and antigen retrieval performed with micro-waving in boiling citrate buffer (pH 6.0) for 10 minutes; sections were then washed in cold water before transferring to PBS. Frozen sections were thawed at room temperature for 30 minutes before fixing in cooled Acetone (-20°C) for 10 minutes. Sections were then left at room temperature for 30 minutes to allow for evaporation of acetone before being transferred to PBS.

Table 2.5 Immunohistochemistry antibodies and conditions.

Primary Antibody	Specificty	Species	Dilution	Antigen retrieval	Source
Ki-67 (MIB-1)	S-phase marker	Mouse	1:200	Pressure cook in sodium citrate buffer	Novacastra
Secondary Antibody IgG biotin-conjugate	Anti-rabbit	Swine	1:500	Applied as secondary layer	DAKO

2.6.1 Chromogen

Sections were first blocked with a serum-free protein block (Dako, UK) for 10 minutes followed by incubating with streptavidin for 15 minutes and then biotin, also for 15 minutes, at room temperature (Vector Laboratories, Peterborough, UK). The primary antibody - mouse anti-human CCO subunit 1 IgM (1:500; Invitrogen, UK) - was applied for 35 minutes at room temperature. Sections were washed for 5 minutes in PBS x3 followed by 35 minutes incubation with a biotinylated anti-mouse immunoglobulin (Dako, UK). After the final PBS washes, sections were incubated with streptavidin peroxidase (Dako, UK) for another 35 minutes, washed, and developed in a solution containing 4 mmol/L diaminobenzidine and 0.2% hydrogen peroxide (Dako, UK) for 2-5 minutes. All antibodies were diluted in PBS. Sections were then dehydrated through alcohol (75%, 95% and 100%), cleared with xylene, and mounted with DePeX.

2.7 *In situ* hybridization

Following dewaxing, sections were incubated in 1mM sodium thiocyanate (Sigma UK) in distilled water for 10 minutes at 80°C. Afterwards, sections were digested

using 0.4w/v pepsin (Sigma, UK) in 0.1M hydrochloric acid at 37°C. Optimisation time trials were employed to define digestion times, which varied between 10 to 30 minutes for human colonic tissue. Thereafter, sections were incubated in 0.2% glycine (Merck, USA) in double concentration phosphate buffered saline (PBS) to halt digestion. Fixation was then performed for 2 minutes using 4% paraformaldehyde (PFA). Sections were dehydrated through 70%, 95% and 100% ethanol and air-dried.

ISH for *LGR5* expression was performed on 5 μm sections using the RNAscope 2.0 High Definition (Red or Brown) assay according to the manufacturers instructions (Advanced Cell Diagnostics, Hayward, CA). Briefly, samples were baked at 60°C for 1 hour, followed by deparaffinization and incubation with Pretreat 1 buffer for 10 minutes at room temperature (RT). Slides were boiled in Pretreat 2 buffer for 15 minutes, followed by incubation with Pretreat 3 buffer for 30 minutes at 40°C. Slides were incubated with the relevant probes for 2 hours at 40°C, followed by successive incubations with Amp1 to 6 reagents. Staining was visualized with 3,3′-diaminobenzine (DAB) or Fast Red for 10 minutes, then lightly counterstained with Gill's haemotoxylin. RNAscope probes used were *LGR5* (NM_003667.2, region 560–1589), *POLR2A* (positive control probe, NM_000937.4, region 2514–3433) and *dapB* (negative control probe, EF191515, region 414–862). *LGR5* expression at the crypt base was quantified according to the five-grade scoring system recommended by the manufacturer (0 = No staining or less than 1 dot to every 10 cells (40× magnification), 1 = 1–3 dots/cell (visible at 20–40× magnification), 2 = 4–10 dots/cell, very few dot clusters (visible at 20–40× magnification), 3 = > 10 dots/cell, less than 10% positive cells have dot clusters (visible at 20× magnification), 4 = > 10 dots/cell. More than 10% positive cells have dot clusters (visible at 20× magnification).

2.8 Methylation analysis

2.8.1 Laser capture micro-dissection and DNA extraction for methylation analysis

LCMD was performed as described previously (see Methods 2.2.2). Whole crypts from IBD colon were LCMD for methylation analysis; at least 3 serial *on-edge* sections were micro-dissected for each crypt. For CCO^- clones within crypts, the blue and brown cell populations were micro-dissected separately from all serial *en-face* sections of the crypt into two laser capture tubes.

DNA was extracted using 14 µl of proteinase K digestion buffer (Arcturus Bioscience, USA) for a minimum of 3 hours digestion. A negative control tube containing only digestion buffer and no laser capture material was also included. After digestion, tubes were briefly centrifuged and proteinase K deactivated by heating to 95°C for 10 minutes. DNA lysate was stored at -20°C.

2.8.2 Bisulphite treatment

For methylation analysis, extracted DNA was bisulphite treated using the EpiTect® Plus Bisulphite Kit (Qiagen, UK) according to the manufacturer's instructions. A sodium bisulphite mix is prepared and run on a thermal cycling programme overnight and the mix then spun through an EpiTect® spin column with a buffer to promote binding of the converted DNA to the column membrane. Bound DNA is then washed to removed residual sodium bisulphite, de-sulphonated, eluted from the spin column into a 1.5ml micro-centrifuge tube and then stored at -20°C until further use. An aliquot of the digestion buffer was also bisulphite treated as a negative control. Bisulphite treatment results in the efficient conversion of un-methylated cytosine to

uracil, but yields low DNA concentrations. Thus, in order to successfully PCR amplify the bisulphite treated DNA a two-round, nested PCR was used. CpG islands on the following genes were amplified: Myoblast determination protein 1 (*MYOD1*; Chromosome arm 11p); Cardiac-specific homeobox (*CSX*; Chromosome arm 5q); and Biglycan (*BGN*; Chromosome arm Xq). These genes are not expressed in the colonic epithelium, demonstrate age related methylation, and have been previously suggested for use as clonal markers in human colon crypts (Taylor et al. 2003; Greaves et al. 2006).

Specific primers flanking the target CpG islands for each gene were designed using the Primer 3 website (MIT, Cambridge, Massachusetts, USA), and reaction conditions (reagent concentrations and annealing temperatures) were preoptimised for each primer pair using cell-line DNA. Successful PCR amplification was confirmed by gel electrophoresis and only samples with an uncontaminated negative control were taken forward for cloning.

2.8.3 TA-cloning of PCR products

To achieve single strand resolution, PCR products were cloned using a TA-cloning kit, utilising the pGEM®-T vector (Promega, UK), according to the manufacturer's instructions. Taq DNA polymerase adds a terminal 3'-A overhang to the end of each PCR product and this enables it to be directly cloned into a linearized cloning vector that has single base 3'-T overhangs - *TA cloning*. The pGEM®-T is a linearised vector with a single 3'-T overhang at each end, and contains a *LacZ* gene and β-Lactamase coding region. PCR products are cloned in a ligation reaction containing PCR product, buffer, vector and T4 DNA ligase. The recombinant vectors are then transformed into

competent JM109 cells (Promega, UK) and colonies grown overnight on agar growth medium containing ampicillin, X-galactose (X-gal) and Isopropyl β-D-1-thiogalactopyranoside (IPTG). Incorporation of the PCR product into the vector disrupts the *LacZ* operon means that successfully transformed clones are easily identified by blue/white colour discrimination. White clones were PCR amplified using M13 or T7/SP6 primer pairs that flanked the insertion point within the plasmid. The PCR product was then purified and sequenced as previously described (see Methods 1.3.2).

2.9 Somatic mutation and analysis of pseudopolyps

Fresh frozen human pseudopolyps were collected as previously described (see Methods 2.1). Serial sections were cut at 8 μm onto normal glass slides for tissue macrodissection, with every 1st section cut at 4 μm onto normal glass slides for haematoxylin and eosin staining to enable accurate histopathological assessment by expert GI pathologists (Professor Sir N.A. Wright, Head of Tumour Biology, Bart's Cancer Institute, London and Dr I T Saeed, Consultant Histopathologist, Queen's Hospital, London). Sections were then stained for CCO-histochemistry as detailed in 2.5.1. Tissue macro-dissection, PCR and sequencing were all done as previously detailed (see Methods 2.2.1, 2.3.5, 2.3.6, 2.3.6.1, and 2.3.6.2.). For details of all primer sequences, PCR reagent and thermal cycler protocols see Tables 2.1-2.4.

2.9.1 Somatic *TP53* mutation screening

Exons 5-8 of the *TP53* TSG, where the vast majority of somatic mutations in *TP53* occur, were amplified from whole tissue scrapes and/or individual crypts using an established nested, two-round PCR specific for these exons (see section 2.3.6; 2.3.6.1

and Table 2.2).

2.9.2 Somatic *CDKN2A (p16)* mutation screening

The regions where the vast majority of somatic mutations in *CDKN2A* occur, were amplified from whole tissue scrapes and/or individual crypts using an established nested, two-round PCR specific for this region of the gene (see section 2.3.6; 2.3.6.1 and Table 2.3).

2.9.3 Somatic *KRAS* mutation screening

Oncogenic *KRAS* mutations tend to occur at codons 12 and 13, and occasionally codon 61 (COSMIC: Catalogue of Somatic Mutations in Cancer database; cancer.sanger.ac.uk). Therefore, *KRAS* mutation screening of DNA lysate from whole tissue scrapes and/or individual crypts was performed using an established nested, two-round PCR specific for this region of the gene (see section 2.3.5 and Table 2.4).

2.10 MicroRNA Extraction

FFPE tumour tissue sections on haematoxylin and eosin (H&E) stained slides were scored by gastrointestinal pathologists Dr Ibtisam Saeed, Dr Manuel Rodriguez-Justo, and Professor Sir Nicholas Wright and the tumour tissue marked out with a thin pen on the back of the slide. Slides were cut and H&E stained by the pathology department (Core Pathology Department, Queen Mary University of London).

Ten sections, each of 10 μm were used, producing a final depth of 100 μm to reduce cell damage and loss of miRNA, as recommended in the manufacturer's

protocol. The RecoverAll Total Nucleic Acid Isolation Kit (Ambion, AM1975) was used to isolate the miRNA from these slides. The tumour tissue on non-stained slides was scraped off using a scalpel into a centrifuge tube and the protocol was followed to deparaffinise, protease digest and isolate the RNA. RNA was eluted in 60 µl of RNase-free water, the concentration determined by nanodrop and then stored at -80 °C until needed.

2.11 Statistical analysis

All statistical analysis was performed using Graph pad Prism version 5. If data was normally distributed then a Student's T-tests or a one way analysis of variance was applied (ANOVA). All test were two-tailed with significance set at $p<0.05$. Correction was made for multiple testing where appropriate using Bonferroni correction. The sum of squares f test was used to test for differences between best fit curves.

CHAPTER 3 INVESTIGATING CLONAL EXPANSION OF HUMAN INTESTINAL CRYPTS IN INFLAMMATORY BOWEL DISEASE PATIENTS

3.1 Introduction

Owing to the intrinsic constraints of examining human tissue *in vivo*, investigating human intestinal stem cell dynamics continues to be problematic. Methylation patterns of non-expressed genes at CpG island loci provide a way to examine stem cell dynamics and permit extrapolation of clonal expansion rates within human tissues (Yatabe et al. 2001; Kim and Shibata, 2004; Nicolas et al. 2007) (see Introduction 1.16).

The CpG loci studied here are within non-expressed genes and are the same as those used by previous studies to analyse human colon crypt stem cell dynamics: (i) Cardiac specific homeobox (*CSX*), expressed specifically during the differentiation of cardiac myocytes; (ii) Myoblast determination protein-1 (*MYOD1*), specifically expressed during myoblast differentiation. The *CSX*, and *MYOD1* CpG islands have eight, and five CpG sites respectively, and are located in the coding sequence of these non-expressed genes. PCR amplification of bisulphite-treated DNA using methylation specific primers followed by cloning of individual PCR strands allows the methylation status of each gene-specific CpG island for a defined cell population – an individual crypt or clones within crypts - to be sampled (see Materials and Methods section 2.3 & Figure 3.1). This can then be represented as a binary code termed a *methylation tag*, where '1' represents a methylated CpG site and '0' an un-methylated CpG site (Figure 3.1). Similarly, the methylation tags are also represented visually whereby a methylated CpG site is marked with a filled circle, and un-methylated CpG site by an

un-filled circle (Figure 3.1).

As very small quantities of DNA were being bisulphite-treated when micro-dissecting clones from within crypts, at times merely 400-500 cells, the ability of the assay to reliably measure methylation pattern diversity in small clonal populations was tested by colleagues in the lab (Graham et al. 2011). Following DNA extraction of the clone or crypt, the DNA lysate was split into two aliquots and each was subjected to independent bisulphite-sequencing analysis. The two aliquots always produced near identical methylation patterns, confirming the sensitivity and reliability of the assay (Graham et al. 2011). Further, exhaustive cloning analysis demonstrated the following: the percent methylation and intra-crypt distance were largely independent of the number of methylation tags analysed per crypt, whereas the number of unique tags per crypt increased asymptotically with clone number. These results corroborate with the validation of these techniques performed by previous authors (Yatabe, 2001), and demonstrated that the accuracy of the summary statistics are not significantly improved if more than 8 cloned PCR products are successfully sequenced.

3.1.1 Hypothesis and aims

The hypotheses tested in this chapter were as follows: (i) that an approximation of the dynamics of niche succession could be made based on methylation pattern evaluation of CCO-deficient clones within crypts; and (ii) that crypt fission is increased in the inflamed epithelium in the context of IBD. The aim was to study the methylation patterns of CCO-deficient cell populations in IBD patients to allow the recording of the ancestry and stem cell dynamics in this group of patients.

Bisulphite Conversion

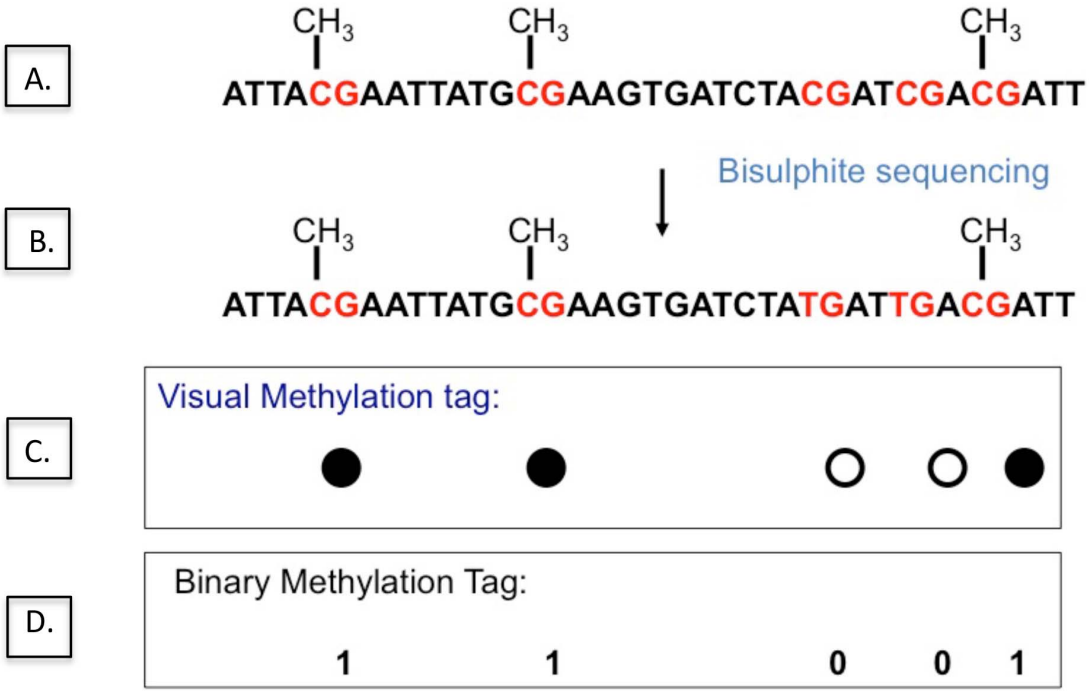

Figure 3.1. The methylation status of a DNA sequence can be determined using sodium bisulphite sequencing. Methylation of DNA occurs only on CpG residues. CpG-rich areas are known as CpG islands, and have a GC content of more than 55%. Incubation of the target DNA with sodium bisulphite results in conversion of unmethylated cytosine residues into uracil and the methylated cytosines remaining unaffected. **A.** An example of a DNA sequence containing 5 CpG sites that is either methylated (CH_3) or unmethylated. **B.** Extracted DNA from a clone undergoes sodium bisulphite conversion where all unmethylated cytosine residues are converted to uracil. Following this, amplification using PCR specific primers for the methylated sequence flanking the CpG site, with subsequent TA-cloning of individual PCR products and sequencing of the products reveals the methylation status. **C.** The methylation status can be depicted as a binary tag or **D.** a visual methylation tag.

3.2 Results

3.2.1 Clinicopathological details of patients

CCO^- mutations are rarely detected in human colon before the age of 40 years (Greaves et al. 2006) and hence the patients selected below are all in their fourth decade of life or older (Table 3.1). In addition, the nature of these experiments requires freshly frozen resection specimens, and intact mucosa to allow the identification of clonal crypts, which explains the limited sample size available.

Table 3.1 Clinicopathological details of the ulcerative colitis patients analysed.

Patient	Age	Sex	Disease Activity
1	54 years	Male	Quiescent
2	52 years	Male	Mildly active
3	47 years	Female	Quiescent
4	67 years	Female	Quiescent
5	35 years	Male	Quiescent

3.2.2 Identification of clonally related patches and their methylation signatures provide a record of crypt ancestry

Several individual cells from CCO^- and neighbouring CCO^+ crypts were laser captured, micro-dissected and the mitochondrial genome amplified and sequenced. This allowed the identification of clonal mutations within the CCO^- cells, thus confirming that the CCO^- cell populations are clonally related and derived from a single stem cell lineage (see Methods 2.5.3). Figure 3.2 demonstrates colonic crypts from a UC patient with quiescent colitis. Following histochemical staining for CCO on frozen sections, a discrete population of CCO^- crypts can be identified. Evidence

that all the CCO^- cells within the crypt were from a distinct clonal population and derived from a single stem cell lineage was corroborated by mtDNA sequencing of the CCO^- cells (Figure 3.2).

For the CCO^- crypts in Figure 3.2 the mtDNA mutation was located in the *MT-ND4* gene that encodes for the nicotinamide adenine di-nucleotide (NADH)-ubiquinone oxidoreductase chain subunit 4 (complex I). A G>A missense mutation at nucleotide position 11246 (Figure 3.2) caused an amino acid change from Alanine to Threonine. However, these crypts have distinct methylation patterns (Figure 3.2).

Using single cell LCMD this finding was repeated in a second patient (patient 2 in Table 3.1), a 52 year old male with mildly active UC (Figure 3.3). Clonality was confirmed in all CCO^- crypts. A missense mutation caused an amino acid change, G>A Alanine to Threonine in Mt-RNR2 (mitochondrially encoded 16S RNA), at nucleotide position 3127 (Figure 3.3). However, this patch of adjacent CCO^- and, therefore, clonally-derived crypts had similar methylation patterns (Figure 3.4). The clonal relation indicated by adjacent crypts having CCO-deficiency was mirrored by the consistency of the crypt methylation patterns across the *MYOD* locus examined. In conditions of active inflammation, both adjacent clonally related CCO^- crypts and adjacent unrelated crypts had similar methylation patterns indicating recent crypt fission.

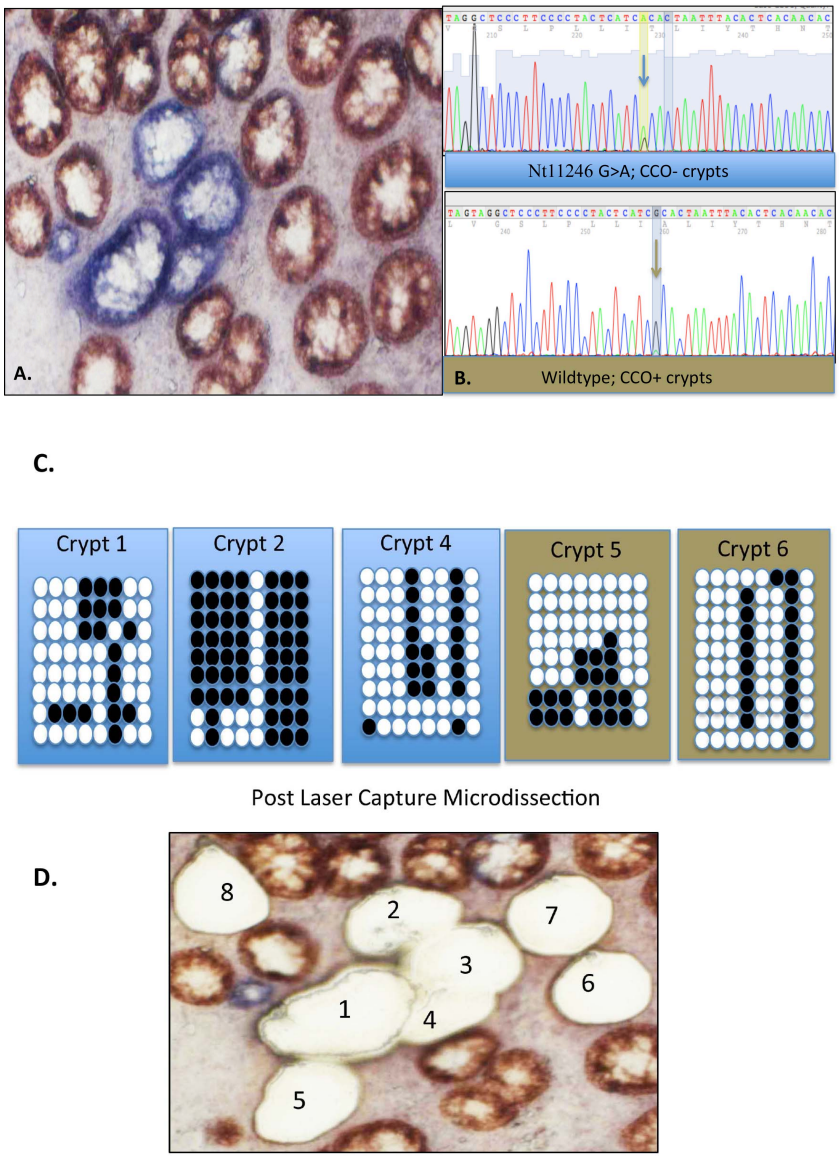

Figure 3.2 Cytochrome *c* oxidase staining of ulcerative colitis tissue identifies stem cell clones within crypts. A. Cytochrome *c* oxidase staining of *en face* section of UC mucosa from a 54 year old male shows a patch of CCO^- crypts with a distinct population of CCO-deficient, blue cells. **B.** CCO^- cells with clonal mutation in mtDNA (G>A Alanine>Threonine in NADH dehydrogenase at nt11246). All CCO^+ cells are wild-type. **C.** *CSX* Methylation patterns for CCO^- (clonal mutant blue) crypts and CCO^- (wildtype brown) crypts. **D.** Post LCMD of whole crypts. Although adjacent CCO deficient crypts are clonal, they share no similar methylation patterns, and are as dissimilar as non-related CCO^+ adjacent crypts.

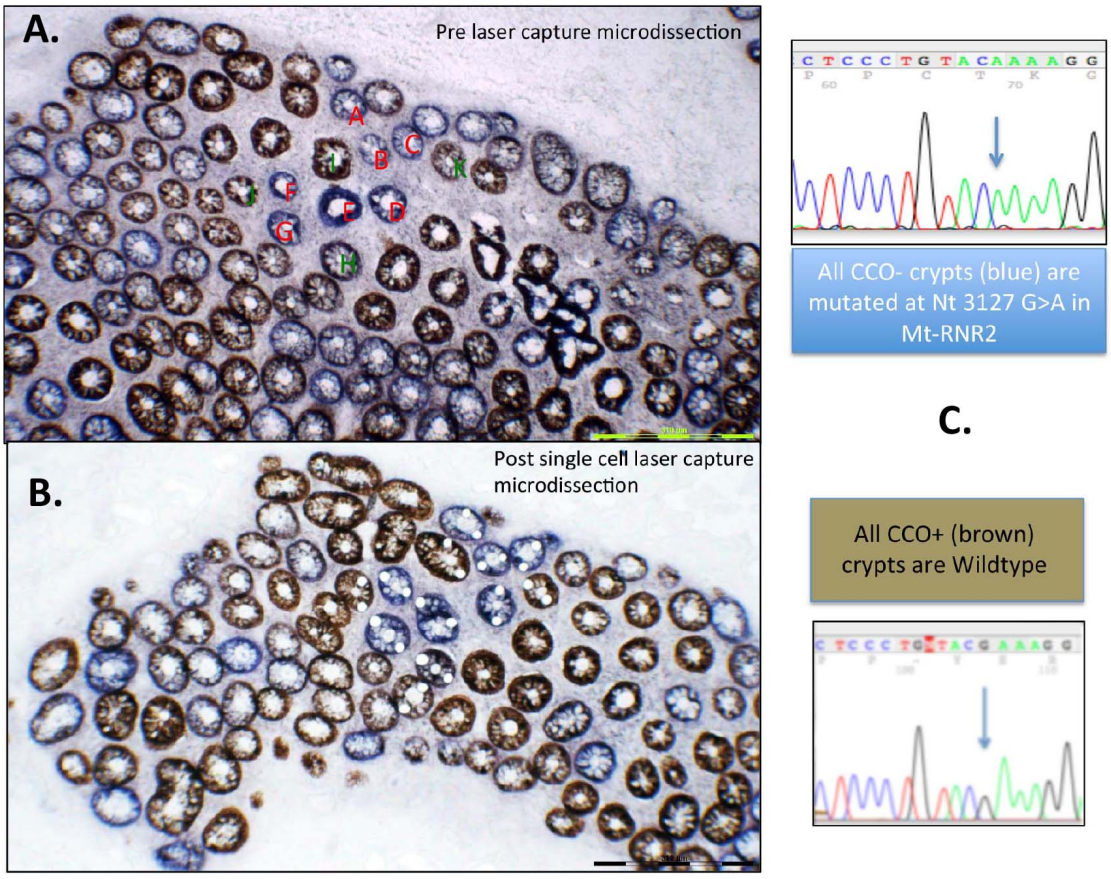

Figure 3.3 Cytochrome *c* oxidase staining of serial *en face* sections allows the identification of stem cell clones within crypts. A. Serial section stained from a second UC patient, a 52 year old male with mildly active UC. **B.** Laser capture microdissection (LCMD) of CCO^- and CCO^+ cells within the crypt, and of CCO^+ cells from adjacent crypts. **C.** The CCO^- population contains a clonal mutation in their mtDNA, in this case a G>A Alanine>Threonine in Mt-RNR2 at position nt3127. All the CCO^+ cells are wildtype.

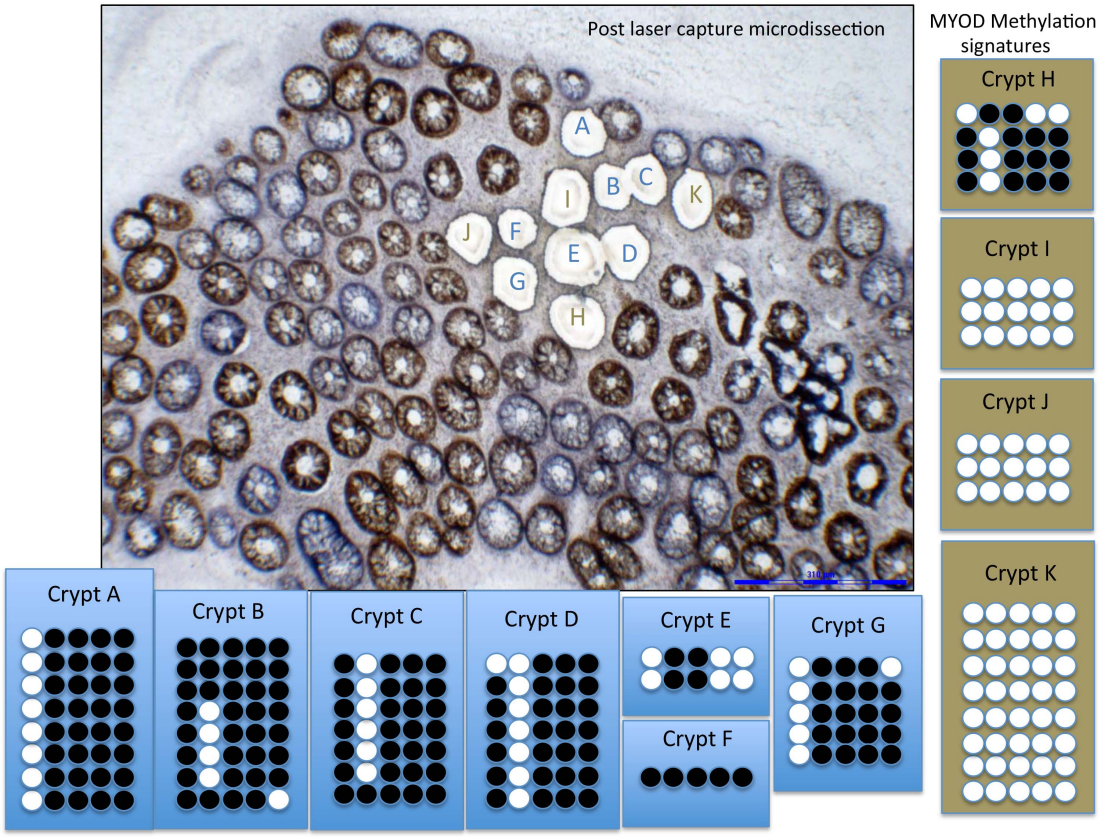

Figure 3.4 Post laser capture microdissection of stem cell clones within crypts. Post LCMD of whole crypts. The *MYOD* methylation status of each crypt is depicted using the visual methylation tags described earlier. CCO^- clones are depicted in blue and CCO^+ clones are depicted in brown. The clonally related CCO^- blue crypts have obvious similar methylation signatures indicating recent crypt fission in this patient with mildly active disease. CCO^+ crypts I, J and K have 0% methylation which makes interpretation of stem cell dynamics in those crypts difficult.

A third patient was analysed, a 47 year old female with UC (Table 3.1). LCMD and mtDNA sequencing of a patch of adjacent CCO-deficient crypts demonstrated the presence of the same, clonal mtDNA point mutation in all crypts, confirming that they are clonally derived by fission (Figure 3.5). For the CCO^- crypts in Figure 3.5 the mtDNA mutation was located in the *MT-CO3* gene that encodes for the cytochrome *c* oxidase subunit III gene and the point mutation was C>T at position 9641. On analysis of the methylation signatures of clonal and non-clonal crypts, clonally related crypts have different, distinct methylation patterns (Figure 3.5).

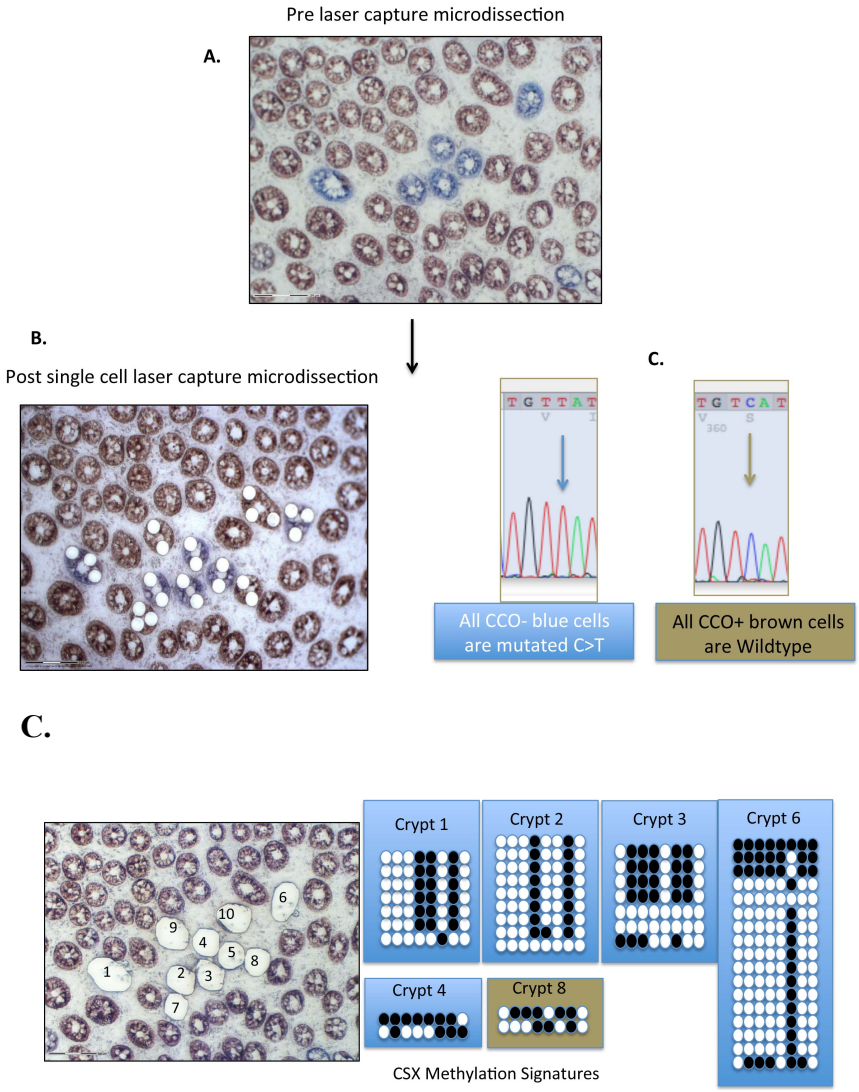

Figure 3.5 Cytochrome *c* oxidase staining of ulcerative colitis tissue identifies stem cell clones within crypts. A. Cytochrome *c* oxidase staining of an *en face* UC mucosa section from a 47 year old female shows a patch of CCO^- crypts with a distinct population of CCO-deficient, blue cells. **B.** Post single cell laser capture microdissection of CCO^- cells from CCO^- crypts, and CCO^+ cells from adjacent CCO^+ crypts. The CCO^- population contain a clonal mtDNA mutation (C>T mutation at position 9641). **C**. Post laser capture microdissection of CCO^- and CCO^+ crypts. The *CSX* methylation status of each crypt is depicted using visual methylation tags. Here, the clonally related crypts share very few similar methylation signatures.

These observations were extended through investigation of a large clonal expansion of CCO-deficient colonic crypts across a considerable physical distance (Figure 3.6). Figure 3.6 shows colonic crypts from a 67 year old UC patient with quiescent colitis (Table 3.1). Following histochemical staining for CCO, a large discrete population of CCO^- crypts can be identified across a considerable distance in the section analysed. Interestingly, two clonal populations were identified via mtDNA sequencing of the CCO^- cells (Figures 3.7-3.8). Here, the first of the clonal populations was defined by a synonymous mutation, A>G in the MT-ND4 gene at position 11924. A further clonal mutation (synonymous mutation A>T) was identified in the MT-ND2 gene at position 5238. The methylation patterns did not corroborate with clonality. Clonally derived crypts did not share similar methylation signatures in either locus examined (Figures 3.10-3.11). In the methylation tags analysed from the *MYOD* locus there did appear to be a high degree of hypomethylation, and so was not optimally informative; *CSX* demonstrated a lack of epigenetic similarity (Figure 3.10).

The final patient analysed was a 35 year old male with UC (Table 3.1). Histochemistry and LCMD of single cells within a clonal patch was performed (Figure 3.12). The CCO^- cell population had a synonymous mutation (silent substitution), a T>C mutation at nucleotide position 14783, in the mitochondria encoded cytochrome B gene, (Mt CYB) that did not cause an amino acid change (Figure 3.12).

Pre laser capture microdissection

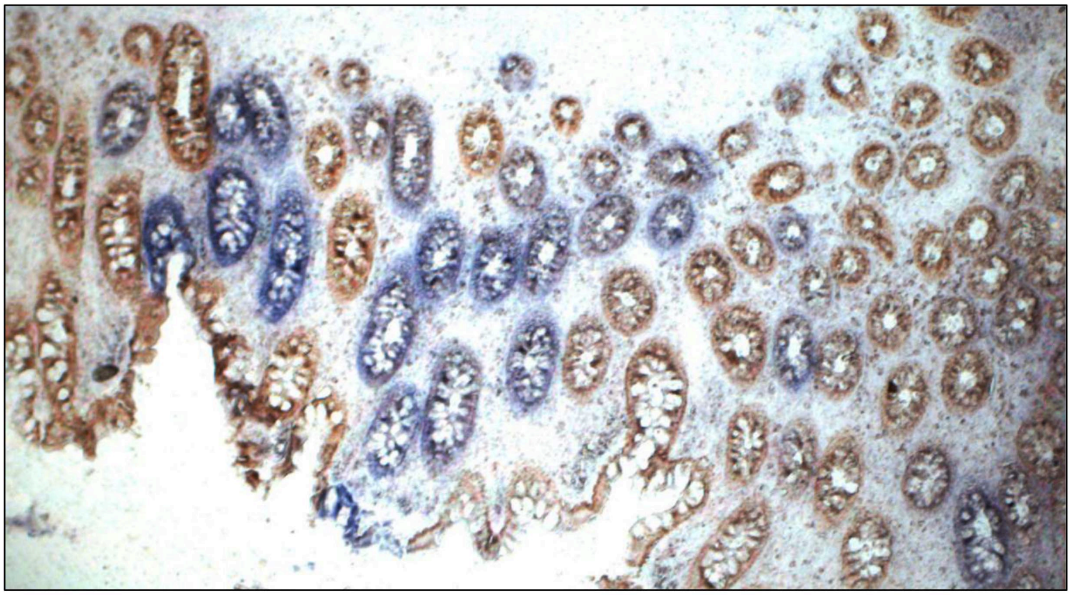

Figure 3.6 Cytochrome *c* oxidase staining of ulcerative colitis tissue identifies stem cell clones within crypts. A. Cytochrome *c* oxidase staining of an *en face* section of UC mucosa from a fourth patient, a female aged 67 years, demonstrating a patch of CCO^- crypts containing a distinct population of cytochrome *c* oxidase-deficient, blue cells.

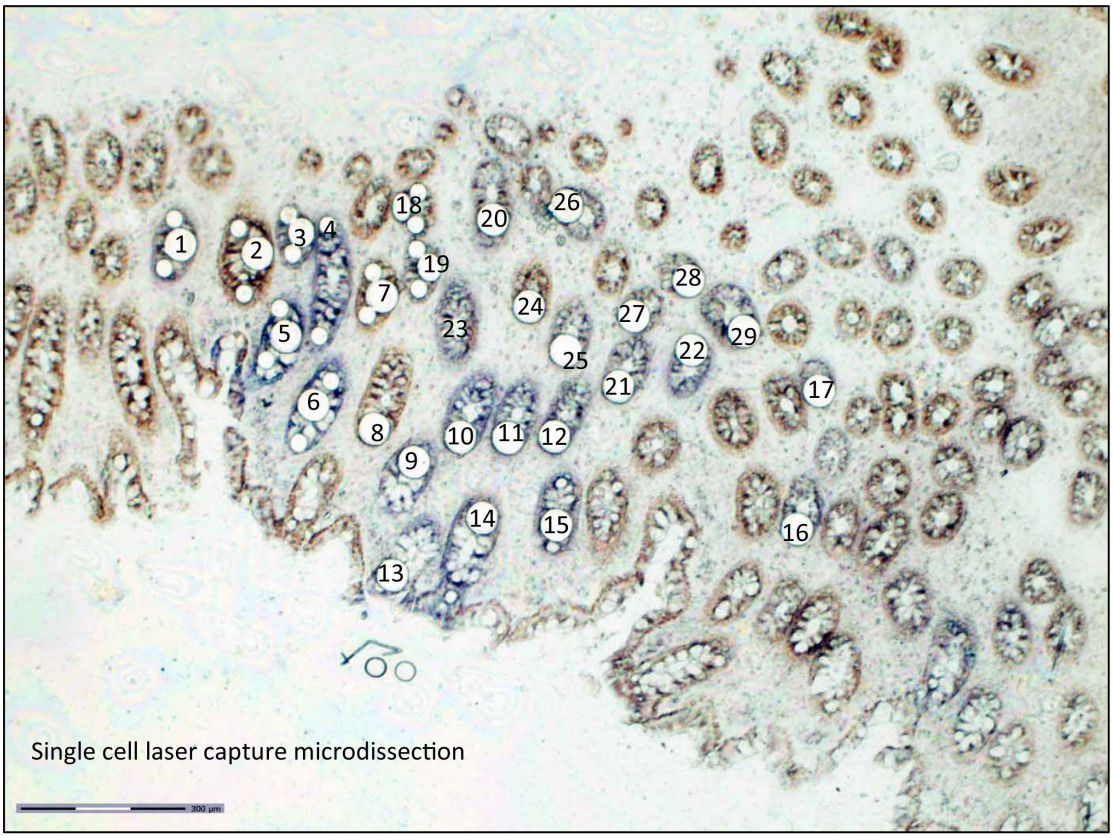

Figure 3.7 Post single cell laser capture microdissection of CCO^- cells from the CCO^- crypts, and of CCO^+ cells from adjacent CCO^+ crypts. CCO^- and CCO^+ crypts have been numbered to aid analysis.

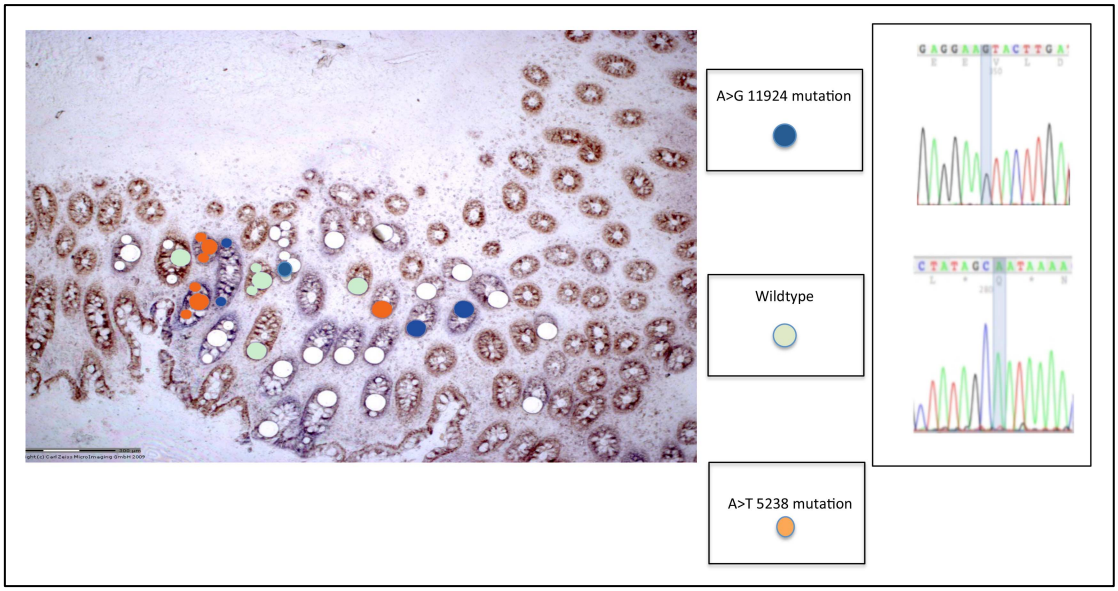

Figure 3.8 MtDNA Sequencing of CCO$^-$ cells from the CCO$^-$ crypts identifies two clonal populations. One clone was defined by a synonymous mutation, A>G in the MT-ND4 gene at position 11924. Both the mutation and wildtype sequence are shown on the right, and are colour coded to highlight the clonal crypts on the image on the left, and the wildtype crypts (CCO$^+$/brown crypts). A further clonal mutation (synonymous mutation A>T) was identified in the MT-ND2 gene at position 5238, depicted by an orange circle (mutation sequence not shown). Thus two, clones exist here in a patch and appear to map cross a considerable physical distance across the section.

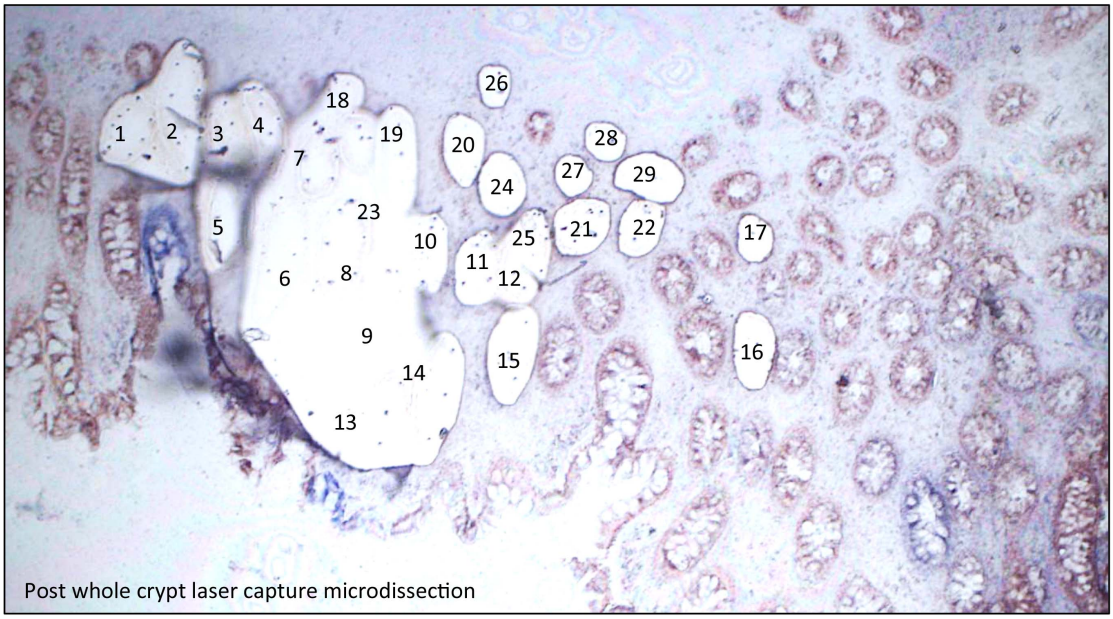

Figure 3.9 Post laser capture microdissection of CCO^- and CCO^+ crypts. This is to allow the DNA to be bisulphite treated and used for PCR.

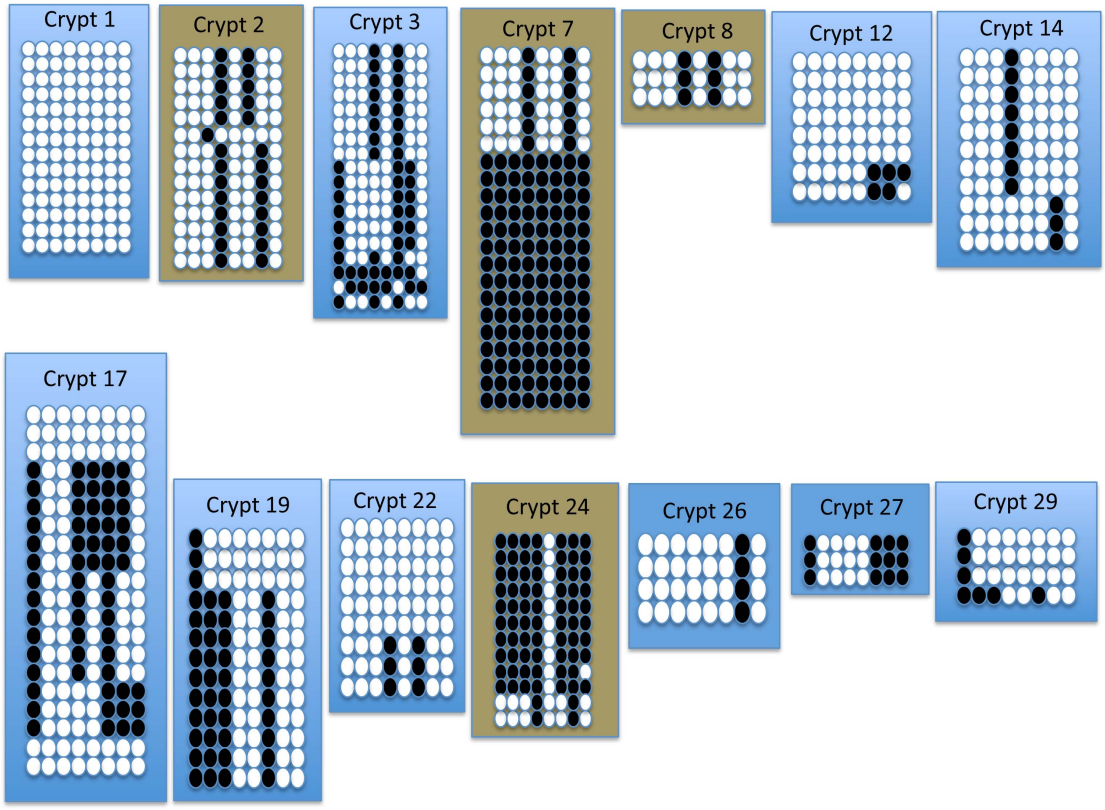

Figure 3.10 Post laser capture microdissection of a clonal patch demonstrating methylation signatures for the *CSX* locus. PCR products were cloned and individual clones were then sequenced. *CSX* methylation tags are shown for blue and brown crypts. Here the clonally related crypts have very dissimilar methylation patterns.

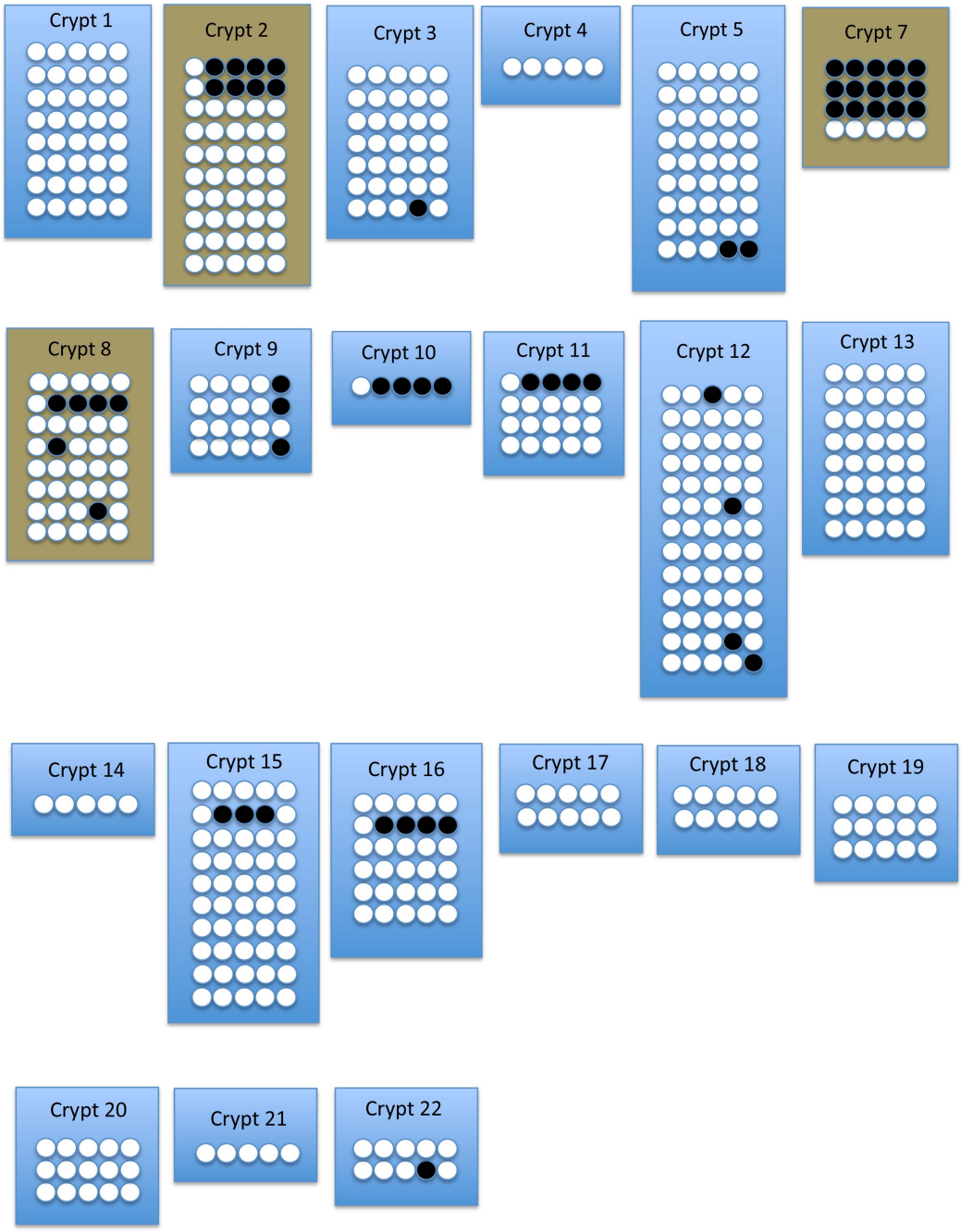

Figure 3.11 Post laser capture microdissection of clonal patch demonstrating methylation signatures for the *MYOD* locus. PCR products were cloned and individual clones then sequenced. *MYOD* methylation tags are shown for blue and brown crypts. The clonally related crypts have a high degree of hypomethylation making interpretation of methylation signatures suboptimal.

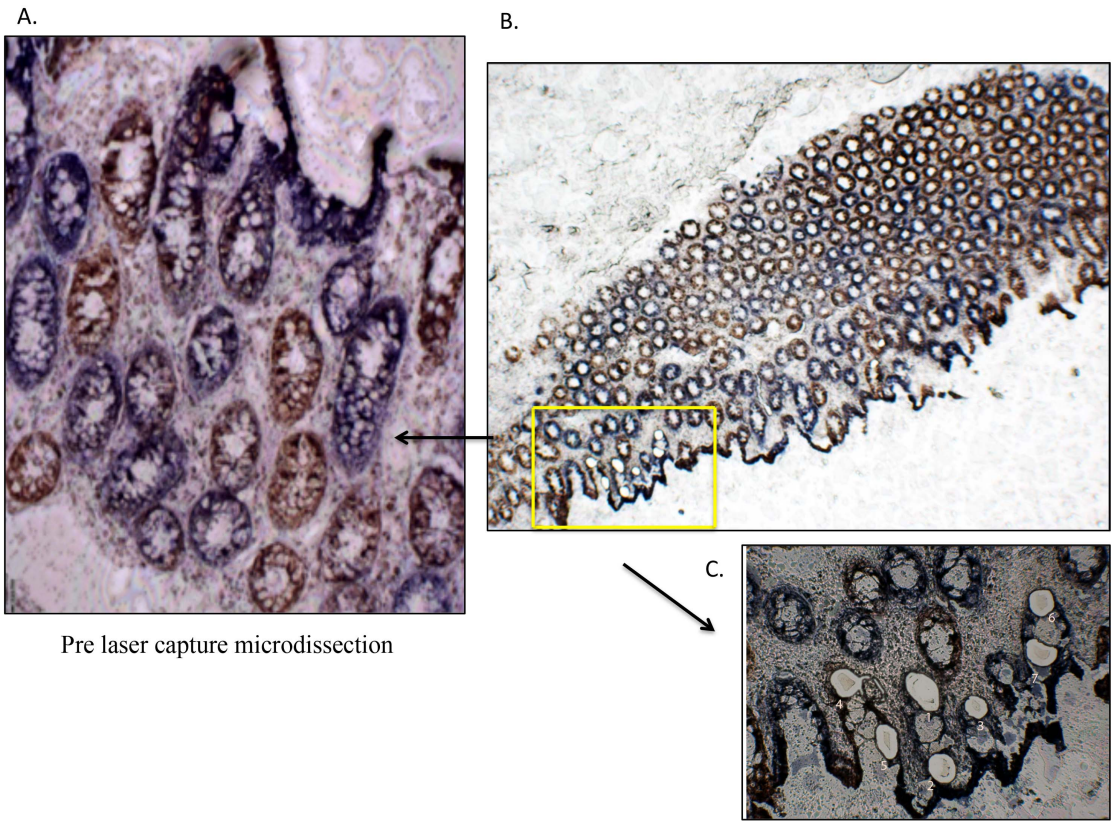

D.

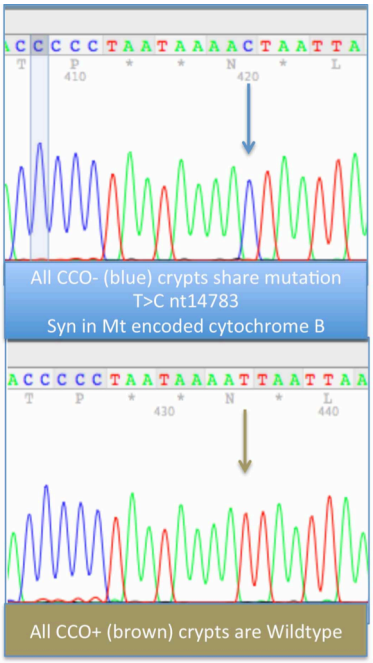

Figure 3.12 Cytochrome *c* oxidase staining of ulcerative colitis tissue identifies stem cell clones within crypts of a 35 year old male. A. Cytochrome *c* oxidase staining of UC mucosa showing patch of CCO^- crypts with distinct CCO-deficient, blue cells. **B.** Overview of patch (boxed). **C.** Post single cell laser capture microdissection of CCO^- crypts and CCO^+ cells from adjacent crypt. D. CCO^- cells have a clonal mtDNA mutation (T> at nt14783, Mt CYB gene); CCO^+ cells are wildtype.

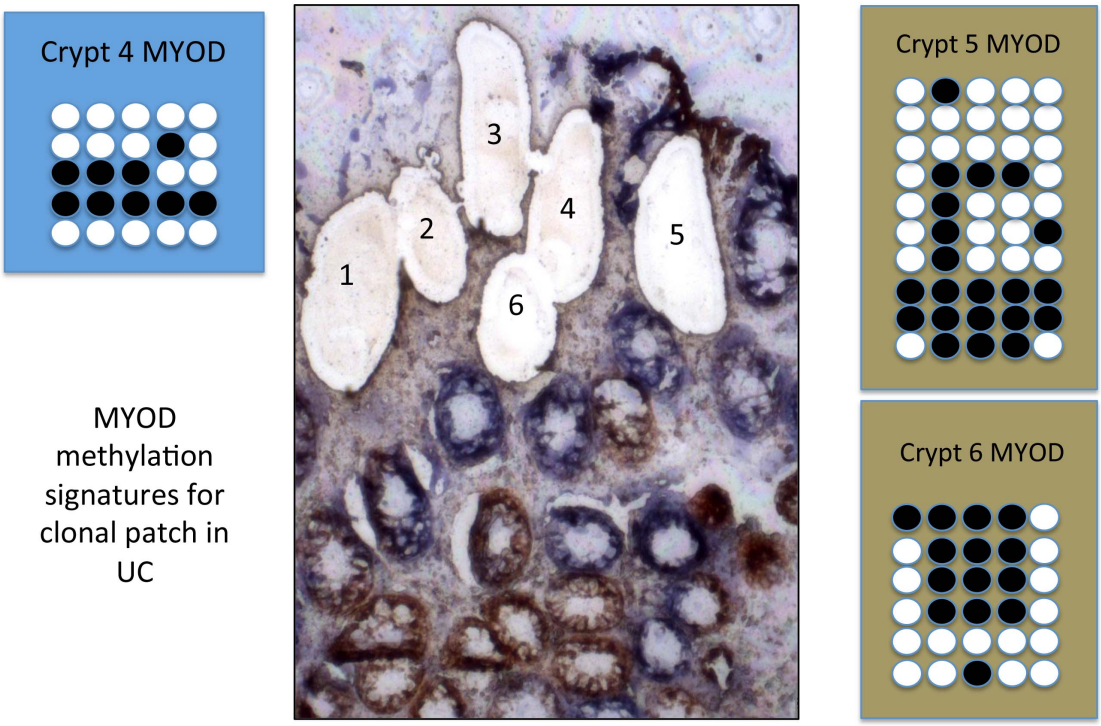

Figure 3.13 Post laser capture microdissection of clonal patch demonstrating methylation signatures for the *MYOD* locus. PCR products were cloned and individual clones were then sequenced. *MYOD* methylation tags are shown for blue and brown crypts. Only one population of blue crypts is shown here because the quality of the DNA extracted was not sufficient for PCR amplification, making interpretation of clonal expansion difficult.

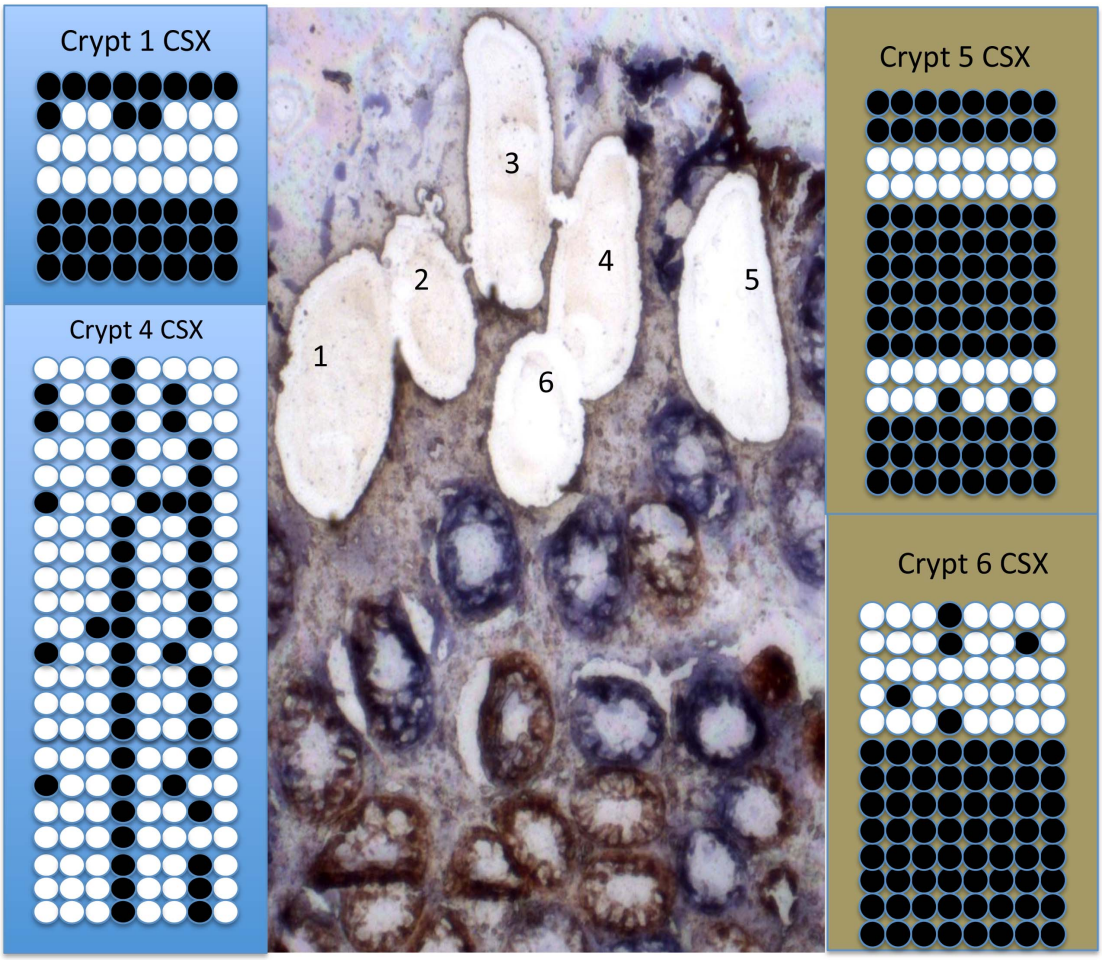

CSX methylation signatures for clonal patch in UC

Figure 3.14 Post laser capture microdissection of a clonal patch demonstrating methylation signatures for the *CSX* locus. PCR products were cloned and individual clones were then sequenced. *CSX* methylation tags are shown for blue and brown crypts. The clonally related crypts share no similar methylation patterns.

The clonal patch methylation signatures in Figures 3.13-3.14 showed there was no relationship between crypts that are clonally related, although for Figure 3.13 only one blue crypt was PCR amplified successfully. Two clonally related crypts for the *CSX* were analysed, and there was no relationship between the methylation patterns and crypts that were clonally related. They were as dissimilar as unrelated crypts.

3.2.3 Niche succession is increased in active IBD

The number of unique methylation patterns in crypts (tags) in patients with active IBD was compared to those with inactive disease. An increased rate at which a single stem cell populates the niche within active IBD crypts was found (Figure 3.15). There was a significant difference between the numbers of unique patterns in crypts from active compared to inactive IBD ($p<0.0001$; two-tailed Students's t-test). Such expansion may facilitate the establishment of protumourigenic mutations within crypts.

3.2.4 Stem cell dynamics are altered by CCO-deficiency

To show that stem cell dynamics of CCO^- crypts were no different to wild-type CCO^+ crypts, statistical analysis of crypt methylation tags comparing blue and brown crypts was performed. The *inter-crypt distance* (the average similarity of all methylation patterns in the first crypt to all the methylation patterns in the second crypt) did indicate that the *MYOD* methylation patterns were similar in adjacent CCO^- crypts ($p<0.0001$, two-tailed Student's t-test) (Figure 3.16). However, no significant difference was observed at the *CSX* locus ($p=0.2596$, two-tailed Student's t-test) (Figure 3.17), although the overall trend showed the intercrypt distance in the related crypts was lower than in the unrelated crypts, as seen in the *MYOD* data set.

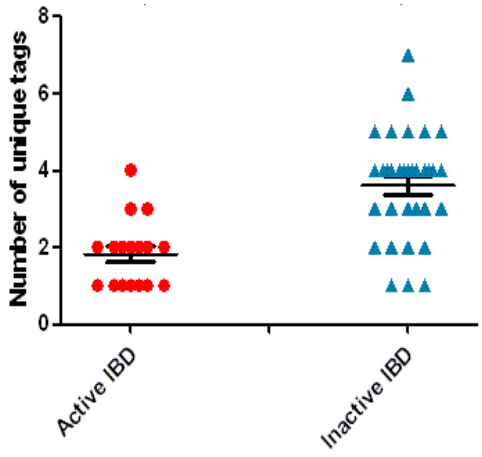

Figure 3.15 Unique methylation patterns in crypts from active inflammatory bowel disease compared to inactive disease. There was a statistically significant difference between the numbers of unique methylation tags in active IBD compared to inactive IBD (n=5 patients; p<0.0001; two-tailed Student's t-test). Although there were more unique methylation tags in the active than the inactive IBD crypts this cannot be generalised to patients on account of the small number of subjects.

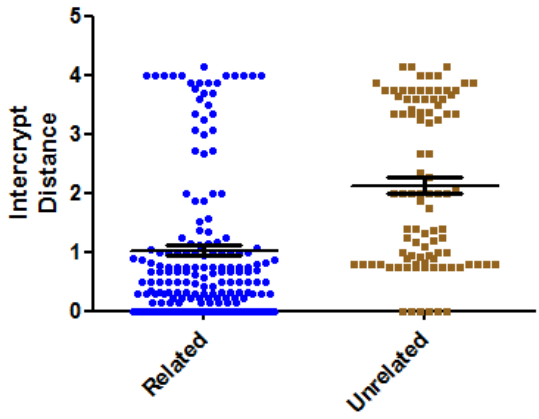

Figure 3.16 Epigenetic distances for the *MYOD* locus comparing related CCO^- crypts versus unrelated CCO^+ crypts. There was a statistically significant difference between the intercrypt distances of CCO^+ and CCO^- crypts (n=5 patients; p <0.0001; Two-tailed Students's t test;). Both related and unrelated crypts have a subpopulation closely related in terms of methylation patterns and a subpopulation that is more unrelated (>3), despite related crypts being more similar overall.

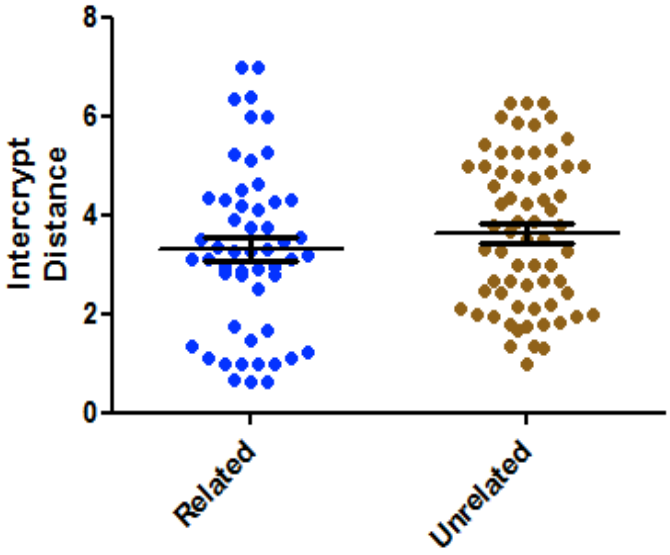

Figure 3.17. The epigenetic distances for the *CSX* locus comparing related CCO^- crypts versus unrelated CCO^+ crypts. There was no statistically significant difference between the intercrypt distances of related CCO^- and unrelated CCO^+ crypts (n=5 patients; p=0.2596; two tailed Student's t-test). Both groups appear to have 2 discrete populations some with high intercrypt distance (>3), some low (<2), suggesting a sharing of some features between related and unrelated cyrpts.

3.2.5 Patches of related crypts have similar *MYOD* methylation patterns indicating recent crypt fission

It is most probable that patches of adjacent CCO^{-} crypts are derived from an ancestral CCO^{-} crypt that underwent fission (Taylor et *al*. 2003; Greaves et *al*. 2006). In human IBD colon, adjacent clonally related CCO^{-} crypts had similar methylation patterns indicating recent crypt fission, as evidenced by the use of the *MYOD* locus ($p<0.0001$). However, when the *CSX* gene was used there was no statistically significant difference between the two groups, although the overall trend was that adjacent clonally related CCO^{-} crypts had a lower intercrypt distance than the unrelated crypts. This indicated that crypt fission was likely to have occurred more recently as there was less time for the methylation patterns to diversify. Previous studies suggested that of the two genes, *CSX* is the more reliable; but not as many colonies were sampled here compared to the *MYOD* PCR, and this meant, perhaps, that the *CSX* results did not reach statistical significance. Ideally, for future studies a third gene would be used to support these findings. In contrast, adjacent unrelated crypts had dissimilar methylation patterns, indicating that crypt fission rates are slow and resemble that of normal colon. The numbers of unique methylation patterns in crypts from active IBD were significantly less than those obtained from inactive IBD patients suggesting that niche succession is elevated in IBD.

The *intercrypt distance*, which measures the average similarity of all methylation patterns in the first crypt to all the methylation patterns in the second crypt, indicated that *MYOD* methylation patterns were more similar in adjacent CCO^{-} crypts ($P = <0.0001$, Student's t test). However, no significant difference was observed at the *CSX* locus. Therefore, the clonal relation indicated by adjacent crypts both having CCO-

deficiency was not mirrored by increased similarity of the methylation patterns of the 2 crypts across all loci studied.

3.4 Discussion

In human IBD colon, adjacent clonally related CCO^- crypts had similar methylation patterns, indicating recent crypt fission. This was found when the *MYOD* locus was examined. Using the *CSX* locus, there was no statistically significant difference between the methylation patterns of adjacent clonally related and adjacent unrelated crypts, however, the overall trend was that the intercrypt distance between methylation signatures of clonally related crypts was lower than the intercrypt distance of unrelated crypts indicating that they had less time to diversify, thus crypt fission was quicker than in unrelated crypts.

This would imply that crypt fission rates are slow, as a long time has passed to allow the methylation patterns to diversify. These results resemble that of normal colon (Shibata et *al*. 2001; Graham et *al*. 2011). It would be expected that *CSX* would be a more sensitive and robust molecular clock marker than *MYOD* given the fact that it has considerably more CpG islands than *MYOD*. However, the selection of methylation-susceptible locus also influences the ability to infer clonality. Certainly in the study by Graham and colleagues (Graham et *al*. 2011) the *CSX* tags appeared to record ancestry more effectively than *MYOD1* or *BGN*. This differential ability to record ancestry is probably secondary to both the locus and CpG-site specific (de)methylation rates and the summary statistic used. Contrary to expectations, merely increasing the number of CpG sites probed does not, in the long-term, result in a decrease in the average pair-wise distance between the methylation tags from related

crypts. This is because epigenetic drift through random methylation is more significant when a greater number of CpG sites are considered. Although X-linked loci in males (mono-allelic loci) simplify clonality inference, utilizing summary statistics to compare relative diversity between clones allows the use of non-X-linked loci. Summary statistics to describe methylation pattern diversity must also be chosen with care. Sampling more tags from a clone, for example, will uncover occasional new methylation patterns, which may signify *de novo* methylation events in the non-stem cell compartment. Average measures, like the intraclone distance are more robust methylation pattern diversity markers. The discrepancy between loci may also be due to intrinsic differences in the properties of CpG islands: it may be that *MYOD* is slower to diversify, such that methylation patterns appear more closely related despite them being not closely related.

It has been described and documented in the past that different loci representing molecular clocks do not always concur (Graham et *al*. 2011). Sometimes a third locus has been used, for example biglycan (*BGN*). I did try to analyse *BGN* methylation signatures in one patient however it was very heavily methylated and future work needs to select with care a third non-expressed neutral locus to test.

A study that examined the difference between methylation patterns of CRC crypts disagrees with the findings in IBD crypts. Siegmund and colleagues found that the methylation patterns did not correlate with the physical separation of the crypts. They drew the conclusion that carcinogenesis was typified by initial rapid expansion ensued by a phase of relative size restriction (Siegmund et *al*. 2009). Yet, the reliability of methylation patterns as clonal markers in CRCs is debatable. Whether methylation

rates in cancer tissue are analogous to those in normal tissues is ambiguous. In UC patients, for example, there are increased levels of methylation (Issa et al. 2001). Increased methylation rates lead to a more accelerated disturbance of any ancestral epigenetic log. Furthermore, Graham and colleagues showed (Graham et *al*. 2011), that the increased stem cell number expected in cancer crypts, (Barker et al. 2007; Siegmund et *al*. 2009), and the altered niche dynamics (Kim et *al*. 2004) and propensity for asymmetric crypt budding in dysplasia (Preston et *al*. 2003), further complicate clonality inference from methylation patterns.

It is estimated that individual CpGs change their methylation status at the low rate of 2×10^{-5} per division. Yet in normal colon, CCO^{-}clones occupying large areas of a crypt showed multiple methylation patterns, suggesting that niche succession occurs sufficiently slowly to allow *de novo* methylation (Graham et *al*. 2011). To obtain niche succession rates from methylation patterns, this necessitates an exact knowledge of the methylation rate and stem cell division rates. Yet, previous studies also imply that niche succession is slow occurring over many years: the proportion of wholly O-acetyltransferase (OAT) defective crypts in radiotherapy-treated $OAT^{-/+}$ individuals increases slowly over 30 years post-radiation therapy, suggesting that OAT^{-} cells can take over a decade to achieve dominance in some crypts (Campbell et *al*. 1996).

Elevated crypt fission in IBD may explain the extensive dispersion of protumourigenic clones previously observed in IBD. Subsequent cycles of crypt atrophy and mucosal healing by crypt fission may provide a key growth stimulus in the inflamed colon. Furthermore, there appears to be an increased rate at which a single stem cell populates the niche within IBD crypts. Studies have demonstrated that

protumourigenic mutations can spread through the entire inflamed colon suggesting that this occurs at a considerable rate indicating stem cell dynamics are altered in IBD (Galandiuk et *al*. 2012, Leedham et *al*. 2009). Such expansion facilitates the establishment of protumourgenic mutations within crypts.

In summary this chapter has shown that niche succession dynamics can be based on an evaluation of methylation patterns of CCO-deficient clones within crypts. Furthermore, evidence from the *MYOD* locus indicated that clonally related crypts share a more recent common ancestor. Perhaps crypt fission rates are faster in clonally related adjacent IBD crypts. These data support the hypothesis that, in the context of IBD, crypt fission is increased in the inflamed epithelium.

The next chapter will demonstrate the use of mitochondrial DNA mutation patch size analysis to examine the rate of crypt fission in UC compared with data from the normal colon.

CHAPTER 4 DETERMINING STEM CELL AND CRYPT DYNAMICS IN INFLAMMATORY BOWEL DISEASE- PATCH SIZE ANALYSIS

4.1 Introduction

In this chapter I will present the use of mitochondrial DNA mutation patch size analysis to examine the rate of crypt fission in UC compared with normal mucosa data. It has been shown that in normal colonic mucosa, patch size increases with age due to multiple crypt fission events (Greaves et al. 2006).

4.1.1 Hypothesis and aims

Inflammation promotes crypt fission as a reparative response to tissue damage, and as such the proliferative drive induced by continuous inflammation and repair in UC will promote the accumulation of age related mtDNA mutations. Increased crypt fission rate will enhance the expansion of clonally related patches. Thus, my hypothesis is that fission, and therefore patch size will be greater in patients with UC than aged-matched normal controls. Here, I aim to investigate the effect of inflammation on the expansion of clones throughout the intestine by using a neutral marker of clonal expansion.

4.2 Methods

Fresh frozen normal colon (n=15) and UC colon (n=6) tissue samples were collected and sectioned in an *en face* orientation. Two-colour enzyme histochemistry for cytochrome *c* oxidase (CCO) activity was performed to identify clonal populations as detailed in Materials and Methods section 2.5.1 Adjacent crypts completely deficient of CCO activity were recorded as a 'CCO deficient patch' and those with a fraction of

the crypt that was CCO-deficient were designated as 'partial crypts'. The CCO-deficient clone fraction in partial crypts was estimated by recording the number of pixels within the CCO-deficient (blue) and CCO-proficient (brown) areas. Pixel numbers were generated automatically by highlighting the blue and brown areas using the program Photoshop. The numbers and size of clonal patches in colitis patients was compared to non-UC controls.

4.3 Results

As in the healthy colon, CCO-deficient clonal patches accumulate in an age dependent fashion in the UC colon. The mean number of crypts within a CCO-deficient patch was significantly larger in the UC colon than in the normal colon ($p<0.025$, extra sum-of-squares F test; Figure 4.1). In addition we observe a larger percentage of wholly ($p=0.30$, two-tailed Student's t test) and partially CCO-deficient crypts in the UC colon when compared to normal healthy controls (Student's t test; $p= 0.12$) (Figure 4.2).

4.4 Discussion

The proliferative drive induced by continuous inflammation and mucosal repair in UC appears to promote the expansion of CCO-deficient patches. The increase in the proportion of wholly and partially mutated crypts in UC could be explained by crypt hyperplasia with more stem cells present driving fission. An alternative explanation may be that the increase in the proportion of wholly and partially mutated crypts in UC may indicate that either more mtDNA mutations are being generated, or that they are more likely to go to fixation in the cell. This increased rate of clonal expansion

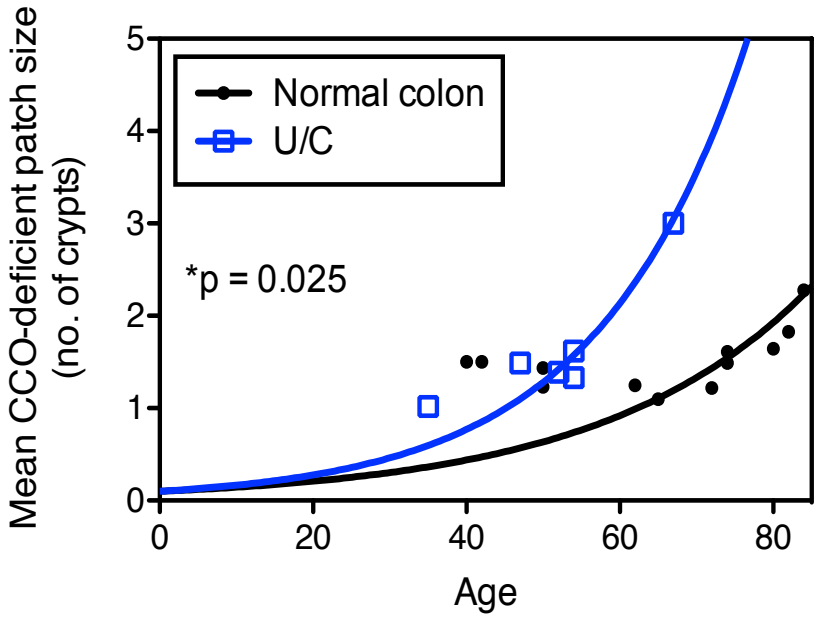

Figure 4.1. Mean CCO-deficient patch size in UC colon (n=6) compared to normal healthy controls. The mean CCO-deficient patch size is statistically significantly greater in UC versus normal healthy controls ($p = 0.025$) by the extra sum-of-squares F test used to test for differences between best-fit curves (n=15). Although there was a statistically significant difference in patch size between UC patients and controls the non-comparable age distributions could be a confounding factor.

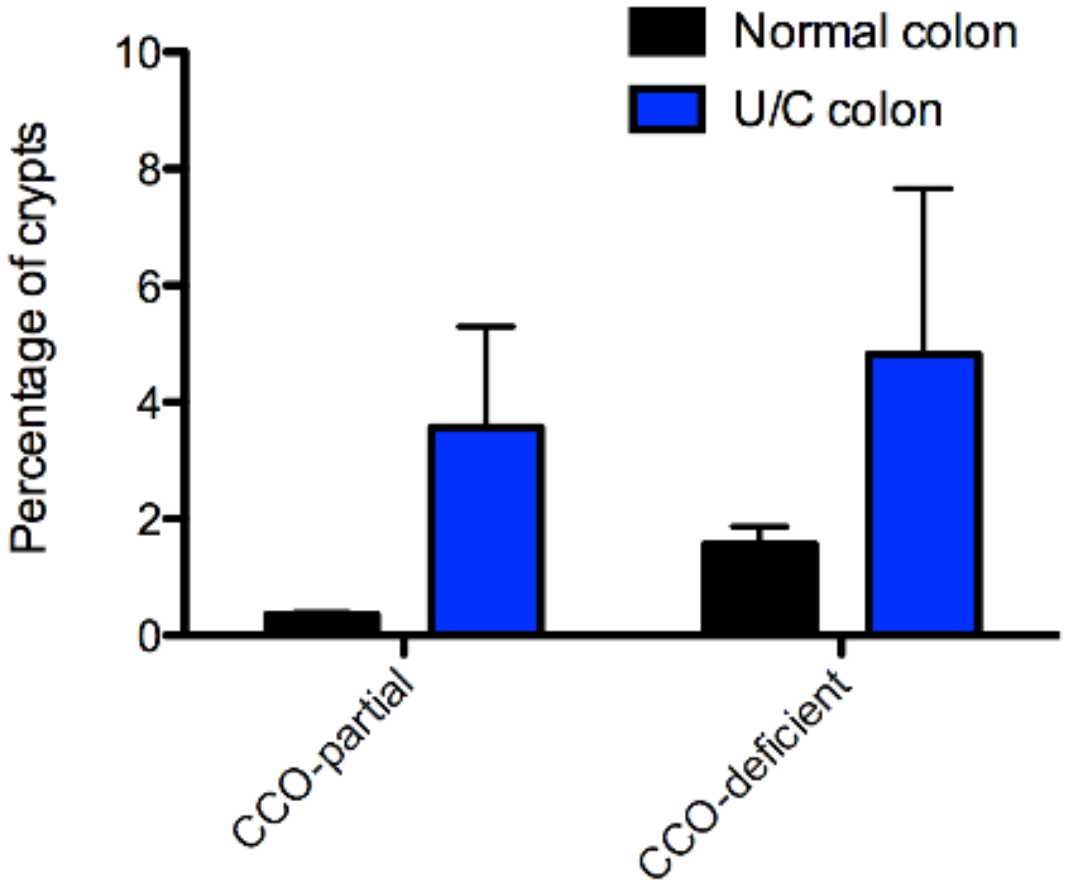

Figure 4.2. Percentage of CCO-deficient (mutant) and partially mutated crypts in UC versus normal healthy controls. There is an increase in the number of partials and wholly mutated crypts compared to normal controls, although this was not significant. Data for normal colon was provided courtesy of McDonald, Greaves and Cereser (Greaves et al. 2006).

may contribute to the increased rate of tumorigenesis in the colitic bowel, however analysis of a larger patient cohort is needed.

Nishikawa and colleagues (Nishikawa et al. 2005) were one of the first groups to show an association with mtDNA mutations in CACRC. They had previously reported that oxidative stress as a result of chronic inflammation increased the mutation of mtDNA, which possibly correlated with a precancerous status (Nishikawa et al. 2001) As severe oxidative stress occurs in the colorectal mucosa of UC patients, they examined the occurrence of mtDNA mutations in the inflammatory colorectal mucosa and colitic cancer specimens. Colorectal mucosal specimens were obtained from UC individuals with and without colitic cancer and from healthy control subjects. The frequency of mtDNA mutations was higher in colorectal mucosal specimens from patients with UC than that from control subjects. The levels of 8-hydroxy-2′-deoxyguanosine, a DNA adduct by reactive oxygen species, were significantly higher in UC than in control. Specimens from patients with colitic cancer had a significantly higher number of mtDNA mutations. Nishikawa and colleagues suggested that the injury followed by the regeneration of intestinal mucosal cells associated with chronic inflammation caused accumulation of mtDNA mutations (Nishikawa et al. 2001). These workers further suggested that the increased instability of genes, including those on the mtDNA, corroborated with the high and multicentric incidence of CRC in UC patients. In some respects, their findings do support our observational data, albeit with small numbers (n=6), on the larger percentage of wholly mutated and partially mutated crypts seen in UC compared to normal individuals. Perhaps, then, a partial explanation for our observations is that increased injury and repair promotes accumulation of mtDNA mutations, via increased ROS. Plus the increased

proliferative drive induced by continuous inflammation and mucosal repair in UC promotes the expansion of CCO-deficient patches.

A second study published last year implicated mt DNA mutations as an associated factor in UC carcinogenesis. The authors concluded that CCO loss precedes tumour progression in UC and may be a biomarker in UC cancer progression (Ussakli et al. 2013). The authors suggested that loss of CCO represents a reduction of the number of mitochondria in preneoplasia and that this is restored in cancers, and detectable by quantification of mtDNA. It is surprising that there was only limited consideration given to the possibility that some of the changes found were due to the clonal expansion of CCO-deficient colonic stem cells.

The suggestion made by Ussakli and colleagues that CCO deficiency is causative in the development of dysplasia/carcinoma in IBD remains unsubstantiated (Ussakli et al. 2013). The data could equally be explained by a series of large clonal expansions. Previous work by the Brentnall group indicated that carcinogenesis in IBD involves large clonal expansions in the premalignant epithelium (Salk et al. 2013) and this has been repeatedly confirmed: Salk and colleagues identified clonal expansions in non-dysplastic epithelium in a UC patient with cancer (Salk et al. 2009). Such passenger mutations have been proposed as markers of clonal cell lineages in emerging neoplasia.

CCO-deficiency marks clonal expansions, which provides an alternative explanation as to why CCO-deficiency predicts the emergence of dysplasia. A critical technical limitation of the study by the Ussakli group is the absence of clonal or

mutational analyses; they observed higher CCO expression in cancer than in surrounding mucosa suggestive of no clonal link between the CCO^- clone and the cancer (Ussakli et al. 2013). Moreover, CCO-deficiency occurs stochastically and is probably selectively neutral, which goes some way to explaining the observed limited specificity of CCO as a biomarker. If indeed CCO is mainly marking a clonal expansion, that expansion may or may not be of a carcinogenic clone. Furthermore, it is always preferable to show CCO expression in frozen sections with double-enzyme histochemistry (Taylor et al. 2003). With regard to the immunohistochemical patterns of CCO expression shown by Ussakli et al. (2013), a single section is insufficient to interpret CCO distribution within a crypt, which requires serial sectioning and reconstruction (Taylor et al. 2003). Moreover, several figures presented in this publication do not appear to show non-specific staining, including non-specific granule-staining in possible Paneth cell metaplasia. A more informative way for Ussalki and colleagues to analyse their data might be to look instead for clonal expansions.

To summarise, the proliferative drive induced by continuous inflammation and mucosal repair in UC appears to promote the expansion of clonal CCO-deficient patches. Thus, the data presented here supports the hypothesis that fission, and therefore patch size are greater in patients with UC than aged-matched normal controls.

I will now turn to the examination of non-clonally related, but spatially adjacent crypts to determine clonal expansion in IBD.

CHAPTER 5 ANALYSIS OF METHYLATION PATTERNS IN ADJACENT AND NON-ADJACENT CRYPTS FROM INFLAMMATORY BOWEL DISEASE PATIENTS

5.1 Introduction

Human colons remain active for many decades following development, but our capacity to decipher ancestral relationships between colonic crypts over the course of the aging process is restricted. However, it is likely that crypts, which are physically distant, probably track their common ancestors to a time near birth.

It is possible to define the destiny of adult crypts using phylogenies - somatic cell trees - to enable the distinction between common ancestor (progenitors) and their descendants (clonal patches), and the distances since common ancestors. Physical distance may function as a proxy for time since a common ancestor. The last possible common ancestor amongst widely spaced crypts is around birth. Thus, neighbouring crypts are likely to be more faithfully related than physically distinct crypts (Kim and Shibata 2004). Using methylation patterns to log crypt lineage, namely to form phylogenies, this connection should be reproduced in the methylation patterns of the crypts**.**

5.1.1 Hypothesis and aims

The hypotheses were as follows: (i) that there is an increased rate of expansion in IBD epithelium; (ii) adjacent crypts are more closely related than non-adjacent crypts because of recent clonal expansion, although this may be dependent on the activity of any inflammatory disease at the time.

The aims of this project was to study the methylation patterns of unrelated cell populations in IBD patients, and in patients with CACRC, and thereby allow a record of the ancestry and stem cell dynamics in this group of patients to be ascertained. Crypts are the functional units of the intestinal epithelium and by comprehending crypt proliferation our understanding of the mechanisms of tumour growth and clonal expansion will be advanced. By studying the methylation patterns of adjacent unrelated crypts, crypt ancestry can be traced.

5.2 Methods

Methylation patterns at CpG sites were measured in colonic crypts from patients described in Table 5.1, that had undergone LCMD. The DNA was bisulphite treated and then half the sample was used for PCR. PCR products were cloned and individual clones were sequenced. Clones with evidence of incomplete bisulphite conversion (ie Cs at non-CpG sites) were eliminated from the analysis. Methylation patterns were sampled at either the CpG rich loci *MYOD* (with 5 CpG sites), and/or *CSX* (8 CpG sites).

Table 5.1 Clinicopathological data of patients analysed.

Patient	Age	Sex	Disease	IBD	Disease Activity
1	50 years	Male	Adenocarcinoma	CD	Quiescent
2	52 years	Male	Adenocarcinoma	UC	Quiescent
3	35 years	Male	Adenocarcinoma	UC	Quiescent
4	29 years	Male	Adenocarcinoma	CD	Quiescent
5	54 years	Male	-	UC	Quiescent
6	29 years	Male	-	UC	Quiescent

Each sequenced molecule is referred to as a 'tag'. Percent methylation was calculated from the number of methylated CpG sites. Distance was calculated by summing the total number of methylation site differences between two methylation tags. Intracrypt distance was the average difference between all possible tag pairs sampled from a single crypt. Intercrypt distance was the average difference between all possible tag pairs sampled between two crypts. Intercrypt distances were measured between adjacent crypts and between non-adjacent crypts (Graham et al. 2011; Kim and Shibata 2004).

5.3 Results

Serial sections of normal colonic tissue taken from a 50 year old male Crohn's patient (Patient no 1; Table 5.1) contained a distinct population of CCO-positive brown crypts (Figure 5.1) and the *MYOD* methylation status of each crypt was established (Figure 5.2). The methylation patterns of neighbouring crypts were very dissimilar, indicating that there was no relationship between the epigenetic distances of crypts that were adjacent versus crypts that were not (Figure 5.2).

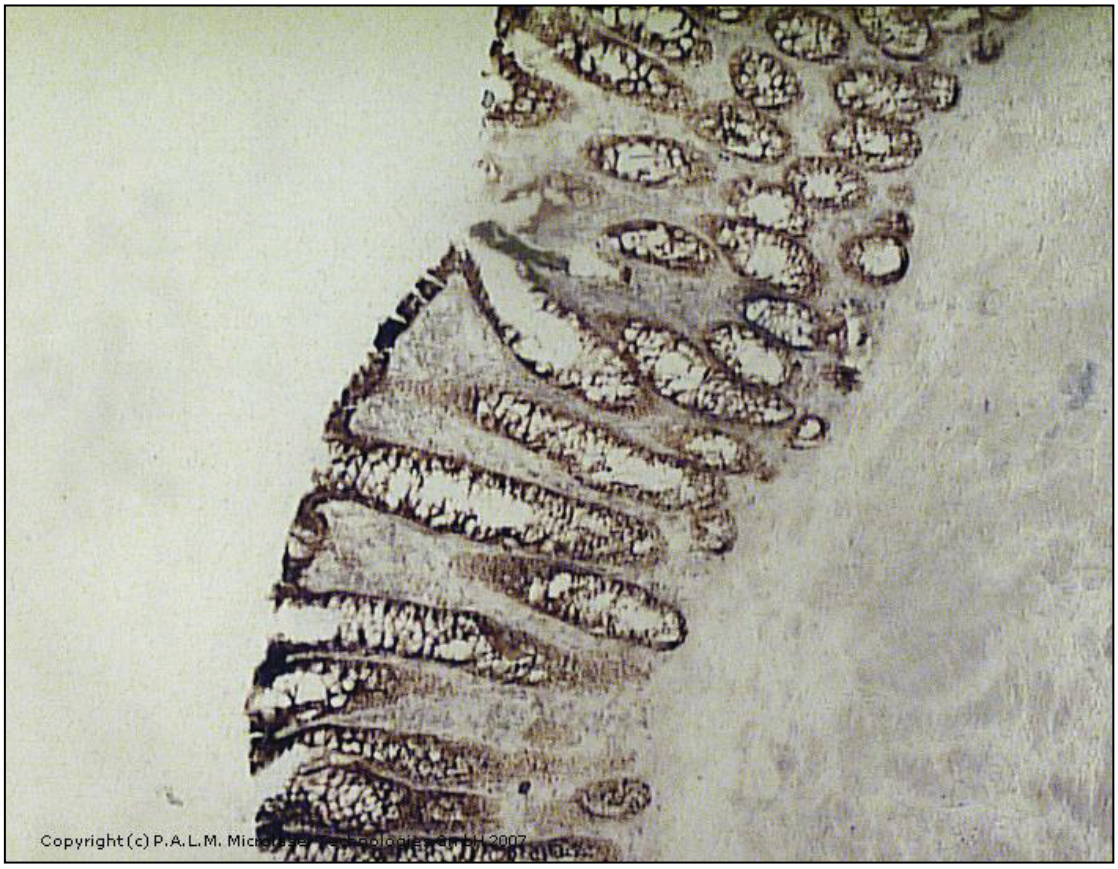

Figure 5.1. Serial section of colonic tissue from a 50 year old male patient with a background history of Crohn's disease, who developed a colitis-associated colorectal cancer. This tissue contains a distinct population of cytochrome *c* oxidase - positive brown crypts taken prior to laser capture microdissection.

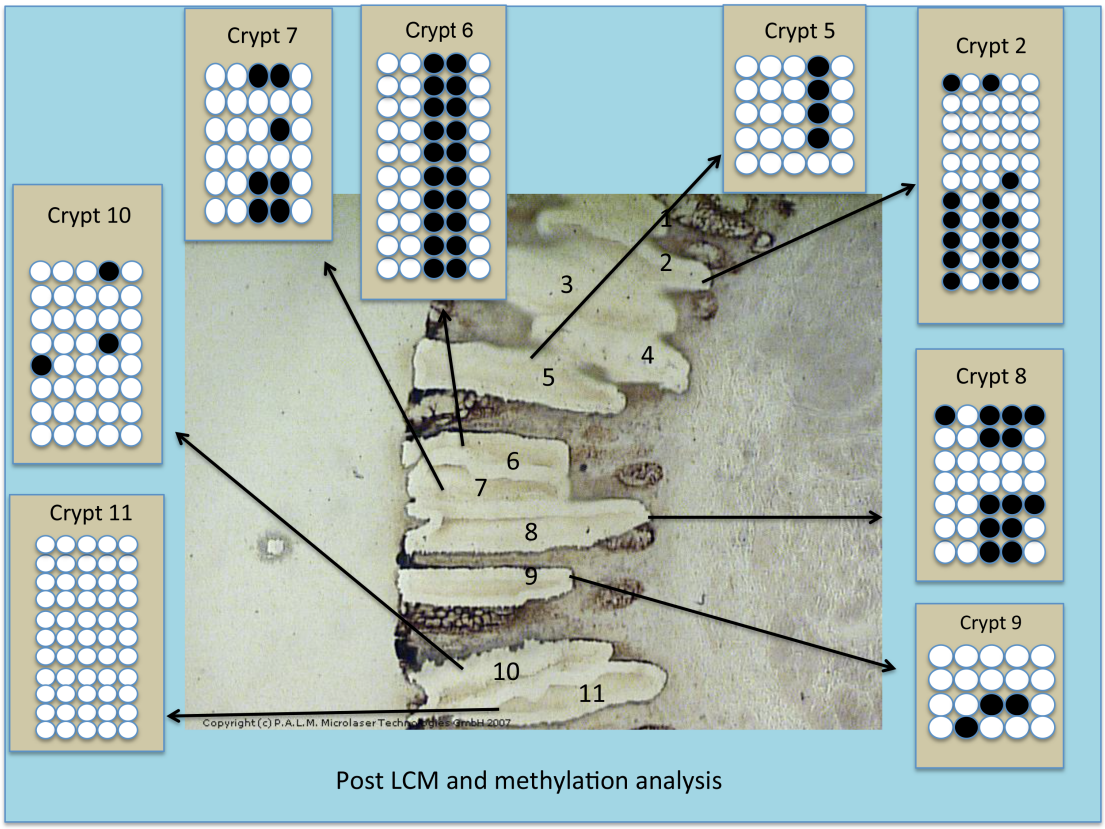

Figure 5.2. Serial section of colonic tissue from a patient with a background history of Crohn's disease who developed a colitis-associated colorectal cancer. The section shows a distinct population of cytochrome *c* oxidase positive brown crypts following laser capture microdissection. The *MYOD* methylation status of each crypt is depicted using the visual methylation tags described earlier. Despite crypts being adjacent or in very close proximity, the methylation patterns appear diverse.

Further analysis was conducted on normal colonic tissue from a 52 year old UC patient (patient number 2; Table 5.1) and *MYOD* signatures established for non-adjacent crypts and adjacent crypts (Figures 5.3-5.7). Although the methylation tags are similar and in some cases identical for neighbouring crypts there was no association between physical distance and the epigenetic status. For example, crypts 1 and 3 (Figure 5.3) have identical methylation signatures although not immediately adjacent to each other (Figure 5.4). Crypts 6 and 7 (Figure 5.5) are adjacent yet their methylation patterns are dissimilar (Figure 5.6). Crypts 7 and 8 are not immediately adjacent (Figure 5.5) but in very close proximity, but share almost identical methylation patterns (Figure 5.6). Crypts 8 and 10 are physically disparate, yet their methylation patterns are almost identical (Figure 5.7).

Figure 5.3. Serial section of colonic tissue from a 52 year old patient with adenocarcinoma of the colon on a background of longstanding ulcerative colitis. This tissue contains a distinct population of cytochrome *c* oxidase -positive brown crypts taken prior to laser capture microdissection.

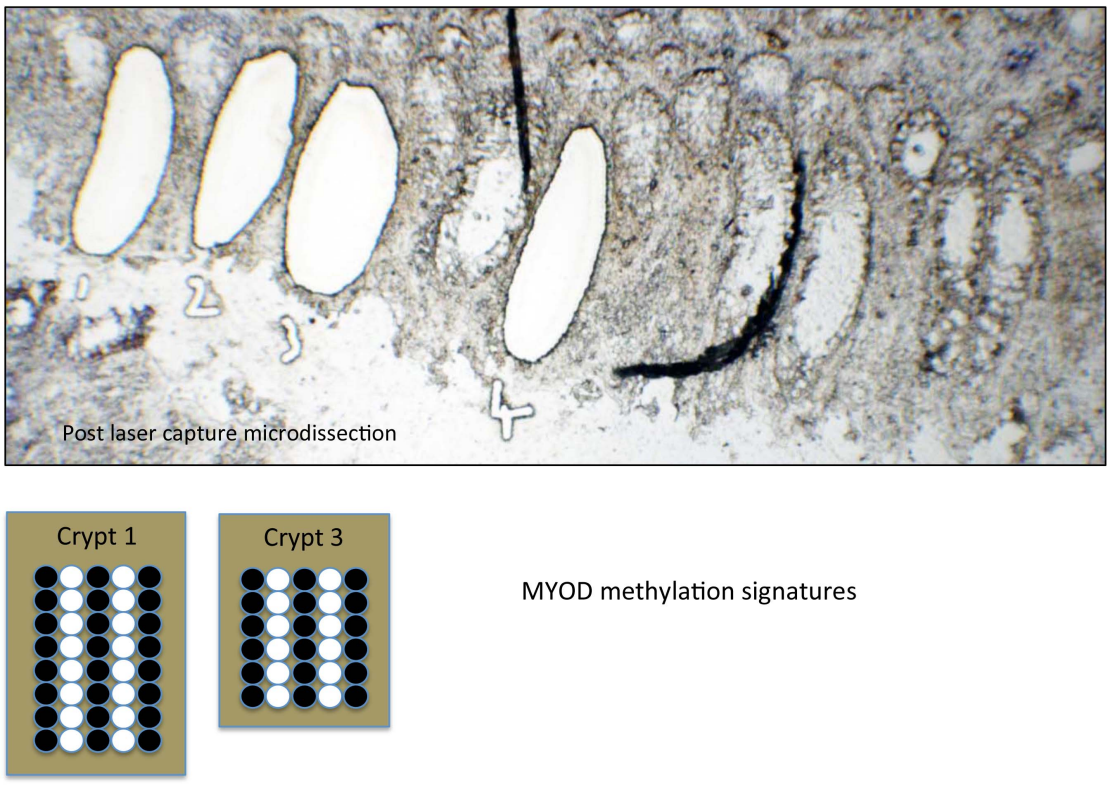

Figure 5.4. Post laser capture microdissection of crypts 1-4 and *MYOD* methylation signatures for crypts 1 and 3 sampled from a 52 year old patient with an adenocarcinoma of the colon on a background of longstanding ulcerative colitis. *MYOD* methylation signatures are illustrated for crypts 1 and 3 and are identical although the crypts are not immediately adjacent to each other.

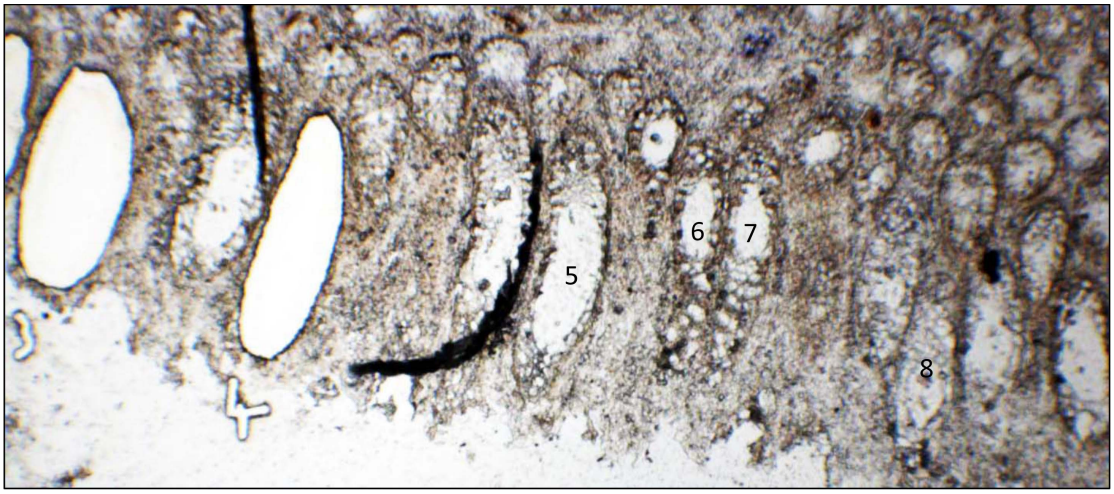

Figure 5.5. Pre laser capture microdissection of crypts 5–8 from a 52 year old patient with an adenocarcinoma of the colon on a background of longstanding ulcerative colitis. Crypts 6 and 7 are adjacent and crypt 8 is at a very short distance to them.

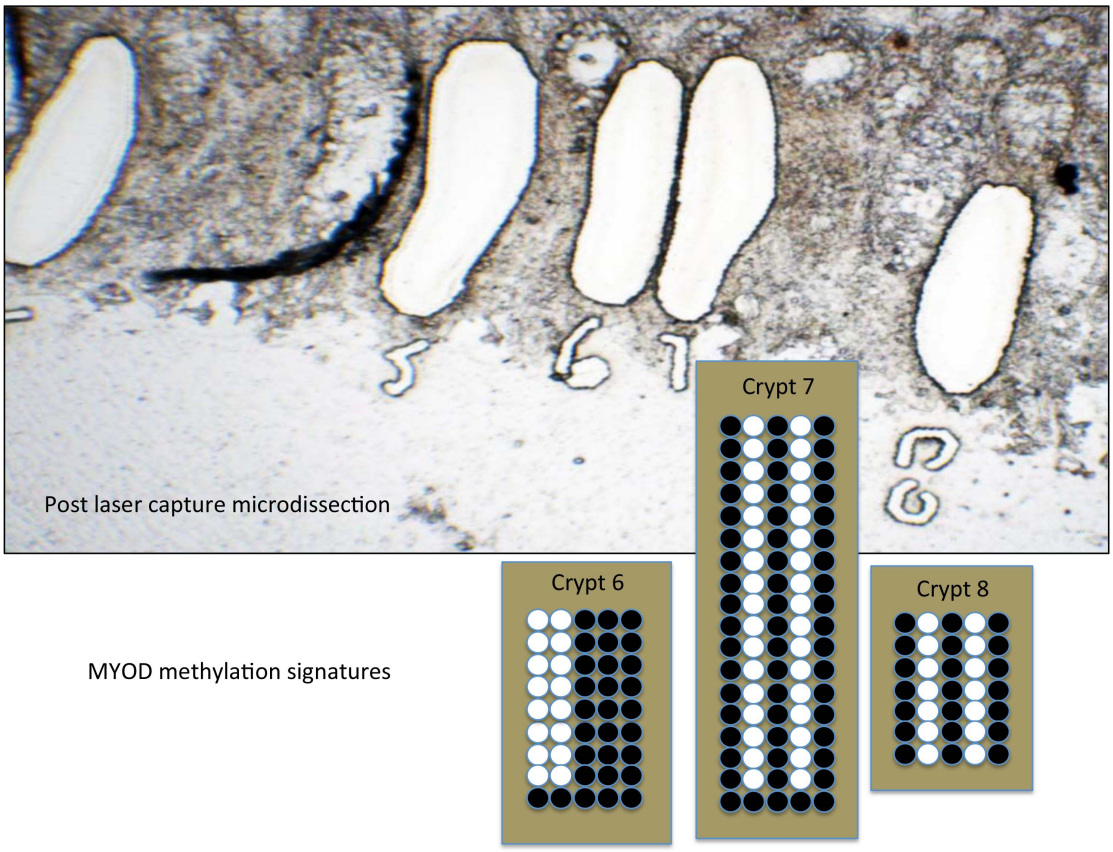

Figure 5.6. *MYOD* methylation signatures for crypts 6, 7 and 8 sampled from a 52 year old patient with an adenocarcinoma of the colon on a background of longstanding ulcerative colitis. Crypts 6 and 7 are adjacent yet their methylation patterns are dissimilar; crypts 7 and 8 are not immediately adjacent but in very close proximity, but share almost identical methylation patterns.

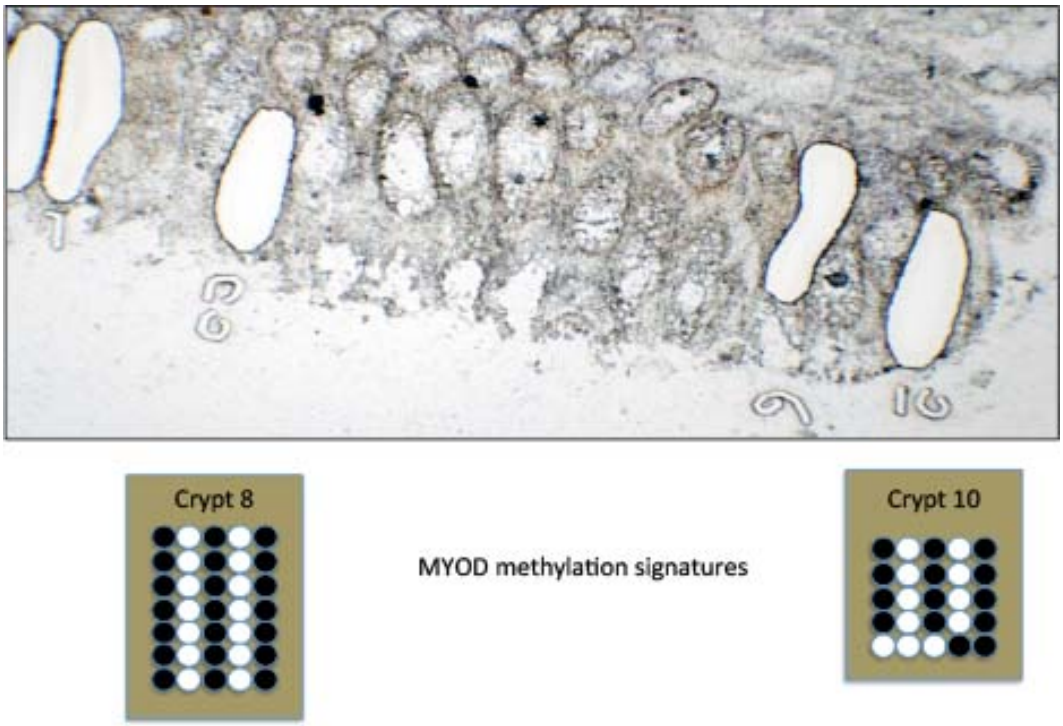

Figure 5.7. Post laser capture microdissection of crypts 8-10 and *MYOD* methylation signatures for crypts 8 and 10 sampled from a 52 year old patient with an adenocarcinoma of the colon on a background of longstanding ulcerative colitis. Crypts 8 and 10 are physically disparate, yet their methylation patterns are almost identical.

The third patient to be analysed was a 35 year old male patient with an adenocarcinoma on a background of UC (patient number 3; Table 5.1). In this example, the gene examined was *CSX*. *CSX* methylation analysis was performed on their colonic tissue (Figures 5.8-5.11) Again, both adjacent crypts and non-adjacent crypts were analysed (Figures 5.8-5.11) and there were no similarities in the methylation patterns between crypts that were adjacent versus crypts that were not (Figure 5.9-5.11). In Figure 5.9 despite all crypts 1-6 being adjacent or in very close proximity, their methylation patterns are very diverse. In Figure 5.10, crypts 6 and 7 are separated and crypts 6 and 10 are also separated at a distance. Similarly, the methylation signatures of these crypts are diverse, despite the crypts being adjacent or in very close proximity. The last crypt sampled, number 12, in Figure 5.11, shows that the methylation patterns in crypt 12 are very different from the methylation patterns seen in neighbouring crypts 6-10 (Figure 5.10).

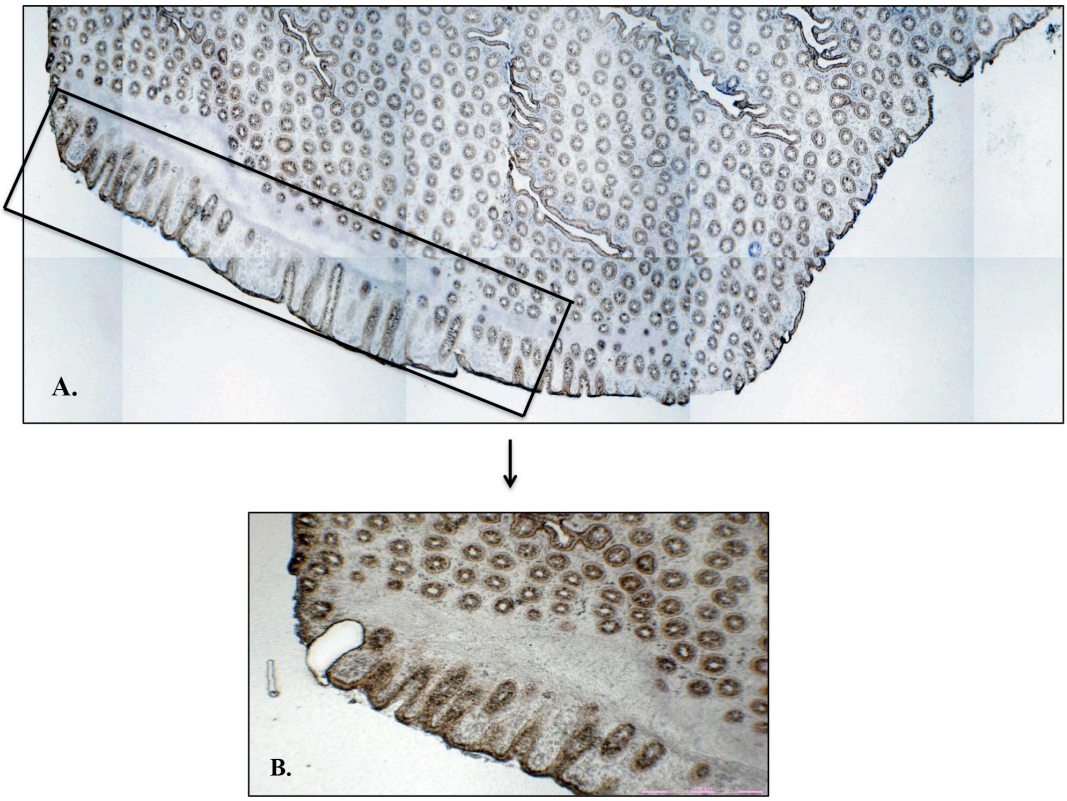

Figure 5.8. Laser capture microdissection of colonic serial sections taken from a 35 year old male with adenocarcinoma of the colon on a background of quiescent ulcerative colitis. A. Selected serial section identified (boxed). **B**. Post laser capture microdissection of crypt 1 (CCO^{+}).

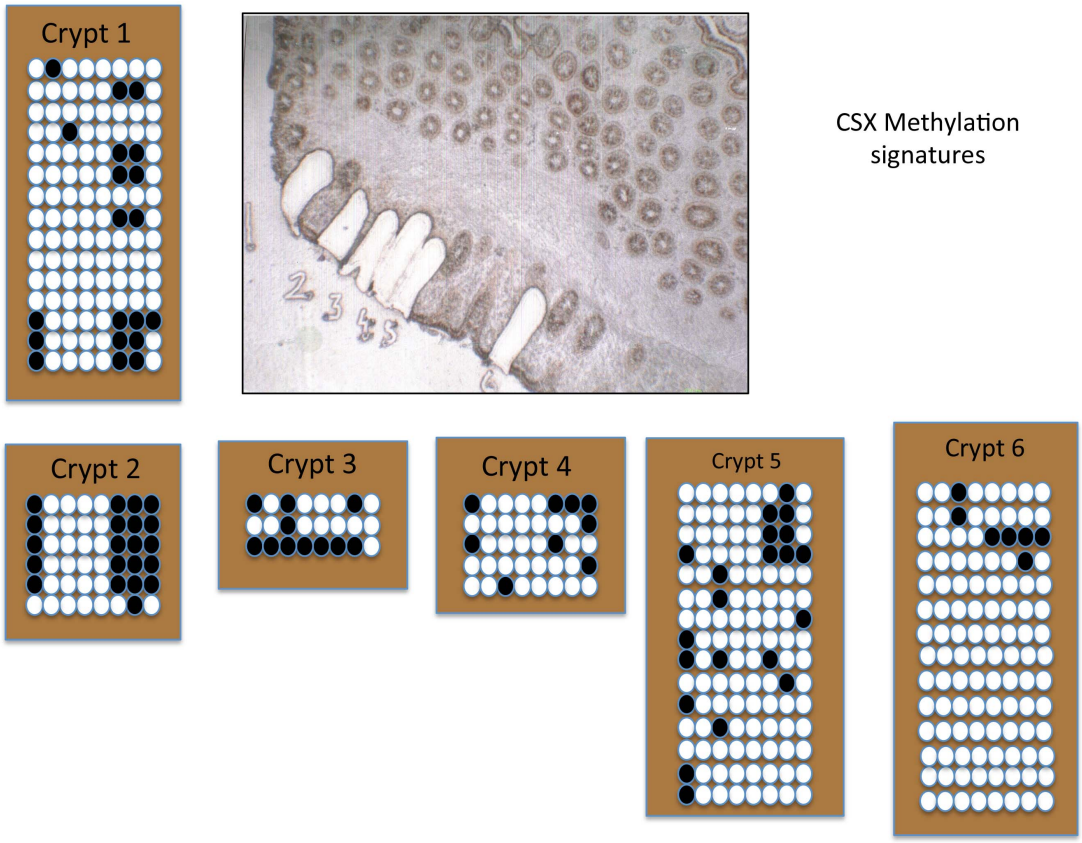

Figure 5.9. Post laser capture microdissection of crypts and methylation signatures depicted for the *CSX* locus for 35 year old male with adenocarcinoma on a background of quiescent ulcerative colitis. Image is taken at x 100 magnification. Despite the crypts being adjacent or in very close proximity, their methylation patterns are very diverse.

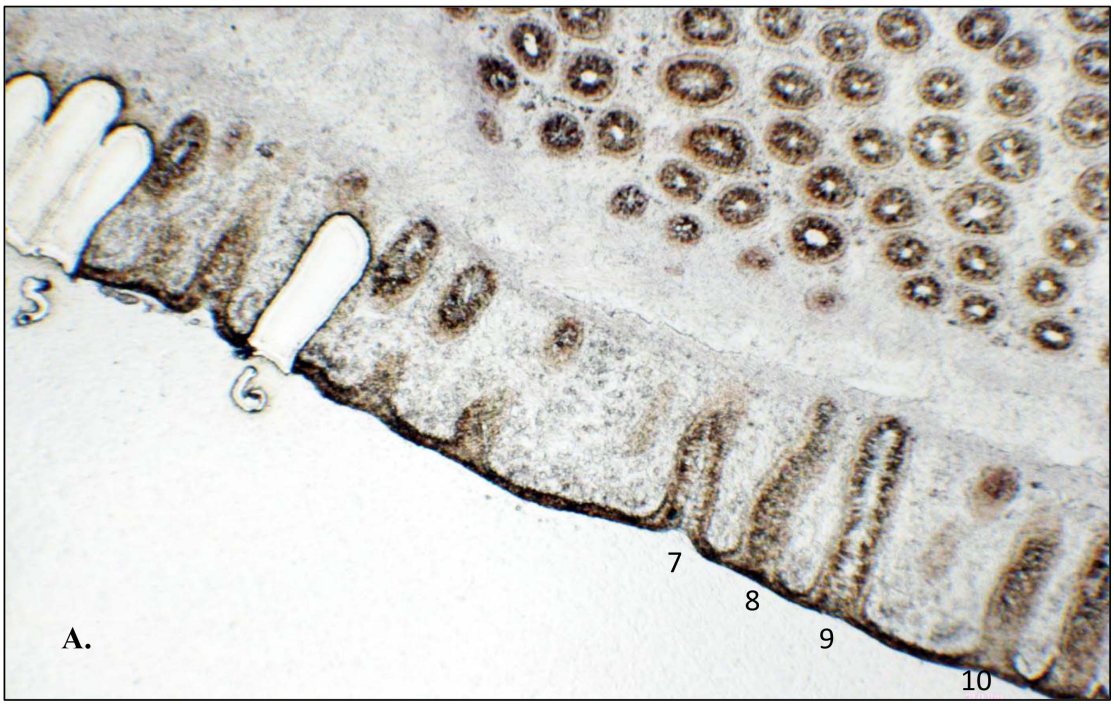

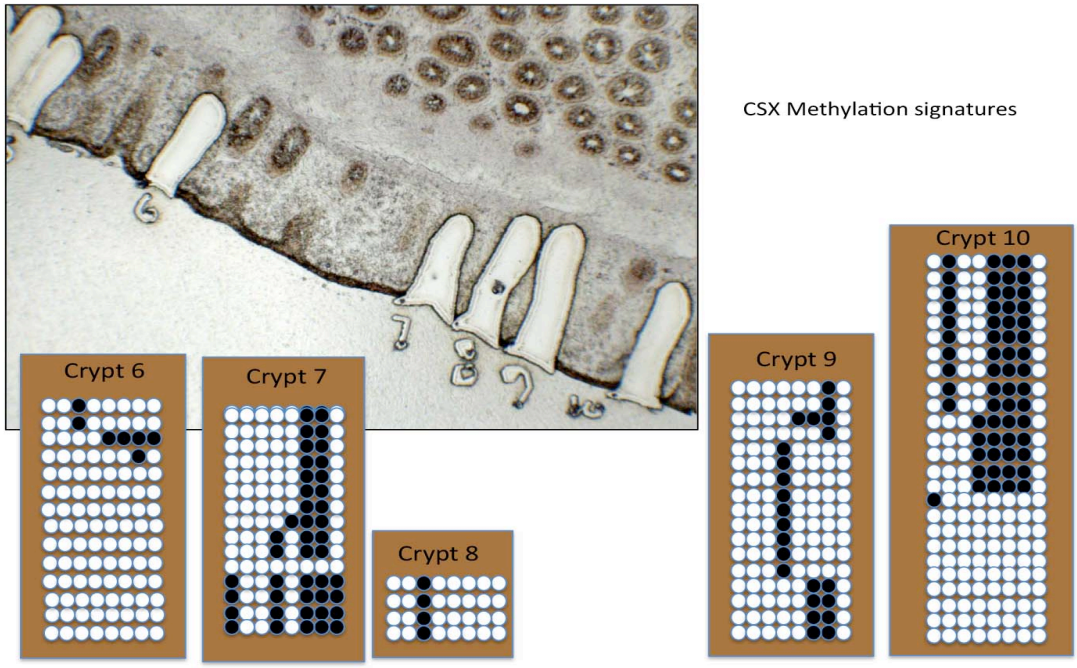

Figure 5.10. Pre and post laser capture microdissection of crypts from a 35 year old UC patient with adenocarcinoma. A. Pre laser capture of crypts 6-10. **B.** Methylation signatures for *CSX* locus for crypts 6-10. Crypts 6 and 7 are separated and crypts 6 and 10 are also separated at a distance. The methylation signatures of these crypts are diverse, despite the crypts being adjacent or in very close proximity.

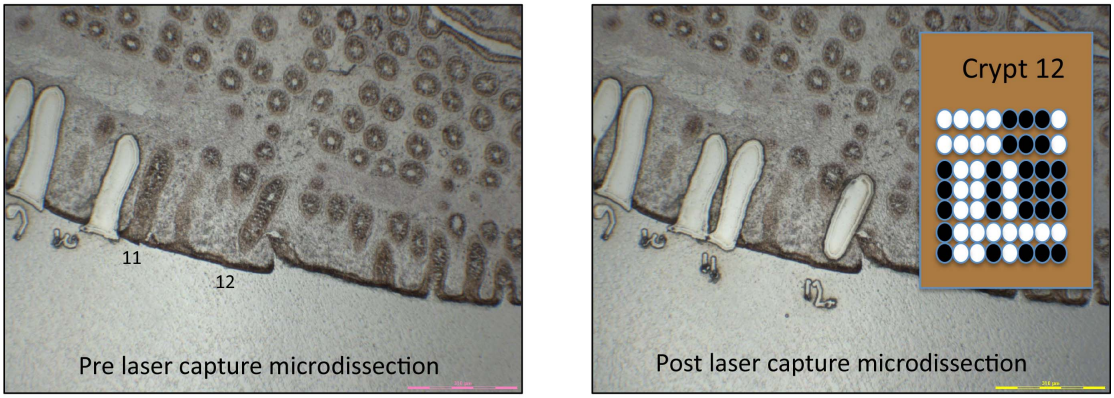

Figure 5.11. Pre and post laser capture microdissection of crypt 12 from a 35 year old UC patient with adenocarcinoma. The methylation signatures for *CSX* for crypt 12 is shown in the post laser capture image. Notably the methylation patterns in crypt 12 are very different from the methylation patterns seen in neighbouring crypts 6-10 (Figure 5.10).

The fourth patient to be examined was a 29 year old male with quiescent Crohn's colitis with an adenocarcinoma (patient number 4; Table 5.1). Adjacent and non-adjacent crypts were LCMD and their *CSX* methylation signatures analysed (Figures 5.12-5.14). In Figure 5.12, crypts 3-7, although adjacent they have *CSX* methylation signatures that are dissimilar. Figure 5.13 demonstrates the methylation signature for the *CSX* locus for crypt 9, again dissimilar to neighbouring crypts 3-7 (Figure 5.12) and crypts 10-11 (Figure 5.13). In Figure 5.14, the adjacent crypts 10 and 11 share no identical methylation signatures, in the *CSX* locus, and are quite diverse. Again, it is overwhelmingly apparent that despite crypts being adjacent, their methylation signatures were no more similar than when you compared them to non-adjacent crypts further along the tissue section (Figures 5.12-5.14).

The fifth patient analysed was a 54 year old male patient with UC (patient number 5; Table 5.1). Figures 5.15 and 5.16 depict pre and post LCM and the *CSX* methylation patterns that were identified. Crypts 6 and 8 are not immediately adjacent. However, they are in close proximity and share some methylation signatures, whilst adjacent crypts 11 and 12 do not (Figures 5.15-5.16). Crypt 12 had some very distinct unique tags not seen in crypts 6, 8 or 11 (Figure 5.16). Thus, in this example, there are some unique tags shared amongst all the crypts, correlating with their physical proximity, but this did not hold true for all crypts (Figure 5.16).

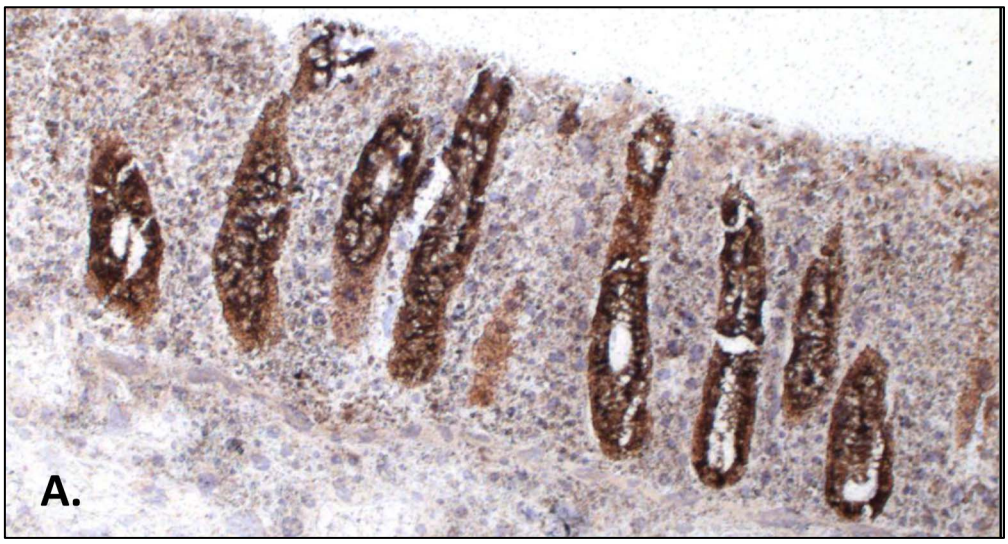

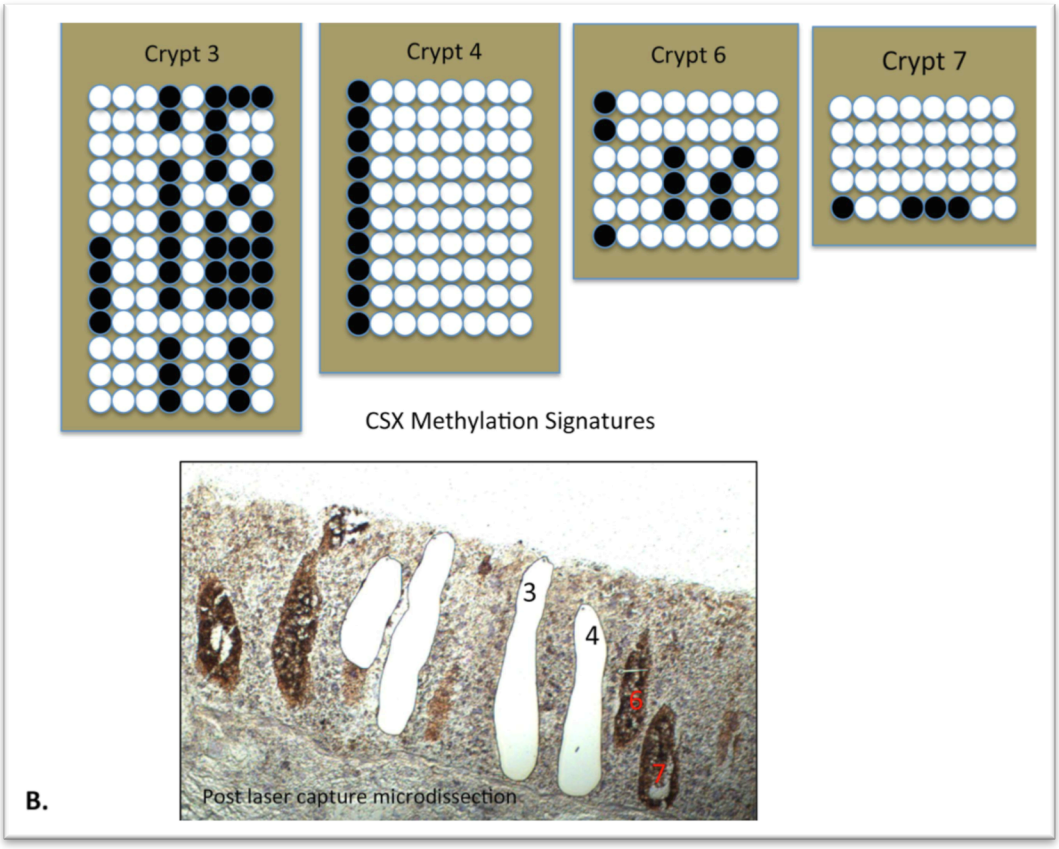

Figure 5.12. Pre and post laser capture microdissection of crypts from a 29 year old CD patient with quiescent disease, who developed an adenocarcinoma. A. Pre laser capture of crypts. **B.** Post LCM of crypts 3 and 4. Methylation signatures for *CSX* locus: crypts 3, 4, 6, 7. Crypts are adjacent, but signatures are dissimilar.

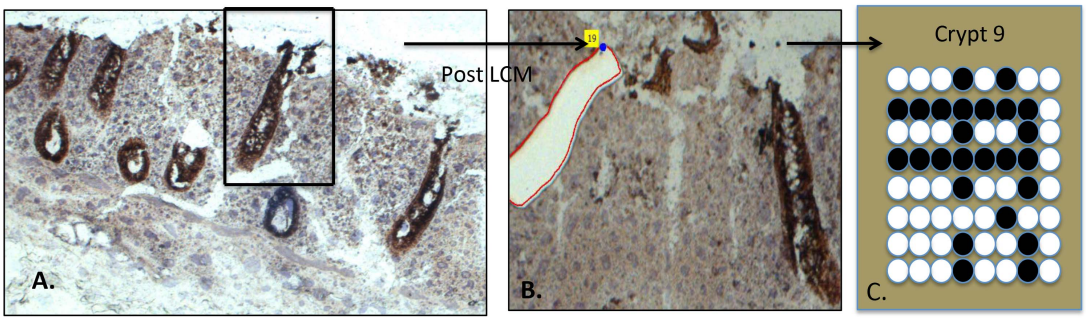

Figure 5.13. Pre and post laser capture microdissection of crypts from a 29 year old CD patient with quiescent disease who developed an adenocarcinoma. A. Pre laser capture of crypt 9 (highlighted in selection box). **B.** Post laser capture microdissection of crypt 9. **C.** Methylation signature for *CSX* locus for crypt 9, which is dissimilar to neighbouring crypts 3-7 (Figure 5.12) and crypts 10-11 (Figure 5.13).

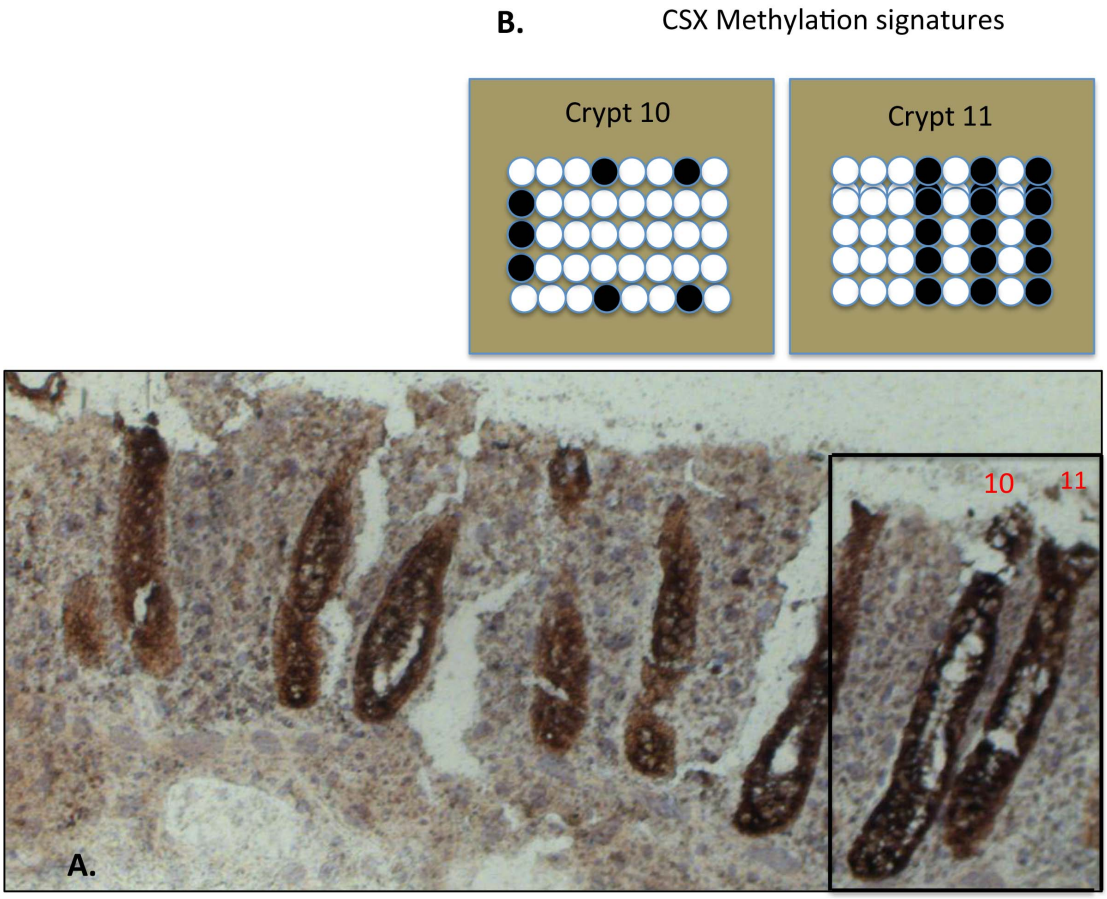

Figure 5.14. Pre laser capture microdissection of crypts 10 and 11 from a 29 year old CD patient with quiescent disease who developed an adenocarcinoma and their methylation signatures. A. Pre laser capture of crypt 10 and 11 (highlighted in selection box). **B.** Methylation signatures for *CSX* locus for crypts 10 and 11. The adjacent crypts share no identical methylation signatures, and are quite diverse.

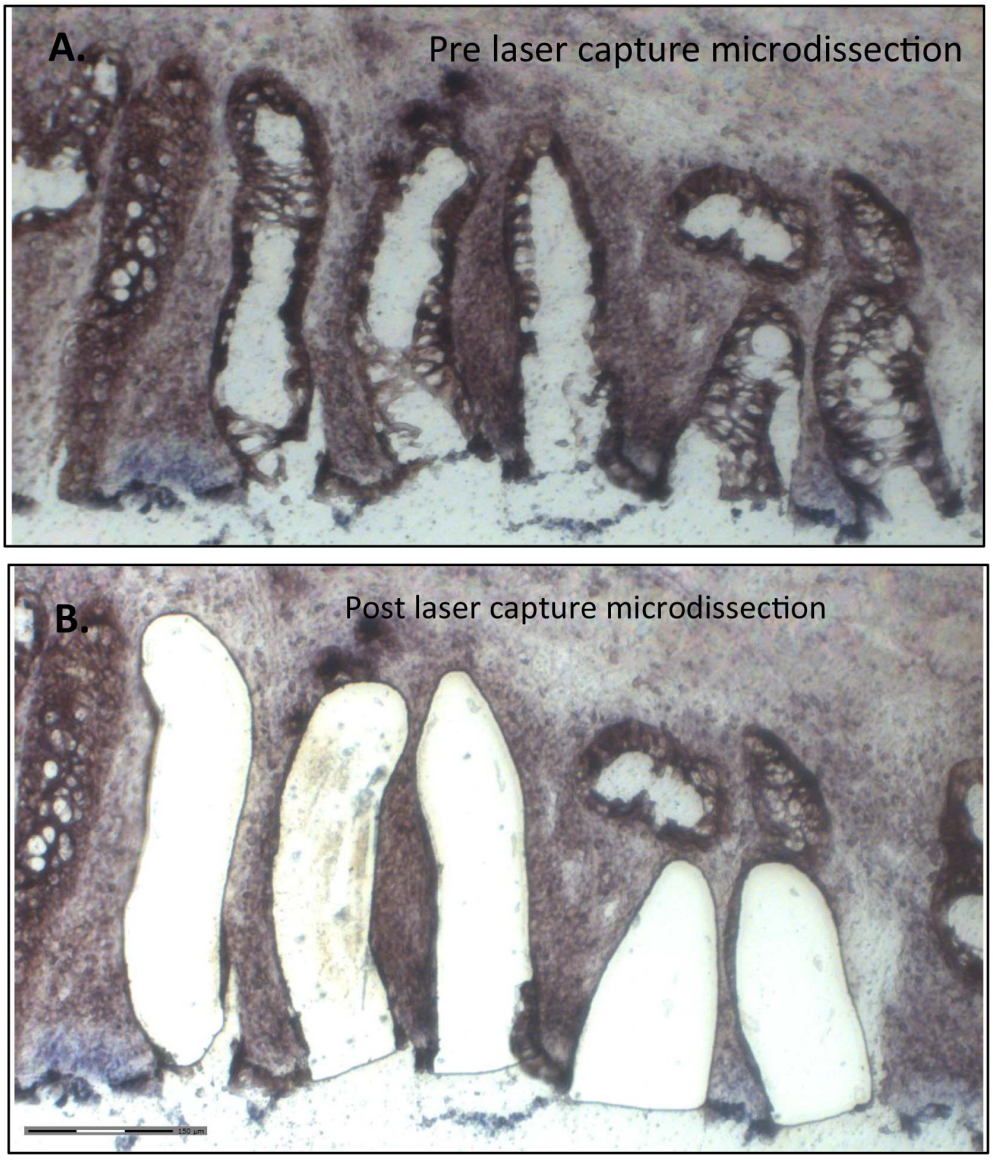

Figure 5.15 Pre and post laser capture microdissection of crypts from a 54 year old male UC patient. A. Pre laser capture of crypts. **B.** Post laser capture microdissection of crypts. These crypts were sampled, as they are all adjacent to one another.

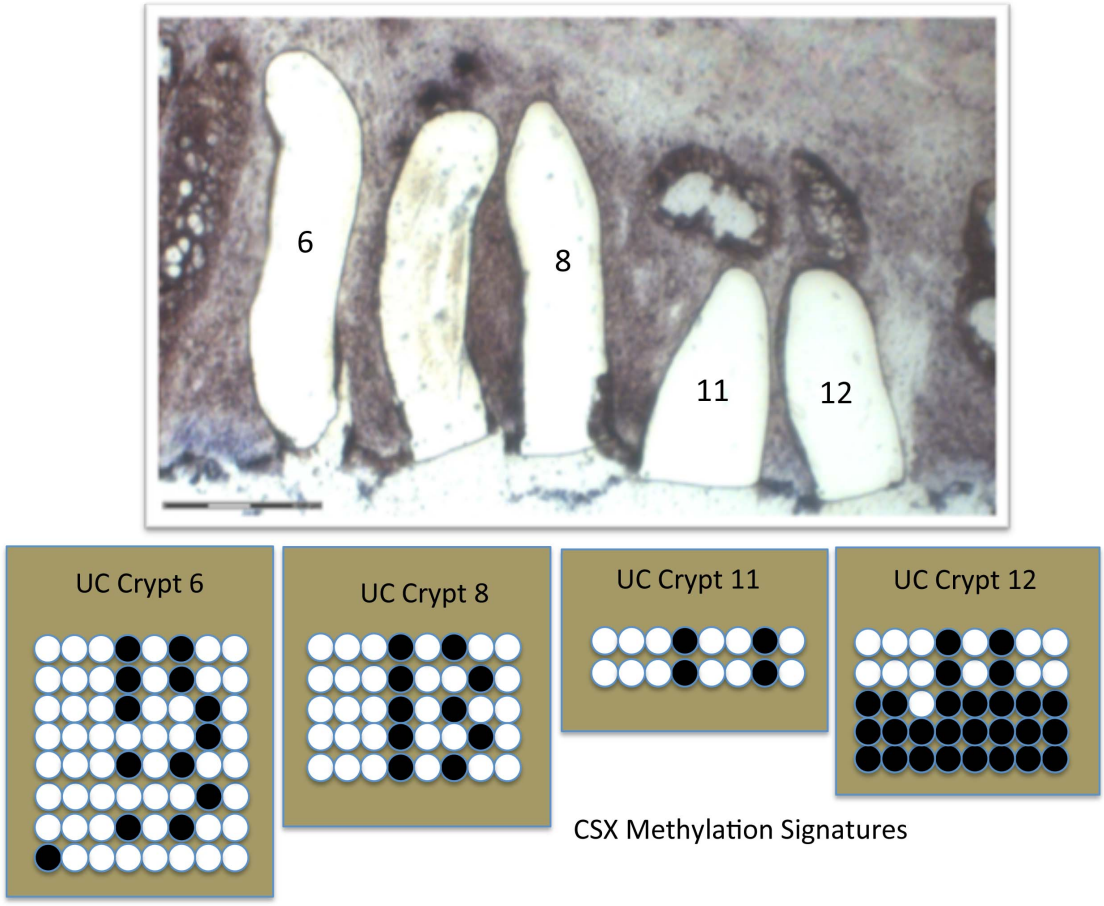

Figure 5.16. Post laser capture microdissection of crypts 6, 8, 11, 12 from a 54 year old UC patient and their methylation signatures. A. Pre laser capture microdissection of crypts 6, 8, 11, and 12. **B.** CSX methylation signatures of crypts 6, 8, 11 and 12. Crypts 6 and 8 share some methylation signatures, but adjacent crypts 11 and 12 do not.

The final patient examined in this chapter was a 29 year old male with inactive UC (patient number 6; Table 5.1). Laser capture microdissection was conducted on their colonic tissue (Figure 5.17). This case provided examples of serial tissue sections with very close spatial proximity of colonic crypts (Figure 5.17). From the original pre LCM picture it is difficult to say whether any of these crypts are actually budding from fission (Figure 5.17). *MYOD* methylation patterns for 7 closely adjacent crypts were determined and some shared unique tags were identified (Figure 5.18). This may explain why some of the unique tags are similar. However, there were some clear dissimilarities in their methylation signatures, for example, between crypt 6 and 7 and the other crypts (Figure 5.18). Due to the high degree of hypermethylation and indeed hypomethylation in the *MYOD* locus examined, interpretation of the methylation signatures here is difficult. The *CSX* locus is much more informative in this case and demonstrates diverse methylation patterns despite the crypts being adjacent (Figure 5.19).

In the next series of crypts examined, there may be fission occurring; the crypt labelled 10 may represent a crypt bud forming as a result of bifurcation of crypt 8 (Figure 5.20-5.21). In Figure 5.20, the *CSX* locus is represented. These crypts share no identical methylation signatures despite being adjacent to each other, or indeed may represent the same crypt if they are in the process of bifurcating (crypts 8 and 10 for example). When the *MYOD* locus was examined in addition to the *CSX* locus, although some crypts showed a high degree of methylation in the *MYOD* locus there were some methylation signatures that were shared amongst all crypts examined (Figure 5.21).

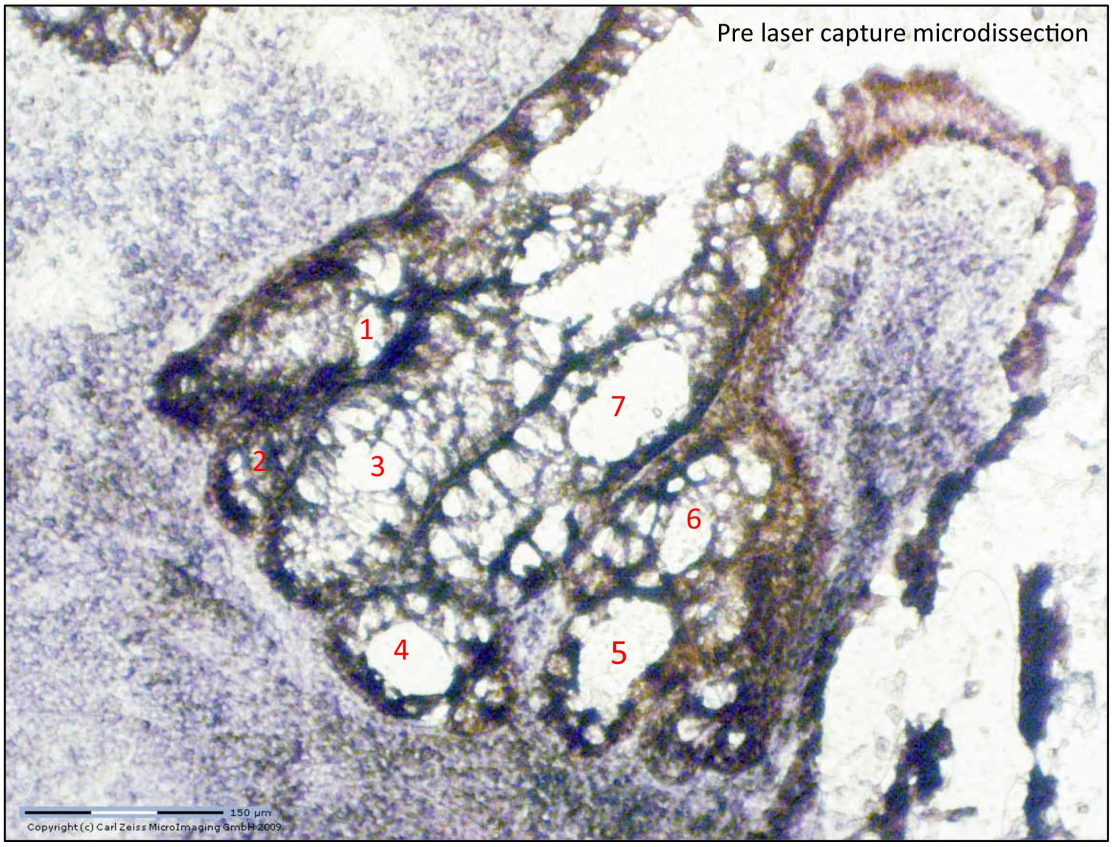

Figure 5.17. Neighbouring crypts 1-7 from a 29 year old male with inactive ulcerative colitis prior to laser capture microdissection. Image is at x100 magnification. These crypts are in very close proximity.

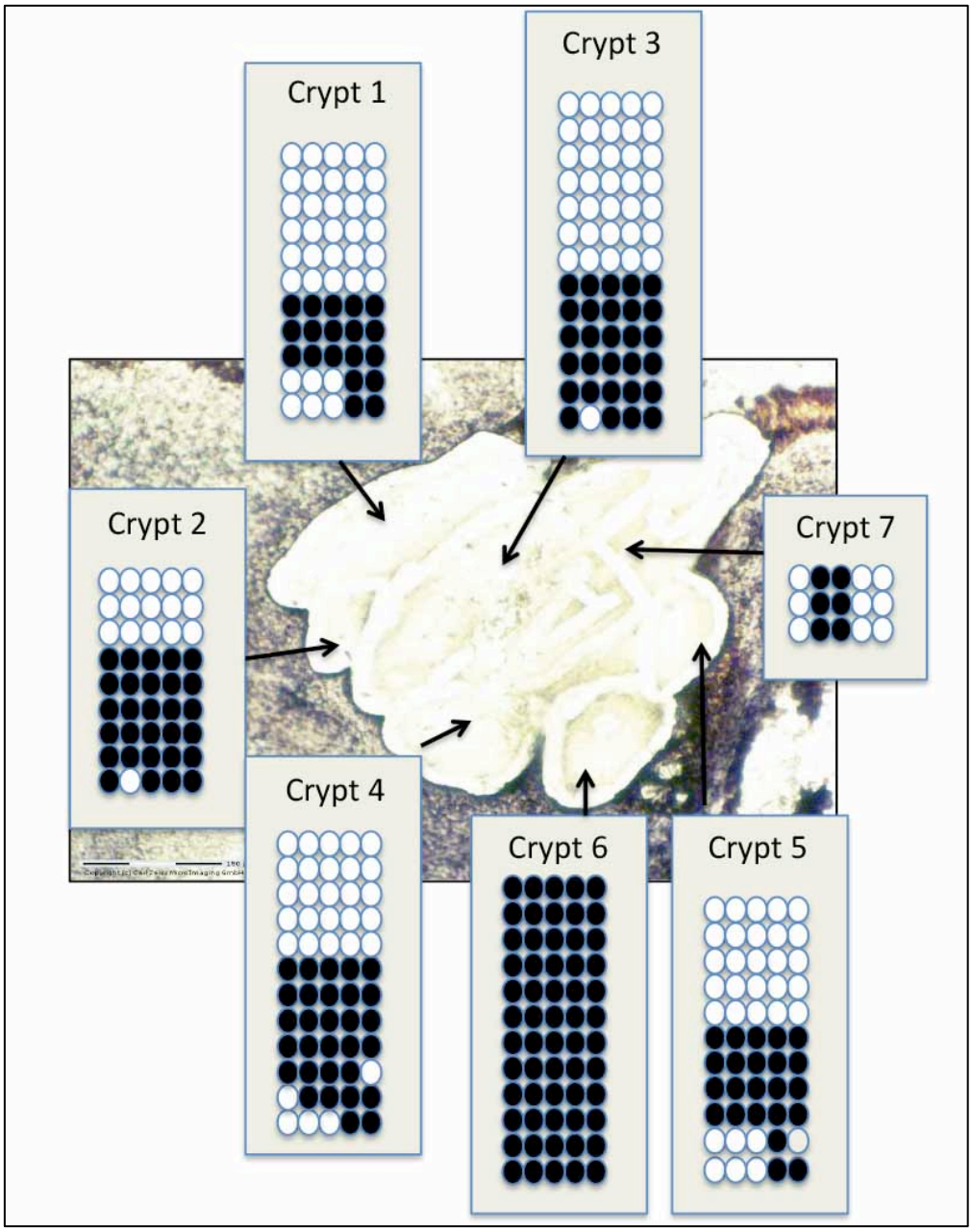

Figure 5.18. Adjacent crypts and buds from the colon of a 29 year old male with inactive ulcerative colitis. *MYOD* methylation signatures given for all the adjacent crypts. The high degree of hypermethylation and hypomethylation in the *MYOD* locus makes interpretation of the signatures difficult. Image is at x100 magnification.

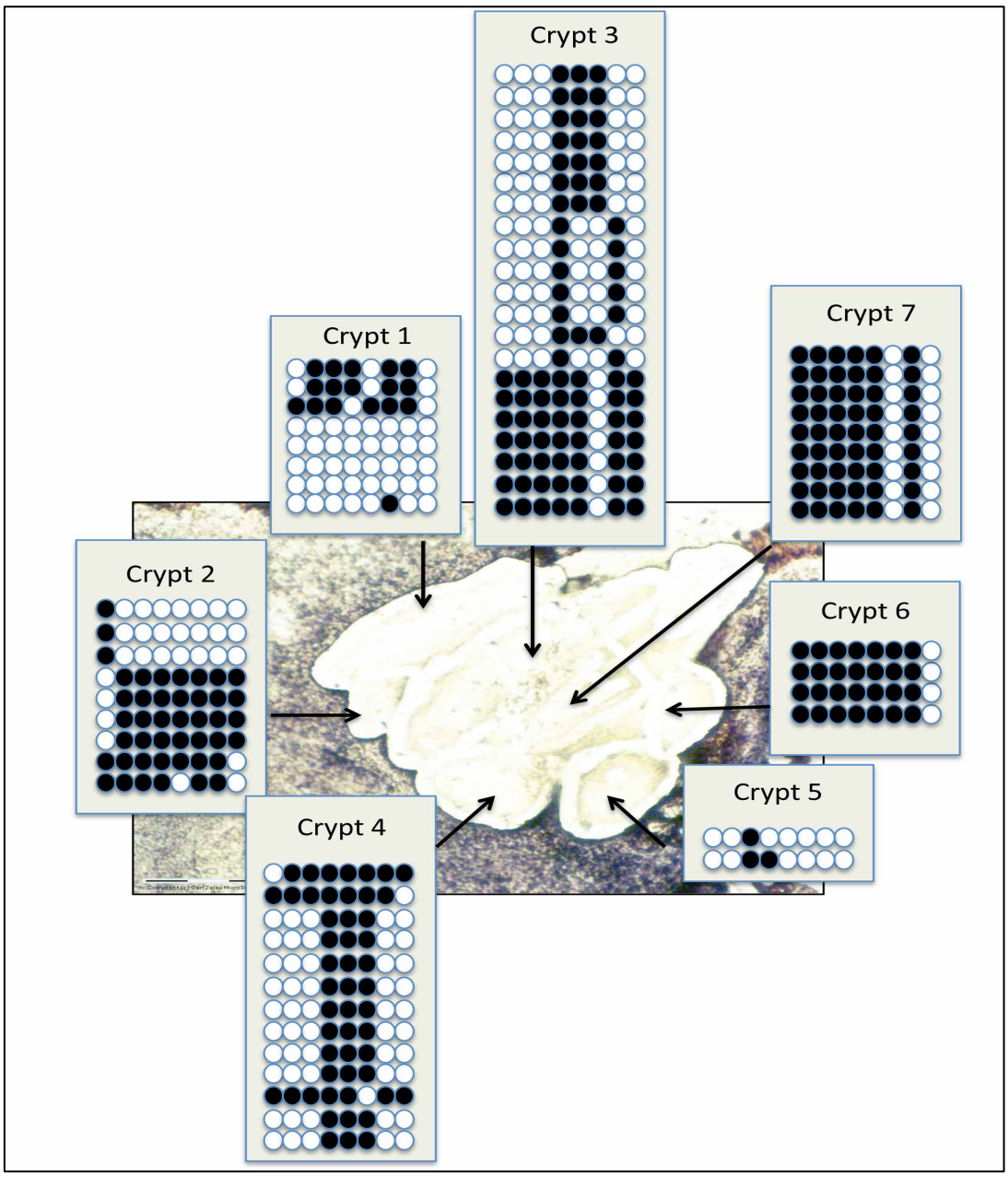

Figure 5.19. Adjacent crypts and buds from the colon of a 29 year old male with inactive ulcerative colitis after laser capture microdissection. Image is at x100 magnification. *CSX* methylation signatures depicted for all the adjacent crypts. The *CSX* locus is much more informative in this case and demonstrates diverse methylation patterns despite the crypts being adjacent.

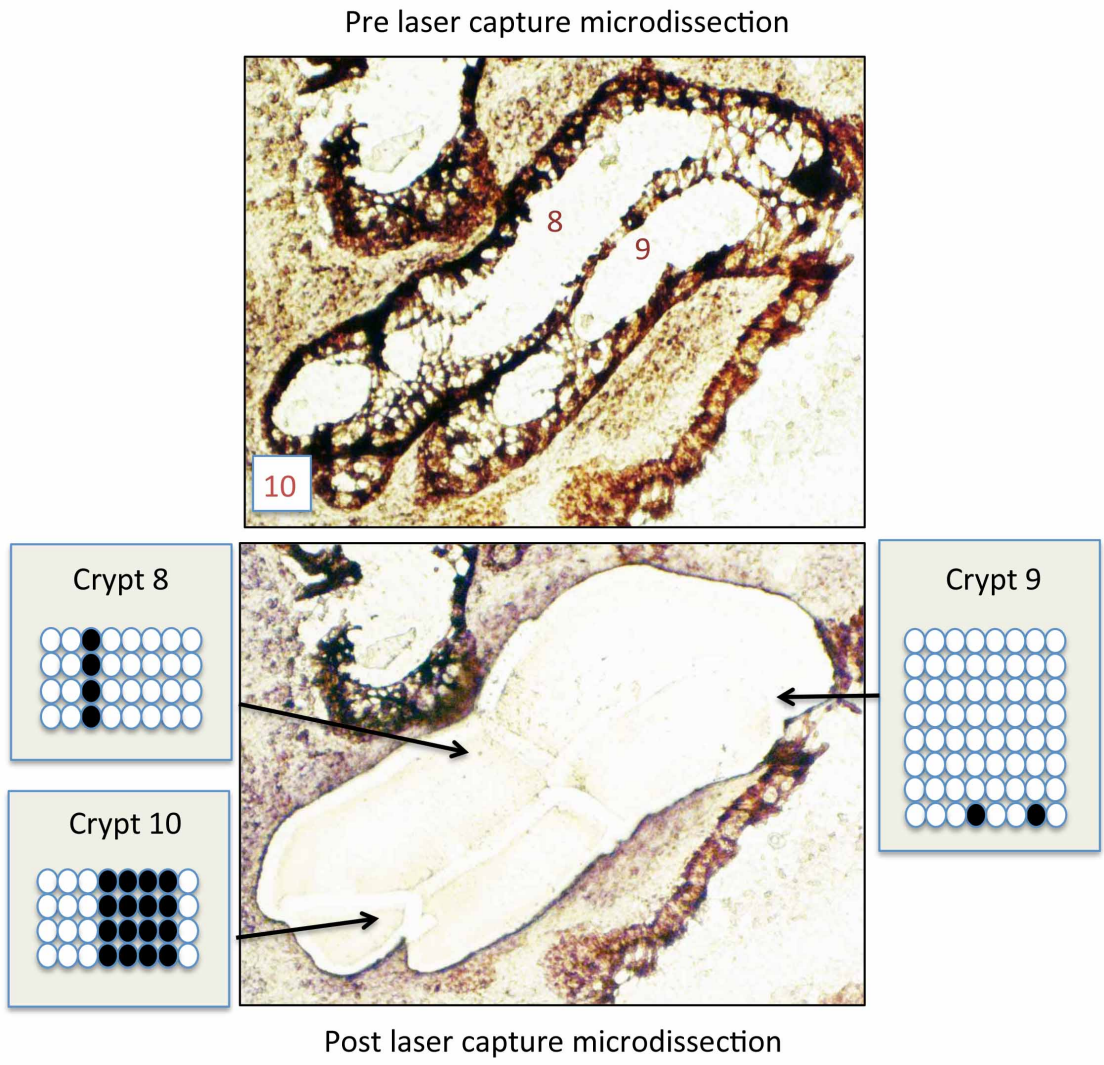

Figure 5.20. Post Laser capture microdissection of crypts from the colon of a 29 year old male with inactive ulcerative colitis and their *CSX* methylation patterns. *CSX* methylation signatures are depicted for all the adjacent crypts. The crypt labelled 10 may represent a crypt bud forming as a result of bifurcation of crypt 8. Image is at x100 magnification. These crypts share no identical methylation signatures despite being adjacent to each other.

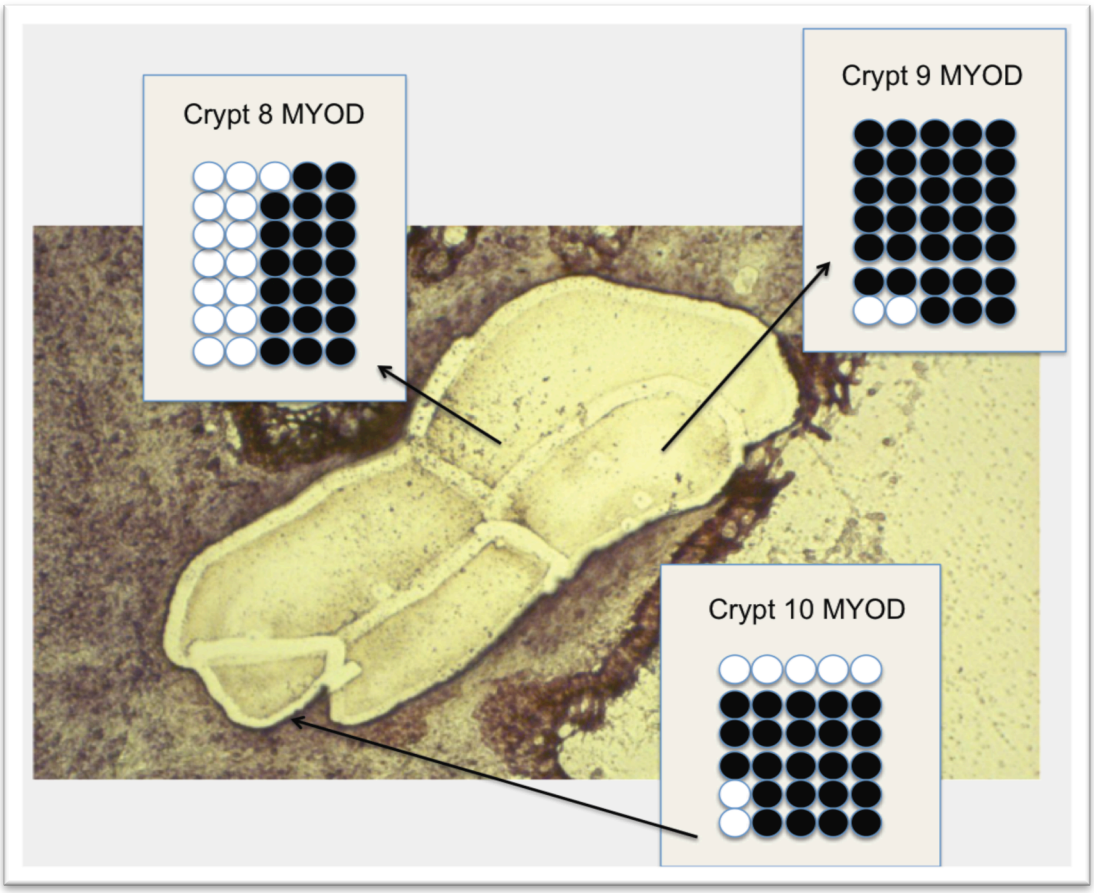

Figure 5.21. Serial section of intestinal mucosa sampled from a 29 year old male with inactive ulcerative colitis post laser capture microdissection. *MYOD* methylation signatures depicted for all the adjacent crypts. The crypt labelled 10 may represent a crypt bud forming as a result of bifurcation of crypt 8. Although some crypts show a high degree of methylation, there are some methylation signatures that are shared amongst all crypts examined. Image is at x100 magnification.

Figures 5.20-5.21 show 2 adjacent crypts 8 and 9 with a bud (crypt 10) forming from crypt 8 (early stages of fission). Whilst crypts 8 and 9 have one shared unique tag amongst them, which is only apparent in the *MYOD* locus and not the *CSX* locus, the crypt bud 10 apparently formed from crypt 8 has no unique tags in common with crypt 8 across both the *CSX* and *MYOD* loci examined (Figures 5.20-5.21).

Finally, statistical analysis was performed examining all patients (Table 5.1) comparing the intercrypt distance between adjacent and non-adjacent crypts across both loci probed. Figure 5.22 shows that rather counter-intuitively, non-adjacent crypts were more similar in their methylation patterns when directly compared to adjacent crypts ($p=0.0040$, two tailed Student's t-test) (Figure 5.22). It would be expected that adjacent crypts would be more similar than non-adjacent crypts. However, this is consistent with previous data from normal colon (Kim and Shibata 2004; Graham et al. 2011). However, *MYOD* as previously documented in Chapter 3 at times, appears to be a less reliable molecular clock marker, and perhaps owing to the fewer number of CpG sites compared to the *CSX* locus (5 versus 9) and to the high degree of hyper- hypo-methylation which is observed occasionally.

Next, a two-tailed Student's t-test was performed on both adjacent and non-adjacent crypts across the *CSX* locus (Figure 5.23). There was no statistically significant difference between the intercrypt distance of adjacent versus non-adjacent crypts ($p=0.3014$) (Figure 5.23). Non-adjacent crypts however, still appeared to follow the general trend having more similar methylation patterns than adjacent crypts with a lower intercrypt distance (Figures 5.22-5.23), again consistent with previous findings (Kim and Shibata 2004; Graham et al. 2011).

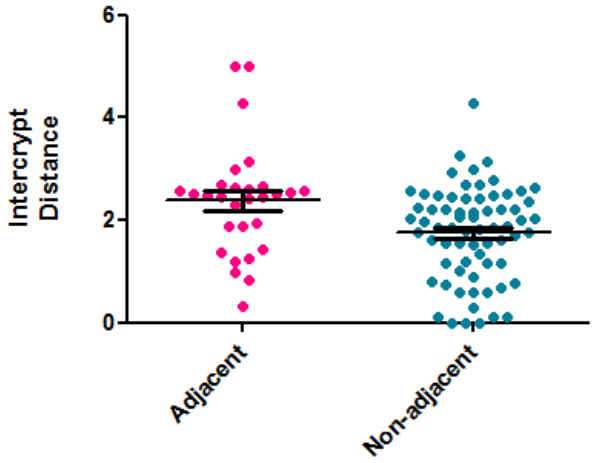

Figure 5.22. Epigenetic distances between *MYOD* tags between adjacent and non-adjacent crypts in IBD. There was a significant difference between the intercrypt distance of adjacent crypts and non-adjacent crypts (p=0.0040, Student's 2 tailed t-test). Non-adjacent crypts were more similar in their *MYOD* methylation patterns than adjacent crypts.

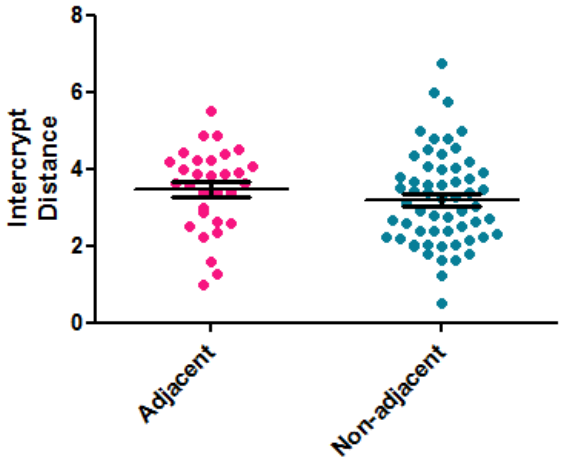

Figure 5.23. Epigenetic distances between *CSX* tags between adjacent and non-adjacent crypts in IBD. No statistically significant difference between the intercrypt distance of adjacent crypts and non-adjacent crypts (p=0.3014, two tailed Student's t-test;). Non-adjacent crypts appear more similar in their methylation patterns than adjacent crypts, demonstrating a modestly lower intercrypt distance.

5.4 Discussion

The epigenetic distances between the *MYOD* tags between adjacent and non-adjacent crypts in IBD showed a statistically significant difference between the intercrypt distance of adjacent crypts and non-adjacent crypts. Non-adjacent crypts were more similar in their *MYOD* methylation patterns than adjacent crypts. However, when the *CSX* locus was examined there were no significant differences between the intercrypt distances analysed from adjacent crypts or non-adjacent crypts. However, the general trend was that the non-adjacent crypts were more similar in their methylation patterns than adjacent crypts (Figure 5.23). Physical propinquity did not correlate with the methylation patterns and were inconsistent with respect to distance. Thus, the time periods between crypt fission events are sufficiently long for methylation patterns of 2 daughter crypts to diverge.

In this chapter I have shown that physical proximity does not appear to correlate with the epigenetic distances of crypts in IBD patients. One would expect that physical distance would be a surrogate marker for time and thus crypts that were adjacent would potentially come from a common ancestor and thus share similar methylation signatures. However, methylation patterns between directly adjacent crypts were not significantly different from non-adjacent crypts in the *CSX* locus. Adult human IBD colonic crypts appear to be long-lived structures that become mosaic with respect to methylation during aging. This corroborates with previous studies in normal human colon (Kim and Shibata 2004, Graham et al. 2011).

A recent study from the host laboratory analysed clonal dynamics of adenomatous crypts within human colorectal adenomatous polyps. Clonal expansion within

adenomas was found to be very restrictive, with relative stasis of growth (Humphries et al. 2013). Their data suggests that most crypt-pairs within adenomas are similarly related to one another. Crypt patches that were recently related were exceptional. These data support a model for tumour growth in which the time to the most recent common ancestor of each crypt-pair is longer than the time taken for the methylation patterns of two clonally-derived daughter crypts to diverge. Furthermore, this group found that crypts that were situated nearby within the adenoma were no more alike in their methylation signatures than crypts that were physically widely spaced. What is compelling is that similar patterns of epigenetic diversity have been documented in advanced CRCs (Siegmund et al. 2009). The advanced lesions demonstrated modest evidence of recent clonal expansions and all cancerous acini were similarly distinct in their methylation signatures (Siegmund et al. 2009). This would infer that relative stasis where clonal expansion occurs slower than the rate of methylation pattern divergence may represent all periods of colorectal tumourigenesis and may indeed be the case in chronic inflammation.

In summary, adjacent crypts in IBD have as dissimilar methylation signatures as non-adjacent crypts, and are not more closely related because of recent clonal expansion, indicating fission is very slow in IBD, although this may be dependent on the activity of any inflammatory disease at the time. The same is true in the apparently normal colon.

In the next chapter, I will examine the methylation patterns in crypts undergoing the active process of fission.

CHAPTER 6. ANALYSIS OF CRYPT METHYLATION PATTERNS IN ACTIVE FISSION IN INFLAMMATORY BOWEL DISEASE PATIENTS

6.1 Introduction

In order to understand how mutations spread in the colitic bowel, the rate of crypt fission needs to be established. Crypts in the large intestine bifurcate to produce neighbouring crypts following injury or indeed expansion (Park et al. 1995; Wright 2000). Bifurcating crypts are only seen in less than 1% of all crypts in human adult colons (Cheng et al. 1986). The rate of crypt fission is increased in pathological conditions, in particular UC and CD (Cheng et al. 1986), as well as in the flat mucosa of FAP (Bjerkness et al. 1997; Wasan et al. 1998) and sporadic adenomas and hyperplastic polyps (Wong et al. 2002). Wong et al (2002) demonstrated that the percentage of crypts undergoing fission within an adenoma is upregulated approximately 80- fold compared to the normal colonic epithelium. Indeed, fission is a vital process in IBD mucosal healing but, although the process is upregulated in IBD, there is little data on the speed with which this process occurs. Thus, this chapter seeks to investigate the rate of fission in IBD.

Kim and Shibata (Kim and Shibata 2004) described methylation patterns of crypts in fission (or branching) and found that they were markedly more diverse than individual crypts and similar to crypts in pairs (i.e. 2 crypts adjacent to one another). The authors explained that this finding may be in accordance with a crypt cycle in which fission occurs following an increase in stem cell number (Park et al. 1995; Wright 2000) since stem cell number is directly proportional to methylation pattern diversity (Yatabe et al. 2001).

Graham and colleagues examined the expansion of stem cell clones in the human colon by using methylation patterns (Graham et al. 2011). They found that the methylation pattern diversity in CCO^- clones residing in only a fraction of a crypt was proportional to clone size. This implied that niche succession occurred at a slow rate within the crypt. In addition, the two arms of bifurcating crypts had distinct methylation patterns, signifying that fission can disturb epigenetic logs of crypt lineage. Neighbouring clonal CCO^- crypts had methylation patterns as dissimilar to one another as the methylation patterns of two unrelated crypts. Mathematical modeling indicated that stem cell dynamics and epigenetic drift might explain the dissimilarity in the methylation pattern the authors found.

6.1.1 Hypothesis and aims

The hypothesis is that in IBD, branched crypts are more closely related than distant crypts because of recent clonal expansion, but this may depend on the activity of the disease. Here, methylation signatures will be used to recognize the time taken for crypts to divide. The aim is to isolate crypts undergoing various stages of crypt fission from different IBD patients with varying disease activity states and to separate the branching arms from the stalk of the crypt. This will permit analysis of the individually separated sections of the crypt and allow the mathematical modeling of crypt fission rates in various activity states in IBD in the future.

6.2 Methods

Fresh colonic tissue samples were immediately subjected to an EDTA crypt isolation technique (see section 2.4 in Materials and Methods chapter).

6.2.2 Patients

Table 6.1 Clinicopathological features for patients

Patient	Age	Sex	IBD	Extent	Activity	Medication
1	17 years	Male	CD	Colonic CD	Quiescent	Infliximab
2	59 years	Female	UC	Pan UC	Mildly active	Asacol, Folic acid
3	51 years	Male	UC	Left sided UC	Mildly active	Balsalazide Pentasa
4	33 years	Female	UC	Pan UC	Mildly active	6-Mercaptopurine Pentasa Salofalk enemas Rectal steroid
5	66 years	Female	CD	Colonic CD	Quiescent	6-Mercaptopurine Corticosteroids
6	28 years	Male	UC	Pan UC	Quiescent	Ciprofloxacin; Metronidazole; VSL3
7	29 years	Male	UC	Pan UC	Quiescent	Salofalk enemas
8	29 years	Male	CD	Colonic CD	Mildly active	Azathioprine refractory; Secondary loss of response to Infliximab; Primary non-responder to Humira; No response to Tacrolimus
9	28 years	Female	CD	Colonic CD	Quiescent	Infliximab

6.3 Results

Crypts were isolated from fresh tissue biopsies taken from IBD patients (Table 6.1) and those crypts in fission were identified microscopically (X 160 magnification). An example of a crypt in late fission from a 17 year old male Crohn's patient (patient 1, Table 6.1) is shown in Figure 6.1. The two arms and the stalk were dissected and separated under high power magnification (X100) and *MYOD* methylation signatures

established (Figure 6.2). As perhaps expected for a young patient few methylated CpG sites were identified and this makes the data uninformative (Figure 6.2). Yet when the *CSX* locus was examined, the stalk (numbered 1), had no similar methylation patterns to its own branching crypt arm (numbered 2; Figure 6.3), In stark contrast, examination of the same gene locus *CSX*, in another early branching crypt from the same patient revealed a high degree of *CSX* methylation in the one of the two buds (bud 5) and the stalk (crypt 4; Figures 6.4 and 6.5). The number of cells across the diameter of each bud was counted and 11 cells were found across the shorter bud (bud 6) and 17 across the larger (bud 5; Figure 6.5). What is remarkable is that the two buds 5 and 6 from the same crypt have such diverse methylation patterns considering the crypt has only just begun the process of fission: the small buds have not yet separated into crypt arms. Bud 5 and the crypt stalk numbered 4 share two identical methylation tags but share no unique tags with bud 6. Thus, rather unexpectedly, the *CSX* methylation signatures of branching buds from a crypt in early fission were dissimilar with a high percentage of methylation in bud 5 (Figure 6.5) suggesting a high degree of dynamic change over only a few cell generations. The number of cells across the maximum diameter of the branching buds was also calculated under the high power microscope: the smaller bud number 6 had 4 cells across the maximum diameter and the larger bud (number 5) had 6 cells (Figure 6.5). Ideally, more bacterial colonies to obtain more unique tags would have been optimal to analyse stalk 4 in more detail.

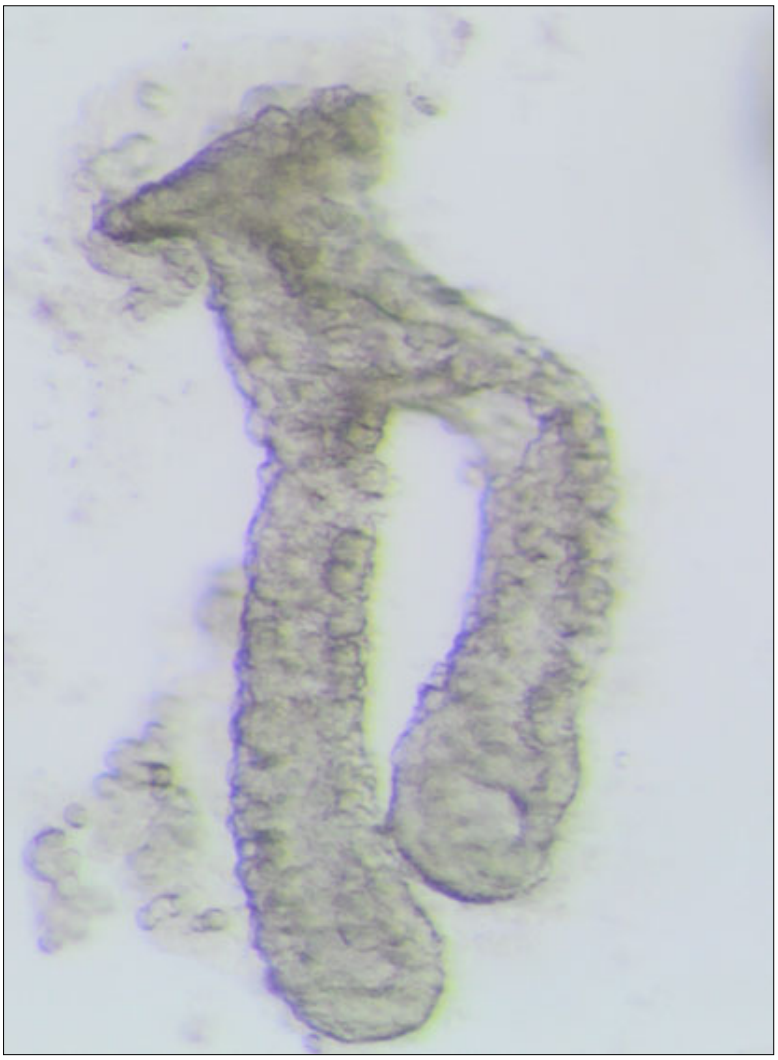

Figure 6.1. Crypt isolation technique used to isolate a crypt in active fission. Crypt was taken from a male patient aged 17 years with Crohn's disease. This crypt is in late fission as indicated by the two long arms about to separate and is imaged at x110 magnification.

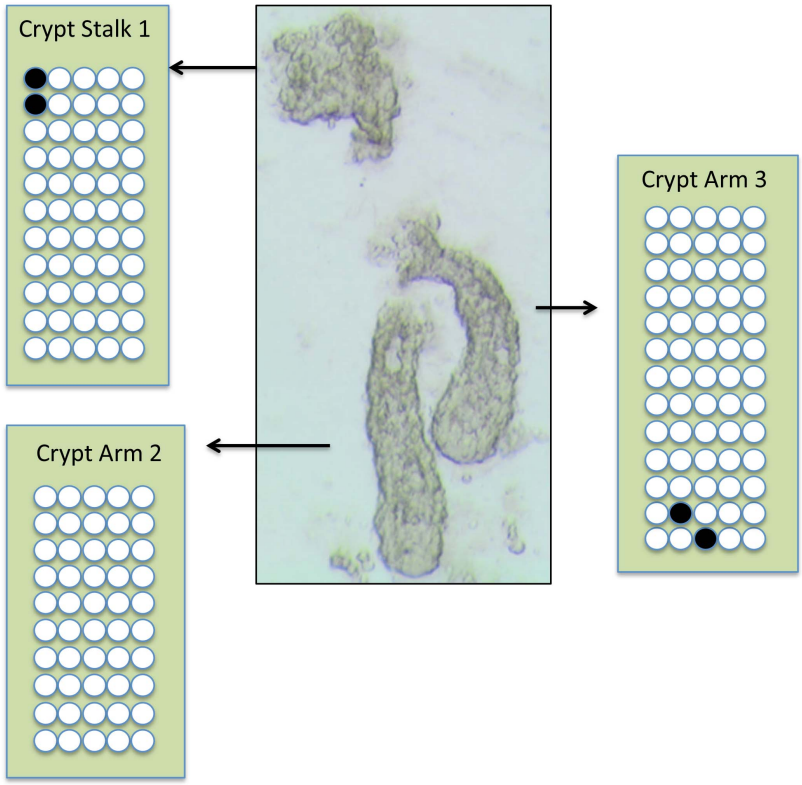

Figure 6.2. Methylation signatures from *MYOD* locus following the separation of the two arms and stalk of a crypt isolated from a male patient aged 17 years with Crohn's disease. *MYOD* methylation signatures for the stalk and two branching arms post dissection. Image is at x160 magnification. There is a high degree of hypomethylation, making interpretation impossible.

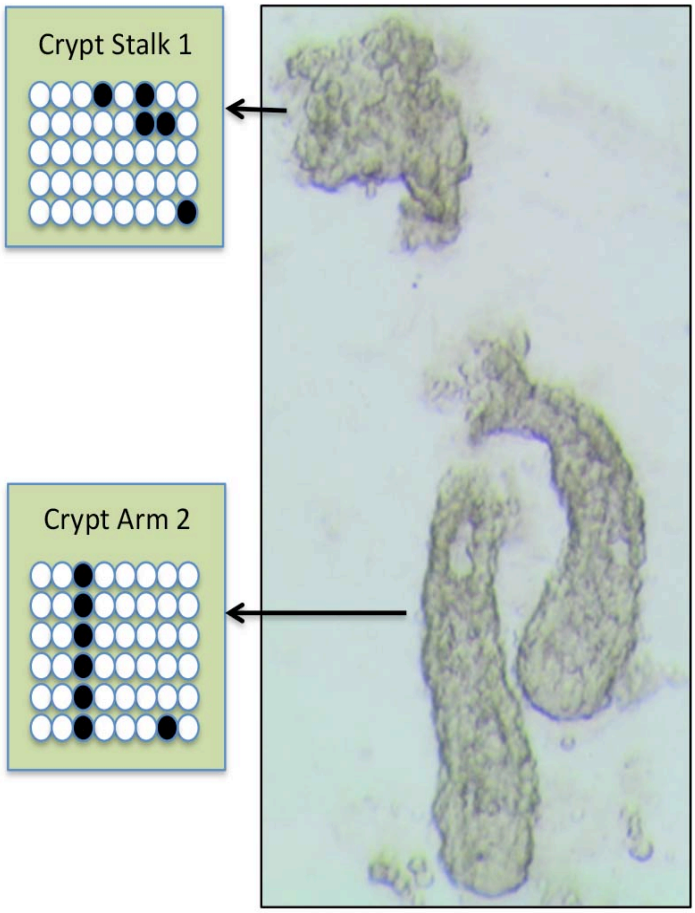

Figure 6.3. Methylation signatures from *CSX* locus following the separation of the two arms and stalk of a crypt isolated from a male patient aged 17 years with Crohn's disease. *CSX* methylation signatures for the stalk and one of the branching arms post dissection. Image is at x160 magnification. The stalk numbered 1 has no similar methylation patterns to the branching crypt arm numbered 2.

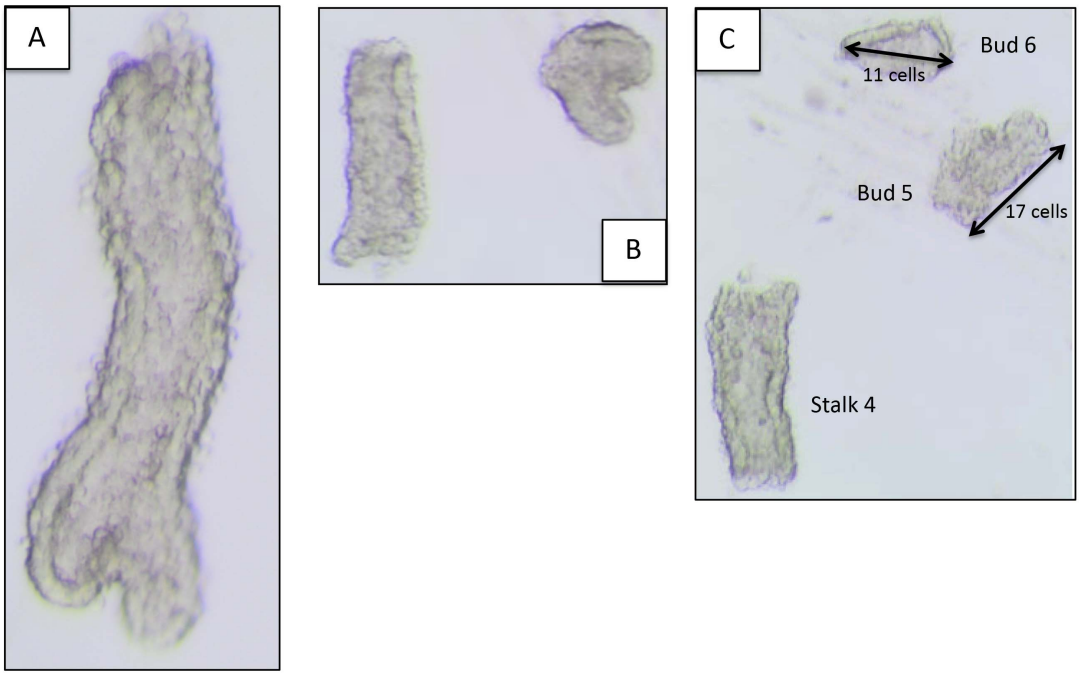

Figure 6.4. A colonic crypt in early fission isolated from a 17 year old male with Crohn's disease. A. Image shows a crypt in early fission. **B**. Post dissection shown of stalk and buds. **C**. Post dissection and separation of 2 branching buds.

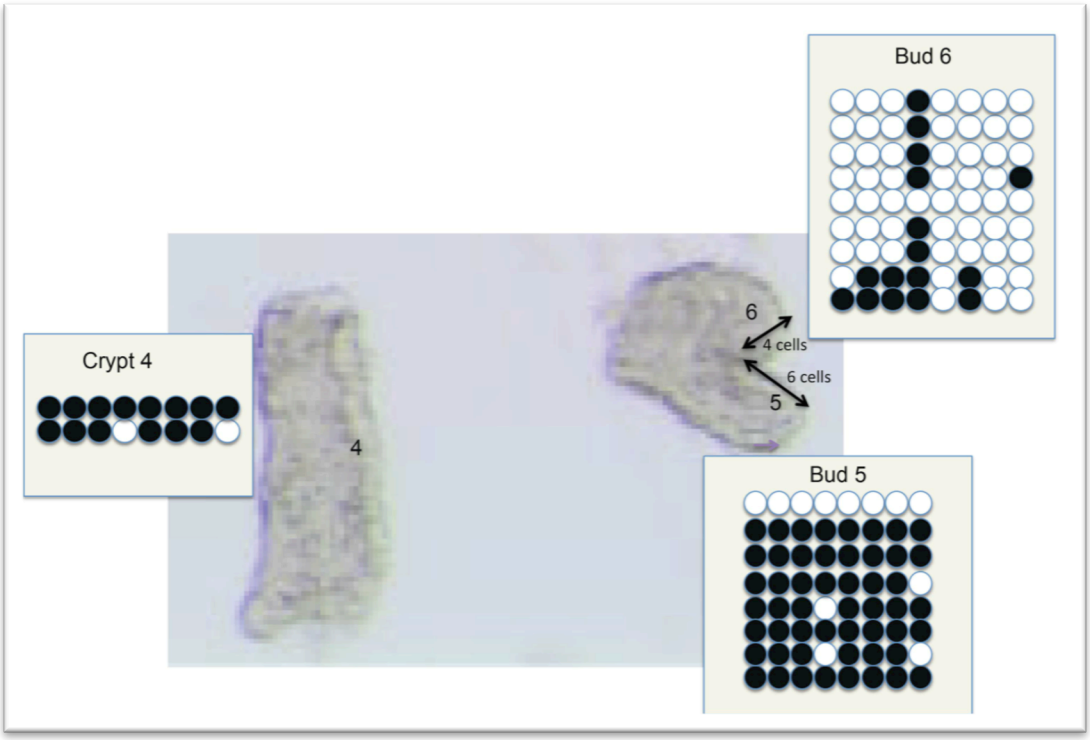

Figure 6.5. Methylation signatures for the *CSX* locus of the stalk and the branching buds. *CSX* methylation signatures for the stalk and two branching arms post dissection of the isolated crypt. Image is at x160 magnification. The two buds 5 and 6 have such diverse methylation patterns considering the crypt has only just begun the process of fission, and given that the small buds not yet separated into crypt arms. Bud 5 and the crypt stalk numbered 4 share two identical methylation tags but share no unique tags with bud 6.

The second patient analysed was a female aged 59 years old (patient 2, Table 6.1) with mildly active UC and multiple crypts in various stages of fission were found in the biopsy sample. In Figure 6.6 a crypt from this patient is undergoing late fission with the two arms bifurcating in the middle and almost at the final stage of forming two independent crypts. It is clear how diverse the methylation signatures are of the two bifurcating arms (Figure 6.6). The branching arms A and B are so diverse that they do not share a single unique tag. A random control crypt was also examined to demonstrate that these methylation patterns are not just due to chance. Figures 6.7 and 6.8 show a second crypt isolated from the same patient, but this time in early fission just as budding to separate is occurring. In both Figures 6.7 and 6.8 the same crypt series are analysed for the *MYOD* locus and *CSX* locus respectively; Bud D, although sharing some identical methylation signatures with its arm C, appears quite diverse in terms of its overall methylation signature. There are two shared unique tags amongst the stalk C and bud D in the *MYOD* locus (Figure 6.7) and across the *CSX* locus there is just one unique tag common to both (Figure 6.8). A random control crypt was also examined to demonstrate that these methylation patterns are not just due to chance.

In the same patient (Patient 2; Table 6.1), a third crypt, again in early fission, was examined and again, bud G is quite diverse to its stalk E (Figure 6.9). In fact, there is only one shared unique tag between stalk E and crypt bud G, otherwise the methylation patterns for *CSX* were all different. At the *MYOD* locus the same pattern emerges: both buds are quite diverse compared to their shared stalk; bud G shares only one unique tag with stalk E; bud F shares only 2 unique tags with stalk E (Figure 6.10). Yet between the buds F and G there was only one shared unique tag.

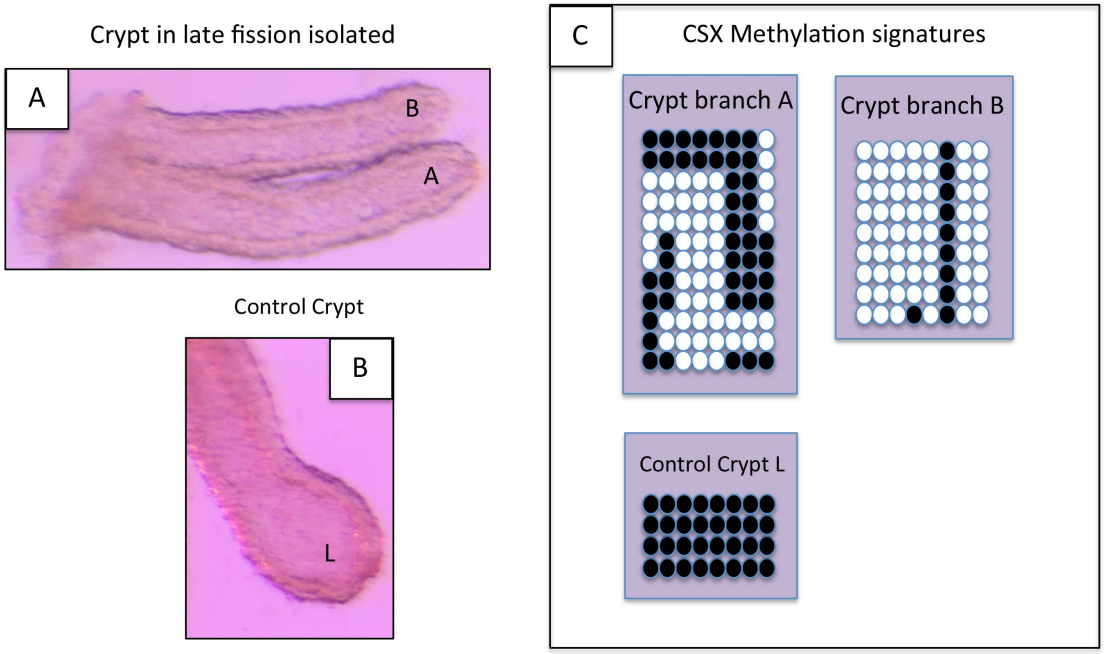

Figure 6.6. *CSX* methylation signatures for crypts isolated from a 59 year old female with mildly active ulcerative colitis. A. A crypt in the process of late fission. **B.** A control crypt L. **C**. Depicted are the *CSX* methylation signatures of the branching arms A and B in panel **A** and of the control crypt L seen in panel **B**. The branching arms A and B are so diverse that they do not share a single unique tag. A random control crypt was also examined to demonstrate that these methylation patterns are not due just to chance.

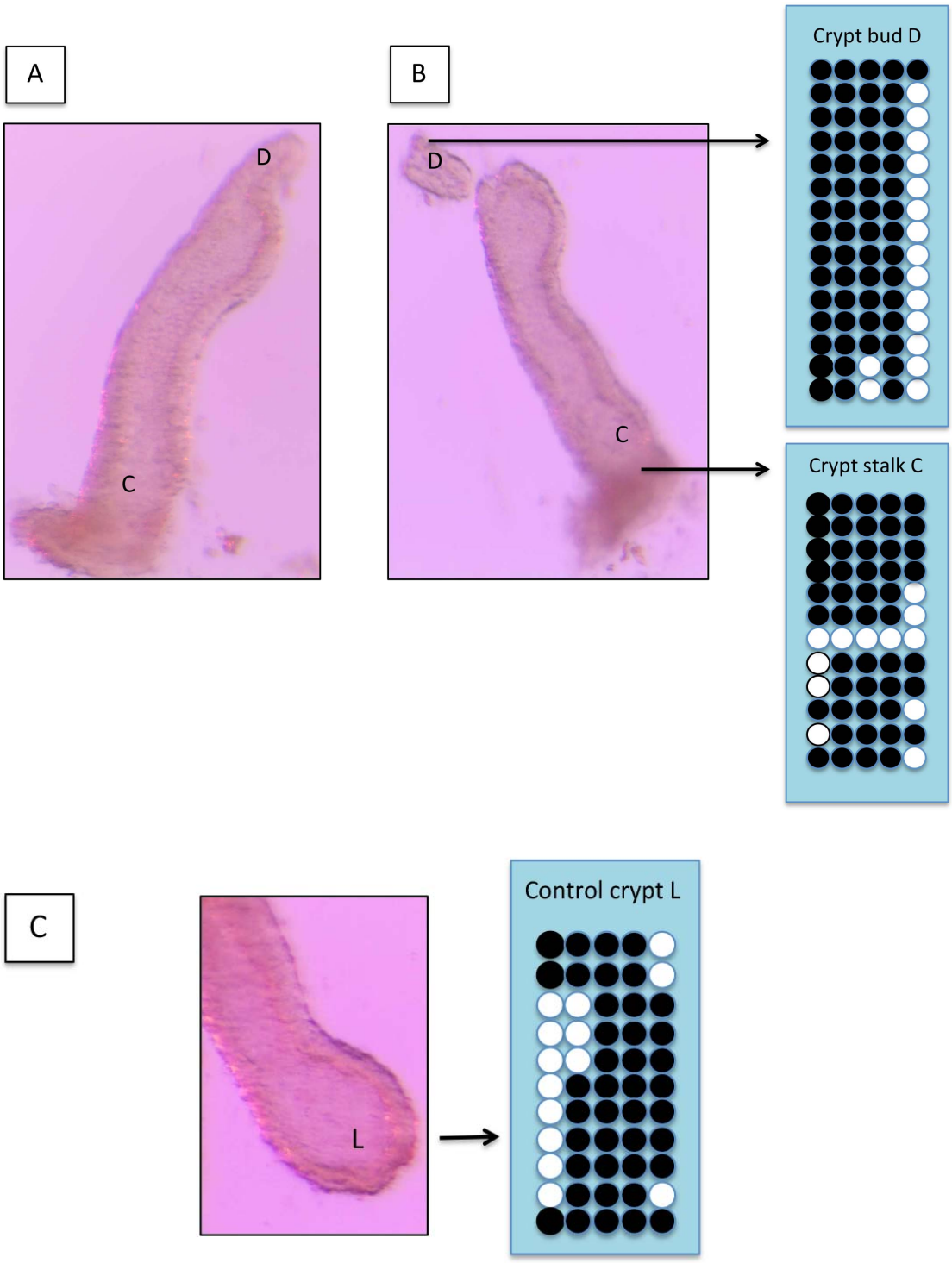

Figure 6.7. *MYOD* methylation signatures crypts isolated from a 59 year old female with mildly active ulcerative colitis. A. Crypt in process of budding; C, stalk of the crypt; D, the bud. **B.** Buds D post dissection and separation from stalk C, the *MYOD* methylation signatures of the stalk C and bud D. **C.** Control crypt L and its *MYOD* methylation signature.

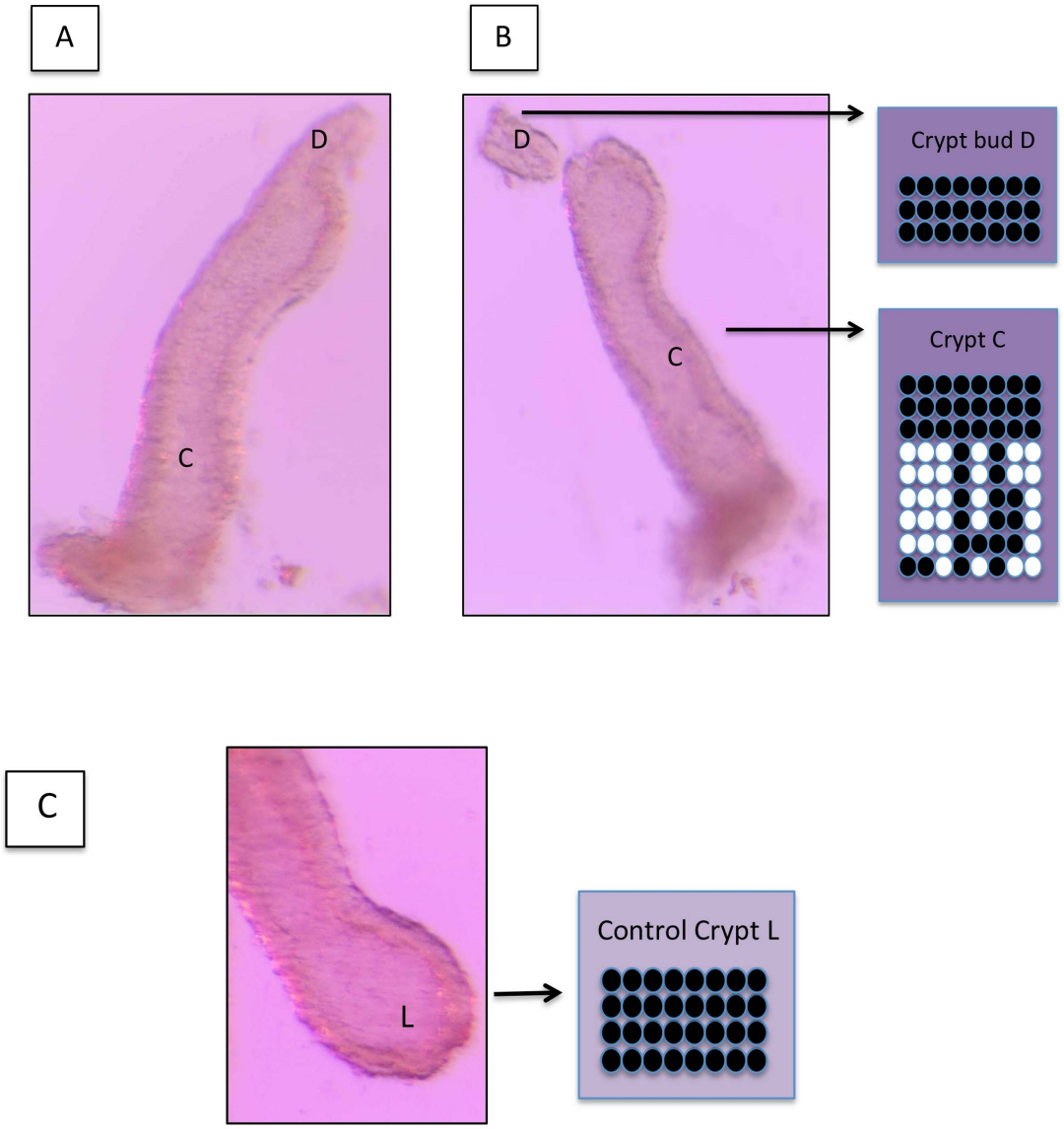

Figure 6.8. *CSX* methylation signatures of a stalk and bud for crypts isolated from a 59 year old female with mildly active ulcerative colitis. A. Crypt in the process of budding to separate. C, the stalk of the crypt; D, the bud. **B.** Buds D post dissection and separation from stalk C, the *CSX* methylation signatures of the stalk C and bud D. **C**. Control crypt L and its respective *CSX* methylation signature. Bud D, although sharing some identical methylation signatures with its arm C, is quite diverse in terms of its overall methylation signature.

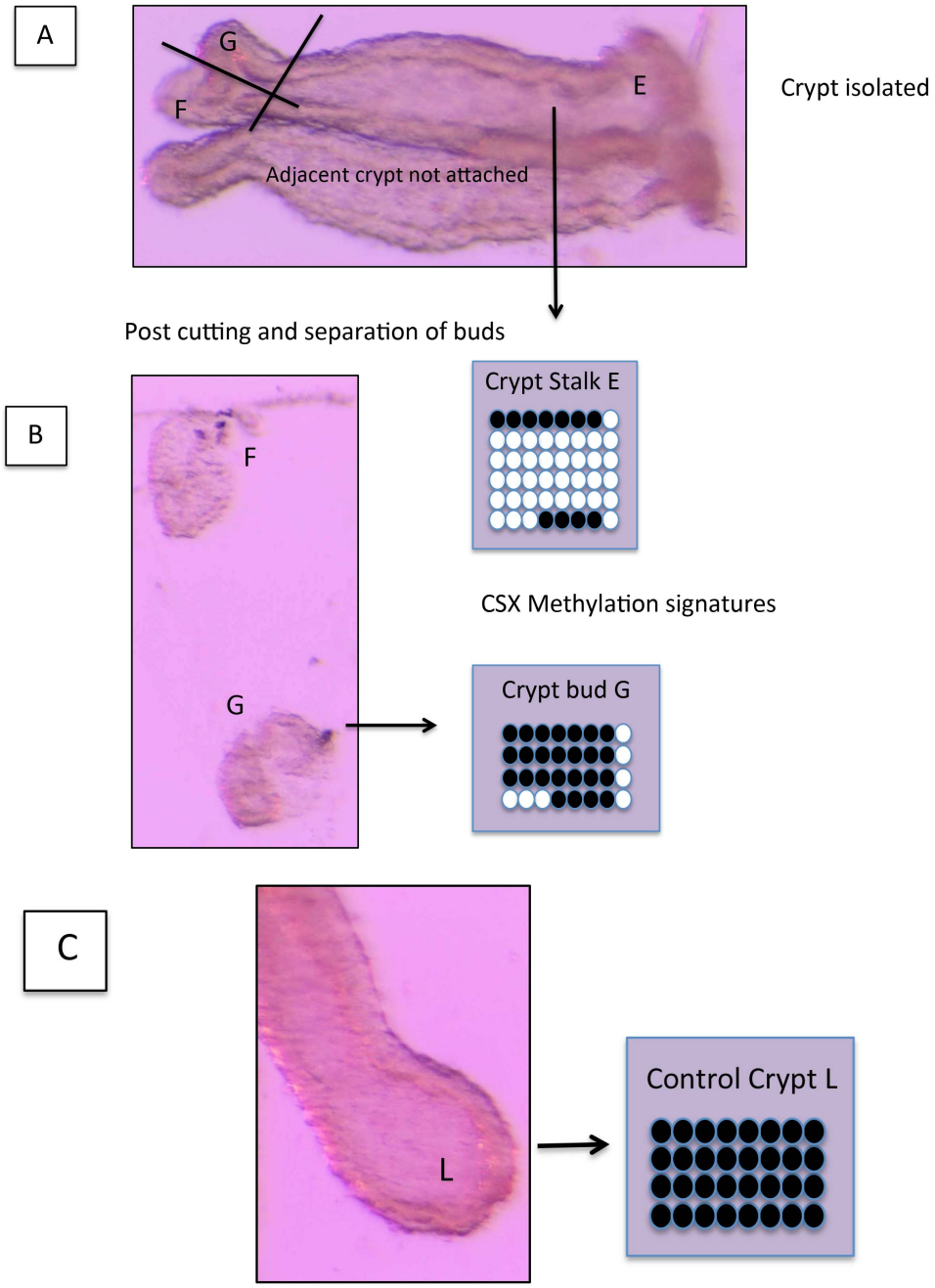

Figure 6.9. Further crypt analysis of the stalk and bud *CSX* methylation signatures. Crypts isolated from a 59 year old female with mildly active ulcerative colitis. **A.** Budding crypt: E, crypt stalk; F and G, buds. Lines show dissection of the branching crypt to separate the buds and stalk. **B.** Buds F and G post dissection and separation from stalk E. *CSX* signatures of stalk E in panel **A** and of bud G in panel **A** and **B. C.** shows the control crypt L and its methylation signature. Bud G has only one shared unique tag with its stalk E, and is quite diverse in its signatures.

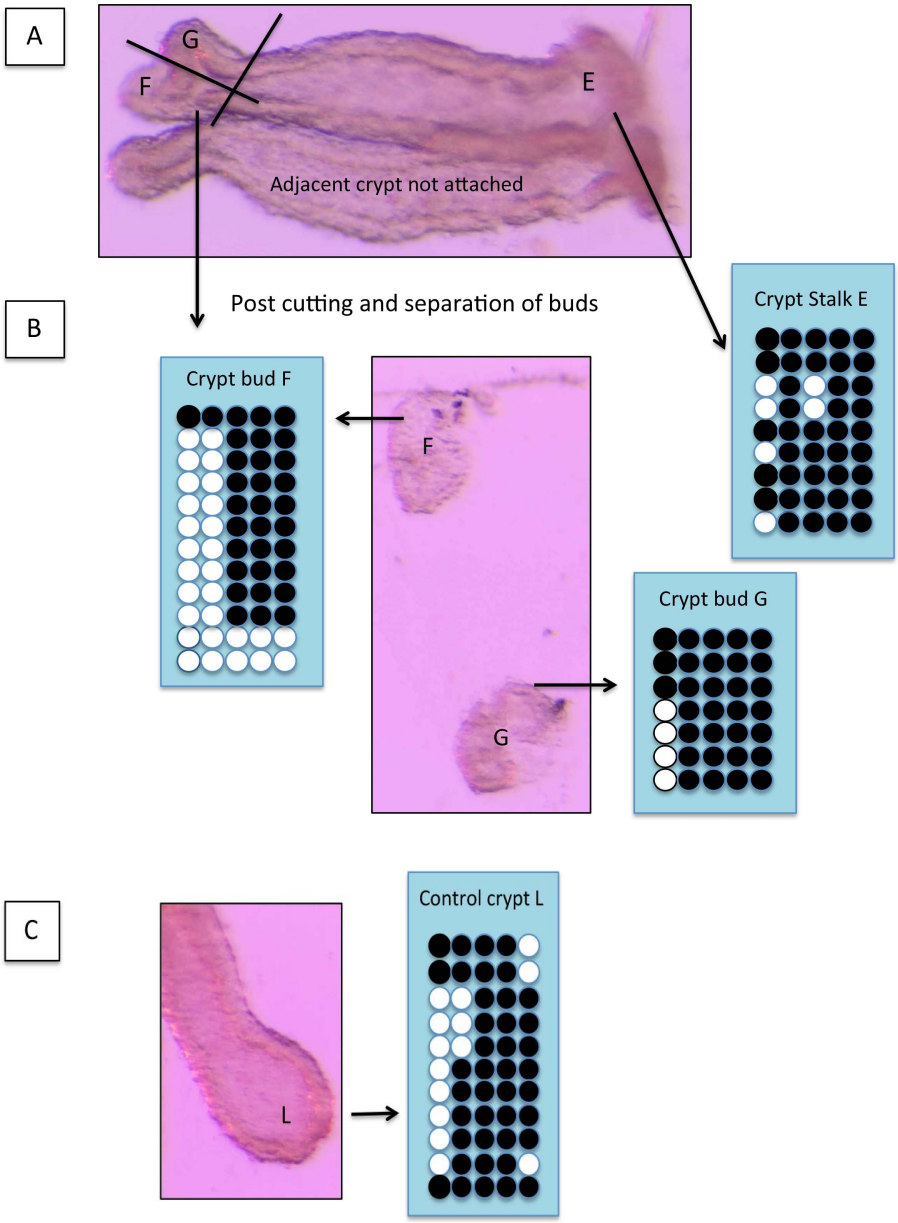

Figure 6.10. Further crypt analysis of the stalk and bud for *MYOD* methylation signatures. A. Crypts isolated from a 59 year old female with mildly active ulcerative colitis. **A**, budding crypt; E, crypt stalk; F and G, the buds. Lines show dissection of the branching crypt to separate buds and stalk. **B.** Buds F and G post dissection and separation from stalk E. *MYOD* methylation signatures of E and F and G. **C**. control crypt L and its *MYOD* methylation signature. Buds F and G are quite diverse in their respective methylation signatures, sharing only one unique tag. Bud G shares only one unique tag with its stalk E, and bud F shares only 2 unique tags with stalk E.

In the last of the crypts in fission analysed from this patient (patient number 2; Table 6.1) (Figures 6.11 and 6.12) there was an unusual looking crypt in the process of early fission: there are two buds (buds K and J) forming from the stalk (I) in the process of budding to separate (Figures 6.11-6.12). The control crypt is lying adjacent in the media but is not attached to the budding crypt (Figures 6.11-6.12).

The crypt stalk I shares only one unique tag at the *CSX* locus with its buds K and J. Bud K has 5 unique tags and has 3 shared unique tags at the *CSX* locus with its bud J (Figure 6.11). Interestingly, across the *MYOD* locus buds K and J are very diverse in their methylation signatures, not sharing a single unique tag between them. Their crypt stalk I shares no unique tags with its bud J, and share only one unique tag with bud K (Figure 6.12).

Patient number 3, a 51 year old male with mild UC, (Table 6.1) shows another crypt undergoing fission. Both buds 2 and 3 share no unique tags whatsoever, and there is only one shared unique tag between the stalk 1 and crypt bud 3 only across the *MYOD* locus (Figure 6.13).

Figure 6.14 depicts patient number 4, a 33 year old female with UC (Table 6.1). The crypts observed are in mid fission. The stalk A shares no unique methylation signatures with its respective bifurcating crypt arms B and C. Indeed crypt arms B and C share no identical methylation patterns (Figure 6.14).

Figure 6.11. CSX methylation signatures for budding crypts. Crypts isolated from a 59 year old female with mildly active ulcerative colitis. Crypt in the process of budding: I, the stalk; J and K, the buds; L, control crypt. *CSX* methylation signatures are given of each area of the crypt/bud and control crypt. The crypt stalk I shares only one unique tag with its buds K and J. Bud K has 5 unique tags and has 3 shared unique tags with its bud J.

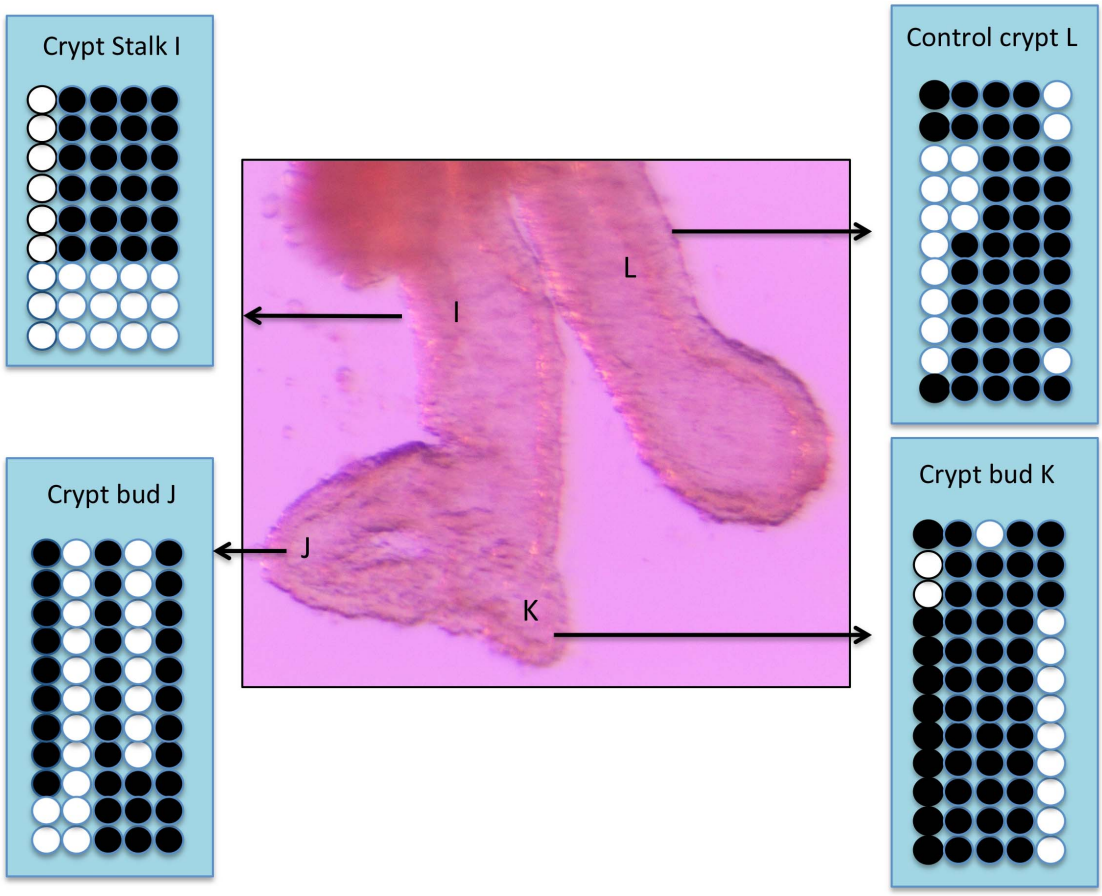

Figure 6.12. *MYOD* methylation signatures for budding crypts. Crypts isolated from a 59 year old female with mildly active ulcerative colitis. Crypt in the process of budding: I, the stalk of the crypt; and J and K, the crypt buds; L, control crypt. *MYOD* methylation signatures of each area of the crypt/bud and control crypt are shown. Buds K and J are very diverse in their methylation signatures, not sharing a single unique tag between them. Their crypt stalk I shares no unique tags with its bud J, and shares only one unique tag with bud K.

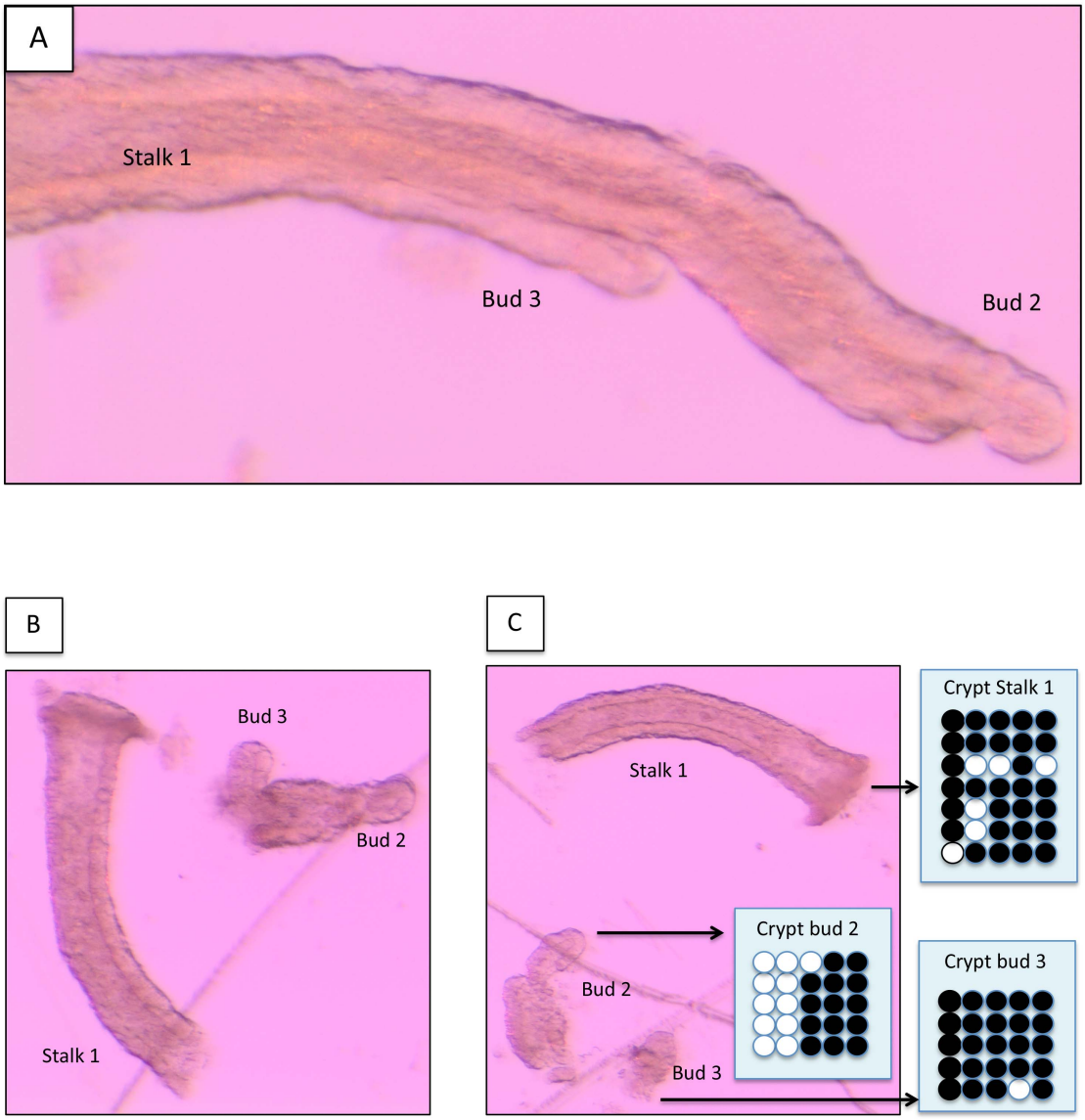

Figure 6.13. Crypt isolated from a 51 year old male with mild ulcerative proctitis. **A.** Crypt beginning budding to separate. Stalk is depicted as 1, and buds are represented as 2 and 3**. B.** Dissection into stalk 1 and buds 2 and 3. **C.** Image taken following dissection and separation of buds 2 and 3 with their respective *MYOD* methylation signatures, including the stalk 1. Buds 2 and 3 are so diverse they share no unique tags at all. In addition, bud 2 does not share a single unique tag with its respective stalk 1, and bud 3 only shares one unique tag with its respective stalk 1.

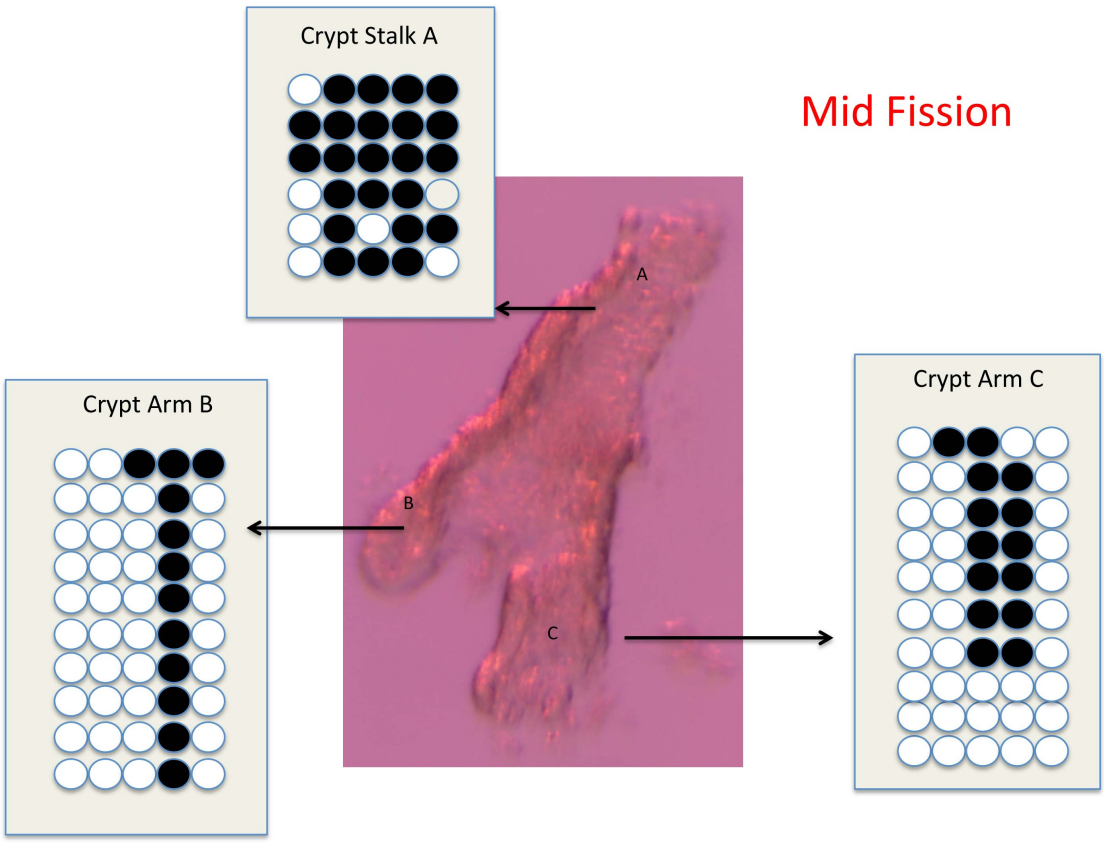

Figure 6.14. *MYOD* methylation signatures depicted from a crypt in mid fission. Taken from a 33 year old female with ulcerative colitis proctitis. The two branching arms and stalk were separated and the *MYOD* methylation signatures were calculated. Image taken at x160 magnification. The stalk A shares no unique methylation signatures with its respective bifurcating crypt arms B and C. Indeed, crypt arms B and C share no identical methylation patterns.

Figure 6.15 depicts a crypt in early fission from a 66 year old female with quiescent colonic CD, (patient number 5; Table 6.1) and shows small buds forming (Sm and L) at the bottom of the stalk (S). The larger bud, L, measures 9 cells across in maximum diameter under the microscope. There are two shared tags between buds Sm and L on analysis of the *MYOD* locus (Figure 6.15). There are 2 shared tags between stalk S and bud Sm and only 1 shared tag between stalk S and bud (Figure 6.15). Examining the same crypt but this time the *CSX* gene, bud Sm shares two unique tags with Stalk S and Bud L shares one unique tag with Stalk S. Yet buds Sm and L share no unique tags (Figure 6.16).

Patient 8, a 29 year old male with CD, (Table 6.1), was analysed using LCMD as this crypt in fission was identified on a tissue stained section of colonic tissue (Figure 6.17). The stalk appears quite diverse in comparison to its respective buds 2 and 3. There are only 2 shared unique tags between the stalk and the buds. The buds are more similar in that they share 3 unique tags between them.

The last patient analysed here was a 28 year old female with quiescent colonic Crohn's, on infliximab, patient number 9 from Table 6.1. The crypts analysed are depicted in Figures 6.18-6.20 and show 2 different crypts in early fission. Although there are only a few colonies available that show the methylation signatures in buds 3 and 4, it is clear that there are two shared unique tags between stalk 1 and bud 2 (Figure 6.18). With buds 3 and 4 there is only one shared unique tag between them and the stalk 1 (Figure 6.18).

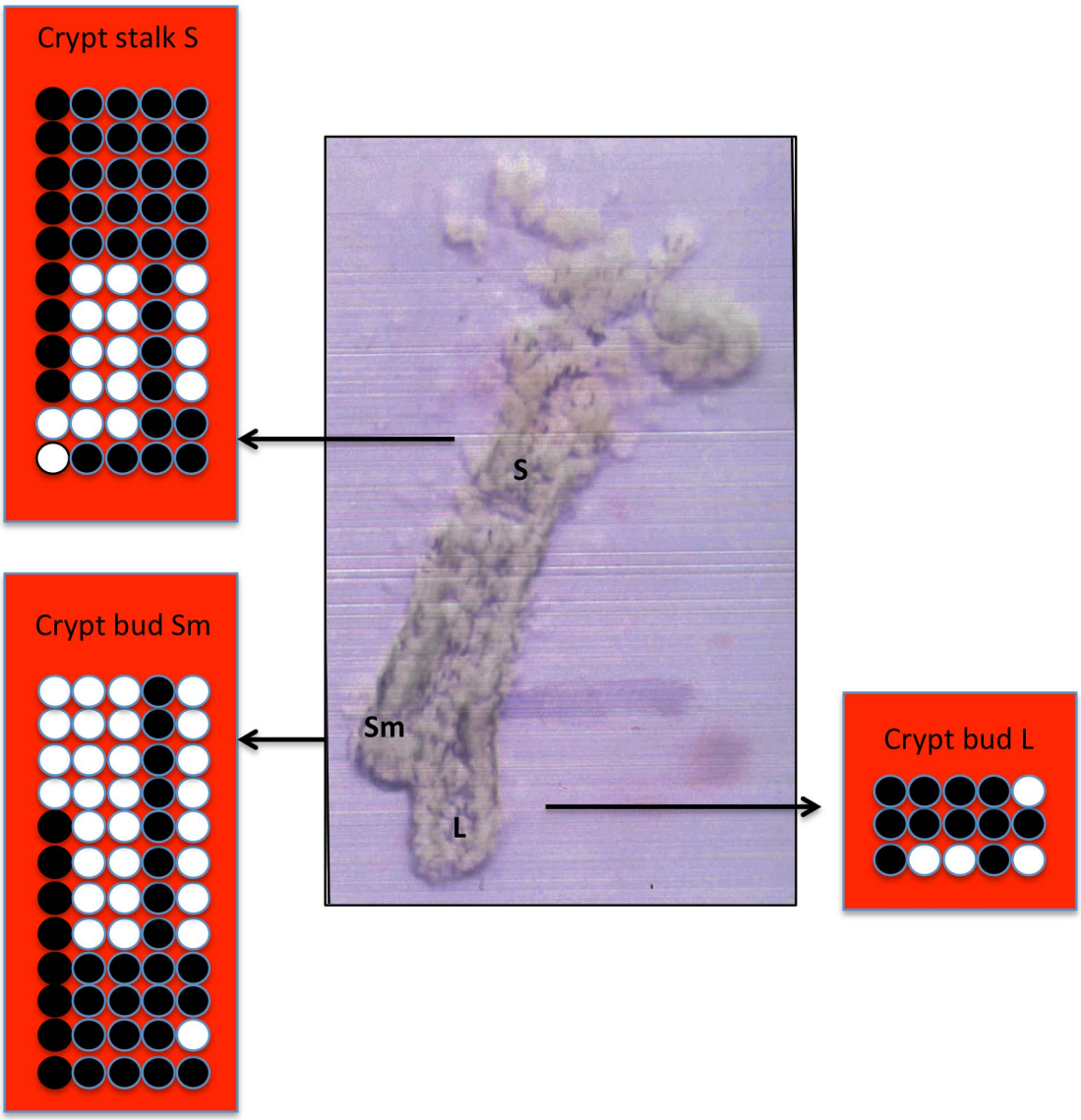

Figure 6.15. Crypt isolated from a 66 year old female with inactive colonic Crohn's disease. A crypt in the process of budding to separate where S represents the stalk of the crypt and Sm and L represent the buds. Buds Sm and L were dissected and separated from stalk S. Depicted are the *MYOD* methylation signatures of the stalk S and of buds Sm and L. There are 2 shared tags between stalk S and bud Sm and only 1 shared tag between stalk S and bud L. There are 2 shared tags between buds Sm and L.

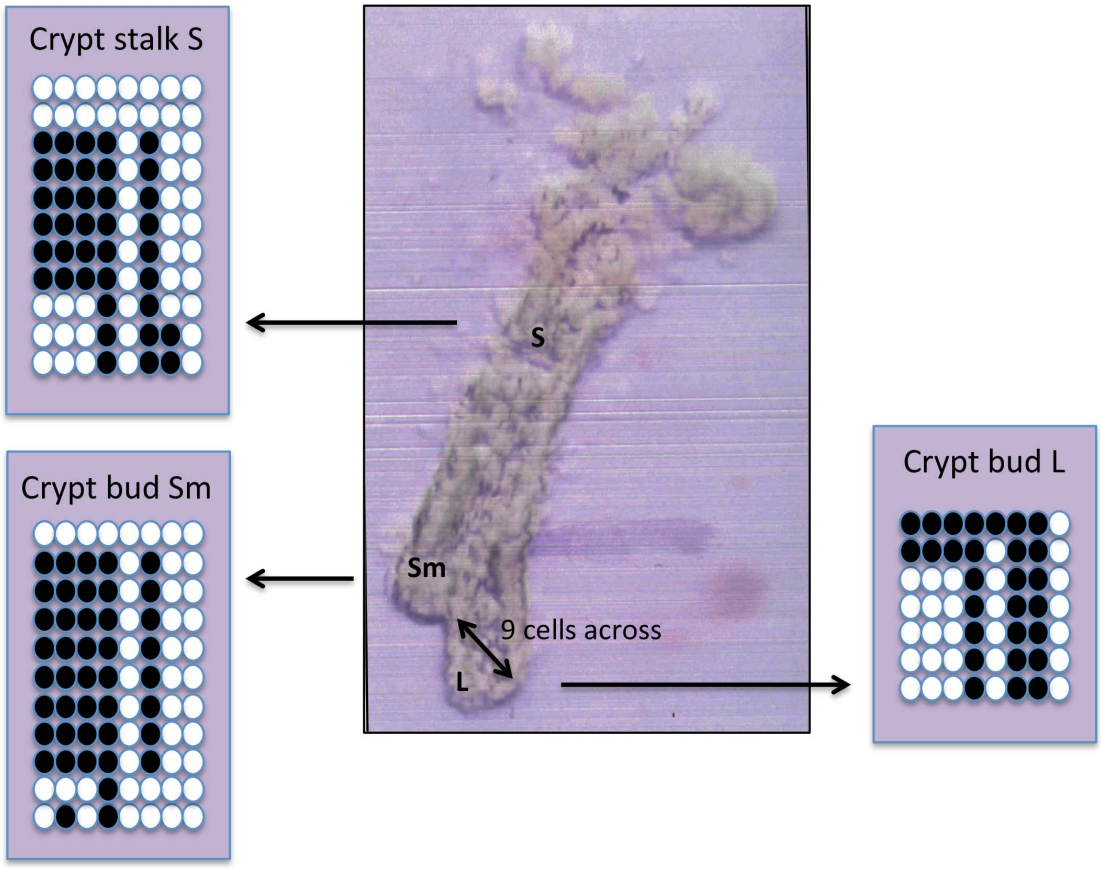

Figure 6.16. Crypt isolated from a 66 year old female with inactive colonic Crohn's disease. A crypt in the process of budding to separate. S represents the stalk of the crypt and Sm and L represent the buds. Buds Sm and L were dissected and separated from stalk S. Depicted are the *CSX* methylation signatures of the stalk S and of buds Sm and L. Bud Sm shares two unique tags with Stalk S and Bud L shares one unique tag with Stalk S. Buds Sm and L share no unique tags.

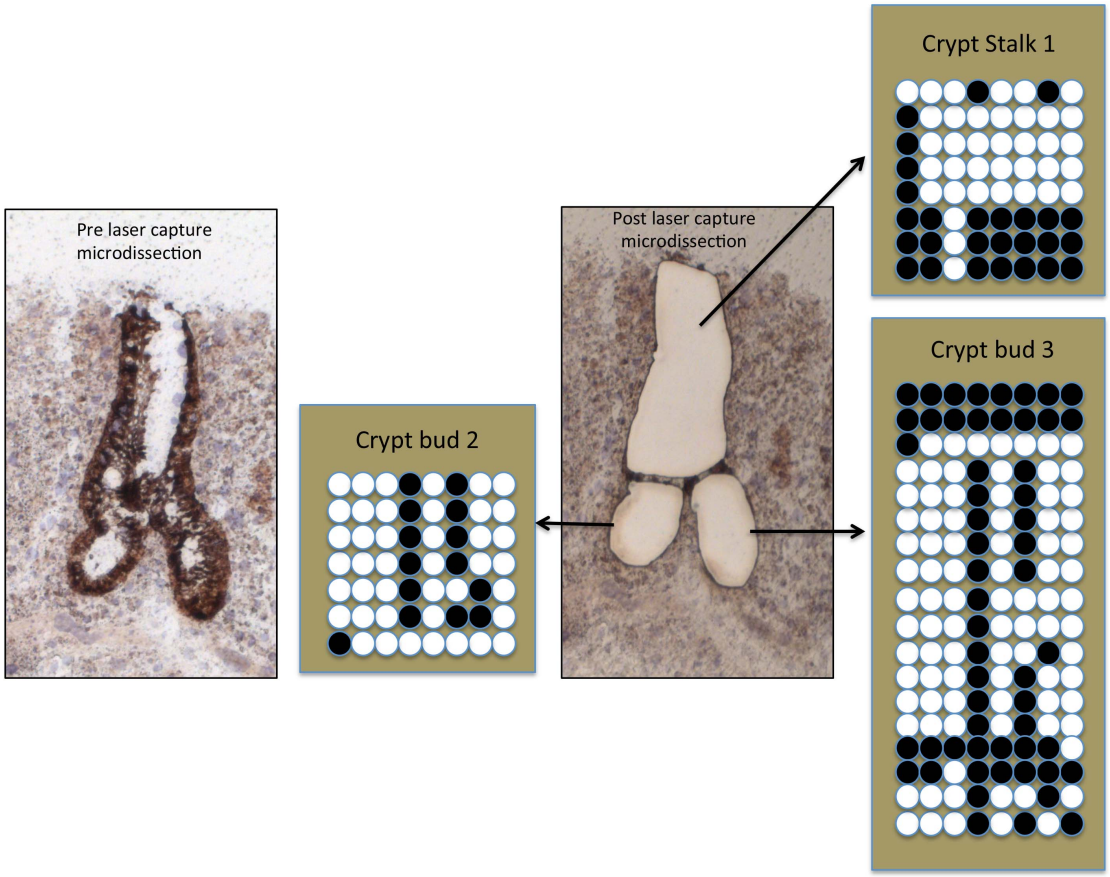

Figure 6.17. Pre and post laser capture microdissection of a crypt in fission sampled from a 29 year old male with Crohn's disease and methylation signatures. The two branching arms and stalk were separated and the *CSX* methylation signatures were calculated. The stalk appears quite diverse in comparison to its respective buds 2 and 3. There are only 2 shared unique tags between the stalk and the buds. The buds are more similar in that they share 3 unique tags between them.

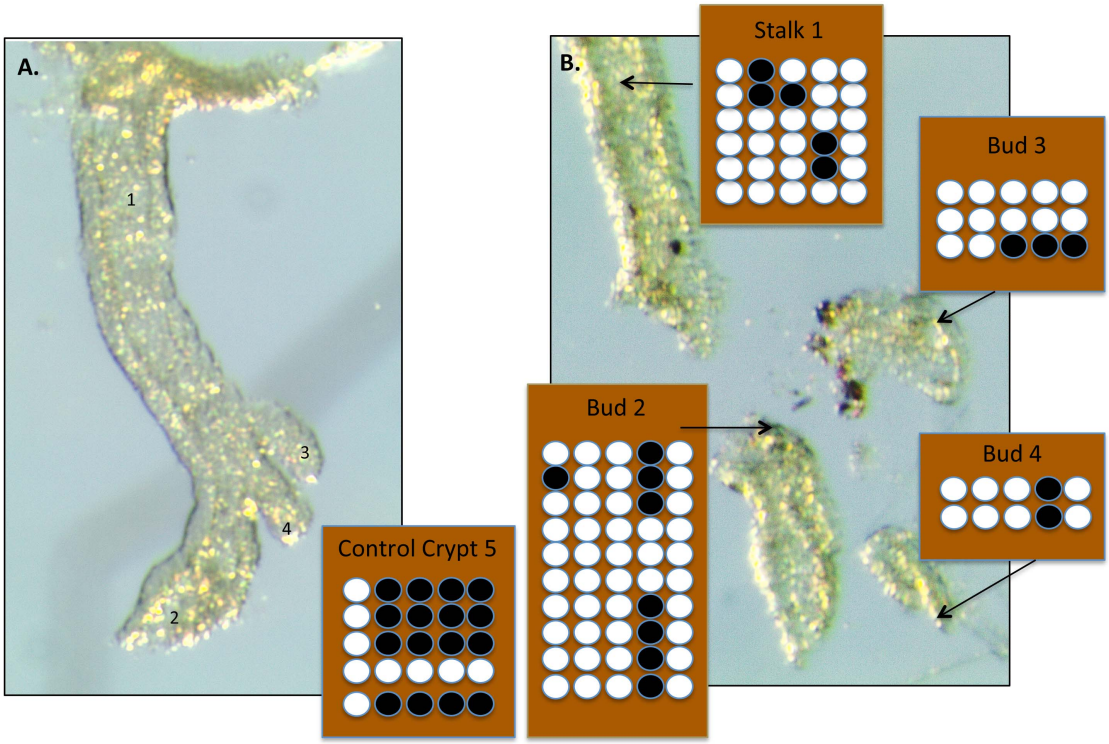

Figure 6.18. Crypt isolated from a 28 year old female with quiescent Crohn's colitis on Infliximab diagnosed aged 8 years. A. The crypt on identification. **B.** The crypt, stalk and buds following dissection and separation and analysis of *MYOD* methylation signatures. The control crypt 5 is not shown. There are two shared unique tags between stalk 1 and bud 2. With buds 3 and 4 there is only one shared unique tag between them and the stalk.

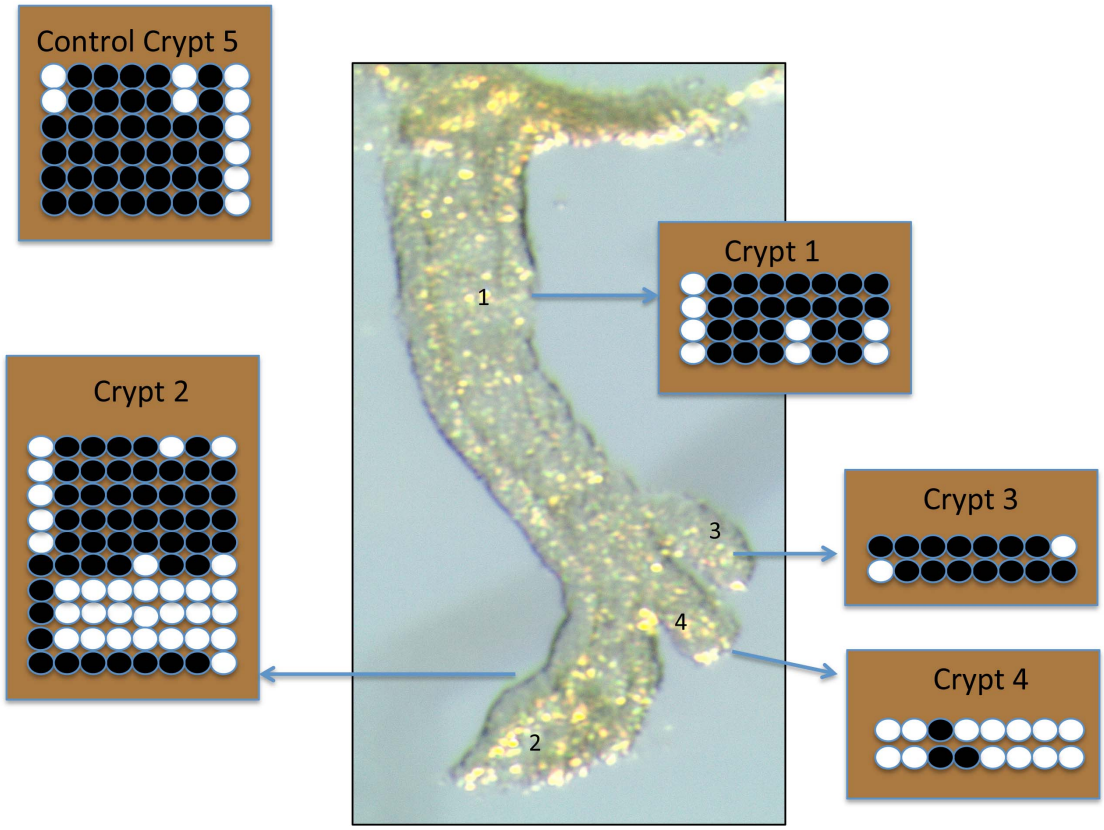

Figure 6.19. Crypt isolated from a 28 year old female with quiescent Crohn's colitis on Infliximab diagnosed aged 8 years. Depicted is the crypt stalk (1) and buds (2, 3 and 4) preceding dissection and separation and analysis of *CSX* methylation signatures. The control crypt 5 is not shown.

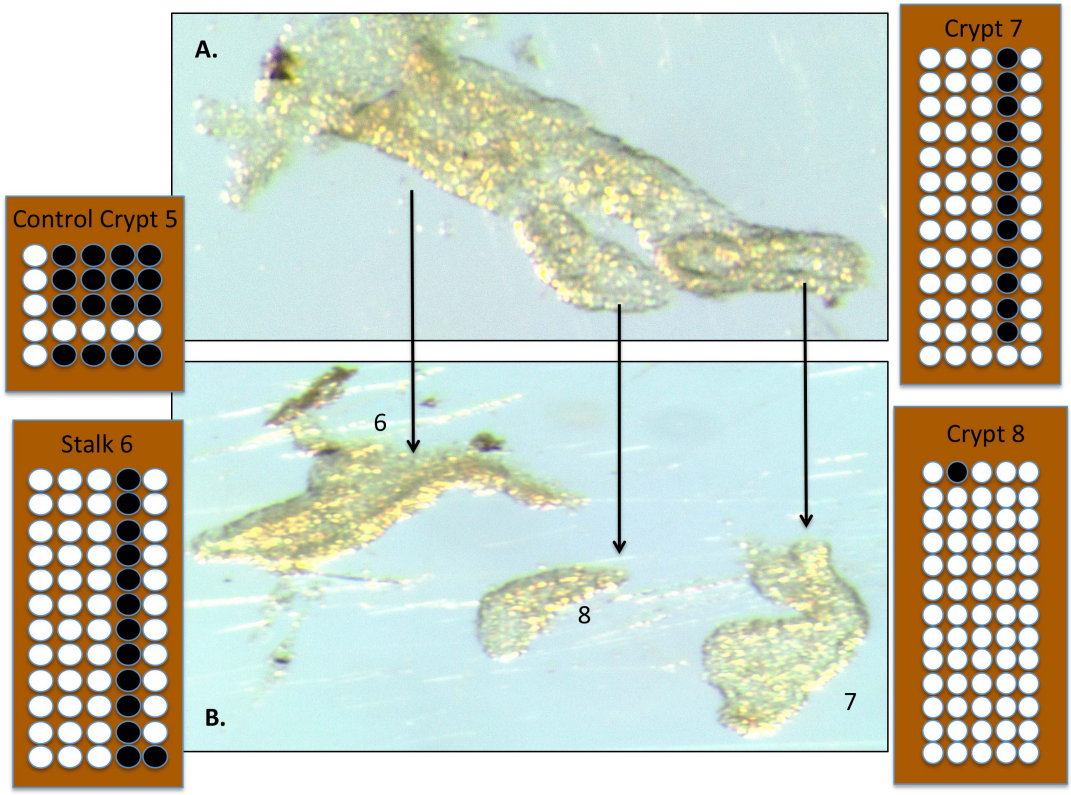

Figure 6.20. A further crypt actively undergoing fission isolated from a 28 year old female with quiescent Crohn's colitis on Infliximab diagnosed aged 8 years. **A.** The crypt on identification. **B** The crypt stalk (6) and buds (7 and 8) following dissection and separation and analysis of *MYOD* methylation signatures. The control crypt 5 is not shown. The stalk 6 and bud 7 are virtually identical except for one unique tag, yet buds 7 and 8 are relatively diverse. Bud 8 shares no unique tags with its stalk 6.

Across the *CSX* locus (Figure 6.19), again buds 3 and 4 have very little unique tags examined, bud 4 shares no unique tags with either buds 2 or 3 or stalk 1; bud 2 shares 2 unique tags with stalk 1 and bud 3 shares one unique tag. In a further crypt examined from the same patient (Figure 6.20), the stalk 6 and bud 7 are virtually identical bar one unique tag, yet buds 7 and 8 are relatively diverse. Bud 8 shares no unique tags with its stalk 6 (Figure 6.20).

There is no statistically significant difference between the epigenetic distances between crypts that are branching – either comparing the two buds or the stalk versus the bud versus a random control crypt (*CSX* locus, p=0.2820; Figure 6.21). However for the *MYOD* locus is very close to significance based on a small sample set (p=0.0536; Figure 6.22).

The epigenetic distances between *CSX* tags in branching crypts in IBD patients showed a statistically significant difference between the intracrypt distance of the stalk compared to buds 1 and 2 versus a random control crypt (p=0.042; one way ANOVA; Figure 6.23). In other words, branching crypt arms or buds show marked diversity compared to its crypt stalk. However the buds here have low intracrypt distances relative to the control crypt, as you would expect because they are from the same crypt. What is striking is the variability in the buds relative to the stalk and the control; the data may be measuring the increase in this variability, which could be related to stem cell number variability.

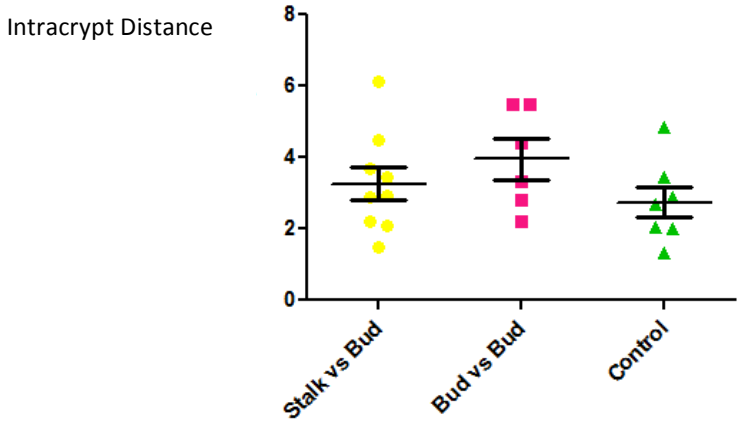

Figure 6.21. Epigenetic distances between *CSX* tags in branching crypts in IBD patients. Lines represent the mean and bars the standard error of the mean. There were no statistically significant difference between the intracrypt distance of the stalk vs bud; bud vs bud compared to random control crypts (p=0.2820; one way ANOVA).

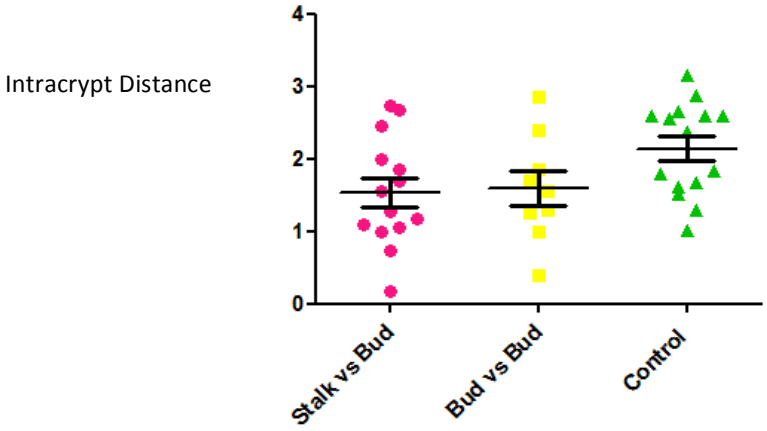

Figure 6.22. The epigenetic distances between *MYOD* tags in branching crypts in IBD patients Lines represent the mean and bars the standard error of the mean. The *MYOD* result approaches significance based on a small sample set when comparing the intracrypt distance of the stalk vs bud and bud vs bud (p=0.0536, one way ANOVA).

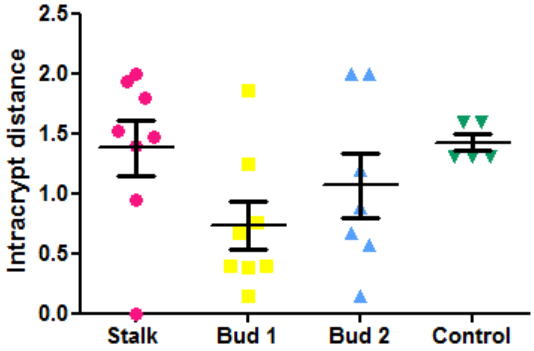

Figure 6.23. Epigenetic distances between *CSX* tags in branching crypts in IBD patients. Lines represent the mean and bars the standard error of the mean. There was a significant difference between the intracrypt distance of the stalk compared to buds 1 and 2 versus a random control crypt (p=0.042; one way ANOVA). What is striking here is the variability in the buds relative to the stalk and the control; the increase in this variability could be related to stem cell numbers.

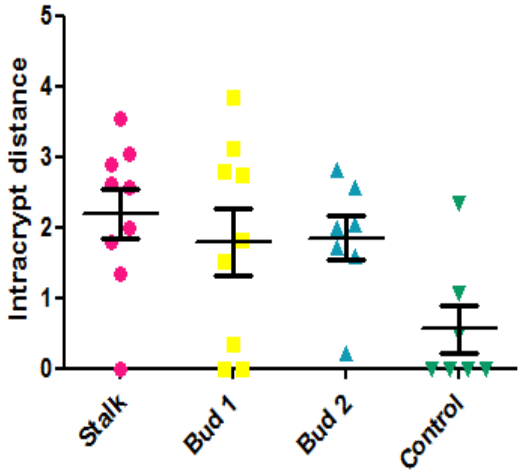

Figure 6.24. Epigenetic distances between *CSX* tags in branching crypts in IBD patients. Lines represent the mean and bars the standard error of the mean. There was a significant difference between the intracrypt distance of the stalk compared to buds 1 and 2 versus a random control crypt (p=0.042; one way ANOVA).

In Figure 6.24 depicting the epigenetic distances between *CSX* tags in branching crypts in IBD patients, the control crypt showed a lower intracrypt diversity compared to branching crypt buds and stalk demonstrating the incredible diversity and distinction in the methylation patterns within branched crypts compared to control crypts. There was a statistically significant difference between the intracrypt distance of the stalk compared to buds 1 and 2 versus a random control crypt ($p=0.042$, one way ANOVA).

6.4 Discussion

During fission how do stem cells segregate into buds? The two bifurcating buds of a crypt are not closely related at all in both *CSX* and *MYOD* loci. Two buds are more distantly related than they are to random crypts, therefore this would imply that fission takes a very long time.

When the crypt begins bifurcation into 2 small buds, how do stem cells segregate; do some stem cells lose some methylation signatures from one bud and another bud gain more stem cells, therefore more diversity and more signatures than the other bud or stalk? This seems to be the case in many examples from the data shown, where one bud may share some tags with its stalk, whereas the other bud is more diverse. In addition in some cases (Figure 6.24), the control crypt showed a lower intracrypt diversity compared to branching crypt buds and stalk demonstrating the remarkable diversity and distinction in the methylation patterns within branched crypts compared to control crypts.

Intracrypt distances reflect stem cell number. The intracrypt distances within segments

of branching crypts are more dissimilar than random control crypts when the *CSX* locus was probed (p=0.042; one way ANOVA) (Figure 6.24). Yet in Figure 6.23 examining the *MYOD* locus, there was no statistically significant difference between the stalk, buds 1 and 2 compared to random control crypts (p=0.1208; one way ANOVA) As expected the intracrypt distances for the buds were lower than the stalk and compared to random control crypts, yet this was not the case in the *CSX* gene. If we consider the *CSX* locus to be more reliable given previous data published and the fact that it has more CpG sites to probe, one would conclude that fission is clearly a long process with sufficient time for methylation signatures to diversify.

5.4.1 Branching segments of crypts undergoing fission are as dissimilar as random whole crypts

On examination of multiple branching crypts from a variety of age groups the branching stalks and bifurcating buds/arms were as dissimilar in terms of their epigenetic distance compared to whole random crypts (see Figures 6.21-6.22). This was corroborated in both *CSX* and *MYOD*.

The fate of human intestinal crypts remains enigmatic. Some murine studies have permitted the examination of crypt behaviour in terms of development, but not ageing due to the short lifespan of mice. The intestinal epithelium is a rapidly proliferating tissue and represents a dynamic evolving population. In order to accommodate such prolific growth, crypts bifurcate longitudinally into two daughter crypts through a process termed fission. It is thought that the crypt fission time in mice is approximately 108 days (Wright 2000). The corporal separation of branched crypts takes between 12 hours and 5 days, in order to form two new daughter crypts (Wright

2000). Fission is pronounced in early murine life but regresses with age (Cheng and Bjerknes 1985). Crypt fission in human adult colon is thought to recur through life, and is detected at a very low level in the ageing colon, and has been documented as less than 1% of all crypts in normal adult colons (Cheng et al. 1986). Crypt fission is upregulated in IBD by approximately 44% (Cheng et al. 1986). In keeping with this finding, in healing tissue, as a result of epithelial damage, the proportion of crypts in fission increases (Cheng et al 1986; Park et al. 1995; Totafurno et al. 1987). Quantitative analysis of genetic lineage tracing studies in mice have shown the low basal rate of crypt fission in the normal murine large bowel is increased 30-fold by oncogenic *KRAS* mutation (Snippert et al. 2014). Furthermore, it is the fission of a transformed crypt, not the aberrant growth of cells *per se*, that promotes the initial expansion of colorectal adenomas (Wong et al. 2002; Preston et al. 2003). In spite of the pivotal role of crypt fission in colorectal cancer initiation, the evolutionary dynamics of the human intestinal crypt population remains unclear. It would seem from the data presented that crypt fission, although occurring more often in IBD as described by Cheng et al. in 1986, following the cycles of inflammation and repair driving this process, however, as the crypts enter this fission state, they may remain as such for a prolonged period of time, akin to normal colon (Graham et al 2011).

According to our findings, branched crypts were no different in terms of epigenetic distances to non-branching crypts. This would imply that fission is occurring very slowly to account for the lack of variability. An alternative explanation could be that once crypts are committed to separate into two daughter crypts, they remain stuck in fission in a limbo state for sometime until they then separate. In this regard, Graham *et al* (Graham et al. 2011) assessed epigenetic distances between crypts known to be

clonally-related through the sharing of a common mtDNA mutation; adjacent clonal CCO^{-} crypts showed methylation patterns as divergent to one another as methylation patterns of two unrelated crypts, while the arms of bifurcating crypts had distinct methylation patterns, indicating that fission disrupts epigenetic records of crypt ancestry. This is in keeping with the data presented here, where the bifurcating arms or buds of a crypt in fission show distinct methylation signatures relative to each other. It was estimated that normal colonic crypts divided approximately every 17–25 years.

We know that mutant clones expand via crypt fission in the human intestine (Greaves et al. 2006; Gutierrez-Gonzalez and Wright 2008). We know fission is a rarity in the normal colon but in IBD this rate is elevated (Cheng et al. 1986). However, having driver tumorigenic mutations may further increase the crypt fission rate. A prospective candidate for growth impetus would be the chronic cycling of atrophy and mucosal healing, characteristic of chronic inflammation. Certainly, Galandiuk et al. (Galandiuk et al. 2012) showed that mutant clones were only located in actively inflamed regions of the bowel. However, it seems questionable that a mutant clone could maintain this rapid growth, especially if this process is occurring as slowly as it appears in this data set. Obviously the methylation changes detected in this data set are completely neutral as the genes are not transcribed. There may be an alternative mechanistic process, such as stem cell migration between crypts, comparable to the migration between niches noted in the Drosophila ovary (Nystul and Spradling 2007). This seems more likely given the data presented, where crypt arms and buds are very diverse in comparison to each other, and where very few methylation tags are shared with the stalk. There is very little data on the processes that activate crypt fission. Certainly

mathematical modeling has proposed that intestinal crypt fission occurs when a certain threshold of crypt stem cells has been reached. This is corroborated by murine intestinal lineage tracing studies, (Paulus et al. 1993; Loeffler et al. 1997). Further support for this notion is provided by two studies by Totafurno and colleagues, (Totafurno et al. 1987; Totafurno et al. 1988). These workers found that crypts undergoing fission were actually bigger in size than non-branching crypts. Perhaps pre-tumour mutations could increase the basal crypt fission rate and propel clonal expansion. Pre tumour mutations could feasibly, increase the number of stem cells in a crypt via Wnt signaling, this could drive the spread of clones (Humphries et al. 2013). Certainly in the data presented, the branching crypt arms and buds appear very diverse in comparison to their respective crypt stalks, perhaps representing increased stem cell number following pre tumour mutations driving clonal expansion in IBD.

In summary the data demonstrates that there is no difference between the epigenetic distances of crypts in various stages of fission and that fission is clearly a long process with sufficient time for methylation signatures to diversify.

The final results chapter will turn to pseudopolyp lesions in IBD, examining their malignant potential and their possible ability to drive clonal expansion in IBD.

CHAPTER 7 ANALYSIS OF FEATURES ASSOCIATED WITH THE EARLY STAGES OF MALIGNANT PROGRESSION IN PSEUDOPOLPS

7.1 Introduction

Inflammatory pseudopolyps are irregularly shaped islands of residual intact colonic mucosa that are the direct consequence of the mucosal ulceration and regeneration that is a predominant characteristic of IBD (Goldgraber 1965). These polyps are typically multiple, often filiform and scattered throughout the inflamed region of the colon.

In this chapter I will investigate whether there is any evidence that pseudopolyps have characteristics more usually associated with malignant progression: firstly, I present an observational study on pseudopolyps; followed by assessing cellular proliferation as measured by Ki67 immunolabelling; expansion of the stem cell component in the form of increased numbers of *LGR5*$^{+}$ cells by ISH; presence of oncogenic mutations and microarray profiles more consistent with dysplasia than apparently normal mucosa from IBD patients.

7.2 Do inflammatory bowel disease patients with pseudopolyps develop pre-malignant lesions and/or CRC?

7.2.1 Hypothesis

The hypothesis is that pseudopolyps are a pre-malignant marker for progression to CRC. Therefore, an observational study was carried out on pseudopolyps in IBD

patients who subsequently went on to develop pre-malignant lesions and or CRC on colonoscopy. This was postulated to be both spatially and temporally correlated.

7.2.2 Aims

Pseudopolyps have historically been regarded as benign markers of inflammation associated with IBD, and current colonoscopic surveillance programmes do not focus on them being of clinical importance. Consequently they are not recorded with the same accuracy or managed in the same treatment pathway as adenomatous polyps, a known risk factor for CRC development. Based on recent research findings of genetic markers in pseudopolyps known to predispose to colitis-associated cancers I planned to investigate pseudopolyps as possible pre-malignant markers and potential sites of development of CRC. A retrospective case-control observational study was carried out using patients registered for treatment of IBD within Bart's Health NHS Trust, Queens University Hospital, University College Hospital and The Homerton University Hospital. The aim was to investigate both the location of pseudopolyps and the pre-malignant lesion and or CRC to see if they are in the same area, as well as examining other related variables, such as treatment factors, and pre-existing family history of CRC.

7.2.3 Methods

7.2.3.1 Source population

Our study cohort comprised IBD patients from the Royal London Hospital, Newham University Hospital, Whipps Cross University Hospital, Queens University Hospital, Romford, University College Hospital and Homerton University Hospital.

7.2.3.2 Selection of cases and controls

To select our initial cohort, a search on the pathology database at the Royal London, for all patients who had been categorised as having both IBD and CRC from histology reports was performed. Their surveillance colonoscopy reports were then interrogated. Further searches were then performed for the categories of IBD patients who had had dysplasia identified on histology, as well as searches for patients with IBD with adenomas and pseudopolyps, IBD and pseudopolyps, and IBD with pseudopolyps and CRC. The Royal London Hospital pathology database includes data from Homerton University Hospital in one amalgamated database. The same searches were then subsequently performed at Newham University Hospital, Queens University Hospital, University College Hospital and Whipps Cross University Hospital, and the results collated into separate lists.

7.2.3.3 Data collection

Patients were retrospectively followed from their date of diagnosis with IBD, or as early as their records allowed, to their development of CRC. Controls were followed from the date of development of their IBD to a corresponding date as their cases developed CRC. Data was collected both from electronic copies of pathology reports on the hospital pathology database and electronic copies of patient clinic letters and colonoscopy reports, held on the hospital correspondence database.

7.2.3.4 Definition of variables

Criteria were based on prior studies by Velayos et al. (2006) and Rutter et al. (2004b) and examined appearance at colonoscopy and correlated them with long-term risk of

developing CRC in case-control studies. All criteria used have been previously shown to influence the risk of development of CRC in IBD patients, either positively or negatively. Patient, clinical, endoscopic, and treatment data was recorded, as well as demographic data to decrease the risk of confounding factors where possible. Patient adherence was also examined- each patient's colonoscopy reports were examined to check against recommended adherence according to the British Society of Gastroenterology (BSG) guidelines for colonoscopy surveillance in IBD. Each patient should have had, as a minimum, a colonoscopy every ten years, and most of the selected patients should have had more frequent colonoscopies than that, due to their identified risk factors.

7.2.4 Results

From the colon maps depicted, it is possible to track both temporally and spatially the pseudopolyp lesions and the pre-malignant and malignant lesions (Figure 7.1 and Chapter 9 Appendix).

In 21% (12/58) of cases, pre-malignant lesions or cancerous lesions were identified as developing at a site of a previously documented pseudopolyp (IBD+adenoma and pseudopolyps n=38; pseudopolyps and CRC n=13; pseudopolyps/dysplasia n=3; pseudopolyps and dysplasia associated lesion and mass (DALM, n=3; pseudopolyps and hyperplastic polyp n=1; Table 7.1). This suggests that pseudopolyps could be the reservoir for the generation of mutations that may trigger a malignant transformation.

Patient Number	Age	diagnosis	Tissue sites
1	76	UC distal sigmoid	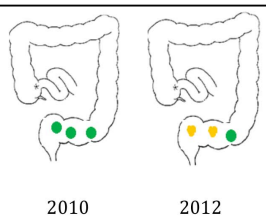 2010 2012
3	60	UC total	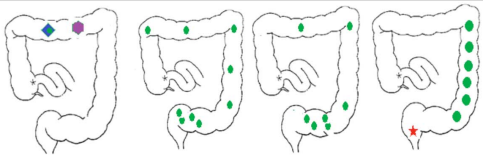 2003 2006 2007 2009
6	73	UC left sided	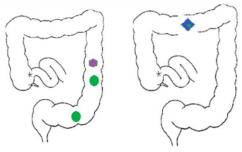 2006 2007
13	77	Colitis	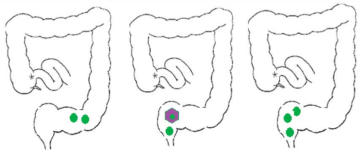 2008 2011 2013
14	64	UC pancolitis	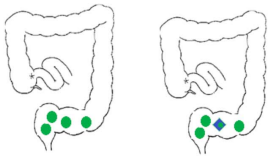 2007 2013

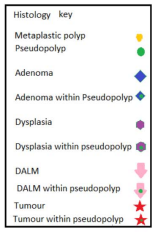

Figure 7.1 Colon maps for 6 patients with pseudopolyps and pre-malignant and/or malignant lesions. The lesions are depicted spatially and temporally.

Table 7.1 Total numbers of patients identified for each set of selection criteria.

Cases	
IBD + CRC	28
IBD + dysplasia	4
IBD + adenoma + pseudopolyps	38
IBD + pseudopolyps + CRC	13
IBD + pseudopolyps	103
IBD + pseudopolyps+dysplasia	3
IBD + adenoma (no pseudopolyps)	3
IBD + pseudopolyps + DALM	3
IBD + pseudopolyps + hyperplastic polyp	1
Total number of cases	196

There were insufficient numbers with dysplasia (n=7; 3 with pseudopolyps) to determine if pseudopolyps were associated with this lesion. However, of the patients who developed adenoma (n=41) there was a significant increase in the incidence of pseudopolyps (38/41; $p<0.0001$, Fisher's exact test) indicating an association between pseudopolyps and development of an adenoma.

A total of 41 patients (IBD+: CRC n=28; pseudopolyps + CRC n=13; Table 7.2) who had developed colitis-associated cancers, were studied, of which 38% had pseudopolyps (13/41; UC, n=9; CD, 4). Of the patients with CRC, statistically fewer had pseudopolyps ($p=0.0018$, Fisher's exact test). However, of the cases with pseudopolyps and cancer, 38% (5/13) developed cancer in the same area as a previously documented pseudopolyp site. Interestingly, one case had synchronous neoplastic lesions, one from the hepatic flexure and one from the rectum, both sites of previously documented pseudopolyps.

In addition, 3 IBD patients had pseudopolyps and DALM and 1 had pseudopolyps and a hyperplastic polyp; giving 45 in total. Of these 45, 16 patients developed changes within a previously documented pseudopolyp 36% (16/45). 27% had UC (12/45), 7% had Crohns (3/45), and in a single case the diagnosis was indeterminate colitis (Table 7.1).

Pseudopolyps may be reconsidered as a pre-malignant marker for CRC, and treated in the same way as other equivalent lesions such as adenomatous polyps, when identified on endoscopic screening. I next consider whether pseudopolyps show increased proliferation and/or increased stem cell number.

7.3 Do crypts in pseudopolyps show increases in proliferation and *LGR5* positive stem cells characteristic of progression?

Pseudopolyps histologically contain more hypertrophied crypts, than in non pseudopolyp IBD tissue. So does that indicate that the proliferative zone is increased in pseudopolyps compared to crypts from control UC tissue? Also, is the percentage of $LGR5^+$ cells in the crypt base altered and is this linked to a change in stem cell number and consequent cellular proliferation?

Proliferation can be measured using Ki67 immunolabelling as the marker is expressed from late G1 to mitosis in the cell cycle, is highly phosphorylated in mitosis and absent in resting cells. This makes Ki67 the marker of choice for observing cellular proliferation. Expression of the Wnt target gene *LGR5* has been demonstrated to be a robust marker of colonic stem cells in mice (Barker, 2007). *In situ* hybridization (ISH) to detect *LGR5* mRNA can be used to determine the number of $LGR5^+$ cells.

7.3.1 Hypothesis and aims

The hypothesis is that there would be more $Ki67^+$ cells in pseudopolyps compared with control IBD crypts because of a stronger survival advantage and reduced apoptosis. Similarly, the number of $LGR5^+$ cells would be increased as a consequence of expansion of the stem cell compartment.

7.3.2 Methods

Details for Ki67 are given in Materials and Methods section 2.6. To test for proliferation rates 30 crypts from pseudopolyp tissue samples were analysed for Ki67

positivity, compared to the total number of cells in one side of the crypt along its longitudinal axis.

In situ hybridisation was performed on serial sections of FFPE pseudopolyp UC tissue (see Materials and Methods 2.7) as the protocol does not work effectively on fresh frozen tissue due to the activation of endogenous RNAses and disruption of the anatomy as a consequence of the various digestion steps.

7.3.3 Results

A total of 30 individual crypts in pseudopolyps and control IBD crypts were counted (n=60). The total cell number was significantly different in pseudopolyps versus controls (mean, 82 and 66.1, respectively; $p< 0.00208$ using a two-tailed Student's t-test; Figure 7.2). There were more $Ki67^+$ cells in the individual crypts of pseudopolyps as compared to control IBD crypts, which was statistically significant ($p<0.0047$, using a two-tailed t-test; Figure 7.2). This showed that there was more actively cycling cells in pseudopolyps compared to controls (29.2% versus 23%). Representative images of Ki67 staining are shown in Figure 7.3.

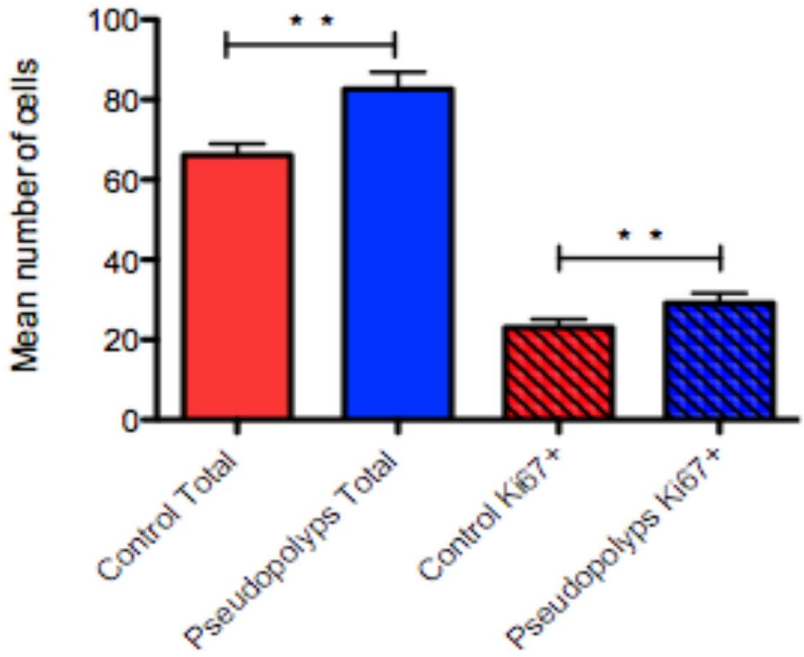

Figure 7.2 The total number of cells and actively cycling cells was higher in pseudopolyps. Mean cell number ± SEM of cells and $Ki67^+$ cells within 30 control IBD crypts and 30 pseudopolyp crypts are shown. There were significantly more cells in pseudopolyps than control IBD crypts ($p< 0.00208$, two-tailed Student's t-test). The mean $Ki67^+$ cell number was larger in pseudopolyps compared to controls (29.2 versus 23%), which was statistically significant $p<0.0047$ using a two-tailed t-test.

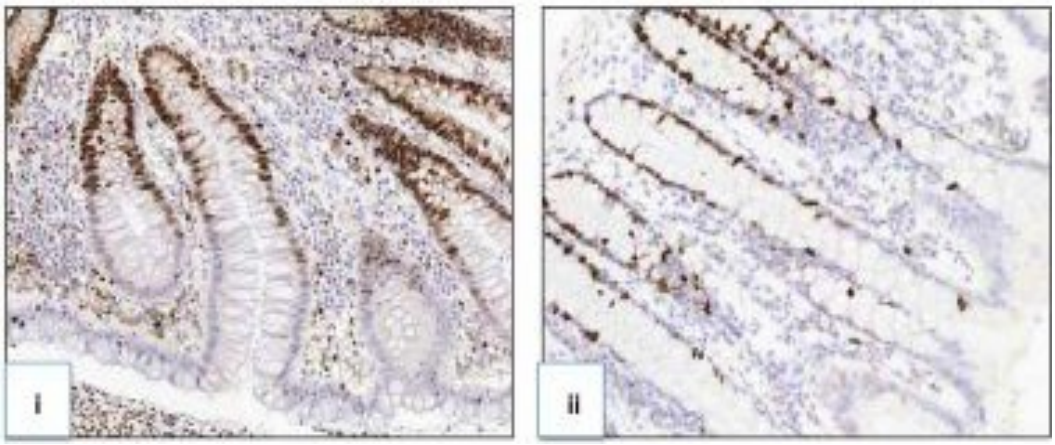

Figure 7.3 Representative examples of Ki67 immunohistochemical staining of UC colonic tissue. (i) extensive Ki67 positive cells within crypts sampled from pseudopolyp tissue. (ii) Ki67 staining in crypts sampled from IBD crypts not within pseudopolyps (control crypts).

7.3.4 Assessment of *LGR5 in situ* hybridisation in Pseudopolyps

Pseudopolyps from IBD tissue exhibit signal for LGR5 mRNA that is specific to the crypt base and the putative stem cell niche compartment (Figure 7.4). There was no obvious increase in $LGR5^+$ stem cell numbers in pseudopolyp crypts.). A total of 20 crypts from 10 IBD patients were examined by counting 10 cells on both sides of the crypt from the base. $LGR5^+$ cells were recorded and give a mean ± sem of 0.07±0.02 positive cells per crypt. The number of $LGR5^+$ cells in the human large bowel is smaller than the murine small intestine for which there is considerable data. The very low number of $LGR5^+$ cells here suggests there was no obvious increase in $LGR5^+$ stem cell numbers in pseudopolyp crypts.

Interestingly, there was an exception where *LGR5* mRNA was present in a row of cells not at the base of a crypt; a possible example of cells with stem cell potential expanding and moving out over the damaged surface, ready to seed growth of a new crypt (Figure 7.4). A further pseudopolyp from another patient demonstrated *LGR5* in cells near the base of crypts that looked to be in the process of bifurcation (Figure 7.5).

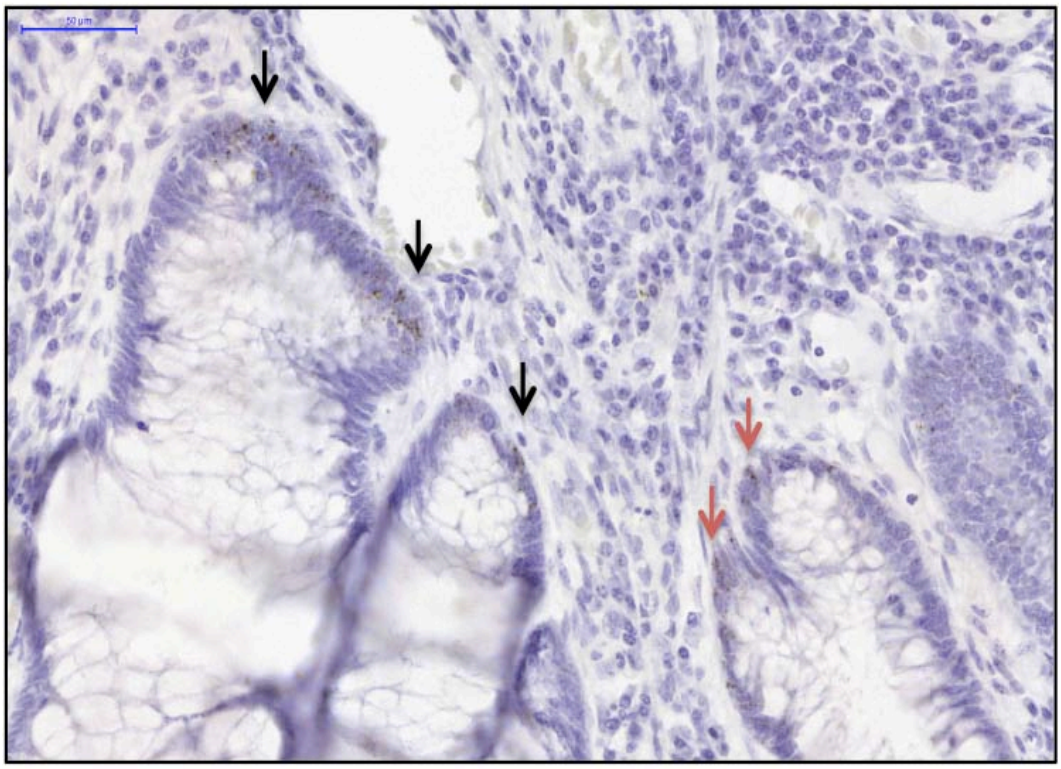

Figure 7.4 Representative example of *LGR5*$^{+}$ stem cells in pseudopolyps. *In situ* hybridisation for *LGR5* mRNA is specific to the basal stem cell niche for all crypts (see black arrowheads). The red arrowheads show *LGR5*$^{+}$ stem cells near the base of crypts that look to be in the process of possible bifurcation.

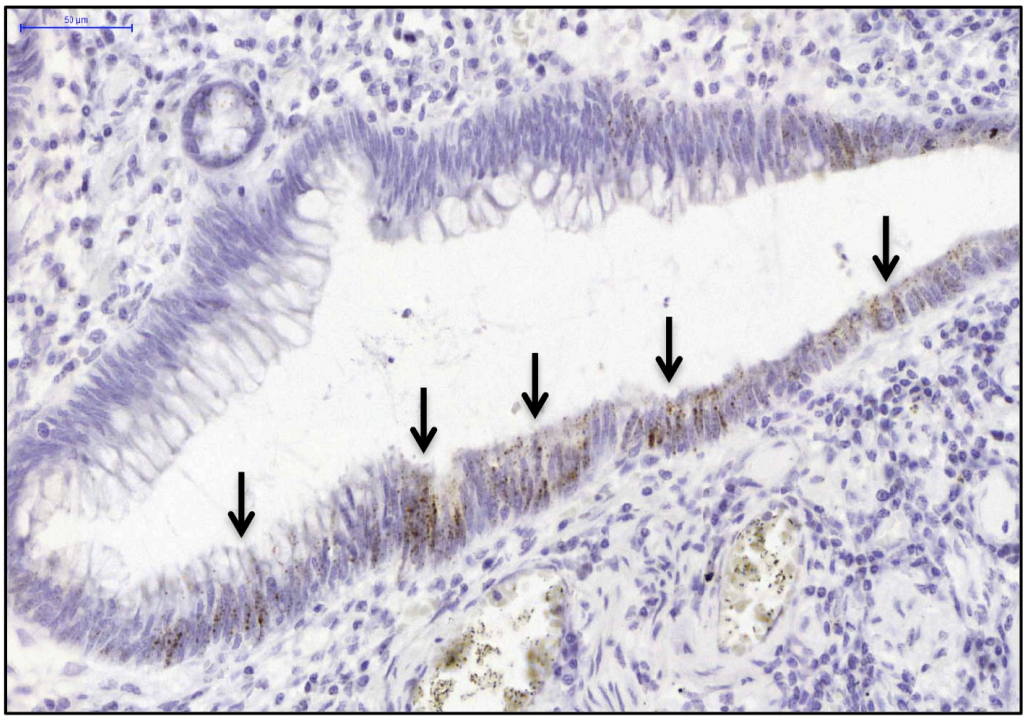

Figure 7.5 *LGR5*$^{+}$ stem cells in a pseudopolyp. The arrows demarcate *LGR5*-positive cells in a row not at the base of the crypt.

7.4 Are pseudopolyps a possible source of pro-tumourigenic mutations in ulcerative colitis?

Traditionally, pseudopolyps are thought to be benign lesions, but when pseudopolyps are grouped in clusters they may be associated with surrounding dysplasia (uptodate; www.uptodate.com). In the characteristic cycle of gastro-intestinal inflammation and epithelial restitution seen in IBD, pseudopolyps, may be the source of the healing colonic epithelium. It has been previously shown that protumourigenic mutations can spread through the entire colon of patients with CACRC (Galandiuk et al. 2012; Leedham et al. 2009). Therefore, pseudopolyps may possess a survival advantage over normal epithelium during inflammation possibly due to a pro-tumourigenic mutation. Restitution of the bowel from such mutated polyps may result in massive expansion through the bowel.

7.4.1 Hypothesis and aims

My primary hypothesis is that pseudopolyps (Figure 7.6) may be the areas where mutations are harboured, acting as a 'nursery' for the genesis of repopulating cells that carry mutations. A secondary hypothesis is that pseudopolyps are clonal expansions of crypts that have acquired a protumourigenic survival advantage over surrounding normal epithelium that frequently perishes in the inflammatory milieu. Here, the aim is to test the hypothesis in vivo, to determine the genetic status of pseudopolyps and frequency of mutated pseudopolyps, by screening thirty IBD patients for mutations in the commonly mutated tumour suppressor and oncogenes seen in CACRC.

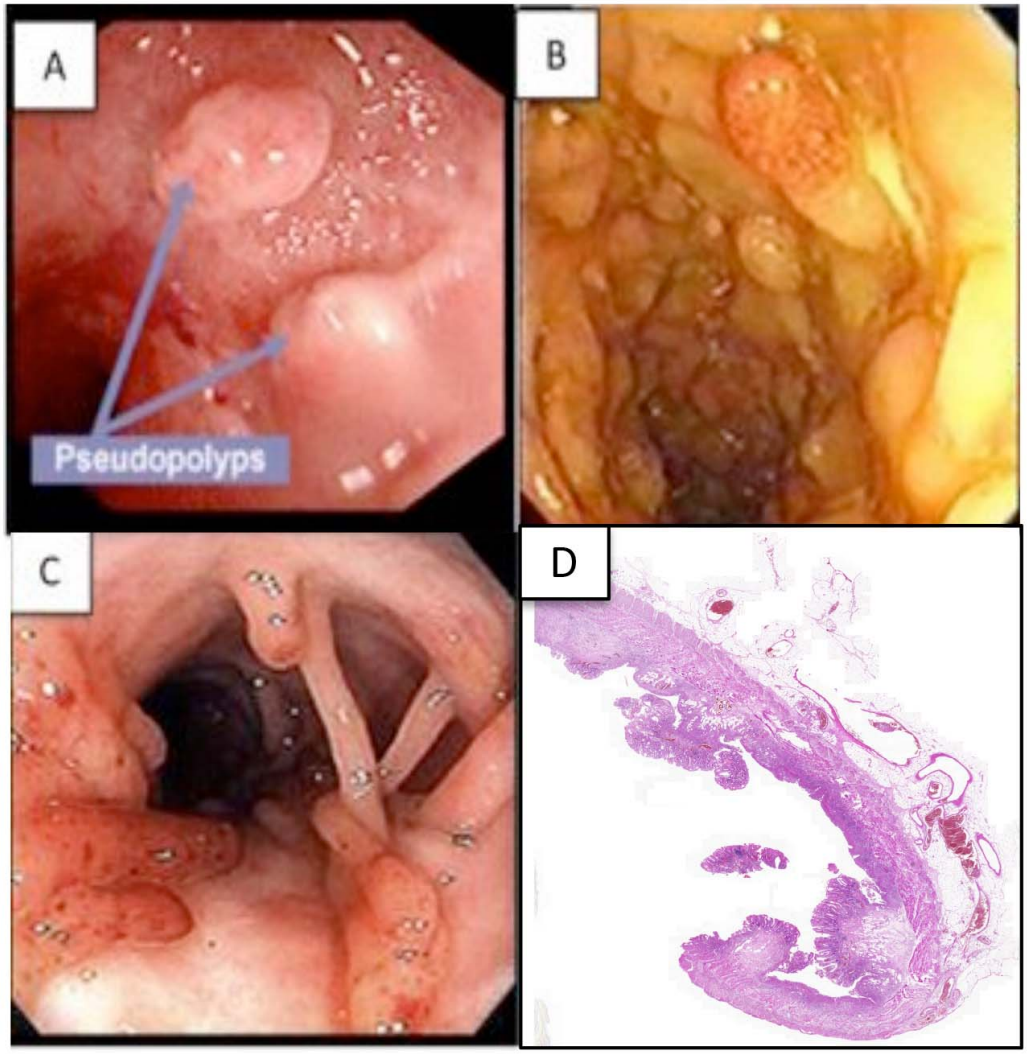

Figure 7.6. Endoscopic view and haematoxylin and eosin staining of pseudopolyps. A. several pseudopolyps at endoscopy; **B**. a 'carpet' of pseudopolyps at endoscopy; **C**. large filiform pseudopolyps at endoscopy; **D**. an H&E stain of a pseudopolyp taken from a UC resection specimen.

7.4.2 Methods

DNA was extracted from macrodissected UC-associated pseudopolyp tissue sections. Thirty patients with IBD and pseudopolyps were examined, 15 female and 15 male, aged between 28-80 years. Nested polymerase chain reaction sequencing of *KRAS*, *CDKN2A* and *TP53* was performed using published protocols (see Materials and Methods section 2.9). Haematoxylin and eosin staining was performed for each specimen (Figure 7.6) as this is the standard practice for the histological analysis of tissue samples from patients with IBD.

7.4.3 Results

Of 30 pseudopolyp samples analysed from 30 different patients, 4 patients had identifiable mutations: *CDKN2A* (c.C387T p.Y129Y); *TP53*-exon7 (c.C735T p.G245G); and *KRAS* (c.G37A p.G13D, and c.G35C p.G12A) (summarised in Table 7.2 with representative traces shown in Figure 7.7). The observation of mutations in pseudopolyps adds considerable weight to the hypothesis that these lesions harbour genetic changes associated with malignant change.

Table 7.2 IBD Pseudopolyp patients and their respective genetic mutations. The 4 informative cases were aged between 30-63years.

Patient	IBD	Mutated Gene
1	UC	*CDKN2A* (c.C387T p.Y129Y)
2	UC	*TP53*-exon7 (c.C735T p.G245G)
3	UC	*K-RAS* (c.G37A p.G13D)
4	UC	*K-RAS* (c.G35C p.G12A)

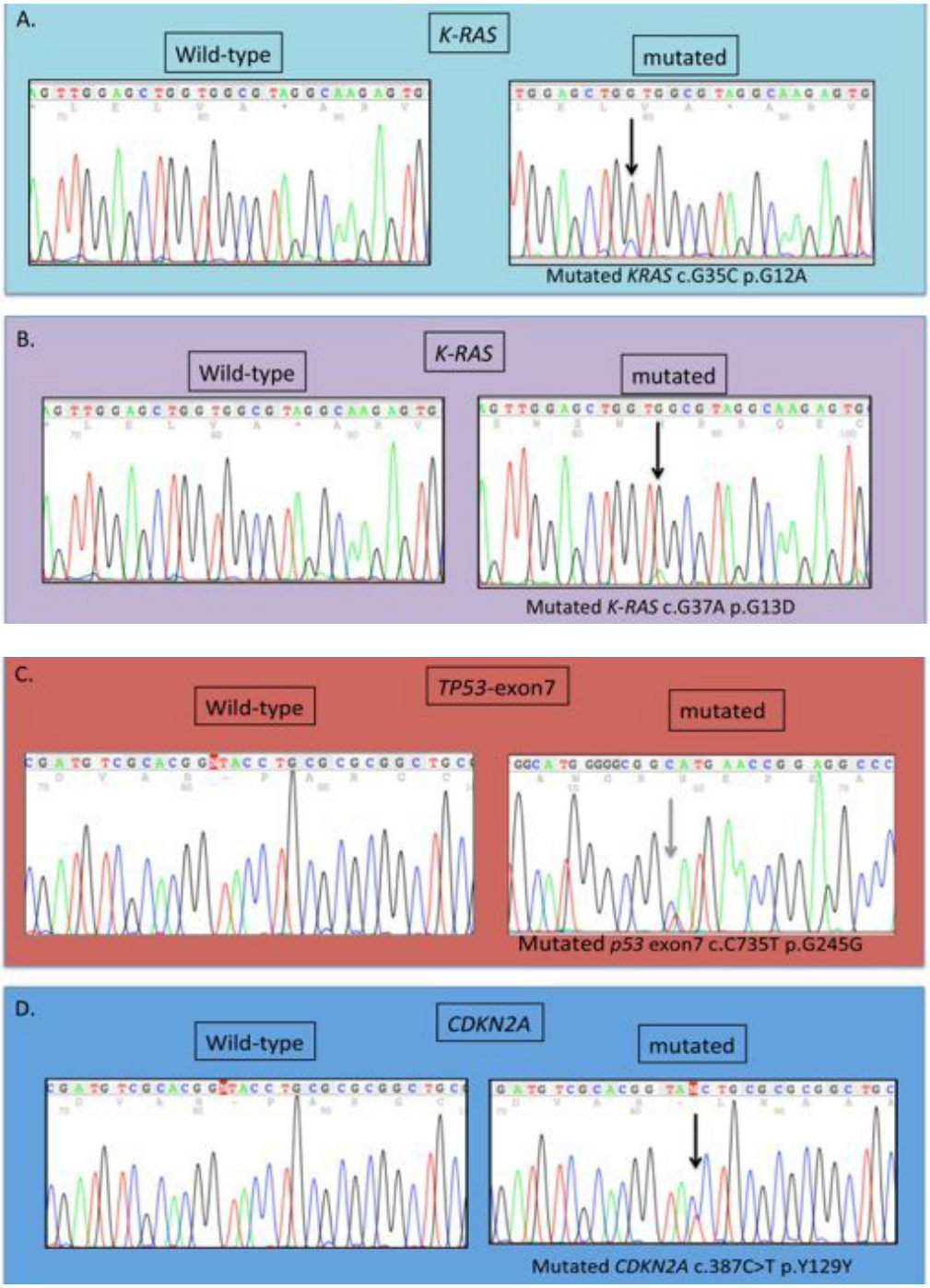

Figure 7.7 Representative Electropherograms of mutations from 4 inflammatory bowel disease patients. A. *KRAS*, c.G35C p.G12A and **B.** *KRAS*, c.G37A p.G13D. **C.** *TP53* (exon 7) c.C735T p.G245G. **D.** *CDKN2A*, c.387C>T p.Y129Y.

7.5 Does microRNA array analyses demonstrate potential for malignant change in pseudopolyps in IBD patients?

Recent studies support a role for dysregulation of microRNAs (miRNAs) in the initiation and progression of cancer (Bartel 2009). Consequently, miRNA profiles have distinct potential as markers for cancer diagnosis and prognosis. MiRNAs negatively regulate mRNA expression through sequence specific interactions and at least one thousand miRNAs are predicted to exist in the human genome, likely regulating almost every cellular process (Bartel 2009). Profiles of microRNAs within tissues are likely to alter as progression toward malignancy takes place. It is therefore possible that pseudopolyps have profiles that are more characteristic of dysplastic lesions than apparently normal IBD mucosa. Ultimately, such profiles may be used as biomarkers to distinguish those pseudopolyps with the highest potential for malignant change. Such MiRNA profiles would eventually be incorporated into a laboratory assay suitable for diagnostic and prognostic use allowing discrimination between abnormal and healthy tissue (Felice et al. 2015).

7.5.1 Hypothesis and aims

The hypothesis is that the inflammation-associated changes to the intestinal mucosa that drive progression to dysplasia and CACRC result in dysregulated expression of miRNAs and that pseudopolyps have profiles more akin to dysplasia than IBD intestinal mucosa. This study aims to establish miRNA profiles in inflammation and pseudopolyps presenting in UC patients. Profiles will be compared with ongoing studies in the laboratory focused across the spectrum of inflammatory disease (dysplasia and CACRC). In particular, miRNAs consistent with dysplasia and CACRC that also feature in pseudopolyps may serve to identify malignant potential in

pseudopolyps. Conversely, the absence of dysplasia and/or CACRC associated miRNAs in pseudopolyps may indicate an absence of potential for further progression.

This project will also seek the mRNA/protein targets of selected miRNAs through literature searches and computational programmes.

7.5.2 Methods

In this study we analysed tissue biopsies collected from UC patients with informed consent and formalin fixed paraffin embedded tissues from the Pathology archive at the Royal London Hospital, UK.

Total RNA including miRNA was extracted using the miRNeasy Mini Kit (Qiagen) or the mirVana miRNA Isolation Kit (Invitrogen). We used the NanoString nCounter Analysis System at UCL Genomics (University College London, UK) to conduct microRNA profiling. Data was analysed using the software NanoStride (Brumbaugh et al. 2012). The raw data were normalised for lane-to-lane variation using spike-in positive controls and corrected for background. Differential expression was determined using DESeq [bioconductor.org] for comparison between two groups and negative binomial based one-way ANOVA for comparison of more than two groups. P-values were adjusted by Benjamini and Hochberg procedure.

7.5.3 Results

Twenty-three samples were analysed in the miRNA profiling: UC-pseudopolyps (UC-PP; n = 5), UC-dysplasia (UC-Dys; n = 5) and UC (UC; inactive, n = 4; mildly active, n = 4; moderate to severely active, n = 5).

Table 7.3 Pseudopolyp patient characteristics

Patient	Age (years)	Sex
1	**28**	**Male**
2	**30**	**Female**
3	**64**	**Female**
4	**39**	**Male**
5	**30**	**Male**

We identified 36 miRNAs that were differentially expressed in the three groups (adjusted p-value < 0.05). Fourteen of these miRNAs were selectively upregulated in UC-pseudopolyps compared to UC and UC-dysplasia, suggesting there are miRNAs whose expression is specific to this group. These included miR-493 (UC-PP Vs UC, 5 fold, UC-PP Vs UC-Dys, 5.4 fold; adjusted p-value = 1.52×10^{-06}), which has been reported to suppress liver metastasis in a subset of colon cancer (Okamoto et al. 2012). In addition, the pseudopolyp samples demonstrated reduced expression of miR-29a and miR29c (Table 7.4 and Figure 7.8). These miRNA have been reported to be dysregulated in IBD previously (Nijhuis et al. 2014, Brain et al. 2013).

Table 7.4. Differentially Expressed MicroRNAs for Pseudopolyps Sampled from 5 Ulcerative Colitis Patients. The reference miRNA numbers given in the left hand column. UC, ulcerative colitis; PP, pseudopolyp; Dys, dysplasia; p values from ANOVA are adjusted for multiple correction.

Regulation	Base Mean			P value	Fold change
Up	UC	PP	Dys		PP/UC
493	19.3	97.6	18.1	0.000002	5.1
1253	16.0	32.3	17.2	0.002486	2.0
1303	5.0	13.4	6.0	0.002486	2.7
548i	20.6	43.6	18.9	0.008370	2.1
1261	8.7	17.1	8.7	0.008651	2.0
Down					
362-3p	90.8	13.8	89.3	0.000069	6.6
192	4759.7	965.9	3268.6	0.001481	4.9
142-3p	5259.7	1265.1	2420.9	0.001473	4.2
29c	712.1	95.0	288.2	0.001615	7.5

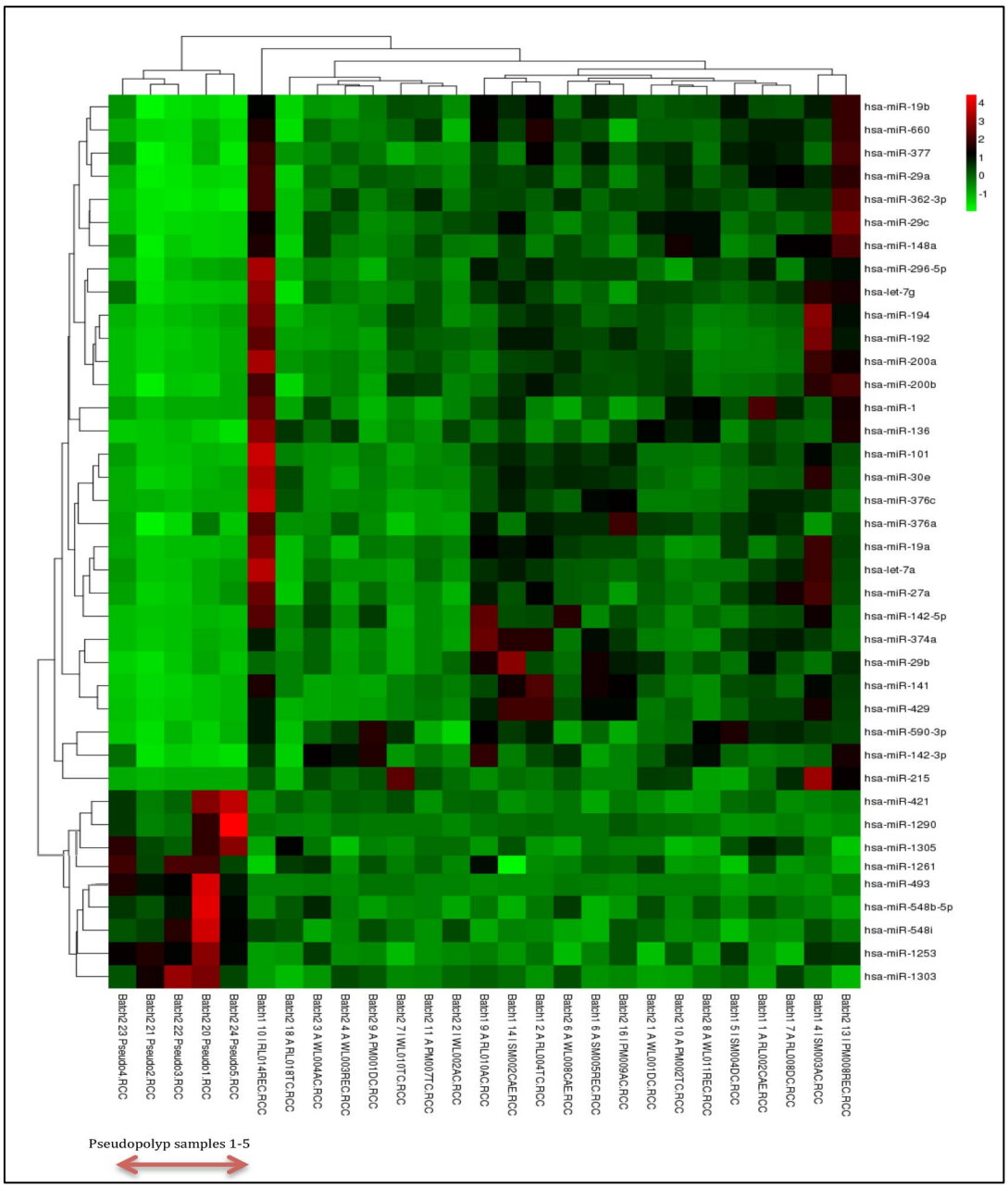

Figure 7.8 Relative expression of microRNAs significantly differentially expressed in pseudopolyps, inactive UC, active UC and dysplastic tissue from UC patients. Heat map demonstrating the 36 significantly differentially expressed microRNAs (ANOVA). In the pseudopolyp samples there is reduced expression of the miR-29a, miR-29b, miR-29c depicted in red. miRNA-308 was removed from the analysis because this has been reassigned and is no longer considered a microRNA.

The DIANA miRPath v.2.0 microRNA target prediction website [Diana.imis.athena-innovation.gr] was used for the simultaneous analysis of the microRNA presented in Table 7.4 (Vlachos et al. 2012). The pathway union for the microRNA gene list was calculated using predicted microRNA targets from the microT-coding DNA sequence (CDS) database. Data from Kyoto Encyclopedia of Genes and Genomes (KEGG) pathways are presented as a heatmap (Figure 7.9). Pathways in cancer showed the most significant score ($p=1.54 \times 10^{-13}$; Figure 7.10).

7.6 Discussion

We have previously shown that pseudopolyps may be a source of protumourigenic mutations in IBD. Preliminary data from this study appears to support this finding demonstrating that the presence of pseudopolyps may be possible sites of pre-malignant disease. This is in support of previous data demonstrating pseudopolyps as predictive of cancer risk (Rutter et al. 2004b; Velayos et al. 2006). In just over a third of the cancer cases (38%), pseudopolyps that were previously documented were the site for the development of neoplasia. This study adds additional complexities to endoscopic surveillance in patients with multiple post-inflammatory polyps.

Analysis of $Ki67^{+}$ cells per 30 crypts in pseudopolyps and 30 control IBD crypts presented here demonstrate a statistically significant increase in the mean number of Ki67 positive cells within pseudopolyps versus control IBD crypts. In addition, the larger crypt size of pseudopolyps crypts may be explained by this increase in cell number. It is also possible the cells are increased in size within the pseudopolyp as a result of increased cellular metabolism.

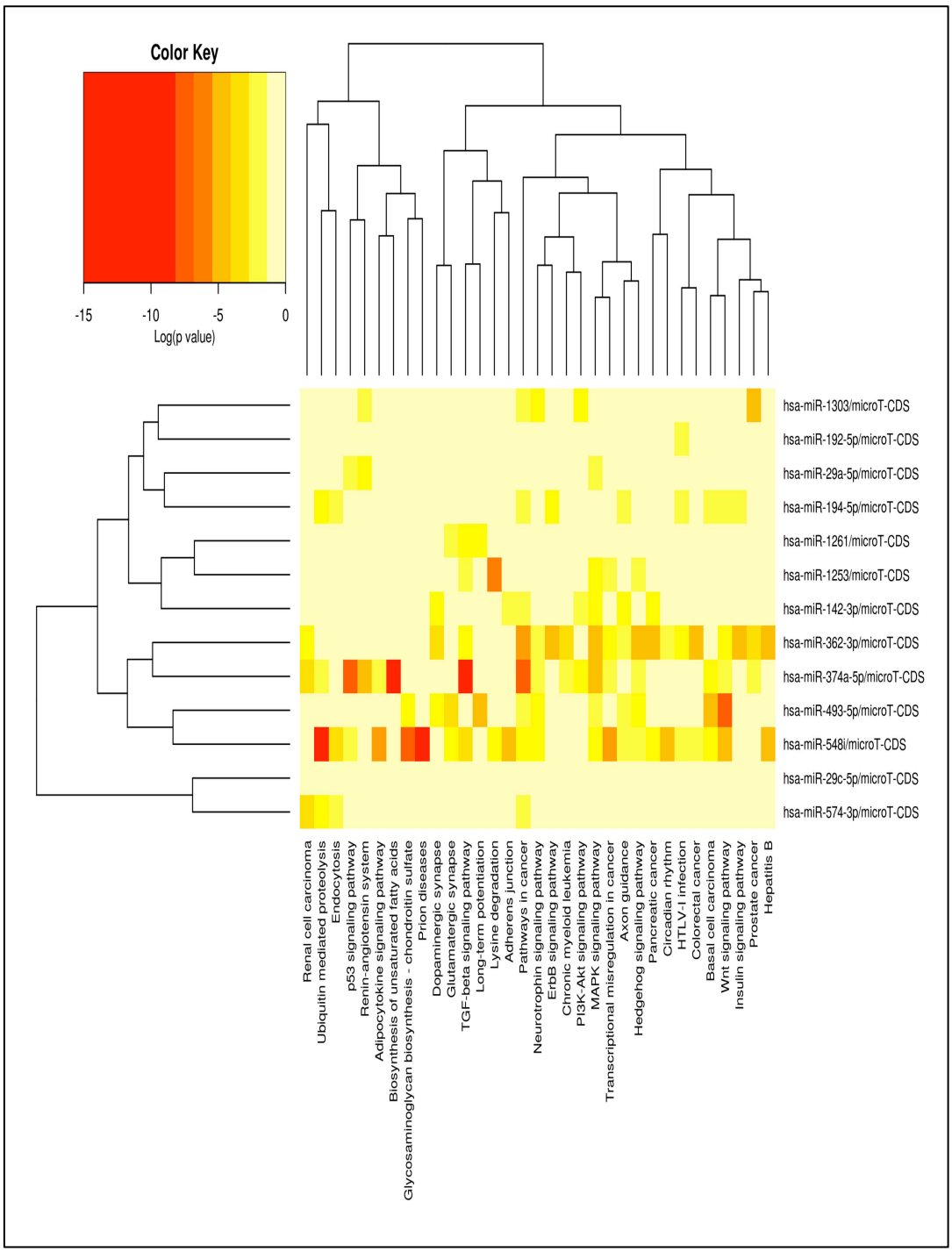

Figure 7.9. Pathways targeted by microRNAs differentially expressed in pseudopolyps. MicroRNAs presented on right hand side, pathways on x-axis. Both up and down regulated microRNAs are included in this algorithm. Only pathways with a significant false discovery rate (FDR) corrected value $p<0.05$ are included.

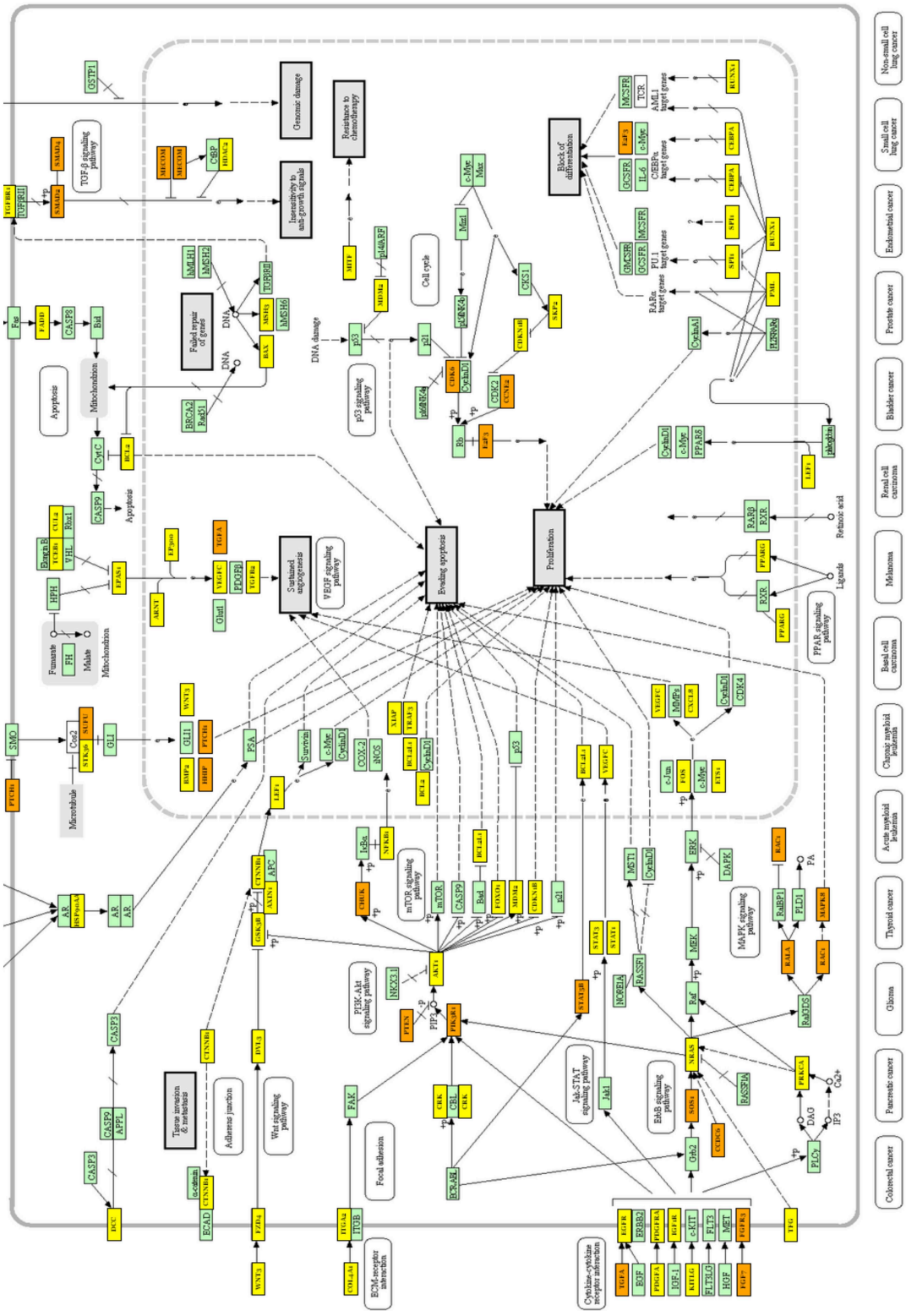

Figure 7.10. Pathways in Cancer. Genes in yellow are targeted by one miRNA in list; genes in orange are targeted by more than one microRNA in list. Pathways in cancer showed the most significant score ($p=1.54 \times 10^{-13}$).

Regarding the question, does crypt size alter the percentage of *LGR5*$^{+}$ cells? The slightly bigger crypts that are found within pseudopolyps may reflect an expansion of the proliferative zone. The ISH experiments suggest that the larger crypts might have a greater rate of crypt cell production. This hypothesis now needs testing by microdissecting out and counting metaphases. In mice for example, vincristine could be utilized to block cell division and the metaphases counted at a fixed time thereafter. It would not be possible to know how many proliferative zone cells there were unless flash labelled with fluorescent thymidine analogue was performed before fixing, for example. An alternative would be to see how many stem cell *LGR5* positive cells there were per crypt by microdissecting and staining, or imaging many thin serial sections and reconstructing them into a 3-dimensional representation.

Sequencing of DNA extracted from pseudopolyps indicates that these lesions are a potential source of protumourigenic mutations in UC. In addition, pseudopolyps may possibly be the sites within the inflamed epithelium where mutations are harboured and where there is no competition from neighbouring epithelium, as it has been denuded following previous inflammation. Thirdly, pseudopolyps are a potential source of regeneration within the epithelium and repair will involve population of 'new' epithelium by cells carrying oncogenic mutations. More numbers are needed for analysis and this is planned for future work. Next generation sequencing will also identify additional novel mutations harboured by pseudopolyps. This work is important, as these lesions have been traditionally thought to be benign, genetically inert, incidental findings, characteristic of chronic inflammation. Although the data here is preliminary, the findings propose an exciting paradigm shift in the way we

consider pseudopolyps and more detailed mutational profiling may alter endoscopic management of these lesions in the future.

The MiRNA expression analysis conducted here suggests that miRNAs do differ between pseudopolyps and that of UC-Dys and mucosa. Hence, there is potential in using these changes as biomarker particularly if there is a functional consequence, namely a role for miRNA dysregulation in tumour progression. Future work needs to be conducted to validate these finding in independent cohorts of IBD patients. Our laboratory is currently conducting such a large-scale trial involving some 12 IBD surveillance centres around the country. Addition work also needs to focus on identifying the mRNA targets of miRNAs and the molecular pathways altered by at the protein level by miRNA changes in expression. Use of the mRNA and protein target, as the actual biomarker maybe more applicable than directly assaying the miRNA profiles. Investigations should also look at whether dysregulated miRNAs and/or their targets are targetable by novel therapies (Felice et al. 2015).

With respect to other studies, Kanaan et al (2012) assayed six IBD patients with IBD associated-dysplasia/cancers, yet this included only 2 patients with UC. Five miRNAs were demonstrated to be significantly downregulated in CRC progression from non-neoplasia to dysplasia to cancer (miR-193b, miR-373, let-7e, miR-15b and miR-372). There are no overlaps between these miRNAs with those identified in this research data at this stage, which may be explained by the very small number of UC samples involved in the published study. Another group, Olaru and colleagues, performed a miRNA microarray analysis of 8 chronically inflamed and 8 IBD-associated dysplastic rectal tissues (Olaru et al. 2011). Their research demonstrated 32 miRNAs

that have increased in expression and 10 that had decreased expression. In the study performed here, differentially expressed miRNA in UC-dysplasia, two miRNAs, miR-203 and miR-183, also featured on the Olaru list of upregulated miRNA in IBD-dysplasia. The Olaru study predominantly homed in on miR-31, which in their sample set was 11 fold higher in neoplastic specimens from IBD patients compared with chronically inflamed specimens from IBD patients. This same miRNA was examined in our cohort, however, no significant difference between the UC dysplasia samples and the other UC control samples by NanoString array analysis was found. In fact, following correction for background and normalisation, miR-31 is expressed only in some of the samples (UC-inactive, 2 out of 8; UC-active, 6 out of 13; UC-dysplasia, 1 out of 4). This discrepancy could be due to comparing UC samples with general IBD samples and/or the use by Olaru et al (2011) of archival material against our prospectively collected sample. Future experiments should focus on miR-203 and miR-183. The miR-RNA 203 is upregulated in bladder cancer and is known to target Akt2 and Src. Its functions include inhibiting cell proliferation, invasion and migration; and inducing cell cycle arrest and apoptosis (see Table 1 in section 1.18.3). The targets of MiR-183 are as yet unknown and hence its function has not been described in cancers or IBD.

Regarding the miR-29 family, as in Table 3, section 1.18.4, there is upregulation of miR-29a in sigmoid biopsies of active UC when compared to control tissue. However, in support of our findings, the identification of miR-29a and miR-29c as down regulated miRNAs is interesting, as the miR-29 family has been implicated in cardiac, hepatic and pulmonary fibrosis (reviewed in Felice et al. 2015). Furthermore, our laboratory has investigated the expression of miR-29a, miR-29b and miR-29c in

mucosa overlying a stricture in CD patients (SCD) paired with mucosa from non-strictured areas (NSCD) (Nijhuis et al. 2014). There was marked down- regulation of the miR-29 family in mucosa overlying SCD comparatively to mucosa overlying NSCD. These data implicate the miR-29 family in the pathogenesis of intestinal fibrosis in CD.

Another study from Brain et al. (2013) demonstrated that the intracellular sensor NOD2 induces miRNA-29 expression in human dendritic cells to limit IL-23 release. IL-23 as well as IL-6 are needed for induction of T helper 17 (Th17) CD4+ T cells, a response vital for antimicrobial immunity at mucosal surfaces and a trademark of the inflammatory response in Crohn's (Brain et al. 2013). This study demonstrated that in DSS-induced colitis, the colitis was worse in miR-29-deficient mice and was associated with elevated IL-23 and T helper 17 signature cytokines in the intestinal mucosa. CD patient DCs expressing NOD2 polymorphisms failed to induce miR-29 upon pattern recognition receptor stimulation and showed enhanced release of IL-12p40 on exposure to adherent invasive *E.coli*. Thus the researchers suggest that loss of miR-29-mediated immunoregulation in CD DCs might contribute to elevated IL-23 in this disease (Brain et al. 2013). This corroborates with the downregulation of the miR-29 family observed in pseudopolyps.

Further evaluation of miR-29 family members as biomarkers in UC and CD and development of pseudopolyps and their role in disease manifestation is also warranted. Interestingly, miR-493 has been reported to suppress liver metastasis in a subset of colon cancer suggesting a possible link to disease progression that requires

further investigation (Okamoto et al. 2012). MiRNA profiles may help determine the malignant potential of pseudopolyps.

In summary, the experiments presented here add weight to the hypothesis that pseudopolyps have characteristics usually associated with malignant progression: increased cellular proliferation; limited expansion of the stem cell component as marked by *LGR5*$^{+}$ cells; and microarray profiles differ from IBD mucosa and dysplasia. Overall, these findings suggest that pseudopolyps are not benign entities and require further detailed investigation to identify robust biomarkers to identify those requiring removal at endoscopy. This study remains ongoing, as my findings warrant further investigation and pose an exciting paradigm shift in the stratification and management of IBD patients.

CHAPTER 8 GENERAL DISCUSSION

Most of our existing knowledge on the location of the intestinal stem cell niche, stem cell number and dynamics of clonal expansion within crypts is based on lineage labelling experiments in mice, utilising techniques that are impractical in humans. In this thesis the rates of niche succession and crypt fission in humans have been examined. Niche succession and fission are the methods by which tumorigenic mutations in stem cells become fixed within the IBD epithelium. My investigations were focussed on human IBD colonic tissue and the methylation patterns at CpG loci of non-expressed genes in CCO-deficient cell populations. Patches of clonal CCO-deficient crypts generated by (multiple) fission events, appear disparate by their methylation patterns, thus there is sufficient time (years) between fission events to allow divergence. Mathematical modelling demonstrates that the lower limit by which two crypts appear distinct by their methylation patterns is 10 years, suggesting this is the lower limit for crypt fission events in normal human colon.

8.1 The major findings

The most important finding from this thesis are summarised below:

1) Crypt fission cycles in inflammatory bowel diseased colon are protracted. Each stage of crypt fission appears to be slow. This maybe dependent on the activity of any inflammatory disease at the time.
2) Patches of clonal CCO-deficient crypts generated by (multiple) fission events, are larger than the CCO deficient patches within normal colon. The proliferative drive induced by continuous inflammation and mucosal repair in UC appears to promote the expansion of CCO-deficient patches.

3) Overall, clonally related adjacent IBD crypts seem to share a more recent common ancestor than non-related IBD crypts. These data support the hypothesis that, in the context of IBD, crypt fission rates may be increased in the inflamed epithelium. Furthermore niche succession appears to be faster in active IBD.
4) Pseudopolyps are not genetically inert and are a potential source of protumourigenic mutations in UC. Pseudopolyps are a potential source of regeneration within the epithelium and, as shown here, have a faster proliferative drive than background mucosa in IBD patients. Hence, pseudopolyps might well be the site within the inflamed epithelium where mutations are harboured and where there is no competition from neighbouring epithelium, as it has been denuded following previous inflammation.
5) MiRNA expression in pseudopolyps differs from that of UC-Dys and mucosa. In particular, the MiR-29 family was downregulated in pseudopolyps, a miRNA family that has been implicated in intestinal fibrosis formation in stricturing Crohn's disease. The MiR-493 was upregulated in pseudopolyps.

The significance of these findings has been summarised in the discussion sections of the relevant chapters. This work has raised many fascinating questions about stem cell dynamics in IBD and about the characterisation of pseudopolyp lesions and these questions will be discussed in the following sections.

8.2 Alteration in stem cell dynamics and IBD – an intimate and complex relationship

It is interesting that up to 15% of CRCs that occur in patients with IBD are diagnosed within the first 7 years of disease (Beaugerie et al. 2013; Lutgens et al. 2008). Yet the excess risk of colitis-associated cancer becomes epidemiologically apparent afterwards, (Lutgens et al. 2013). Could this be explained by the apparent increased expansion of clonal patches in IBD colonic tissue compared to the normal colon?

The risk of CACRC increases linearly, with a steeper slope in patients with extensive colitis. As mentioned in the Introduction, features of previous or currently active colitis, including pseudopolyps and mucosal inflammation, are independent risk factors for CRC. The observation from this thesis that clonally related adjacent IBD crypts seem to share a more recent common ancestor than non-related IBD crypts support the hypothesis that, in the context of IBD, crypt fission is increased in the inflamed epithelium. Furthermore, that niche succession appears to be faster in active IBD; this might explain accelerated tumourigenesis in IBD.

In contrast to the relatively high risk of CRC suggested in a 2001 meta-analysis (approximately 0.5 to 1% per year) (Eaden et al. 2001), a progressive decrease in the excess risk of CRC in IBD patients has been reported over time, with no excess risk found in a Danish population based study (Jess et al. 2007). This was further supported by another meta-analysis (Lutgens et al. 2013). The explanation put forward being better control of inflammation, stricter colonoscopic surveillance, increased colectomy rates in some countries, and the possible chemopreventitive effect of 5-aminosalicylates (5-ASAs), which remain controversial. The goal of mucosal healing

as an end point in the medical management of IBD has resulted in lowering the risk of CRC in IBD in recent studies. More patients achieving mucosal healing may mean that crypt fission cycles approach that of the normal colon and this may explain some of the findings presented here whereby the stem cell dynamics in the IBD bowel approaches that of the normal colon.

The apparent increase in the clonal patch size in IBD compared to normal colon might go some way to account for the increased likelihood of 'fields' of genetic change of cancer associated molecular modifications prior to any histological evidence of dysplasia developing. The increase in the proportion of wholly and partially mutated crypts in UC may indicate that either more mtDNA mutations are being generated, or that they are more likely to go to fixation in the cell, allowing the rapid fixation and spread of pro tumourigenic mutations, perhaps explaining the increased development of field cancerisation in IBD.

It has been demonstrated following the analysis of fields of mtDNA mutant crypts, that a normal colon crypt divides around once every 30-40 years, and the division rate is increased in adenomas by at least an order of magnitude (Baker et al. 2014). In IBD this rate may also be increased. Clearly, mathematical modelling is required on larger numbers. However, this thesis supports the notion that an increase in the clonal population patch size in UC compared to normal colon may substantiate the increased rate of tumourigenesis in the IBD bowel.

8.3 Pseudopolyps; not as innocent as they look

Pseudopolyps, are islands of intact colonic mucosa following severe inflammation in IBD. The presence of pseudopolyps increases the risk of CRC by up to 2.5 times when found on endoscopy of IBD patients. This risk was attributed to the belief that pseudopolyps were purely a marker of inflammation severity, which caused their development in the first place. That the pseudopolyps are *per se,* a pre-cursor lesion for carcinoma was not considered. Indeed, they are generally believed to be benign without any pre-cancerous genetic change, but could decrease the sensitivity of colonoscopy screening by obscuring true adenomatous polyps (Velayos et al. 2006).

Results from this study have the potential to cause a paradigm shift in our approach to the management of pseudopolyps. Important questions have been raised with relatively small numbers regarding their pre-malignant potential and this warrants further investigation using a much larger study cohort. The longer term aim would be to stratify patients in terms of their risk of cancer progression based on mutation and/or biomarker (miRNA/*LGR5*/Ki67, for example) profiling.

8.4 Limitations of this work

There are a number of limitations to the data presented in this study that require consideration. The numbers of samples analysed are small and the experiments very time consuming; the data is hard-won. The mt DNA mutations necessary for the analytical experiments are rarely observed in patients below the age of 40 years (Greaves et al. 2006) and most of the resections that take place for IBD patients, usually for a colitis-associated cancer or disease refractory to medical therapy, are in younger patients who have no mt DNA mutations and therefore no CCO-deficient

patches to analyse. The tissue always needs to be fresh frozen for this particular type of analysis thereby limiting sample size further. Nevertheless, I collected over 20 fresh frozen IBD colonic tissue samples from 20 IBD patients undergoing surgical resections over the course of my PhD and every one was screened for CCO-deficient patches, but only 5 had CCO-deficient patches to permit analysis. To add to the patch size analysis, IHC for CCO on some IBD FFPE blocks was conducted (n=30 in patients over 50 years), but as the samples were biopsies the number of CCO-deficient crypts was very small. This is a limitation of the study design and the methodologies currently available. Further work is required to ensure a representative data set can be acquired. The estimates of the dynamics of clonal expansion using the methylation status at CpG islands of non-expressed genes rely on the legitimacy of the numerous inferences made. Hence, the data needs to be carefully interpreted. Furthermore, observational data has inherent bias associated with study design and data collection, analysis and interpretation. Additional work on an independent cohort is necessary to validate any conclusions.

Another limitation is that all fresh frozen tissue needs to have intact mucosa to allow the visualisation of the crypt architecture to permit the analysis. This then limits the tissue analysed to quiescent diseased mucosa; mucosa that is severely ulcerated and inflamed could not be analysed as it was denuded and no epithelium exists to analyse. However, as mentioned previously, the overwhelming majority of surgical resections that take place for IBD patients are for severe colitis refractory to medical therapy. This limits the number of patients that can be analysed and restricts the disease severity that can be analysed, which may perhaps create bias in the data.

Most patients analysed had been on different forms of medical therapy including immunosuppressants (azathioprine, 6-mercaptopurine and methotrexate) anti-Tumour Necrosis Factor alpha (anti-TNFα) treatment and 5-aminosalicylic acid; often those currently on no treatment had received extensive medical treatment in the past. Treatment is likely to influence some of the results. With a small sample population, it is always difficult to control all variables: medical therapy, sex, age and degree of disease activity; but on the positive side, different patients on all types of treatment were analysed.

The sequencing for mutations in the DNA of pseudopolyps was performed on FFPE archival tissue. This allowed for well-orientated samples necessary to identify the pseudopolyps and permitted extraction of adequate amounts of DNA for directional sequencing. The risk of contamination, from both unintentionally dissected tissue and artefactual contaminants was high. The risk of the former was reduced by very careful tissue macrodissection under a high powered microscope, and the latter rigourously inspected for using negative controls in every PCR reaction. Any contamination of control samples would results in the entire batch being discarded and re-dissected.

Any observational study has several limitations. I found that, although Barts Health NHS Trust is the largest NHS trust in the UK, the sample numbers were less than anticipated. The pathology archive data recording computer system and also the endoscopy reporting tool systems were only introduced in 2004 limiting successful retrieval of archival specimens. Unfortunately, this problem is inherent to most NHS Trust Pathology and Endoscopy reporting tools nationwide. In addition, the presence of IBD and CRC is relatively rare. If this study was extended further to incorporate

other trusts within the UK, and also possibly abroad, the patient numbers would increase correspondingly providing more statistical power. In addition, the self-reporting of pseudopolyps by the endoscopist and their site is operator dependent and not systematic. Currently, there is no standard endoscopy reporting system for pseudopolyps nationally, which limits subsequent analyses. Other potential biases include possible skewing due to the hospital Trust demographic, the majority of the patients were from East London, a further study would be required to examine whether our findings held with other patient populations from different areas.

8.5 Future Directions

Not unexpectedly, this work has generated as many questions as it has answered, but has provided a framework for a great deal of further investigations. This section will briefly explore potential future paths.

Taking the observational study forward, it would be important to expand to include a larger cohort from a variety of different areas across the United Kingdom, and ultimately, globally, in order to validate the results. Any hypotheses should be tested by designing and conducting a prospective cohort study to provide a detailed analysis of the location of pseudopolyps in relation to CRC. Additional analyses of genetic changes to the pseudopolyps that occur over time, to adenomas associated with IBD and CACRC should be conducted to link mutations to progression. These data may provide for potential biomarkers and identify molecular pathways for novel therapeutic interventions.

Investigations of stem cell dynamics in pseudopolyp lesions has distinct potential and

should involve the examination of both clonal patches within pseudopolyps and non clonal patches and a statistical comparison of their methylation patterns. I would employ the same techniques outlined in the earlier chapters. Longitudinal barium and endoscopic studies demonstrate that adenomas grow very slowly; in fact 18% of small (<1cm) adenomas regress over 5 years. Modelling of mutation burdens reveal that adenomas take 15-20 years to progress to cancer (Muto, 1975; Jones et al. 2008). Recent studies from our lab show that human adenomas demonstrate punctuated growth with relative quiescence with occasional cycles of rapid clonal expansion (Humphries et al. 2013). If pseudopolyps are thought to be potential pre-malignant lesions, perhaps they too may demonstrate a staccato type growth with relative rapid points of fast clonal expansion. Certainly, colorectal carcinogenesis is characterised by relative stasis punctuated by occasional clone growth – does the same hold true for colitis-associated cancers in that case?

The mutation burden of pseudopolyps in UC via deep next generation sequencing of a PCR-based gene panel or preferably whole-genome sequencing should be determined. The programme of experiments would involve selecting 3 UC patients of interest: those patients who developed cancer and who also have pseudopolyps. Paired surrounding mucosal samples along with pseudopolyp tissue at 3 different time points (2 preceding cancer development, one at cancer diagnosis) should be used as the source for DNA. FFPE tissue would be used and the extracted DNA prepped via PCR for deep next generation sequencing. Certain next generation sequencing methods are not suitable with FFPE tissue, so this would need to be taken into account when choosing the panel. This experiment would allow the assessment of mutation identification and burden within

pseudopolyps.

Questions generated from this work: Do pseudopolyps possess some survival advantage? Are growth factors upregulated and are repair mechanisms enhanced in pseudopolyps? Is it possible to determine all the mutated genes (this should include mutational profiling of promoter CpG islands) and the relevant molecular pathways that become dysfunctional as a result?

Future work would also include gene expression arrays for profiling to quantify the number and determine the type of genes that are dysregulated through mutation and methylation changes. These should be validated with RT-PCR and protein expression assessed by IHC. We are currently analysing microRNA arrays on more pseudopolyp samples and comparing results to active and inactive disease and CRC. Do changes in miRNAs alter regulation of key genes needed for repair and survival? This represents a very novel area for research.

8.6 Summary

In summary, a number of major and intriguing findings have been made during the course of my PhD studies and these provide the impetus for further studies to understand the stem cell biology of the IBD intestine and their pivotal role in the development of pathology associated with colitis. Additional work to decipher the dynamics of neoplastic growth in IBD will improve the clinical management of patients and permit the development of targeted chemoprevention based on the identification of novel molecular targets.

REFERENCES

Al-Hajj M, Wicha MS, Benito-Hernandez A, Morrison SJ, Clarke MF. 2003. Prospective identification of tumorigenic breast cancer cells. Proc Natl Acad Sci USA A100: 3983-3988.

Allegra CJ, Jessup JM, Somerfield MR, Hamilton SR, Hammond EH, Hayes DF, McAllister PK, Morton RF, Schilsky RL. 2009. American Society of Clinical Oncology provisional clinical opinion: testing for KRAS gene mutations in patients with metastatic colorectal carcinoma to predict response to anti-epidermal growth factor receptor monoclonal antibody therapy. J Clin Oncol. 27: 2091-2096.

Alspach E, Flanagan KC, Luo X, Ruhland MK, Huang H, Pazolli E, Donlin MJ, Marsh T, Piwnica-Worms D, Monahan J, Novack DV, McAllister SS, Stewart SA. 2014. p38MAPK plays a crucial role in stromal-mediated tumorigenesis. Cancer Discov. 4: 716-729.

Ambros V. 2004. The functions of animal microRNAs. Nature 431: 350-355.

Anastas JN, Moon RT. 2013. WNT signalling pathways as therapeutic targets in cancer. Nat Rev Cancer 13: 11-26.

Ang PW, Loh M, Liem N, Lim PL, Grieu F, Vaithilingam A, Platell C, Yong WP, Iacopetta B, Soong R. 2010. Comprehensive profiling of DNA methylation in colorectal cancer reveals subgroups with distinct clinicopathological and molecular features. BMC Cancer 10: 227.

Arijs I, Li K, Toedter G, Quintens R, Van Lommel L, Van Steen K, Leemans P, De Hertogh G, Lemaire K, Ferrante M, Schnitzier F, Thorez L, Ma K, Song XY, Marino C, van Assche G, Vermeire S, Geboes K, Schuit F, Rutgeerts. 2009. Mucosal gene signatures to predict response to infliximab in patients with ulcerative colitis. Gut 58: 1612-1619.

Ashton KJ, Willems L, Holmgren K, Ferreira L, Headrick JP. 2006. Age-associated shifts in cardiac gene transcription and transcriptional responses to ischemic stress. Exp Gerontol. 41: 189-204.

Aust DE, Terdiman JP, Willenbucher RF, Chang CG, Molinaro-Clark A, Baretton GB, Loehrs U, Waldman FM. 2002. The APC/beta-catenin pathway in ulcerative colitis-related colorectal carcinomas: a mutational analysis. Cancer 94: 1421-1427.

Baker AM, Cereser B, Melton S, Fletcher AG, Rodriguez-Justo M, Tadrous PJ, Humphries A, Elia G, McDonald SA, Wright NA, Simons BD, Jansen M, Graham TA. 2014. Quantification of crypt and stem cell evolution in the normal and neoplastic human colon. Cell Rep. 8:940-9477.

Barker N, van Es JH, Kuipers J, Kujala P, van den Born M, Cozijnsen M, Haegebarth A, Korving J, Begthel H, Peters PJ, Clevers H. 2007. Identification of stem cells in small intestine and colon by marker gene *Lgr5*. Nature 449: 1003-1007.

Barker N, Ridgway RA, van Es JH, van de Wetering M, Begthel H, van den Born M, Danenberg E, Clarke AR, Sansom OJ, Clevers H. 2009. Crypt stem cells as the cells-of-origin of intestinal cancer. Nature 457: 608-611.

Bartel DP. 2009. MicroRNAs: target recognition and regulatory functions. Cell 136: 215-233.

Baylin SB, Herman JG, Graff JR, Vertino PM, Issa JP. 1998. Alterations in DNA methylation: a fundamental aspect of neoplasia. Adv Cancer Res 72: 141-196.

Bea S, Tort F, Pinyol M, Puig X, Hernandez L, Hernandez S, Fernandez PL, van Lohuizen M, Colomer D, Campo E. 2001. BMI-1 gene amplification and overexpression in hematological malignancies occur mainly in mantle cell lymphomas. Cancer Res 61: 2409-2412.

Beaugerie L, Svrcek M, Seksik P, Bouvier AM, Simon T, Allez M, Brixi H, Gornet JM, Altwegg R, Beau P, Duclos B, Bourreille A, Faivre J, Peyrin-Biroulet L, Fléjou JF, Carrat F; CESAME Study Group. 2013. Risk of colorectal high-grade dysplasia and cancer in a prospective observational cohort of patients with inflammatory bowel disease. Gastroenterology 145:166-175.

Befrits R, Hammarberg C, Rubio C, Jaramillo E, Tribukait B. 1994. DNA aneuploidy and histologic dysplasia in long-standing ulcerative colitis. A 10-year follow-up study. Dis Colon Rectum 37: 313-319; discussion 319-320.

Bienz M, Clevers H. 2000. Linking colorectal cancer to Wnt signaling. Cell 103: 311-320.

Bigas A, Espinosa L. 2012. Hematopoietic stem cells: to be or Notch to be. Blood 119: 3226-3235.

Bjerknes M, Cheng H. 1999. Clonal analysis of mouse intestinal epithelial progenitors. Gastroenterology 116: 7-14.

Bodmer WF. 1999. 1998 Runme Shaw Memorial Lecture: somatic evolution of cancer. Ann Acad Med Singapore 28: 323-329.

Bodmer W, Bielas JH, Beckman RA. 2008. Genetic instability is not a requirement for tumor development. Cancer Res 68: 3558-3560; discussion 3560-3551.

Bonnett D, Dick JE. 1997. Human acute myeloid leukaemia is organised as a hierarchy that originates from a primitive hematopoietic cell. Nature Medicine 3: 730-737.

Braakhuis BJ, Tabor MP, Kummer JA, Leemans CR, Brakenhoff RH. 2003. A genetic explanation of Slaughter's concept of field cancerization: evidence and clinical implications. Cancer Res. 63: 1727-1730.

Brain O, Owens BM, Pichulik T, Allan P, Khatamzas E, Leslie A, Steevels T, Sharma S, Mayer A, Catuneanu AM, Morton V, Sun MY, Jewell D, Coccia M, Harrison O,

Maloy K, Schönefeldt S, Bornschein S, Liston A, Simmons A. 2013. The intracellular sensor NOD2 induces microRNA-29 expression in human dendritic cells to limit IL-23 release. Immunity 39: 521-36.

Brentnall TA, Crispin DA, Rabinovitch PS, Haggitt RC, Rubin CE, Stevens AC, Burmer GC. 1994. Mutations in the p53 gene: an early marker of neoplastic progression in ulcerative colitis. Gastroenterology 107: 369-378.

Brittan M, Wright NA. 2004. Stem cell in gastrointestinal structure and neoplastic development. Gut 53: 899-910.

Brumbaugh CD, Kim HJ, Giovacchini M, Poumand N. 2012. NanoStriDE: normalisation and differential expression analysis of Nano String nCounter data. BMC Bioinformatics 12: 479.

Buczacki SJ, Zecchini HI, Nicholson AM, Russell R, Vermeulen L, Kemp R, Winton DJ. 2013. Intestinal label-retaining cells are secretory precursors expressing Lgr5. Nature 495: 65-69.

Burmer GC, Rabinovitch PS, Haggitt RC, Crispin DA, Brentnall TA, Kolli VR, Stevens AC, Rubin CE. 1992. Neoplastic progression in ulcerative colitis: histology, DNA content, and loss of a p53 allele. Gastroenterology 103: 1602-1610.

Cai WB, Roberts SA, Bowley E, Hendry JH, Potten CS. 1997. Differential survival of murine small and large intestinal crypts following ionizing radiation. Int J Radiat Biol. 71: 145-155.

Cairnie AB, Millen BH. 1975. Fission of crypts in the small intestine of the irradiated mouse. Cell Tissue Kinet 8: 189-196.

Cairns J. 1975. Mutation selection and the natural history of cancer. Nature 255: 197-200.

Campbell F, Williams GT, Appleton MA, Dixon MF, Harris M, Williams ED. 1996. Post-irradiation somatic mutation and clonal stabilisation time in the human colon. Gut 39: 569-573.

Chekulaeva M, Filipowicz W. 2009. Mechanisms of miRNA-mediated post-transcriptional regulation in animal cells. Curr Opin Cell Biol. 21: 452-460.

Cheng H, Leblond CP. 1974. Origin, differentiation and renewal of the four main epithelial cell types in the mouse small intestine. V. Unitarian Theory of the origin of the four epithelial cell types. Am J Anat 141: 537-561.

Cheng H, Bjerknes M. 1985. Whole population cell kinetics and postnatal development of the mouse intestinal epithelium. The Anatomical record 211: 420-426.

Cheng H, Bjerknes M, Amar J, Gardiner G. 1986. Crypt production in normal and diseased human colonic epithelium. The Anatomical record 216: 44-48.

Chen H, Wang LD, Guo M, Gao SG, Guo HQ, Fan ZM, Li JL. 2003. Alterations of p53 and PCNA in cancer and adjacent tissues from concurrent carcinomas of the esophagus and gastric cardia in the same patient in Linzhou, a high incidence area for esophageal cancer in northern China. World J Gastroenterol. 9: 16-21.

Chen J, Li Y, Yu TS, McKay RM, Burns DK, Kernie SG, Parada LF. 2012. A restricted cell population propagates glioblastoma growth after chemotherapy. Nature 488: 522-526.

Chen R, Rabinovitch PS, Crispin DA, Emond MJ, Bronner MP, Brentnall TA. 2005. The initiation of colon cancer in a chronic inflammatory setting. Carcinogenesis 26: 1513-1519.

Chu MW, Siegmund KD, Eckstam CL, Kim JY, Yang AS, Kanel GC, Tavare S, Shibata D. 2007. Lack of increases in methylation at three CpG-rich genomic loci in non-mitotic adult tissues during aging. BMC medical genetics 8: 50.

Cocciadiferro L, Miceli V, Kang KS, Polito LM, Trosko JE, Carruba G. 2009. Profiling cancer stem cells in androgen-responsive and refractory human prostate tumor cell lines. Ann N Y Acad Sci. 1155: 257-262.

Connell WR, Talbot IC, Harpaz N, Britto N, Wilkinson KH, Kamm MA, Lennard-Jones JE. 1994. Clinicopathological characteristics of colorectal carcinoma complicating ulcerative colitis. Gut 35: 1419-1423.

Crohn BB, Ginzburg L, Oppenheimer GD. 1932. Regional ileitis: a pathologic and clinical entity. JAMA 99: 1323-1329.

Cummins AG, Catto-Smith AG, Cameron DJ, Couper RT, Davidson GP, Day AS, Hammond PD, Moore DJ, Thompson FM. 2008. Crypt fission peaks early during infancy and crypt hyperplasia broadly peaks during infancy and childhood in the small intestine of humans. Journal of pediatric gastroenterology and nutrition 47: 153-157.

Cummins AG, Jones BJ, Thompson FM. 2006. Postnatal epithelial growth of the small intestine in the rat occurs by both crypt fission and crypt hyperplasia. Dig Dis Sci. 51: 718-723.

Curtin K, Slattery ML, Samowitz WS. 2011. CpG island methylation in colorectal cancer: past, present and future. Patholog Res Int. 2011: 902674.

Dalerba P, Cho RW, Clarke MF. 2007. Cancer stem cells: models and concepts. Annu Rev Med. 58: 267-284.

Danese S, Fiocchi C. 2011. Ulcerative colitis. N Engl J Med 365: 1713-1725.

Dekaney CM, Rodriguez JM, Graul MC, Henning SJ. 2005. Isolation and characterization of a putative intestinal stem cell fraction from mouse jejunum. Gastroenterology 129: 1567-1580.

Dekaney CM, Fong JJ, Rigby RJ, Lund PK, Henning SJ, Helmrath MA. 2007. Expansion of intestinal stem cells associated with long-term adaptation following ileocecal resection in mice. Am J Physiol Gastrointest Liver Physiol. 293: G1013-1022.

Driessens G, Beck B, Caauwe A, Simons BD, Blanpain C. 2012. Defining the mode of tumour growth by clonal analysis. Nature 488: 527-530.

Ekbom A, Helmick C, Zack M, Adami HO. 1990. Ulcerative colitis and colorectal cancer. A population-based study. N Engl J Med. 323: 1228-1233.

Fearon ER, Vogelstein B. 1990. A genetic model for colorectal tumorigenesis. Cell 61: 759-67.

Felice C, Lewis A, Armuzzi A, Lindsay JO, Silver A. 2015. Review article: selective histone deacetylase isoforms as potential therapeutic targets in inflammatory bowel diseases. Aliment Pharmacol Ther. 4: 26-38.

Fellous TG, Islam S, Tadrous PJ, Elia G, Kocher HM, Bhattacharya S, Mears L, Turnbull DM, Taylor RW, Greaves LC, Chinnery PF, Taylor G, McDonald SA, Wright NA, Alison MR. 2009a. Locating the stem cell niche and tracing hepatocyte lineages in human liver. Hepatology 49: 1655-1663.

Fellous TG, McDonald SA, Burkert J, Humphries A, Islam S, De-Alwis NM, Gutierrez-Gonzalez L, Tadrous PJ, Elia G, Kocher HM, Bhattacharya S, Mears L, El-

Brahrawy M, Turnbull DM, Taylor RW, Greaves LC, Chinnery PF, Day CP, Wright NA, Alison MR. 2009b. A methodological approach to tracing cell lineage in human epithelial tissues. Stem Cells 27: 1410-1420.

FitzGerald AJ, Mandir N, Goodlad RA. 2005. Leptin, cell proliferation and crypt fission in the gastrointestinal tract of intravenously fed rats. Cell Prolif. 38: 25-33.

Fodde R, Smits R, Clevers H. 2001. APC signal transduction and genetic instability in colorectal cancer. Nat Rev Cancer 1: 55-67.

Fre S, Huyghe M, Mourikis P, Robine S, Louvard D, Artavanis-Tsakonas S. 2005. Notch signals control the fate of immature progenitor cells in the intestine. Nature 435: 964-968.

Friedman RC, Farh KK, Burge CB, Bartel DP. 2009. Most mammalian mRNAs are conserved targets of microRNAs. Genome Res. 19: 92-105.

Fuller CE, Davies RP, Williams GT, Williams ED. 1990. Crypt restricted heterogeneity of goblet cell mucus glycoprotein in histologically normal human colonic mucosa: a potential marker of somatic mutation. Br J Cancer 61: 382-384.

Galandiuk S, Rodriguez-Justo M, Jeffery R, Nicholson AM, Cheng Y, Oukrif D, Elia G, Leedham SJ, McDonald SA, Wright NA. 2012. Field cancerization in the intestinal epithelium of patients with Crohn's ileocolitis. Gastroenterology 142: 855-864 e858.

Garrity-Park MM, Loftus EV, Jr., Sandborn WJ, Bryant SC, Smyrk TC. 2010. Methylation status of genes in non-neoplastic mucosa from patients with ulcerative colitis-associated colorectal cancer. Am J Gastroenterol. 105: 1610-1619.

Giannakis M, Stappenbeck TS, Mills JC, Leip DG, Lovett M, Clifton SW, Ippolito JE, Glasscock JI, Arumugam M, Brent MR, Gordon JL. 2006. Molecular properties of adult mouse gastric and intestinal epithelial progenitors in their niches. J Biol Chem. 281: 11292-11300.

Gillen CD, Walmsley RS, Prior P, Andrews HA, Allan RN. 1994. Ulcerative colitis and Crohn's disease: a comparison of the colorectal cancer risk in extensive colitis. Gut 35: 1590-1592.

Goldgraber MB. 1965. Diseases of the colon and rectum 8: pp 355-363.

Graham TA, Humphries A, Sanders T, Rodriguez-Justo M, Tadrous PJ, Preston SL, Novelli MR, Leedham SJ, McDonald SA, Wright NA. 2011. Use of methylation patterns to determine expansion of stem cell clones in human colon tissue. Gastroenterology 140: 1241-1250.

Graham TA, Humphries A, Wright N. 2011. Use of methylation patterns to determine expansion of stem cell clones in human colon tissue. Gastroenterology 140:1241-1250.

Greaves LC, Preston SL, Tadrous PJ, Taylor RW, Barron MJ, Oukrif D, Leedham SJ, Deheragoda M, Sasieni P, Novelli MR, Jankowski JA, Turnbull DM, Wright NA, Mcdonald SA. 2006. Mitochondrial DNA mutations are established in human colonic stem cells, and mutated clones expand by crypt fission. Proc Natl Acad Sci U S A 103: 714-719.

Greenstein AJ. 2000. Cancer in inflammatory bowel disease. Mt Sinai J Med 67: 227-240.

Gutierrez-Gonzalez L, Wright NA. 2008. Biology of intestinal metaplasia in 2008: more than a simple phenotypic alteration. Dig Liver Dis 40: 510-522.

Gyde SN, Prior P, Macartney JC, Thompson H, Waterhouse JA, Allan RN. 1980. Malignancy in Crohn's disease. Gut 21: 1024-1029.

Hamburger AW, Salmon SE. 1977. Primary bioassay of human tumor stem cells. Science 197: 461-463.

Haramis AP, Begthel H, van den Born M, van Es J, Jonkheer S, Offerhaus GJ, Clevers H. 2004. De novo crypt formation and juvenile polyposis on BMP inhibition in mouse intestine. Science 303: 1684-1686.

Harvey KF, Zhang X, Thomas DM. 2013. The Hippo pathway and human cancer. Nat Rev Cancer 13: 246-257.

He L, Hannon GJ. 2004. MicroRNAs: small RNAs with a big role in gene regulation. Nat Rev Genet. 5: 522-531.

Herbst JJ, Sunshine P. 1969. Postnatal development of the small intestine of the rat. Changes in mucosal morphology at weaning. Pediatric research 3: 27-33.

Hofstad B, Vatn MH, Andersen SN, Huitfeldt HS, Rognum T, Larsen S, Osnes M. 1996. Growth of colorectal polyps: redetection and evaluation of unresected polyps for a period of three years. Gut 39: 449-56.

Humphries A, Cereser B, Gay LJ, Miller DS, Das B, Gutteridge A, Elia G, Nye E, Jeffery R, Poulsom R, Novelli MR, Rodriguez-Justo M, McDonald SA, Wright NA, Graham TA. 2013. Lineage tracing reveals multipotent stem cells maintain human adenomas and the pattern of clonal expansion in tumor evolution. Proc Natl Acad Sci U S A. 110: E2490-2499.

Hussain SP, Amstad P, Raja K, Ambs S, Nagashima M, Bennett WP, Shields PG, Ham AJ, Swenberg JA, Marrogi AJ, Harris CC. 2000. Increased p53 mutation load in noncancerous colon tissue from ulcerative colitis: a cancer-prone chronic inflammatory disease. Cancer Res. 60: 3333-3337.

Iborra M, Bernuzzi F, Correale C, Vetrano S, Fiorino G, Beltrán B, Marabita F, Locati M, Spinelli A, Nos P, Invernizzi P, Danese S. 2013. Identification of serum and tissue micro-RNA expression profiles in different stages of inflammatory bowel disease. Clin Exp Immunol. 173: 250-8.

Issa JP, Ahuja N, Toyota M, Bronner MP, Brentnall TA. 2001. Accelerated age-related CpG island methylation in ulcerative colitis. Cancer Res. 61: 3573-3577.

Itzkowitz SH, Yio X. 2004. Inflammation and cancer IV. Colorectal cancer in inflammatory bowel disease: the role of inflammation. Am J Physiol Gastrointest Liver Physiol. 287: G7-17.

Itzkovitz S, Blat IC, Jacks T, Clevers H, van Oudenaarden A. 2012. Optimality in the development of intestinal crypts. Cell 148: 608-619.

Jass JR. 2002. Pathogenesis of colorectal cancer. Surg Clin North Am. 82: 891-904.

Jeffrey SS. 2008. Cancer biomarker profiling with microRNAs. Nat Biotechnol. 26: 400-401.

Jeffrey SS. Cancer biomarker profiling with microRNAs. 2008. Nat Biotechnol. 26: 400-401.

Jess T, Simonsen J, Jørgensen KT, Pedersen BV, Nielsen NM, Frisch M. 2012. Decreasing risk of colorectal cancer in patients with inflammatory bowel disease over 30 years. Gastroenterology 143:375-381.

Jones S, Chen WD, Parmigiani G, Diehl F, Beerenwinkel N, Antal T, Traulsen A, Nowak MA, Siegel C, Velculescu VE, Kinzler KW, Vogelstein B, Willis J,

Markowitz SD. 2008. Comparative lesion sequencing provides insights into tumor evolution. Proc Natl Acad Sci U S A. 105: 4283-4288.

Kambara T, Simms LA, Whitehall VL, Spring KJ, Wynter CV, Walsh MD, Barker MA, Arnold S, McGivern A, Matsubara N, Tanaka N, Higuchi T, Young J, Jass JR, Leggett BA. 2004. BRAF mutation is associated with DNA methylation in serrated polyps and cancers of the colorectum. Gut 53: 1137-1144.

Kanaan Z, Rai SN, Eichenberger MR, Barnes C, Dworkin AM, Weller C, Cohen E, Roberts H, Keskey B, Petras RE, Crawford NP, Galandiuk S. 2012. Differential microRNA expression tracks neoplastic progression in inflammatory bowel disease-associated colorectal cancer. Hum Mutat. 33: 551-560.

Karnoub AE, Dash AB, Vo AP, Sullivan A, Brooks MW, Bell GW, Richardson AL, Polyak K, Tubo R, Weinberg RA. 2007. Mesenchymal stem cells within tumour stroma promote breast cancer metastasis. Nature 449: 557-563.

Keller R, Foerster EC, Kohler A, Floer B, Winde G, Terpe HJ, Domschke W. 2001. Diagnostic value of DNA image cytometry in ulcerative colitis. Dig Dis Sci. 46: 870-878.

Kelly JK, Gabos S. The pathogenesis of inflammatory polyps. 1987. Dis Colon Rectum. 30: 251-254.

Kim JY, Siegmund KD, Tavare S, Shibata D. 2005. Age-related human small intestine methylation: evidence for stem cell niches. BMC Med 3: 10.

Kim JY, Tavare S, Shibata D. 2006. Human hair genealogies and stem cell latency. BMC Biol 4: 2.

Kim KM, Shibata D. 2002. Methylation reveals a niche: stem cell succession in human colon crypts. Oncogene 21: 5441-5449.

Kim KM, Shibata D. 2004. Tracing ancestry with methylation patterns: most crypts appear distantly related in normal adult human colon. BMC Gastroenterol. 4: 8.

Kim M, Morshead CM. 2003. Distinct populations of forebrain neural stem and progenitor cells can be isolated using side-population analysis. J Neurosci 23: 10703-10709.

Kinzler KW, Vogelstein B. 1996. Lessons from hereditary colorectal cancer. Cell 87: 159-170.

Kozar S, Morrissey E, Nicholson AM, van der Heijden M, Zecchini HI, Kemp R, Tavaré S, Vermeulen L, Winton DJ. 2013. Continuous clonal labeling reveals small numbers of functional stem cells in intestinal crypts and adenomas. Cell Stem Cell 13: 626-633.

Kulis M, Esteller M. 2010. DNA methylation and cancer. Adv Genet. 70: 27-56.

Lai LA, Risques RA, Bronner MP, Rabinovitch PS, Crispin D, Chen R, Brentnall TA. 2012. Pan-colonic field defects are detected by CGH in the colons of UC patients with dysplasia/cancer. Cancer Lett. 320: 180-188.

Lamlum H, Papadopoulou A, Ilyas M, Rowan A, Gillet C, Hanby A, Talbot I, Bodmer W, Tomlinson I. 2000. APC mutations are sufficient for the growth of early colorectal adenomas. Proc Natl Acad Sci U S A. 97: 2225-2228.

Lee G, Goretsky T, Managlia E, Dirisina R, Singh AP, Brown JB, May R, Yang GY, Ragheb JW, Evers BM, Weber CR, Turner JR, He XC, Katzman RB, Barrett TA. 2010. Phosphoinositide 3-kinase signaling mediates beta-catenin activation in intestinal epithelial stem and progenitor cells in colitis. Gastroenterology 139: 869-881, 881 e861-869.

Leedham SJ, Wright NA. 2008. Expansion of a mutated clone: from stem cell to tumour. J Clin Pathol. 61: 164-171.

Leedham SJ, Graham TA, Oukrif D, McDonald SA, Rodriguez-Justo M, Harrison RF, Shepherd NA, Novelli MR, Jankowski JA, Wright NA. 2009. Clonality, founder mutations, and field cancerization in human ulcerative colitis-associated neoplasia. Gastroenterology 136: 542-550 e546.

Leggett B, Whitehall V. 2010. Role of the serrated pathway in colorectal cancer pathogenesis. Gastroenterology 138:2088-2100.

Levine DS, Rabinovitch PS, Haggitt RC, Blount PL, Dean PJ, Rubin CE, Reid BJ. 1991. Distribution of aneuploid cell populations in ulcerative colitis with dysplasia or cancer. Gastroenterology 101: 1198-1210.

Li C, Heidt DG, Dalerba P, Burant CF, Zhang L, Adsay V, Wicha M, Clarke MF, Simeone DM. 2007. Identification of pancreatic cancer stem cells. Cancer Res. 67: 1030-1037.

Lin WR, Lim SN, McDonald SA, Graham T, Wright VL, Peplow CL, Humphries A, Kocher HM, Wright NA, Dhillon AP, Alison MR. 2010. The histogenesis of regenerative nodules in human liver cirrhosis. Hepatology 51: 1017-1026.

Liu J, Zheng M, Tang YL, Liang XH, Yang Q. 2011. MicroRNAs, an active and versatile group in cancers. Int J Oral Sci. 3: 165-175.

Loeb KR, Loeb LA. 1999. Genetic instability and the mutator phenotype. Studies in ulcerative colitis. Am J Pathol. 154: 1621-1626.

Loeffler M, Bratke T, Paulus U, Li YQ, Potten CS. 1997. Clonality and life cycles of intestinal crypts explained by a state dependent stochastic model of epithelial stem cell organization. Journal of theoretical biology 186: 41-54.

Loftus EV, Sandborn WJ. 2002. Epidemiology of inflammatory bowel disease. Gastroenterol Clin North Am. 31: 1-20.

Loh YH, Jakszyn P, Luben RN, Mulligan AA, Mitrou PN, Khaw KT. 2011. N-Nitroso compounds and cancer incidence: the European Prospective Investigation into Cancer and Nutrition (EPIC)-Norfolk Study. Am J Clin Nutr. 93: 1053-1061.

Lopez-Garcia C, Klein AM, Simons BD, Winton DJ. 2010. Intestinal stem cell replacement follows a pattern of neutral drift. Science 330: 822-825.

Lutgens MW, Vleggaar FP, Schipper ME, Stokkers PC, van der Woude CJ, Hommes DW, de Jong DJ, Dijkstra G, van Bodegraven AA, Oldenburg B, Samsom M. 2008. High frequency of early colorectal cancer in inflammatory bowel disease. Gut 57:1246-1251.

Lutgens MW, van Oijen MG, van der Heijden GJ, Vleggaar FP, Siersema PD, Oldenburg B. 2013. Declining risk of colorectal cancer in inflammatory bowel disease: an updated meta-analysis of population-based cohort studies. Inflamm Bowel Dis. 19:789-99.

Lv LL, Cao YH, Ni HF, Xu M, Liu D, Liu H, Chen PS, Liu BC. 2013. MicroRNA-29c in urinary exosome/microvesicle as a biomarker of renal fibrosis. Am J Physiol Renal Physiol. 305: F1220-1227.

Lyda MH, Noffsinger A, Belli J, Fischer J, Fenoglio-Preiser CM. 1998. Multifocal neoplasia involving the colon and appendix in ulcerative colitis: pathological and molecular features. Gastroenterology 115: 1566-1573.

Lyda MH, Noffsinger A, Belli J, Fenoglio-Preiser CM. 2000. Microsatellite instability and K-ras mutations in patients with ulcerative colitis. Hum Pathol. 31: 665-671.

Maley CC, Galipeau PC, Li X, Sanchez CA, Paulson TG, Reid BJ. 2004. Selectively advantageous mutations and hitchhikers in neoplasms: p16 lesions are selected in Barrett's esophagus. Cancer Res. 64: 3414-3427.

Maskens AP, Dujardin-Loits RM. 1981. Kinetics of tissue proliferation in colorectal mucosa during post-natal growth. Cell Tissue Kinet. 14: 467-477.

McDonald SA, Preston SL, Greaves LC, Leedham SJ, Lovell MA, Jankowski JA, Turnbull DM, Wright NA. 2006. Clonal expansion in the human gut: mitochondrial DNA mutations show us the way. Cell Cycle 5: 808-811.

McDonald SA, Greaves LC, Gutierrez-Gonzalez L, Rodriguez-Justo M, Deheragoda M, Leedham SJ, Taylor RW, Lee CY, Preston SL, Lovell M, Hunt T, Elia G, Oukrif D, Harrison R, Novelli MR, Mitchell I, Stoker DL, Turnbull DM, Jankowski JA, Wright NA. 2008. Mechanisms of field cancerization in the human stomach: the expansion and spread of mutated gastric stem cells. Gastroenterology 134: 500-510.

Melville DM, Jass JR, Morson BC, Pollock DJ, Richman PI, Shepherd NA, Ritchie JK, Love SB, Lennard-Jones JE. 1989. Observer study of the grading of dysplasia in ulcerative colitis: comparison with clinical outcome. Hum Pathol. 20: 1008-1014.

Miyoshi Y, Nagase H, Ando H, Horii A, Ichii S, Nakatsuru S, Aoki T, Miki Y, Mori T, Nakamura Y. 1992. Somatic mutations of the APC gene in colorectal tumors: mutation cluster region in the APC gene. Hum Mol Genet. 1: 229-233.

Montgomery RK, Carlone DL, Richmond CA, Farilla L, Kranendonk ME, Henderson DE, Baffour-Awuah NY, Ambruzs DM, Fogli LK, Algra S, Breault DT. 2011. Mouse telomerase reverse transcriptase (mTert) expression marks slowly cycling intestinal stem cells. Proc Natl Acad Sci U S A. 108: 179-184.

Mueller MM, Fusenig NE. 2004. Friends or foes - bipolar effects of the tumour stroma in cancer. Nat Rev Cancer 4: 839-849.

Muñoz J, Stange DE, Schepers AG, van de Wetering M, Koo BK, Itzkovitz S, Volckmann R, Kung KS, Koster J, Radulescu S, Myant K, Versteeg R, Sansom OJ, van Es JH, Barker N, van Oudenaarden A, Mohammed S, Heck AJ, Clevers H. 2012. The Lgr5 intestinal stem cell signature: robust expression of proposed quiescent '+4' cell markers. EMBO J. 31: 3079-3091.

Muto T, Bussey HJ, Morson BC. 1975. The evolution of cancer of the colon and rectum. Cancer 36: 2251-2270.

Nicolas P, Kim KM, Shibata D, Tavare S. 2007. The stem cell population of the human colon crypt: analysis via methylation patterns. PLoS Comput Biol. 3: e28.

Nishimura H, Sakagami H, Uezu A, Fukunaga K, Watanabe M, Kondo H. 2003. Cloning, characterization and expression of two alternatively splicing isoforms of Ca2+/calmodulin-dependent protein kinase I gamma in the rat brain. J Neurochem. 85: 1216-1227.

Nooteboom M, Johnson R, Taylor RW, Wright NA, Lightowlers RN, Kirkwood TB, Mathers JC, Turnbull DM, Greaves LC. 2010. Age-associated mitochondrial DNA mutations lead to small but significant changes in cell proliferation and apoptosis in human colonic crypts. Aging cell 9: 96-99.

Novelli M, Cossu A, Oukrif D, Quaglia A, Lakhani S, Poulsom R, Sasieni P, Carta P, Contini M, Pasca A, Palmieri G, Bodmer W, Tanda F, Wright N. 2003. X-inactivation patch size in human female tissue confounds the assessment of tumor clonality. Proc Natl Acad Sci U S A. 100: 3311-3314.

Novelli MR, Williamson JA, Tomlinson IP, Elia G, Hodgson SV, Talbot IC, Bodmer WF, Wright NA. 1996. Polyclonal origin of colonic adenomas in an XO/XY patient with FAP. Science 272: 1187-1190.

Nystul T, Spradling A. 2007. An epithelial niche in the Drosophila ovary undergoes long-range stem cell replacement. Cell Stem Cell 1: 277-285.

O'Brien MJ, Yang S, Mack C, Xu H, Huang CS, Mulcahy E, Amorosino M, Farraye FA. 2006. Comparison of microsatellite instability, CpG island methylation phenotype, BRAF and KRAS status in serrated polyps and traditional adenomas

indicates separate pathways to distinct colorectal carcinoma end points. Am J Surg Pathol. 30: 1491-1501.

O'Brien CA, Pollett A, Gallinger S, Dick JE. 2007. A human colon cancer cell capable of initiating tumour growth in immunodeficient mice. Nature 445: 106-110.

Olaru AV, Selaru FM, Mori Y, Vazquez C, David S, Paun B, Cheng Y, Jin Z, Yang J, Agarwal R, Abraham JM, Dassopoulos T, Harris M, Bayless TM, Kwon J, Harpaz N, Livak F, Meltzer SJ. 2011. Dynamic changes in the expression of MicroRNA-31 during inflammatory bowel disease-associated neoplastic transformation. Inflamm Bowel Dis. 17: 221-231.

O'Sullivan JN, Bronner MP, Brentnall TA, Finley JC, Shen WT, Emerson S, Emond MJ, Gollahon KA, Moskovitz AH, Crispin DA, Potter JD, Rabinovitch PS. 2002. Chromosomal instability in ulcerative colitis is related to telomere shortening. Nat Genet. 32: 280-284.

Okamoto K, Ishiguro T, Midorikawa Y, Ohata H, Izumiya M, Tsuchiya N, Sato A, Sakai H, Nakagama H. 2012. miR-493 induction during carcinogenesis blocks metastatic settlement of colon cancer cells in liver. EMBO. 31: 1752-1763.

Park HS, Goodlad RA, Wright NA. 1995. Crypt fission in the small intestine and colon. A mechanism for the emergence of G6PD locus-mutated crypts after treatment with mutagens. Am J Pathol. 147: 1416-1427.

Park HS, Goodlad RA, Wright NA. 1997. The incidence of aberrant crypt foci and colonic carcinoma in dimethylhydrazine-treated rats varies in a site-specific manner and depends on tumor histology. Cancer Res. 57: 4507-4510.

Paulus U, Loeffler M, Zeidler J, Owen G, Potten CS. 1993. The differentiation and lineage development of goblet cells in the murine small intestinal crypt: experimental and modelling studies. J Cell Sci. 106: 473-483.

Potten CS, Kovacs L, Hamilton E. 1974. Continuous labelling studies on mouse skin and intestine. Cell Tissue Kinet. 7: 271-283.

Potten CS. 1978. Small intestinal cryptogenic cells in W/Wv mutant mice. Radiat Res. 74: 139-143.

Potten CS, Kellett M, Rew DA, Roberts SA. 1992. Proliferation in human gastrointestinal epithelium using bromodeoxyuridine in vivo: data for different sites, proximity to a tumour, and polyposis coli. Gut 33: 524-529.

Potten CS, Booth C. 1997. The role of radiation-induced and spontaneous apoptosis in the homeostasis of the gastrointestinal epithelium: a brief review. Comp Biochem Physiol B Biochem Mol Biol. 118: 473-478.

Potten CS, Grant HK. 1998. The relationship between ionizing radiation-induced apoptosis and stem cells in the small and large intestine. Br J Cancer 78: 993-1003.

Potten CS, Owen G, Booth D. 2002. Intestinal stem cells protect their genome by selective segregation of template DNA strands. J Cell Sci 115: 2381-2388.

Potten CS, Booth C, Tudor GL, Booth D, Brady G, Hurley P, Ashton G, Clarke R, Sakakibara S, Okano H. 2003. Identification of a putative intestinal stem cell and early lineage marker; musashi-1. Differentiation 71: 28-41.

Powell DW, Mifflin RC, Valentich JD, Crowe SE, Saada JI, West AB. 1999. Myofibroblasts. II. Intestinal subepithelial myofibroblasts. Am J Physiol. 277: C183-201.

Powell SM, Zilz N, Beazer-Barclay Y, Bryan TM, Hamilton SR, Thibodeau SN, Vogelstein B, Kinzler KW. 1992. APC mutations occur early during colorectal tumorigenesis. Nature 359: 235-237.

Preston SL, Wong WM, Chan AO, Poulsom R, Jeffery R, Goodlad RA, Mandir N, Elia G, Novelli M, Bodmer WF, Tomlinson IP, Wright NA. 2003. Bottom-up histogenesis of colorectal adenomas: origin in the monocryptal adenoma and initial expansion by crypt fission. Cancer Res. 63: 3819-3825.

Quintana E, Shackleton M, Sabel MS, Fullen DR, Johnson TM, Morrison SJ. 2008. Efficient tumour formation by single human melanoma cells. Nature 456: 593-598.

Ren F, Wang B, Yue T, Yun EY, Ip YT, Jiang J. 2010. Hippo signaling regulates Drosophila intestine stem cell proliferation through multiple pathways. Proc Natl Acad Sci U S A. 107: 21064-21069.

Ren F, Zheng L, Jiang J. 2010. Hippo signalling regulates yorkie nuclear localisation and activity through dependent and independent mechanisms. Developmental Biology 337: 303-312.

Reya T, Morrison SJ, Clarke MF, Weissman IL. 2001. Stem cells, cancer, and cancer stem cells. Nature 414: 105-111.

Ricci-Vitiani L, Lombardi DG, Pilozzi E, Biffoni M, Todaro M, Peschle C, De Maria R. 2007. Identification and expansion of human colon-cancer-initiating cells. Nature 445: 111-115.

Risques RA, Lai LA, Brentnall TA, Li L, Feng Z, Gallaher J, Mandelson MT, Potter JD, Bronner MP, Rabinovitch PS. 2008. Ulcerative colitis is a disease of accelerated colon aging: evidence from telomere attrition and DNA damage. Gastroenterology 135: 410-418.

Roderburg C, Urban GW, Bettermann K, Vucur M, Zimmermann H, Schmidt S, Janssen J, Koppe C, Knolle P, Castoldi M, Tacke F, Trautwein C, Luedde T. 2011. Micro-RNA profiling reveals a role for miR-29 in human and murine liver fibrosis. Hepatology 53: 209-218.

Rubin CE, Haggitt RC, Burmer GC, Brentnall TA, Stevens AC, Levine DS, Dean PJ, Kimmey M, Perera DR, Rabinovitch PS. 1992. DNA aneuploidy in colonic biopsies predicts future development of dysplasia in ulcerative colitis. Gastroenterology 103: 1611-1620.

Rubin DT, Huo D, Kinnucan JA, Sedrak MS, McCullom NE, Bunnag AP, Raun-Royer EP, Cohen RD, Hanauer SB, Hart J, Turner JR. 2013. Inflammation is an independent risk factor for colonic neoplasia in patients with ulcerative colitis: a case-control study. Clin Gastroenterol Hepatol. 11: 1601-1608.

Rutter M, Saunders B, Wilkinson K, Rumbles S, Schofield G, Kamm M, Williams C, Price A, Talbot I, Forbes A. 2004a. Severity of inflammation is a risk factor for colorectal neoplasia in ulcerative colitis. Gastroenterology 126: 451-459.

Rutter MD, Saunders BP, Wilkinson KH, Rumbles S, Schofield G, Kamm MA, Williams CB, Price AB, Talbot IC, Forbes A. 2004b. Cancer surveillance in longstanding ulcerative colitis: endoscopic appearances help predict cancer risk. Gut 53: 1813-1816.

Rybaczyk L, Rozmiarek A, Circle K, Grants I, Needleman B, Wunderlich JE, Huang K, Christofi FL. 2009. New bioinformatics approach to analyze gene expressions and signaling pathways reveals unique purine gene dysregulation profiles that distinguish between CD and UC. Inflamm Bowel Dis. 15: 971-984.

Sainsbury A, Goodlad RA, Perry SL, Pollard SG, Robins GG, Hull MA. 2008. Increased colorectal epithelial cell proliferation and crypt fission associated with obesity and roux-en-Y gastric bypass. Cancer epidemiology, biomarkers & prevention: a publication of the American Association for Cancer Research, cosponsored by the American Society of Preventive Oncology 17: 1401-1410.

Salk JJ, Salipante SJ, Risques RA, Crispin DA, Li L, Bronner MP, Brentnall TA, Rabinovitch PS, Horwitz MS, Loeb LA. 2009. Clonal expansions in ulcerative colitis identify patients with neoplasia. Proc Natl Acad Sci U S A. 106: 20871-20876.

Salk JJ, Bansal A, Lai LA, Crispin DA, Ussakli CH, Horwitz MS, Bronner MP, Brentnall TA, Loeb LA, Rabinovitch PS, Risques RA. 2013. Clonal expansions and short telomeres are associated with neoplasia in early-onset, but not late-onset, ulcerative colitis. Inflamm Bowel Dis. 19: 2593-2602.

Salzman NH, Underwood MA, Bevins CL. 2007. Paneth cells, defensins, and the commensal microbiota: a hypothesis on intimate interplay at the intestinal mucosa. Semin Immunol. 19: 70-83.

Sangiorgi E, Capecchi MR. 2008. Bmi1 is expressed in vivo in intestinal stem cells. Nat Genet. 40: 915-920.

Samowitz WS, Sweeney C, Herrick J, Abertsen H, Lewin TR, Murtaugh MA, Wolf RK, Slattery ML. 2005. Poor survival associated with the BRAF V600E mutation in microsatellite stable colon cancer. Cancer Res. 65: 6063-6069.

Sato T, Vries RG, Snippert HJ, van de Wetering M, Barker N, Stange DE, van Es JH, Abo A, Kujala P, Peters PJ, Clevers H. 2009. Single Lgr5 stem cells build crypt-villus structures in vitro without a mesenchymal niche. Nature 459: 262-265.

Sato T, van Es JH, Snippert HJ, Stange DE, Vries RG, van den Born M, Barker N, Shroyer NF, van de Wetering M, Clevers H. 2011. Paneth cells constitute the niche for Lgr5 stem cells in intestinal crypts. Nature 469: 415-418.

Schepers AG, Snippert HJ, Stange DE, van den Born M, van Es JH, van de Wetering M, Clevers H. 2012. Lineage tracing reveals Lgr5+ stem cell activity in mouse intestinal adenomas. Science 337: 730-735.

Schwitalla S, Fingerle AA, Cammareri P, Nebelsiek T, Göktuna SI, Ziegler PK, Canli O, Heijmans J, Huels DJ, Moreaux G, Rupec RA, Gerhard M, Schmid R, Barker N, Clevers H, Lang R, Neumann J, Kirchner T, Taketo MM, van den Brink GR, Sansom OJ, Arkan MC, Greten FR. 2013. Intestinal tumorigenesis initiated by dedifferentiation and acquisition of stem-cell-like properties. Cell 152: 25-38.

Sciacco M, Bonilla E, Schon EA, DiMauro S, Moraes CT. 1994. Distribution of wild-type and common deletion forms of mtDNA in normal and respiration-deficient muscle fibers from patients with mitochondrial myopathy. Hum Mol Genet. 3: 13-19.

Scoville DH, Sato T, He XC, Li L. 2008. Current view: intestinal stem cells and signaling. Gastroenterology 134: 849-864.

Seril DN, Liao J, Yang GY, Yang CS. 2003. Oxidative stress and ulcerative colitis-associated carcinogenesis: studies in humans and animal models. Carcinogenesis 24: 353-362.

Shivananda S, Lennard-Jones J, Logan R, Fear N, Price A, Carpenter L, van Blankenstein M. 1996. Incidence of inflammatory bowel disease across Europe: is there a difference between north and south? Results of the European Collaborative Study on Inflammatory Bowel Disease (EC-IBD). Gut 39: 690-697.

Shmelkov SV, Butler JM, Hooper AT, Hormigo A, Kushner J, Milde T, St Clair R, Baljevic M, White I, Jin DK, Chadburn A, Murphy AJ, Valenzuela DM, Gale NW, Thurston G, Yancopoulos GD, D'Angelica M, Kemeny N, Lyden D, Rafili S. 2008. CD133 expression is not restricted to stem cells, and both CD133+ and CD133- metastatic colon cancer cells initiate tumors. J Clin Invest. 118: 2111-2120.

Sieber OM, Tomlinson IP, Lamlum H. 2000. The adenomatous polyposis coli (APC) tumour suppressor--genetics, function and disease. Mol Med Today 6: 462-469.

Siegmund KD, Marjoram P, Woo YJ, Tavare S, Shibata D. 2009. Inferring clonal expansion and cancer stem cell dynamics from DNA methylation patterns in colorectal cancers. Proc Natl Acad Sci U S A. 106: 4828-4833.

Simons BD, Clevers H. 2011. Strategies for homeostatic stem cell self-renewal in adult tissues. Cell 145: 851-862.

Singh SK, Clarke ID, Terasaki M, Bonn VE, Hawkins C, Squire J, Dirks PB. 2003. Identification of a cancer stem cell in human brain tumors. Cancer Res. 63: 5821-5828.

Slaughter DP, Southwick HW, Smejkal W. 1953. Field cancerization in oral stratified squamous epithelium; clinical implications of multicentric origin. Cancer 6: 963-968.

Snippert HJ, van der Flier LG, Sato T, van Es JH, van den Born M, Kroon-Veenboer C, Barker N, Klein AM, van Rheenen J, Simons BD, Clevers H. 2010. Intestinal crypt homeostasis results from neutral competition between symmetrically dividing Lgr5 stem cells. Cell 143: 134-144.

Snover DC. Serrated polyps of the large intestine. Semin Diagn Pathol. 2005. 22: 301-308.

Solberg IC, Lygren I, Jahnsen J, Aadland E, Hoie O, Cvancarova M, Bernklev T, Henriksen M, Sauar J, Vatn MH, Moum; IBSEN Study Group. 2009. Clinical course during the first 10 years of ulcerative colitis: results from a population-based inception cohort (IBSEN Study). Scand J Gastroenterol. 44: 431-440.

St Clair WH, Osborne JW. 1985. Crypt fission and crypt number in the small and large bowel of postnatal rats. Cell Tissue Kinet. 18: 255-262.

Stryker SJ, Wolff BG, Culp CE, Libbe SD, Ilstrup DM, MacCarty RL. Natural history of untreated colonic polyps. Gastroenterology. 1987. 93:1009-1013.

Tada M, Misaki F, Kawai K. 1984. Growth rates of colorectal carcinoma and adenoma by roentgenologic follow-up observations. Gastroenterol Jpn. 19:550-555.

Tarmin L, Yin J, Harpaz N, Kozam M, Noordzij J, Antonio LB, Jiang HY, Chan O, Cymes K, Meltzer SJ. 1995. Adenomatous polyposis coli gene mutations in ulcerative colitis-associated dysplasias and cancers versus sporadic colon neoplasms. Cancer Res. 55: 2035-2038.

Taylor RW, Barron MJ, Borthwick GM, Gospel A, Chinnery PF, Samuels DC, Taylor GA, Plusa SM, Needham SJ, Greaves LC, Kirkwood TB, Turnbull DM. 2003. Mitochondrial DNA mutations in human colonic crypt stem cells. J Clin Invest. 112: 1351-1360.

Taylor RW, Turnbull DM. 2005. Mitochondrial DNA mutations in human disease. Nat Rev Genet. 6: 389-402.

Todaro M, Alea MP, Di Stefano AB, Cammareri P, Vermeulen L, Iovino F, Tripodo C, Russo A, Gulotta G, Medema JP, Stassi G. 2007. Colon cancer stem cells dictate tumor growth and resist cell death by production of interleukin-4. Cell Stem Cell 1: 389-402.

Tomlinson I, Bodmer W. 1999. Selection, the mutation rate and cancer: ensuring that the tail does not wag the dog. Nat Med. 5: 11-12.

Totafurno J, Bjerknes M, Cheng H. 1987. The crypt cycle. Crypt and villus production in the adult intestinal epithelium. Biophysical journal 52: 279-294.

Totafurno J, Bjerknes M, Cheng H. 1988. Variation in crypt size and its influence on the analysis of epithelial cell proliferation in the intestinal crypt. Biophys J. 54: 845-858.

Ussakli CH, Ebaee A, Binkley J, Brentnall TA, Emond MJ, Rabinovitch PS, Risques RA. 2013. Mitochondria and tumor progression in ulcerative colitis. J Natl Cancer Inst. 105: 1239-1248

van der Flier LG, van Gijn ME, Kujala P, Haegebarth A, Stange DE, Begthel H, van den Born M, Guryer V, Oving I, van Es JH, Barker N, Peters PJ, van de Wetering M, Clevers H. 2009. Transcription factor achaete scute-like 2 controls intestinal stem cell fate. Cell 136: 903-912.

van Es JH, van Gijn ME, Riccio O, van den Born M, Vooijs M, Begthel H, Cozijnsen M, Robine S, Winton DJ, Radtke F, Clevers H. Notch/gamma-secretase inhibition turns proliferative cells in intestinal crypts and adenomas into goblet cells. Nature. 2005. 435: 959-963.

Velayos FS, Loftus EV Jr, Jess T, Harmsen WS, Bida J, Zinsmeister AR, Tremaine WJ, Sandborn WJ. 2006. Predictive and protective factors associated with colorectal cancer in ulcerative colitis: A case-control study. Gastroenterology. 130: 1941-1949.

Vermeulen L, Todaro M, de Sousa Mello F, Sprick MR, Kemper K, Perez Alea M, Richel DJ, Stassi G, Medema JP. 2008. Single-cell cloning of colon cancer stem cells reveals a multi-lineage differentiation capacity. Proc Natl Acad Sci U S A. 105: 13427-13432.

Vermeulen L, Morrissey E, van der Heijden M, Nicholson AM, Sottoriva A, Buczacki S, Kemp R, Tavaré S, Winton DJ. 2013. Defining stem cell dynamics in models of intestinal tumor initiation. Science 342: 995-998.

Visvader JE, Lindeman GJ. 2012. Cancer stem cells: current status and evolving complexities. Cell Stem Cell 10: 717-728.

Vogelstein B, Fearon ER, Hamilton SR, Kern SE, Preisinger AC, Leppert M, Nakamura Y, White R, Smits AM, Bos JL. 1988. Genetic alterations during colorectal-tumor development. N Engl J Med. 319: 525-532.

Wallace DC. 2005. The mitochondrial genome in human adaptive radiation and disease: on the road to therapeutics and performance enhancement. Gene 354: 169-180.

Waye JD. The development of carcinoma of the colon. Am J Gastroenterol. 1977 May;67(5):427-9.

Weisenberger DJ, Siegmund KD, Campan M, Young J, Long TI, Faasse MA, Kang GH, Widschwendter M, Weener D, Buchanan D, Koh H, Simms L, Barker M, Leggett

B, Levine J, Kim M, French AJ, Thibodeau SN, Jass J, Haile R, Laird PW. 2006. CpG island methylator phenotype underlies sporadic microsatellite instability and is tightly associated with BRAF mutation in colorectal cancer. Nat Genet. 38: 787-793.

Welin S, Youker J, Spratt JS Jr. 1963. The rates and patterns of growth of 375 tumours of the large intestine and rectum observed serially by double contract enema study (Malmoe technique). Am J Roentgenol Radium Ther Nucl Med. 90: 673-687.

Wicha MS, Liu S, Dontu G. 2006. Cancer stem cells: an old idea--a paradigm shift. Cancer Res 66: 1883-1890; discussion 1895-1896.

Wilks S. 1859. Lectures on pathological anatomy. 2nd ed. Philadelphia: Lindsay & Flakiston; 1870. Pp. 490-492.

Willenbucher RF, Zelman SJ, Ferrell LD, Moore DH, 2nd, Waldman FM. 1997. Chromosomal alterations in ulcerative colitis-related neoplastic progression. Gastroenterology 113: 791-801.

Williams ED, Lowes AP, Williams D, Williams GT. 1992. A stem cell niche theory of intestinal crypt maintenance based on a study of somatic mutation in colonic mucosa. Am J Pathol 141: 773-776.

Winton DJ, Gooderham NJ, Boobis AR, Davies DS, Ponder BA. 1990. Mutagenesis of mouse intestine in vivo using the Dlb-1 specific locus test: studies with 1,2-

dimethylhydrazine, dimethylnitrosamine, and the dietary mutagen 2-amino-3,8-dimethylimidazo[4,5-f]quinoxaline. Cancer Res. 50: 7992-7996.

Wong WM, Mandir N, Goodlad RA, Wong BC, Garcia SB, Lam SK, Wright NA. 2002. Histogenesis of human colorectal adenomas and hyperplastic polyps: the role of cell proliferation and crypt fission. Gut 50: 212-217.

Wright NA, Al-Nafussi A. 1982. The kinetics of villus cell populations in the mouse small intestine. II. Studies on growth control after death of proliferative cells induced by cytosine arabinoside, with special reference to negative feedback mechanisms. Cell Tissue Kinet. 15: 611-621.

Wright NA. 2000. Epithelial stem cell repertoire in the gut: clues to the origin of cell lineages, proliferative units and cancer. Int J Exp Pathol. 81: 117-143.

Wu F, Zikusoka M, Trindade A, Dassopoulos T, Harris ML, Bayless TM, Brant SR, Chakravarti S, Kwon JH. 2008. MicroRNAs are differentially expressed in ulcerative colitis and alter expression of macrophage inflammatory peptide-2 alpha. Gastroenterology. 135: 1624-1635.

Wu F, Zhang S, Dassopoulos T, Harris ML, Bayless TM, Meltzer SJ, Brant SR, Kwon JH. 2010. Identification of microRNAs associated with ileal and colonic Crohn's disease. Inflamm Bowel Dis. 16: 1729-1738.

Yamashita YM, Fuller MT. 2005. Asymmetric stem cell division and function of the niche in the Drosophila male germ line. Int J Hematol. 82: 377-380.

Yatabe Y, Tavare S, Shibata D. 2001. Investigating stem cells in human colon by using methylation patterns. Proc Natl Acad Sci U S A. 98: 10839-10844.

Yin J, Harpaz N, Tong Y, Huang Y, Laurin J, Greenwald BD, Hontanosas M, Newkirk C, Meltzer SJ. 1993. p53 point mutations in dysplastic and cancerous ulcerative colitis lesions. Gastroenterology 104: 1633-1639.

Yoshida T, Mikami T, Mitomi H, Okayasu I. 2003. Diverse p53 alterations in ulcerative colitis-associated low-grade dysplasia: full-length gene sequencing in microdissected single crypts. J Pathol. 199: 166-175.

You J, Nguyen AV, Albers CG, Lin F, Holcombe RF. 2008. Wnt pathway-related gene expression in inflammatory bowel disease. Dig Dis Sci. 53: 1013-1019.

Zhao J, de Vera J, Narushima S, Beck EX, Palencia S, Shinkawa P, Kim KA, Liu Y, Levy MD, Berg DJ, Abo A, Funk WD. 2007. R-spondin1, a novel intestinotrophic mitogen, ameliorates experimental colitis in mice. Gastroenterology 132: 1331-1343.

Chapter 9. Appendix

9.1 PCR primer sequences and reaction conditions

All primers were ordered dry from Sigma-Aldrich, UK, and re-suspended in water to form a 20 micromolar working solution.

9.1.1 Primer details for sequencing of entire mitochondrial genome

Table 9.1 Forward (F) and reverse (R) primers for first-round nested mitochondrial PCR. Primer pairs span the entire mitochondrial genome. See Table 9.5 for PCR reagent and Table 9.8 for thermal cycler protocol.

Name	Sequence 5' to 3'
A(F)	GCTCACATCACCCCATAAAC
A(R)	GATTACTCCGGTCTGAACTC
B(F)	ACCAACAAGTCATTATTACCC
B(R)	TGAGGAAATACTTGATGGCAG
C(F)	CCGTCATCTACTCTACCATC
C(R)	GGACGGATCAGACGAAGAG
D(F)	AATACCCATCATAATCGGAGG
D(R)	GGTGATGAGGAATAGTGTAAG
E(F)	AACCACTTTCACCGCTACAC
E(R)	AGTGAGATGGTAAATGCTAG
F(F)	ACTTCACGTCATTATTGGCTC
F(R)	ATAGGAGGAGAATGGGGGATAG
G(F)	ACCCCCCACTATTAACCTACTG
G(R)	GGTAGAATCCGAGTATGTTGG
H(F)	TATTCGCAGGATTTCTCATTAC
H(R)	AGCTTTGGGTGCTAATGGTG
I(F)	CCCATCCTCCATATATCCAAAC
I(R)	GGTTAGTATAGCTTAGTTAAAC

Table 9.2 Forward (F) primers for second-round nested mitochondrial PCR.

Primers are specific for the amplicons from the first round reaction. See Table 9.5 and Table 9.8 for PCR reagent and thermal cycler protocol.

Name	Sequence 5' to 3'
1(F)	TGTAAAACGACGGCCAGTCACACACACCGCTGCTAAC
2(F)	TGTAAAACGACGGCCAGTTTAAAACTCAAAGGACCTGGC
3(F)	TGTAAAACGACGGCCAGTAACTTAACTTGACCGCTCTGAG
4(F)	TGTAAAACGACGGCCAGTACTGTTAGTCCAAAGAGGAAC
5(F)	TGTAAAACGACGGCCAGTCAGTGACACATGTTTAACGGC
6(F)	TGTAAAACGACGGCCAGTCAGCCGCTATTAAAGGTTCG
7(F)	TGTAAAACGACGGCCAGTACCATCACCCTCTACATCAC
8(F)	TGTAAAACGACGGCCAGTTCGCCCTATTCTTCATAGCC
9(F)	TGTAAAACGACGGCCAGTACACTCATCACAGCGCTAAG
10(F)	TGTAAAACGACGGCCAGTCTCACTCTCTCAATCTTATCC
11(F)	TGTAAAACGACGGCCAGTACCTCAATCACACTACTCCC
12(F)	TGTAAAACGACGGCCAGTAGATTTACAGTCCAATGCTTC
13(F)	TGTAAAACGACGGCCAGTTAGCAGGTGTCTCCTCTATC
14(F)	TGTAAAACGACGGCCAGTATTTAGCTGACTCGCCACAC
15(F)	TGTAAAACGACGGCCAGTGGCTCATTCATTTCTCTAACAG
16(F)	TGTAAAACGACGGCCAGTTCCTAACACTCACAACAAAAC
17(F)	TGTAAAACGACGGCCAGTACAGTTTCATGCCCATCGTC
18(F)	TGTAAAACGACGGCCAGTACCACCCAACAATGACTAATC
19(F)	TGTAAAACGACGGCCAGTATCCTAGAAATCGCTGTCGC
20(F)	TGTAAAACGACGGCCAGTCATCCGTATTACTCGCATCAG
21(F)	TGTAAAACGACGGCCAGTCAACACCCTCCTAGCCTTAC
22(F)	TGTAAAACGACGGCCAGTATCGCTCACACCTCATATCC
23(F)	TGTAAAACGACGGCCAGTTATCCAGTGAACCACTATCAC
24(F)	TGTAAAACGACGGCCAGTTCCTTGTACTATCCCTATGAG
25(F)	TGTAAAACGACGGCCAGTCTCCCTCTACATATTTACCAC
26(F)	TGTAAAACGACGGCCAGTCTCTTCCCCACAACAATATTC
27(F)	TGTAAAACGACGGCCAGTGCCCTTCTAAACGCTAATCC
28(F)	TGTAAAACGACGGCCAGTCGGGTCCATCATCCACAAC
29(F)	TGTAAAACGACGGCCAGTACCTAAAACTCACAGCCCTC
30(F)	TGTAAAACGACGGCCAGTATTAAAGTTTACCACAACCACC
31(F)	TGTAAAACGACGGCCAGTATTCATCGACCTCCCCACC
32(F)	TGTAAAACGACGGCCAGTCATCTTGCCCTTCATTATTGC
D1(F)	TGTAAAACGACGGCCAGTATCGGAGGACAACCAGTAAG
D2(F)	TGTAAAACGACGGCCAGTCTCAACTATCACACATCAACTG
D3(F)	TGTAAAACGACGGCCAGTCCTTAAATAAGACATCACGATG
D4(F)	TGTAAAACGACGGCCAGTGCCACAGCACTTAAACACATC

Table 9.3 Reverse (R) primers for second-round nested mitochondrial PCR.

Primer are specific for the amplicons from the first round reaction. See Table 9.5 and Table 9.8 for PCR reagent and thermal cycler protocol.

Name	Sequence 5' to 3'
1(R)	CAGGAAACAGCTATGACCGATGGCGGTATATAGGCTGAG
2(R)	CAGGAAACAGCTATGACCCTGGTAGTAAGGTGGAGTGGG
3(R)	CAGGAAACAGCTATGACCATTGGTGGCTGCTTTTAGG
4(R)	CAGGAAACAGCTATGACCTCGTGGAGCCATTCATACAG
5(R)	CAGGAAACAGCTATGACCGATTACTCCGGTCTGAACTC
6(R)	CAGGAAACAGCTATGACCGGAGGGGGGTTCATAGTAG
7(R)	CAGGAAACAGCTATGACCAGAGTGCGTCATATGTTGTTC
8(R)	CAGGAAACAGCTATGACCGTTTATTTCTAGGCCTACTCAG
9(R)	CAGGAAACAGCTATGACCGATTTTGCGTAGCTGGGTTTG
10(R)	CAGGAAACAGCTATGACCTGTAGGAGTAGCGTGGTAAGG
11(R)	CAGGAAACAGCTATGACCTAGTCAACGGTCGGCGAA
12(R)	CAGGAAACAGCTATGACCATGGCAGGGGGTTTTATATTG
13(R)	CAGGAAACAGCTATGACCAAGAAAGATGAATCCTAGGGC
14(R)	CAGGAAACAGCTATGACCCATCCATATAGTCACTCCAGG
15(R)	CAGGAAACAGCTATGACCGGCAGGATAGTTCAGACGG
16(R)	CAGGAAACAGCTATGACCTACAGTGGGCTCTAGAGGG
17(R)	CAGGAAACAGCTATGACCGTATAAGAGATCAGGTTCGTC
18(R)	CAGGAAACAGCTATGACCGTTGTCGTGCAGGTAGAGG
19(R)	CAGGAAACAGCTATGACCATTAGACTATGGTGAGCTCAG
20(R)	CAGGAAACAGCTATGACCTAGCCGTTGAGTTGTGGTAG
21(R)	CAGGAAACAGCTATGACCAGGCACAATATTGGCTAAGAG
22(R)	CAGGAAACAGCTATGACCATGATTAGTTCTGTGGCTGTG
23(R)	CAGGAAACAGCTATGACCTAGGTCTGTTTGTCGTAGGC
24(R)	CAGGAAACAGCTATGACCCGTGTGAATGAGGGTTTTATG
25(R)	CAGGAAACAGCTATGACCGTGGCTCAGTGTCAGTTCG
26(R)	CAGGAAACAGCTATGACCCTGATTTGCCTGCTGCTGC
27(R)	CAGGAAACAGCTATGACCGGGAGGTTGAAGTGAGAGG
28(R)	CAGGAAACAGCTATGACCGTTAGGTAGTTGAGGTCTAGG
29(R)	CAGGAAACAGCTATGACCAGGATTGGTGCTGTGGGTG
30(R)	CAGGAAACAGCTATGACCAAGGAGTGAGCCGAAGTTTC
31(R)	CAGGAAACAGCTATGACCGGTTGTTTGATCCCGTTTCG
32(R)	CAGGAAACAGCTATGACCTACAAGGACAGGCCCATTTG
D1(R)	CAGGAAACAGCTATGACCAGGGTGATAGACCTGTGATC
D2(R)	CAGGAAACAGCTATGACCAGATACTGCGACATAGGGTG
D3(R)	CAGGAAACAGCTATGACCCTGGTTAGGCTGGTGTTAGG
D4(R)	CAGGAAACAGCTATGACCTGCTGCGTGCTTGATGCTTG

Table 9.4 Methylation nested PCR, cloning and sequencing primers. **1st** and **2nd** refer to PCR reaction round; primers are specific for bisulphite treated DNA. **F**: Forward primer; **R**: Reverse primer. Reaction notes refer to standard PCR reagent and thermal cycler protocol, (see Materials and Methods and Table 9.8).

Name	Sequence 5' to 3'	Reaction notes
CSX 1st F	GAGTTTGGTAGGGAAGGGATT	Mg 1.5/55ºC
CSX 1st R	AAAACACTCCTAAAAAAACAACTA	Mg 1.5/55ºC
CSX 2nd F	GGAGATTTAGGAATTTTTTTTGTTTT	Mg 1.5/60ºC
CSX 2nd R	CACCAAACTACAAAATCACTCATTACA	Mg 1.5/60ºC
BGN 1st F	TTTTTTTGAAGTTGTTAGGG	Mg 1.5/55ºC
BGN 1st R	AACCAAAAACATCTCTAAATTACT	Mg 1.5/55ºC
BGN 2nd F	TAAATTGTTTAGGAGTGAGTAGTTGTTT	Mg 2.5/60ºC
BGN 2nd R	AAAAACAACTTAAAACCAACCCTACC	Mg 2.5/60ºC
MYOD 1st F	GGGTTTTTTTTTTAGTTGAAGAGGT	Mg 2.5Q/60ºC
MYOD 1st R	ACCTAAAAATTACTCAACAAAT	Mg 2.5Q/60ºC
MYOD 2nd F	TGGAGGGGATTTTTAATTTGG	Mg 1.5Q/55ºC
MYOD 2nd R	AACCCAATCCTTCTTCCCTAA	Mg 1.5Q/55ºC
M13F	GTAAAACGACGGCCAGT	Mg 1.5/55ºC
M13R	CAGGAAACAGCTATGAC	Mg 1.5/55ºC
T7	TAATACGACTCACTATAGGG	Mg 1.5/55ºC
SP6	TATTTAGGTGACACTATAG	Mg 1.5/55ºC
M13 F	GTAAAACGACGGCCAGT	Mg 1.5/55ºC
M13 R	CAGGAAACAGCTATGAC	Mg 1.5/55ºC

Table 9.5 MtDNA PCR reagents

Reagent	**Manufacturer**	**Working Concentration**
Nucleotides	Applied Biosystems	10mM of each
*Buffer	Applied Biosystems	As supplied
Magnesium	Applied Biosystems	25mM
AmpliTaq Gold	Applied Biosystems	5units/µl

Table 9.6 PCR product sequencing reaction protocol. **BDT**: BigDye Terminator (Applied Biosystems, USA); *forward or reverse primer used; **diluted ExoSap-IT purified PCR product.

DNA sequencing reaction reagent protocol

Reagents per well	**Volume per well** (µl) Total= 20 µl per well	**Working Concentration**
BDT	10	10mM of each
*Primer	5	As supplied
H_2O	1	25mM
**PCR Product	4	5units/µl

Table 9.7: Reference sequences of *CSX*, *BGN* and *MYOD1.* Sequences are displayed post-bisulphite treatment. A capital T indicates a thymine base produced by bisulphite conversion of the original cytosine base. CpG sites are assumed methylated and indicated in **bold**. Second round primer binding sites are underlined.

Methylation gene CpG island target sequences.

Locus	**Sequence**
BGN (10 CpGs)	TaaaTtgTTTaggagtgagtagTtgTttt**CG**gtT**CG**T**CG**gaTaTaT**CG**gaTagatag a**CG**tg**CG**ga**CG**gTTTaTTaTTTTagTT**CG**TTaaTtagtTagTTtg**CG**TTtgg **CG**TTtTTTTtTtTTaggtagggTtggTttTaagTtgTTtTT
CSX (8 CpGs)	**G**gagaTTtaggaaTtttttTtgtTTTa**CGCGCG**tttgttTttg**CG**Ta**CG**ggagagtttgt ggg**CG**g**CG**attatgTag**CG**tgTaatgagtgatTTtgTagTTtggtg
MYOD1 (5 CpGs)	tggaggggattTTtaaTTtgggTaggatT**CG**agtttggagagattgg**CGCG**aagTtttagT agTaatTtT**CG**attTTtgtaTaaTTatagTtgggtttTtaag**CG**tTtagggaagaaggaTtg ggTT

Table 9.8 Thermal cycling programme for sequencing of mtDNA PCR products.

MtDNA thermal cycler sequencing programme

Step	Temperature	Time	Time
Temperature 1	96°C	1 minute	
Denaturating	96°C	10 seconds	25 cycles
Annealing	50°C	5 seconds	
Elongation	60°C	4 minutes	
Hold	4°C	Thereafter	

Table 9.9 ExoSap thermal cycler programme

ExoSap-IT Thermal Cycler Programme		
Step	Temperature	Time
Temperature 1	37°C	15 minutes
Temperature 2	80°C	15 minutes
Hold	15°C	Thereafter

9.2 Colon maps for patients with pseudopolyps and pre-malignant and/or malignant lesions

Key to Colon maps

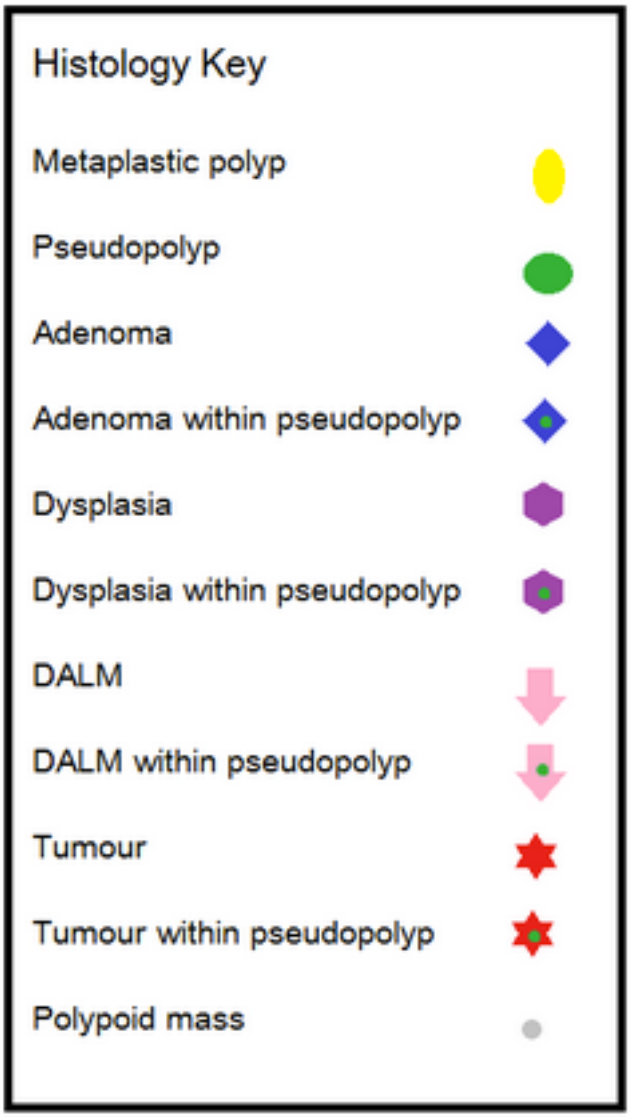

Patient No	Age	Diagnosis	Tissue sites
1	76	UC distal sigmoid	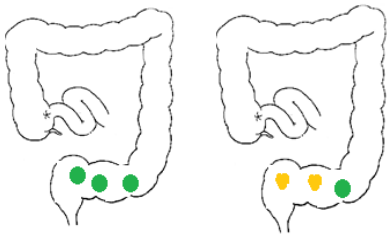 2010 2012
3	60	UC total	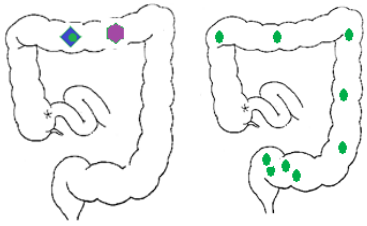 2003 2006 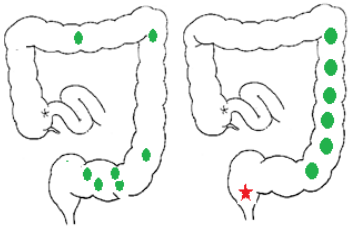 2007 2009
6	73	UC left sided	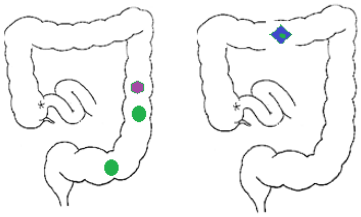 2006 2007
13	77	Colitis	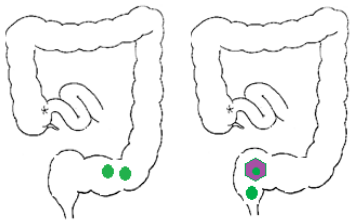 2008 2011 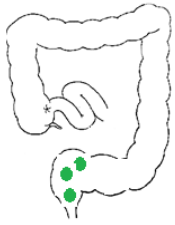

			2013
Patient No	Age	Diagnosis	Tissue sites
14	64	UC Pan-colitis	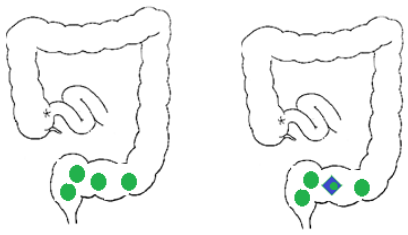 2007 2013
2	73	colitis	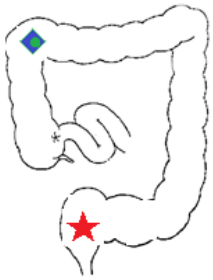 2012
4	60	UC to splenic flexure	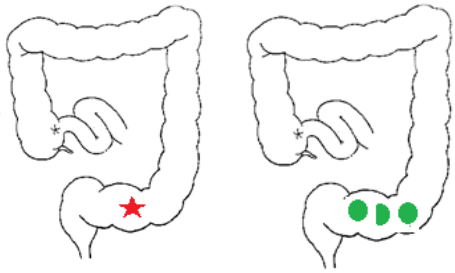 2008 2009 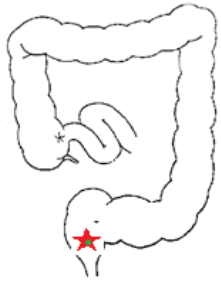 2011
5	64	UC	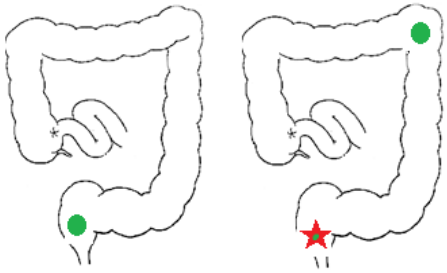 2008 2008

Patient No	Age	Diagnosis	Tissue sites
7	23	Crohn's	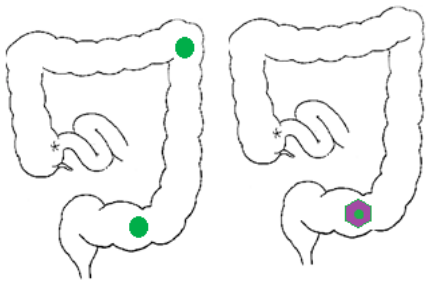 2003 2010
8	20	Crohn's	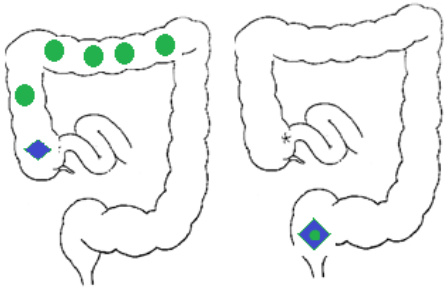 2012 2013
9		UC	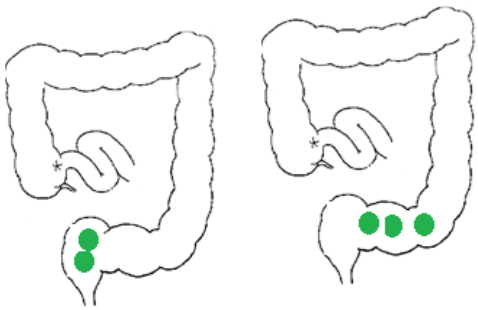 2008 2012 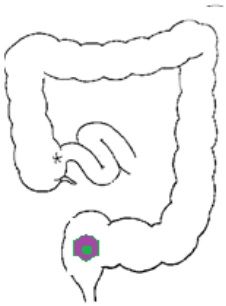 2013
10	45	Sigmoid UC	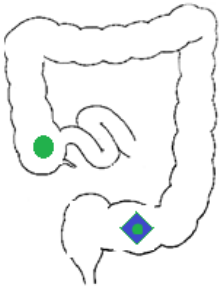 2013

Patient No	Age	Diagnosis	Tissue sites
11	59	Left sided UC	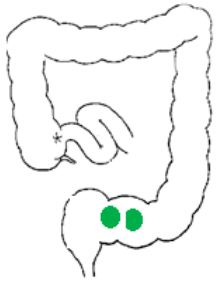 2006 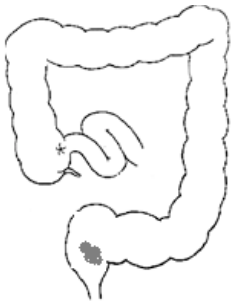 2009 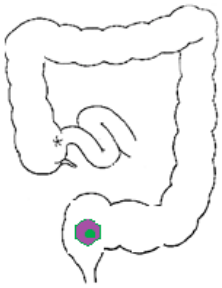 2012
12	44	Pancolitis	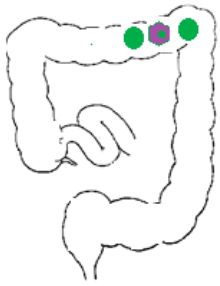 2011
13	40	Distal UC	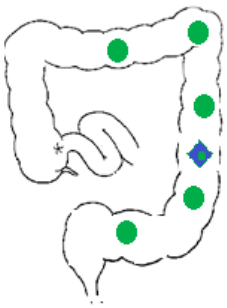 2009 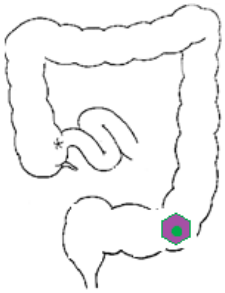 2012
15	68	Crohn's	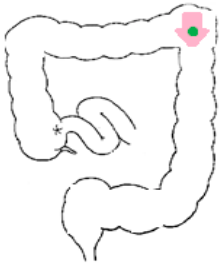 2009